ISSN 0915-6348

NATIONAL INSTITUTE FOR FUSION SCIENCE

Proceedings of Japan-U.S. Workshop P-196 on High Heat Flux Components and Plasma Surface Interactions for Next Devices

(Received – Feb. 23, 1993)

NIFS-PROC-12 Mar. 1993

RESEARCH REPORT
NIFS-PROC Series

NAGOYA, JAPAN

Proceedings of
Japan-U.S. Workshop P-196

on

High Heat Flux Components and Plasma Surface Interactions for Next Devices

at

Kyushu University, Chikushi Campus
Kasuga, Fukuoka
November 17-19, 1992

Edited by
K.N. Wilson, Sandia National Laboratories
and
T. Yamashina, Hokkaido University

National Institute for Fusion Science
Nagoya

Proceedings of
Japan-U.S. Workshop P-196

on

High Heat Flux Components and Plasma Surface Interactions for Next Devices

at

Kyushu University, Chikushi Campus
Kasuga, Fukuoka
November 17-19, 1992

Edited by
K.N. Wilson, Sandia National Laboratories
and
T. Yamashina, Hokkaido University

National Institute for Fusion Science
Nagoya

TABLE OF CONTENTS

Session 3: Developments of HHFC/Divertor and Energy Deposition

Session 4: PFC and PSI Studies in Laboratory

Session 5: Tritium Inventory and Handling

Session 6: Neutron Damage

Session 7: Session Summaries

Summary

K.Wilson and T.Yamashina

The Japan-US Workshop P-196 was successfully carried out in Kyushu University, Chikushi Campus, from November 17 to 19, by the excellent organization due to Prof.Satoshi Itoh, Prof.N.Yoshida and Prof.T.Muroga. The agenda for very many presentations within 3 days period, was well organized by Prof.T.Hino. The last workshop held at Sandia National Laboratories in November of 1991, organized by Dr.W.Gauster, became a largest scale in the series of this workshop. The scale of the present workshop, again, became a largest one, e.g. 48 presentations and 66 participants. Of the 66 participants, 11 were from US, 1 from Canada, 6 from EC and 48 from Japan.

The major concern was on the research and development required both for International Thermonuclear Experimental Reactor(ITER) and Large Helical Device(LHD). Most of the discussion items was similar to that of the last workshop, e.g. PFC and PSI in Large Device, High Heat Flux Component, Laboratory Studies and Neutron Damage. The presentation number concerning High Heat Flux Component was largest.

In the session of PFC and PSI in Large Devices, the result of gas target divertor in DIIID, the prediction of tritium inventory in TFTR, JET divertor program, the status of LHD and the damage of B_4C coated tiles in JT-60U were presented. In addition, the impurity emission in TRIAM-1M was presented. The emphases were the reduction of heat flux, optimization of low Z materials such as boron and beryllium, tritium inventory/retention and control of recycling.

In the field of HHF Component, introduced were the rapid progresses of brazing components in SNL, JAERI and NIFS. Now, the reliable HHF Component, which does not show significant damage after 1000 heat cycles with heat flux up to 20 MW/m^2, is available. The numerous developments for the HHF Component in the Japanese Industries were also introduced.

In the Laboratory Studies, the major concerns were the recycling, the erosion both of low Z and high Z materials and the performance of boronization or boron doped material. It was indicated that emission of hydrogen atom from graphite becomes dominant when the temperature exceeds about 1000K. The relation of the hydrogen solubility with the degree of graphitization, which is useful for the evaluation of retention, was presented. It was also pointed out that the boron evaporation becomes serious when the temperature is over 1000 ^oC.

In the Tritium session, the retention properties of Be were newly introduced based upon numerous data and the experience in JET DT discharge. The attentions in use of tritium and the ion driven permeation in Mo were also discussed. For the graphites and the boron mixed graphites, the deteriorations of thermal conductivity due to neutron damage was also reviewed.

The workshop of this series will be continued and be held in the next year, e.g. December 14-17, 1993, in UCLA.

Finally, we acknowlege the supports for the present workshop by the following Japanese industries ;

Hitachi,
Hitachi Chemicals,
JEOL,
Kawasaki Heavy Industries,
Marubun,
Mitsubishi Atomic Power Industries,
Mitsubishi Chemicals,
Mitsubishi Heavy Industries,
Toshiba Corp.,
Toyo Tanso.

Session 1: Overviews

US ACTIVITIES ON PLASMA FACING MATERIALS AND COMPONENTS

K. L. Wilson
Sandia National Laboratories
Livermore, CA 94550

Japan-US Workshop P196
Kyushu University
November 17-19, 1992

and of course

ITER

US ACTIVITIES IN PFCs

Confinement Systems

DIII-D
TFTR
Alcator C-Mod
ATF
SSAT Conceptual Design

Bi-Lateral Programs

JET
TEXTOR
Tore Supra
JT-60 U
LHD (under discussion)
Monbusho Labs
Russian Federation Labs

U.S. DOE Small Business Innovative Research (SBIR) Program

Carbon-Carbon Composites	NAMCO
Thermal Composite Plasma Facing Materials	ESLI
Joining Technology	TRI
Joining Methodology	Applied Sciences, Inc.
High Thermal Conductivity Carbon-Carbon Composites	Applied Sciences, Inc.
Helium Cooling for HHF Components	CREARE
Carbon-Carbon Composite Joining	MER

US ACTIVITIES IN PFCs

Confinement Systems

DIII-D
TFTR
Alcator C-Mod
ATF
SSAT Conceptual Design

Bi-Lateral Programs

JET
TEXTOR
Tore Supra
JT-60 U
LHD (under discussion)
Monbusho Labs
Russian Federation Labs

U.S. DOE Small Business Innovative Research (SBIR) Program

Carbon-Carbon Composites	NAMCO
Thermal Composite Plasma Facing Materials	ESLI
Joining Technology	TRI
Joining Methodology	Applied Sciences, Inc.
High Thermal Conductivity Carbon-Carbon Composites	Applied Sciences, Inc.
Helium Cooling for HHF Components	CREARE
Carbon-Carbon Composite Joining	MER

and of course

ITER

Tritium Retention in TFTR

(Assumes retention fraction = 0.45)

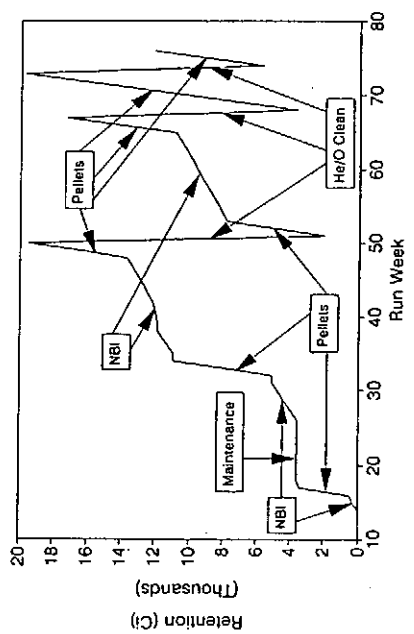

GENERAL ATOMICS

EXTENSIVE EDGE DIAGNOSTICS ON DIII-D

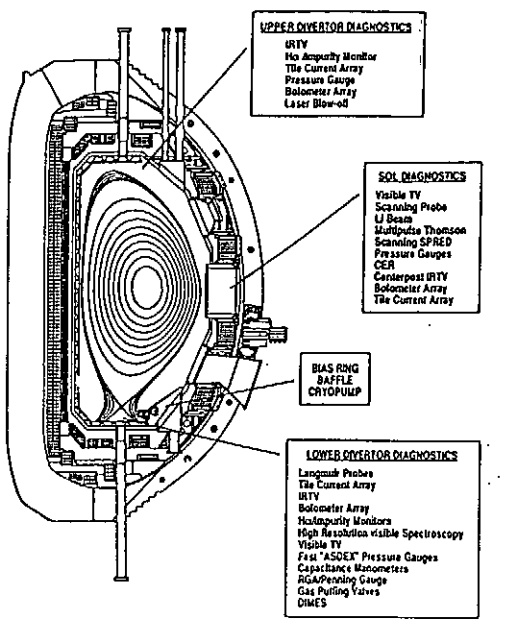

Alcator C-Mod Vessel and First-Wall Hardware

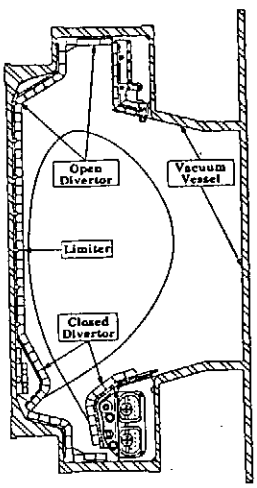

Tokamak Characteristics

High Field: $B_T \leq 9$ Tesla

High Current: $I_p \leq 3$ MA

High Density: $n_{e0} = 10^{19} \rightarrow 10^{21}$ m^{-3}
$T_i \sim T_e \sim 2 \rightarrow 5$ keV $\rightarrow$

Compact: $R_t = 0.67$ m, $a = 0.21$ m

Shaped, Diverted: $\kappa \leq 1.8$, $\delta \sim 0.4$

High Power Density:
$P_{OH} \leq 3$ MW
$P_{ICRF} = 4 \rightarrow 8$ MW (80 MHz)
$P_{LHRF} \leq 4$ MW (4.6 GHz)

$\Rightarrow P_{sep}/A_{sep} \sim 0.5$ MW/m^2 !!

Pulse Length (flattop): 1 sec at 9 Tesla
7 sec at 5 Tesla

First-Wall/Divertor Characteristics

Molybdenum tiles for first phase

Total plasma-facing area 6.7 m^2
Plasma "wetted areas"
Limiter 0.8 m^2
Closed Divertor 0.8 m^2
Open Divertor 0.2 m^2

$\Rightarrow q_{div} \sim 5 \rightarrow 30$ MW/m^2 !!

Mission of the Steady State Advanced Tokamak (SSAT)*

Steady State:

- Demonstrate integrated steady-state operating modes near $q_{95}=3$, $\beta_N=3.0$-3.5 %-m-T/MA.
  - Power and particle handling with divertors.
  - Non-inductive current drive.
  - Reliable plasma operation (no disruptions)
  - Steady state technology (S/C magnets, actively-cooled in-vessel components).

Advanced Tokamak:

- Optimize plasma performance → attractive reactor.
  - Goals: $\tau_E/\tau_L>2$, $\beta_N>3.5$, $I_{BS}/I_P \rightarrow 100\%$.
  - Features:
    - Shaped cross section ($\kappa=2$, $\delta=0.5$)
    - Double null poloidal divertor
    - Deuterium operation
    - High aspect ratio (R/a=4.5)
    - Current profile control

* Also known as the Tokamak Physics Experiment (TPX)

GHN 09/16/92 - 4

TPX PFC SYSTEM FUNCTIONAL REQUIREMENTS

- DIVERTOR
  - EXHAUST PLASMA HEAT AND PARTICLE LOSSES
    PEAK HEAT FLUX - 12 MW/m2 - Obj 1
    20 MW/m2 - Design
  - SUPPORT CLEAN, HIGH PERFORMANCE PLASMAS
  - BE RECONFIGURABLE TO SUPPORT DIVERTOR DEVELOPMENT PROGRAM
- INBOARD LIMITER FOR STARTUP AND VV PROTECTION
- OUTBOARD BELT LIMITERS FOR STARTUP AND PROTECTION OF RF LAUNCHERS AND PASSIVE STABILIZATION PLATES
- ARMOR FOR VV-PROTECTION
- ALL PFC's MUST BE REMOTELY MAINTAINABLE

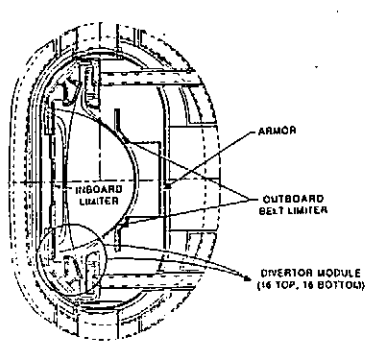

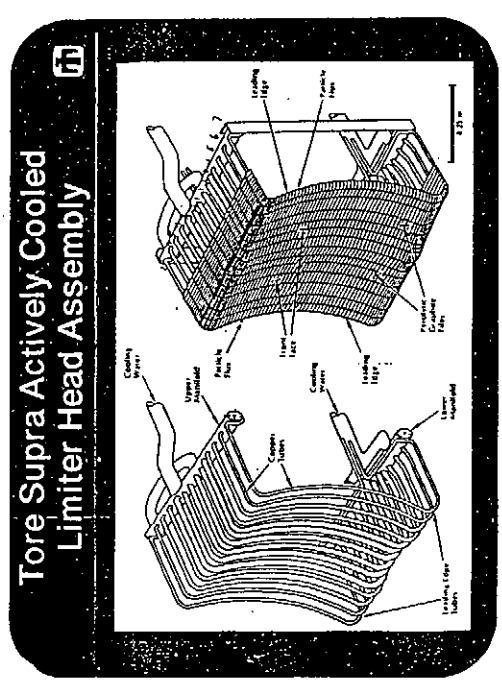

NORMAL FLOW HEAT TRANSFER

A helium-cooled NFHX has a pressure drop which is two orders of magnitude smaller than parallel tubes.

- low coolant velocity
- short flow path
- entire wall sees the entire ΔT

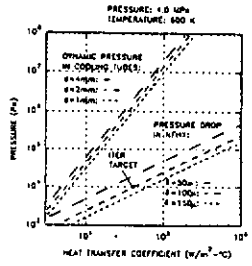

TRITIUM ON THE JET GRAPHITE BELT LIMITER MEASURED BY COUNTING EMITTED BETAS

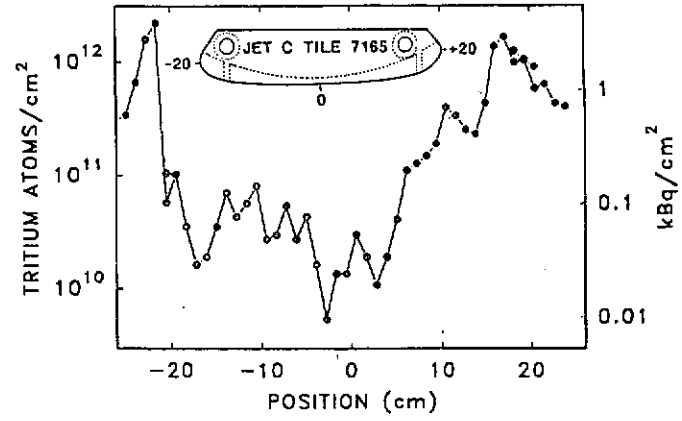

Divertor Development for ITER

Goals

– concept improvement

- qualify gaseous or radiative divertor for power and particle control requirements, and
- reduction of peak and average heat fluxes

– performance maximization

- materials development and validation
- high heat flux technology

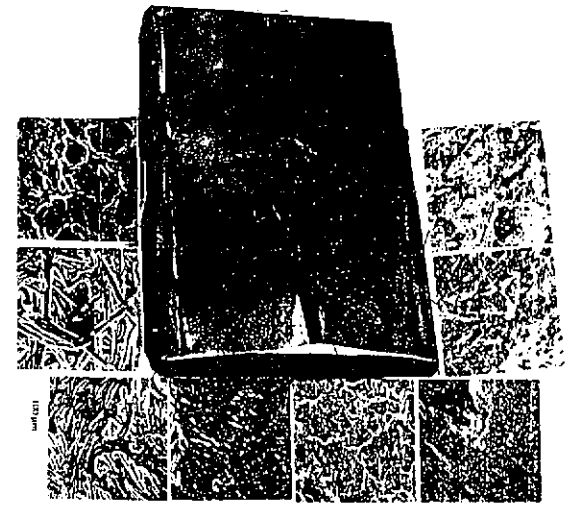

US Capabilities Encompass:

- **Materials development:**

  Examples include

  - Be development for JET,
  - the first use of CFC materials in tokamaks,
  - continued development of high conductivity CFCs and improved Be structures.

- **Heat removal, lifetime and reliability:**

  Extensive experience exists in data base development, prototype testing and component design and fabrication.

- **Boundary layer modification and improved divertor operation:** Examples include

  The Advanced Divertor Program (ADP) on DIII-D which achieves boundary layer modification through

  - gas injection,
  - divertor surface biasing,
  - active divertor region pumping.

  Experiments on PBX/M and Alcator C-Mod

  Additional data base on plasma processes provided by PISCES.

US Capabilities (cont.)

- **Tritium handling and safety:**

  Analysis of tritium inventory, recycling and safety issues for ITER are based on

  - tritium / materials interactions data obtained on the Tritium Plasma Experiment (TPX),
  - extensive measurements of deuterium migration in tokamaks, including TFTR, DIII-D and JET,
  - detailed analytical modeling.

- **Erosion / Redeposition:**

  Predictions of component lifetime and core impurity contamination for ITER are provided by detailed models that have been validated against measurements on TFTR, DIII-D, TEXTOR and other machines.

- **Disruptions:**

  The US program on disruptions includes extensive efforts on both

  - avoidance and mitigation, and
  - component survivability.

- **Helium Exhaust:**

  Options for selective helium removal such as implantation pumping in metal surfaces and semi-permeable membranes are being pursued.

US HHF/PMI Test Facilities

Facility	Institution	Purpose
FELIX	ANL	Disruption electromagnetic forces
DIMES	GA	Exposure of materials to discharges in divertor of DIII-D, erosion-redeposition studies
VAPOR	INEL	Interaction of air or steam with plasma facing materials
Ion Implantation Facility	INEL	Tritium permeation and retention in materials
Beryllium Metallurgy Laboratory	LANL	Production of Be powder, metallurgical processing, including plasma spray
SIRENS	NCSU	Disruption studies
RFTF	ORNL	Wall conditioning and outgassing with application of magnetic field
HFR	ORNL	Water-cooled fission reactor for neutron irradiation studies
EBTS	SNL	High heat flux testing, 30 kW electron beam, beryllium compatible
PMTF	SNL	High heat flux testing, 600 kW electron beam, beryllium compatible
Water Flowloop	SNL	Test specimen cooling, flow rate = 30 l/s max., pressure = 7 MPa, max. temp. = 290°C
Helium Gas Loop	SNL	Test specimen cooling, max. pressure = 4.1 MPa, max. temp. = 450°C, flow capacity = 32 g/s
ACX	SNL	Armor conditioning experiment, wall conditioning at 4.4 T field
TPX-Upgrade	SNL	Plasma drive tritium permeation, tritium retention, beryllium compatible
LAMPE	SNL	Wall conditioning and in-vessel tritium management, beryllium compatible
STOX	SNL	Outgassing and tritium charging of plasma-facing materials, tritium compatible, n-irrad. samples

SNL High Heat Flux Test Capabilities

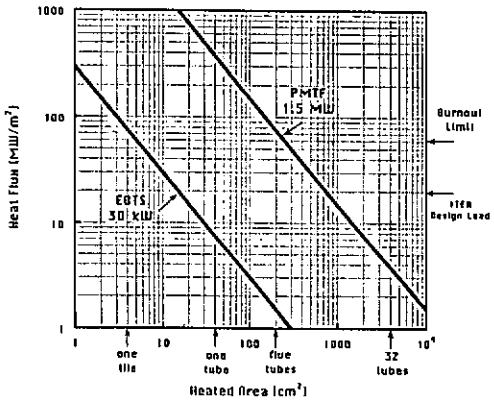

TSRL	SNL	Low pressure plasma-spray facility, beryllium compatible
Surface Analysis	SNL, ANL, UCLA, PPPL, others	Includes accelerator-based diagnostics for non-destructive analysis of tiles and components
PISCES-A	UCLA	Plasma edge management concepts (gaseous divertors); edge plasma turbulence and transport
PISCES-B	UCLA	Plasma-surface interactions: erosion-redeposition, extensive surface diagnostics, beryllium compatible
PISCES-Upgrade	UCLA	Plasma-surface interactions, erosion-redeposition, ITER-relevant parameters, beryllium compatible
PLADIS	UNM	40 kJ plasma gun for study of disruption phenomena, beryllium compatible
IDEAL	PPPL	Proposed steady-state linear divertor simulator

Plasma Interactions Surface-Component Experiment Station

Boundary Layer Physics - PISCES A

- edge plasma turbulence & transport,
- biased divertor simulations,
- slot divertor simulations,
- gaseous divertor simulations.

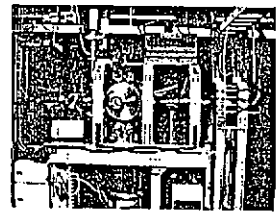

Plasma Materials Interactions - PISCES B

- erosion/redeposition studies,
- outgassing from materials,
- novel materials development eg. bulk boronized graphites.

The Plasma Materials Test Facility Provides Data on

- heat removal and critical heat flux,
- thermal fatigue and lifetime issues,
- design concept and prototype evaluation.

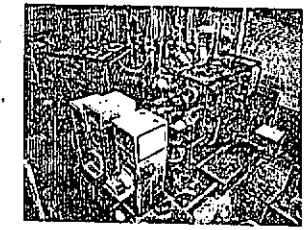

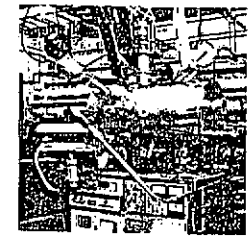

Recent Contrubutions

- CHF data & correlations,
- qualification of actively cooled, brazed armor PFC design options,
- thermal fatigue testing on Be,
- component qualification testing for DIII-D, JET, TFTR, Tore Supra, TEXTOR and other machines.

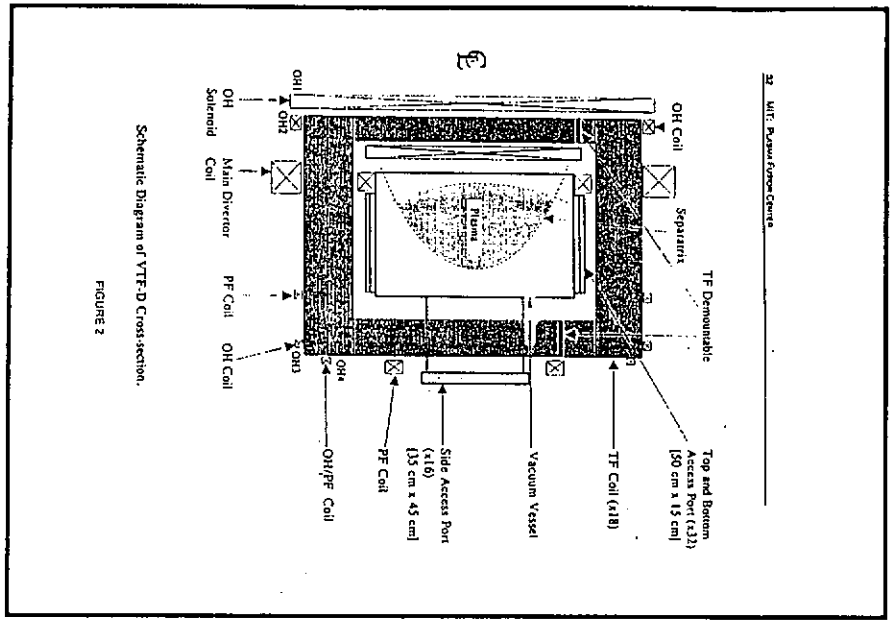

Schematic Diagram of VTF-D Cross-section.

FIGURE 2

32 MIT: Plasma Fusion Center

The Tritium Plasma Experiment (TPX) is a Unique Facility Devoted to Tritium-Material Interaction Studies

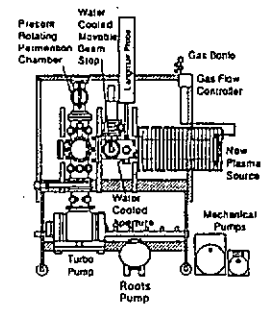

- Qualification of Materials for TFTR D-T Operation
- Insulator Tests for JET and TFTR
- Beryllium Studies for JET
- Tritium Graphite Database for BPX
  - -- Graphites
  - -- Carbon/Carbon Composites
  - -- Pyrolytic Graphite
- Tritium Release Studies (with INEL)
- In-Situ Tritium Removal Techniques
- Tritium Inventory in Neutron-Irradiated Graphites and Beryllium for ITER

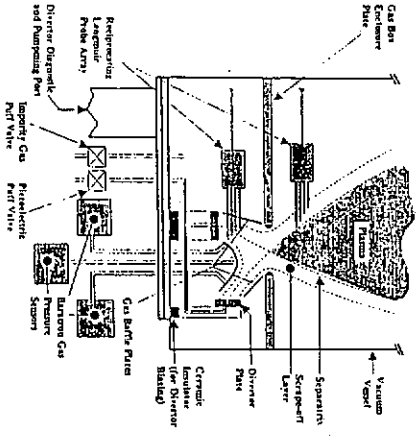

VTF-D Plasma Parameters

Major Radius R_0	0.93 m
Toroidal Field B_0	1.0 T
Plasma Current I_p	250 kA
Minor Radius a_p	0.26 m
Elongation	1.8
Safety Factor q_{95}	2.9
Aspect Ratio A	3.4
Volume Average Beta $\langle\beta\rangle$	2.7%
(Troyon)	
Pulse Length (flat-top) T_p	2 sec
Heating Power	ICRF: 2.3 MW
	NBI Option: 2.3 MW

DIII-D DIVERTOR MATERIAL EVALUATION SYSTEM (DIMES)

- DIMES will allow exposure of various materials to the DIII-D divertor plasma.
- Capabilities:
  - Strike point sweeping across sample.
  - 4.8 cm sample diameter.
  - Exposure for one or more shots.
  - Changeout as often as daily.
  - Active instrumentation and bias can be added.
- DIMES final design, fabrication, and installation are in progress at GA.
- In-situ, on-line measurement technique being developed at SNL-L.

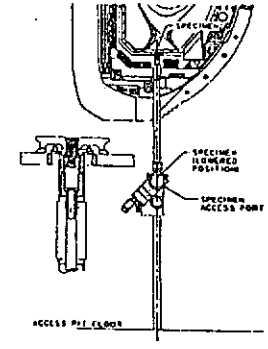

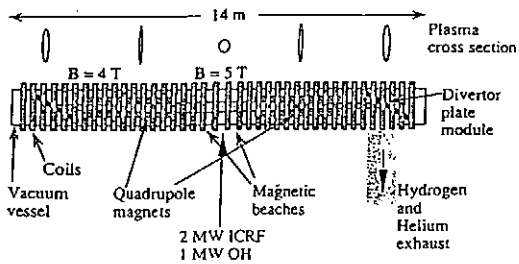

ITER Divertor Experiment and Laboratory: Phase I

Plasma on target plate:	~ 10 cm x 1 m
Predicted peak power flow:	200 MW/m^2
Central plasma density:	5×10^{14} / cm^2
Ion temperature:	~ 300 eV
Electron temperature:	~ 100 eV

Old PFC Task Structure (1988-1992)

PFC-1 First Wall R&D
- 1.1 FW Armor Development
- 1.2 Manufacture of FW Mock-ups
- 1.3 FW Component Testing
- 1.4 Start-up and Passive Shutdown
- 1.5 FW Test Facilities

PFC-2 Divertor R&D
- 2.1 Divertor Armor Development
- 2.2 Manufacture of Divertor Mock-ups
- 2.3 Divertor Component Testing
- 2.4 Divertor Test Facilities

PFC-3 Advanced Divertor Concepts

New PFC Task Structure (1992-?)

PFC-1 Divertor Concept Improvement

PFC-2 Heat Removal, Lifetime, and Reliability

PFC-3 Materials Development

PFC-4 Tritium and Safety

PFC-5 Erosion-Redeposition

PFC-6 Disruptions

PFC-7 Helium Exhaust

R&D Coordinators for Plasma Facing Components Task Area

Sandia National Laboratories - R. Watson

University of California at Los Angeles - Y. Hirooka

Argonne National Laboratory - R. Mattas

General Atomics - C. Wong

Oak Ridge National Laboratory - T. Burchell

Princeton Plasma Physics Laboratory - S. Cohen

Idaho National Engineering Laboratory - S. Piet

Plasma Facing Components Topic Areas

PFC-1: Divertor Concept Improvement

- boundary plasma modification and control
  - DIII-D
  - Alcator C-Mod
  - PISCES-A
- plasma edge computer codes
  - B2, LEDGE, DEGAS, NEWT-1D

PFC-2: Heat Removal, Lifetime, Reliability

- flow enhancement for water and advanced cooling
- CHF data base
- flow instabilities
- diagnostics
- thermal fatigue
- erosion in coolant channels
- testing

PFC-3: Materials Development

- Improved PFM: Be, C, high Z
  - lower oxygen content Be
  - high conductivity carbon fibers
- high strength, high thermal conductivity heat sink structural materials
- associated technologies
  - plasma spray
  - bonding

PFC-4: Tritium and Safety

- control of the at-risk, in-vessel inventory of tritium
  - boundary layer recycling control
  - tritium trapping
  - wall conditioning
- analysis of accident scenarios
  - requires data on interaction of tritium with materials and coolants

PFC-5: Erosion and Redeposition

- measurements of erosion and redeposition in tokamaks (DIMES in DIII-D)
- post-exposure analysis (JET)
- laboratory measurements of fundamental processes (PISCES)
- development and validation of models

PFC-6: Disruptions

- materials response to pulsed loads
  - small plasma guns
  - DIII-D (DIMES)
- model development and validation

PFC-7: Helium Exhaust

- measurements of He transport in tokamaks
- control of exhaust through boundary layer modification
- experiments on selective pumping

PFC Industrial Participation

- Request for Quotations issued June 15, 1992
- Bidders Conference held July 15, 1992
- Proposals received August 3, 1992
- Technical Evaluation completed August 20, 1992
- Contract to be issued 1st quarter FY93

US ITER R&D
Sandia/Industry Contract

Task Descriptions

1. Design and fabrication of small and medium-scale test specimens for high heat flux testing.
2. Finite element thermal and structural design and analyses.
3. Thermal-hydraulic design and analyses.
4. High heat flux testing of small and medium-scale mockups.
5. Non-destructive evaluation of bonded armor tiles.
6. Development of ultra-high thermal conductivity carbon fiber composite armor tiles.
7. Development of plasma sprayed beryllium and tungsten coatings.
8. Modification of the Plasma Materials Test Facility (PMTF).
   - 8.1 Installation and commissioning of the 600 kW electron beam gun
   - 8.2 Design study for a 1 MJ plasma disruption simulator.

Tasks 9-13 were deleted from Sandia contract ... (included in UCLA/Industry contract)

14. Attend design meetings in US and Garching, Germany.

RDW Sandia 9/4/92

New Carbon Materials

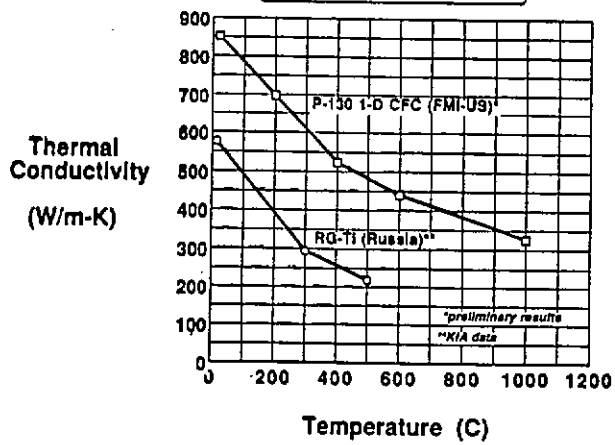

Divertor Thermal Fatigue Tests

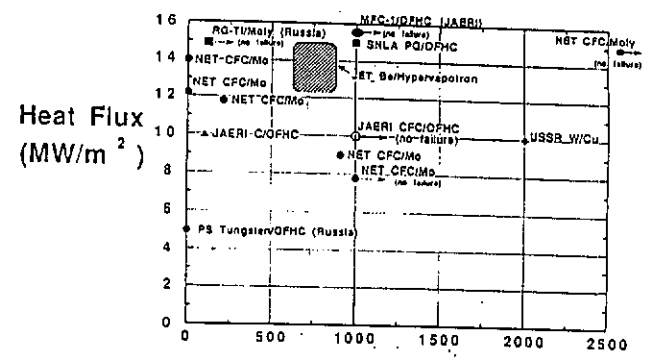

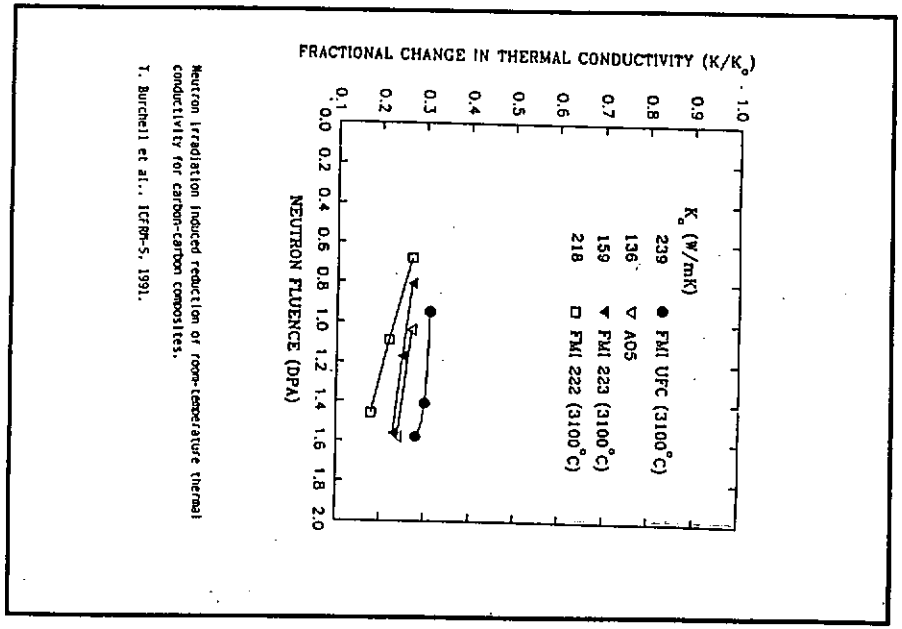

Neutron irradiation induced reduction of room-temperature thermal conductivity for carbon-carbon composites.

T. Burchell et al., ICFRM-5, 1991.

Ultra-High Conductivity Carbon Fiber Composites

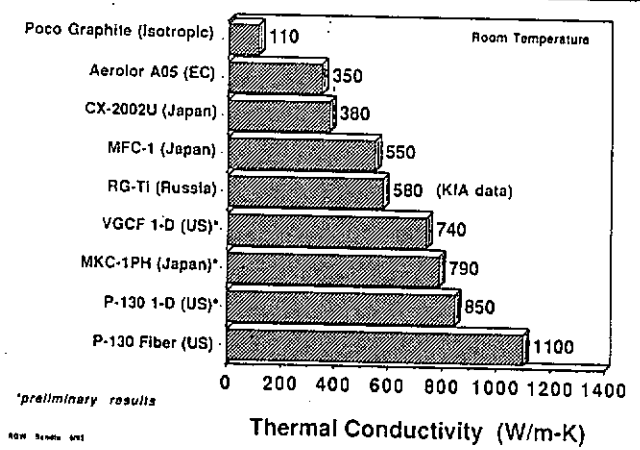

*preliminary results

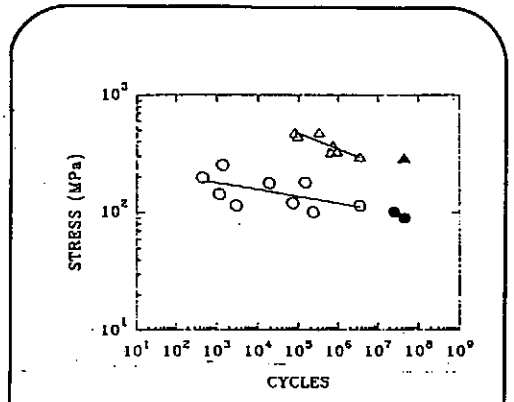

Figure 1. Fatigue data for as-received GLIDCOP A1-15 (triangles) and induction brazed butt joints (circles).

Fusion Power Program

Beryllium Facilites

- Four rooms (2000 sq ft) ventilated by 20,000 CFM fan into HEPA filters
  - Change room & metallography grind and polish
  - Dry box (powder screening, storage, splat quenching), button arc melter, melt spinner, spray chamber, cold iso-press, furnaces, cut-off saw
  - Single crystal furnaces, tented area containing P&W centrifugal atomizer
- Air Quality Permit issued on Sept. 8, 1987 for beryllium operations by New Mexico Environment Department

Los Alamos National Laboratory
Materials Technology: Metallurgy

Support Facilites

- Metallography with SEM & access to TEM
- Container fabrication - TIG, EB & pinch weld, (hot out gassing)
- Two hot isostatic presses (HIP) for consolidation
- Beryllium machine shop
- Mechanical testing - cryogenic & elevated temperatures
- Mechanical fabrication - rolling mills, presses, etc.

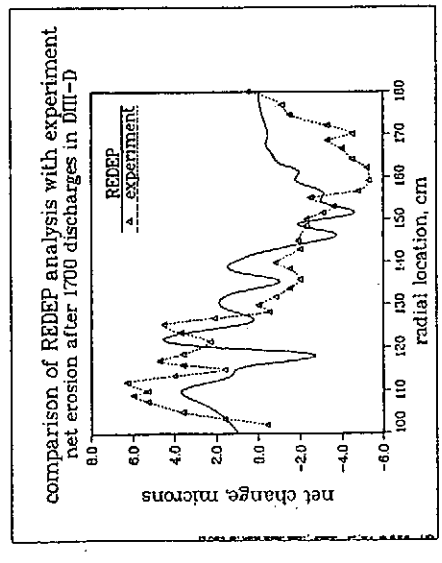

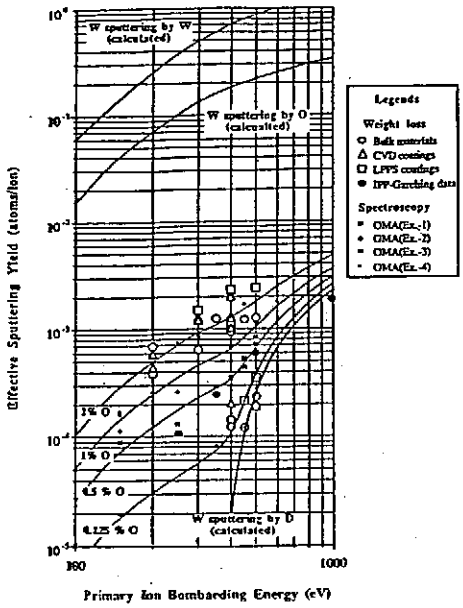

Tungsten erosion by deuterium plasma contaminated with oxygen.

Y. Hirooka, et al., 1992

In-Vessel Tritium Management for ITER (SNL, PPPL)

- Co-deposition is expected to be a major source of in-vessel tritium inventory.
  - Carbon erosion from high flux areas results in redeposition of carbon along with tritium.
  - Tritium concentration ~ 0.4 T/C is expected in a DT device.
  - The thickness of the co-deposited layer increases monotonically with discharge time.
- Tritium co-deposited with eroded carbon is a safety concern.
  - Co-deposited films decompose in air at low temperature.
  - Accidental air exposure would liberate all trapped tritium as HTO.
- Co-deposited carbon-tritium films are volatilized by a helium-oxygen glow discharge.
  - Laboratory studies and proof-of-principle tests in TFTR have demonstrated removal process.
  - CD co-deposits are volatilized to CO, CO_2 and D_2.

What does He/O GCD mean for ITER?

- A crude estimate is that ITER will reach 1 gram of in-vessel tritium after only 1 to 10 discharges in the Physics Phase.
- The allowable at-risk tritium is currently set at 100 grams (depending on siting and fence boundary).
- Therefore, He/O GDC will need to be performed from 10 to 100 times during the ITER Physics Phase.
- Each He/O GDC tritium removal cycle may require zero magnetic field, and take on the order of several days.
- Future Plans: SNL, ORNL, Tore Supra

The INEL Has Completed Exploratory Plasma-Sprayed Be/W - Steam Tests

- Density of Be specimens lower than desired (88% on average)
  - Reaction rates in steam were unacceptably high
    - 150-250 times higher than dense beryllium
    - 3 to 5 times higher than "porous" (~88% dense) Be
- Hydrogen generation in sprayed W - steam tests not significantly different from fully dense W - steam test
- Additional tests of sprayed W samples should be done to understand H2 production as a function of temperature
  - Hydrogen production did not always increase with temperature in the tests
- Volatility of W in sprayed W samples in steam was similar to previous tests of a W alloy in steam

INEL EG&G Idaho, Inc.

Dynamics of Plasma-Vapor Interactions

Stopping Power Calculation for High Energy Beams

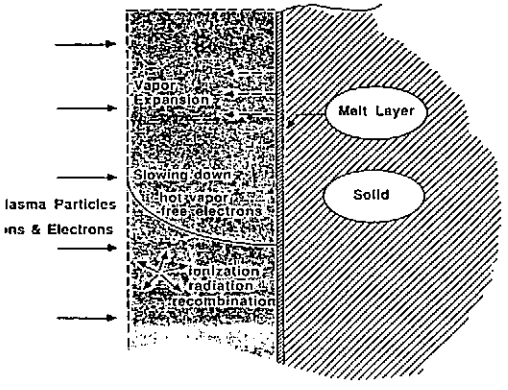

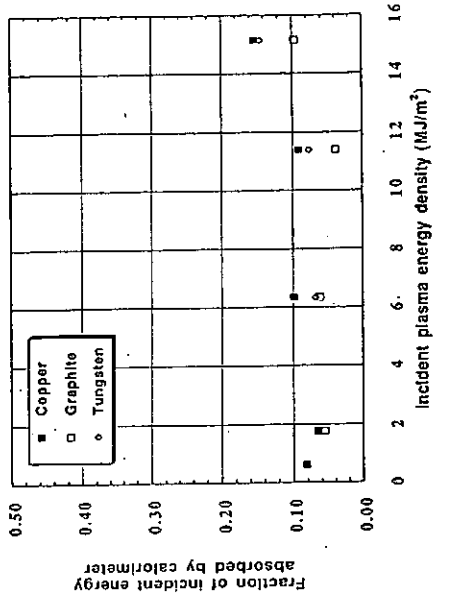

Helium Self-Pumping Experiment*
ANL/SNL/KFA

- Objective: Conduct TEXTOR experiment at KFA Julich. Study helium removal via trapping in deposited nickel surfaces in the HEMOD self-pumping module.
- Personnel:

  ANL: J. Brooks, A. Krauss, R. Mattas D. Smith
  SNL: R. Nygren, B. Doyle
  KFA: K. H. Dippel, K. H. Finken

  and UCLA/ORNL
- Schedule:

  FY 1991 Lab experiments on helium trapping, module design, and assembly, nickel filament testing, installation in TEXTOR

  FY 1992 Conduct experiment at KFA - begin Nov. 1991.

ref: J. N. Brooks et al., J. Nucl. Mat. 176 & 177 (1990) 635.

Fusion Power Program

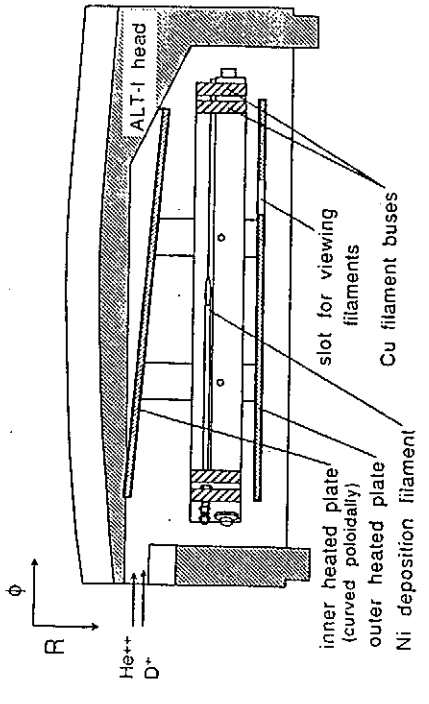

PLASMA HELIUM CONTENT
(FROM 468.6 nm HeII Diagnostic)
H2 REMOVED BY MODULE ≤ 10% OF INITIAL CONTENT ≈ 8 x 10^17 He ATOMS
He (arbitrary units)
Time (Seconds)
Beam Heating
Plasma Shift
He Injection
48859
48860
48861 (Ni deposition)
Beam Off

PFC Technology Development Schedule
93
94
95
96
97
98
Technology Development Program
Tokamak Programs
concept development, analysis and evaluation
component design and fabrication
component qualification
divertor physics - concept improvement
materials technology testing
ITER prototype testing

Schedule and Facilities for
U.S. PMI/HHF Priority Interests and ITER Technical Issues*
Issue
Schedule
Concept Improvement
Lifetime and Reliability
Helium Exhaust
Heat Removal
Materials Development
Erosion/ Redeposition
Disruptions
Tritium & Safety
FY 92
FY 93
FY 94
FY 95
FY 96
FY 97
FY 98
*Does not include International Collaborations

JET AS A TESTBED FOR MATERIALS

K J Dietz and the JET Team

Abstract

Since May 1983 experience has been gained in JET with respect to the interaction of powerful plasmas with the walls of the vacuum vessel. Initially medium-Z materials (NICROFER 7612) were used and heavy damage from runaway electrons was observed. This could be avoided by employing graphite (CFC and fine grain) as wall protection. At a later stage halo currents presented problems which could be solved by redesign of critical components.

The divertor material was graphite and beryllium. Extensive experience is available for both materials. For low density, high ion temperature plasmas, graphite is advantageous compared to beryllium. At high densities, even at full power (40 MW), beryllium is the preferred material because of the absence of density limit disruptions. MHD triggered disruptions are slower and the build-up of runaways is negligible.

JET now undergoes changes which will result in a new machine configuration, called 'Pumped Divertor'.

For the high heat flux elements extensive heat load tests were carried out in the JET neutral beam test bed. It is beryllium compatible and located in a hot cell.

The JET development plan shows that operation will recommence at the end of 1993.

US-Japan Workshop 1992

JET AS TESTBED FOR MATERIALS

K.J. Dietz and the JET Team

MACHINE STATUS

JET DIVERTOR

- Modelling
- Previous Experience
- Concept
- Materials

TEST FACILITIES AND TESTS

FUTURE DEVELOPMENT

CONCLUSION

MODELLING AND CALCULATIONS

PLASMA EDGE

EDGE 2D Fluid Edge Plasma Code

Neutral Particles Simulated by Monte Carlo Calculations (NIMBUS, EIRENE)

CAVEATS (true for all models)

Not Predictive

JET Divertor Geometry not Simulated Properly yet

Code not Validated for High Density

Treatment of Interaction of Plasma with Neutrals Needs Improvement at very low (a few eV) Divertor Temperatures

MODELLING AND CALCULATIONS

Thermomechanic

Thermal Response (ABAQUS)

Anisotropic Materials (CFC)
Nonlinear Properties
Benchmarked

Stresses (ABAQUS)

Bulk Calculation
Singularities Treated with Exact Solutions
Benchmark Tests in Preparation

Thermohydraulic

Heat transfer characteristics measured
Correlation with models (DITTUS-BOELTA, THOM)

Magnetic

EDDY CURRENTS calculated with PROTEUS, SPARK and BARABASCHI 3D

HALO CURRENTS measured, 20% of I_P

JET DIVERTOR

AIMS

- Impurity Control in a Quasistationary Plasma of Thermonuclear Grade
- Determination of Concept and Definition of Geometry and Size for ITER
- Demonstration of Operational Domain

CONCEPT

- Open Divertor with Large Connection Length
- High Density Operation to Reduce
  - -Power Load
  - -Impurity Production and Transport
- Pumping by Cryopump
- Mark I
  - -Radiation Cooled, short pulse (2 - 4 s)
- Mark II
  - -Actively cooled
  - -Long Pulses

JET

PREVIOUS EXPERIENCE

OPERATIONAL CONDITIONS

Normal

Abnormal

- Blooms
- Giant Elms
- Sawtooth Crashes
- Radial Disruptions
- Runaways
- Vertical Instabilities

MATERIALS

- High-Z
  - Nicrofer (eq. to Inconel 600)
- Low-Z
  - Fine Grain Graphite
  - CFC Graphite
  - Beryllium

Slope all joint tiles to hide edges

Tile slope degrees	Flux Density MW/m^2	Time to melt sec
0	4.9	13
2	14.7	1.44
3	19.6	0.82
10	53.8	0.15
90	282	0.004 ← Edge

3 degrees is required

= = > > 20MW of conducted power for 0.8 s

Further modifications required to maintain that value for entire dump plate:

- ⇢ all attachment holes
- ⟶ edges between tiles
- ⟶ tile slots (?)

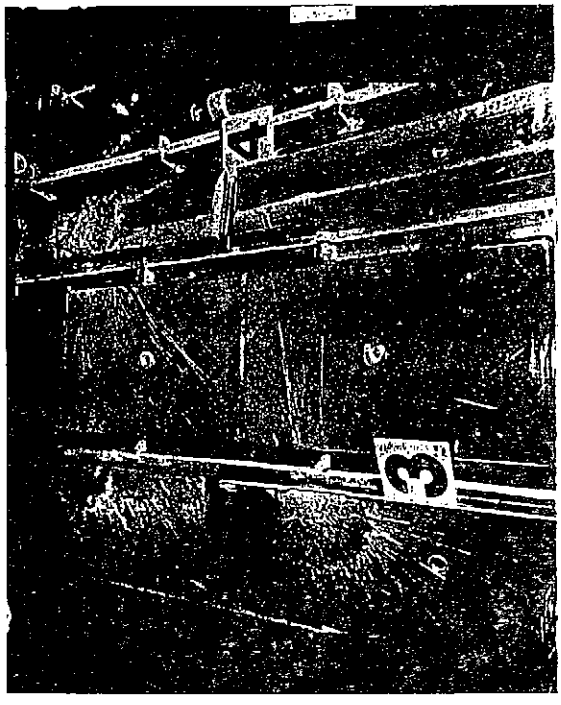

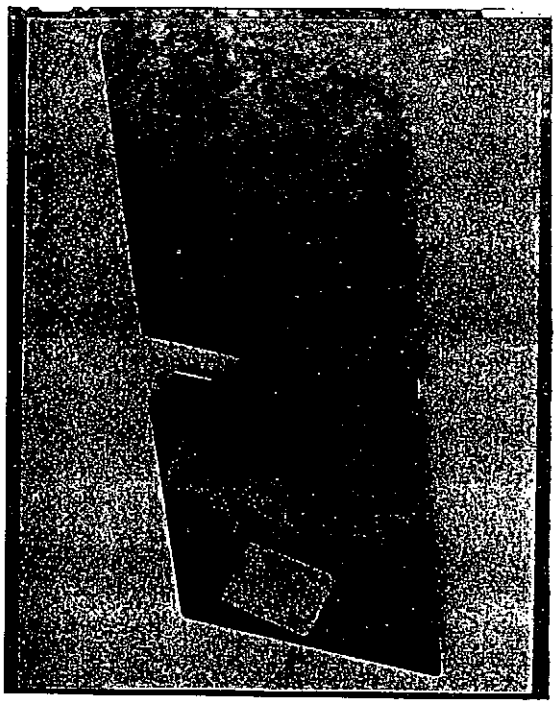

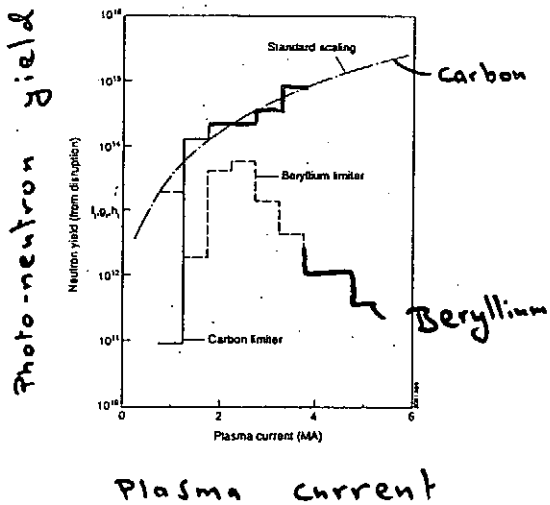
Photo-neutron yield
Standard scaling
Carbon
Beryllium limiter
Carbon limiter
Beryllium
Neutron yield (from disruption)
Plasma current (MA)
Plasma current

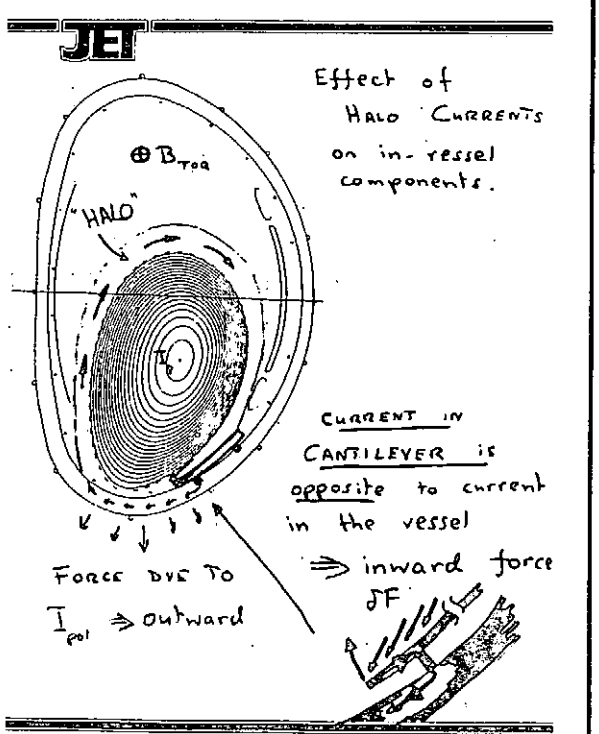
JET
Effect of
Halo Currents
on in-vessel
components.
⊕ B_{TOR}
"HALO"
I_p
Current in
Cantilever is
opposite to current
in the vessel
Force due to
I_{pol} ⇒ outward
⇒ inward force
$\int F$

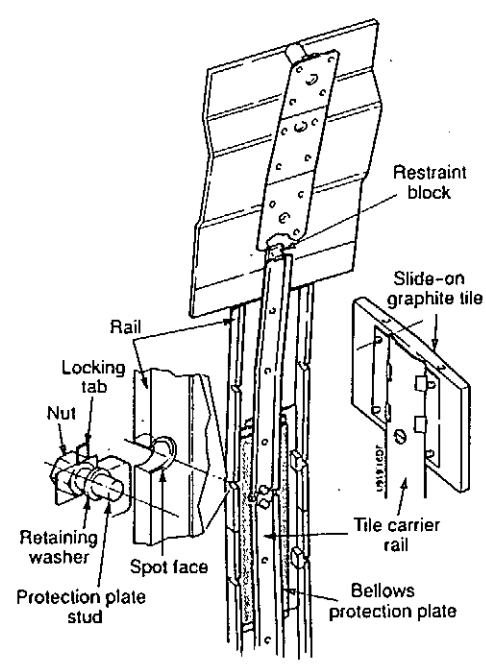
Restraint block
Slide-on graphite tile
Rail
Locking tab
Nut
Retaining washer
Protection plate stud
Spot face
Tile carrier rail
Bellows protection plate

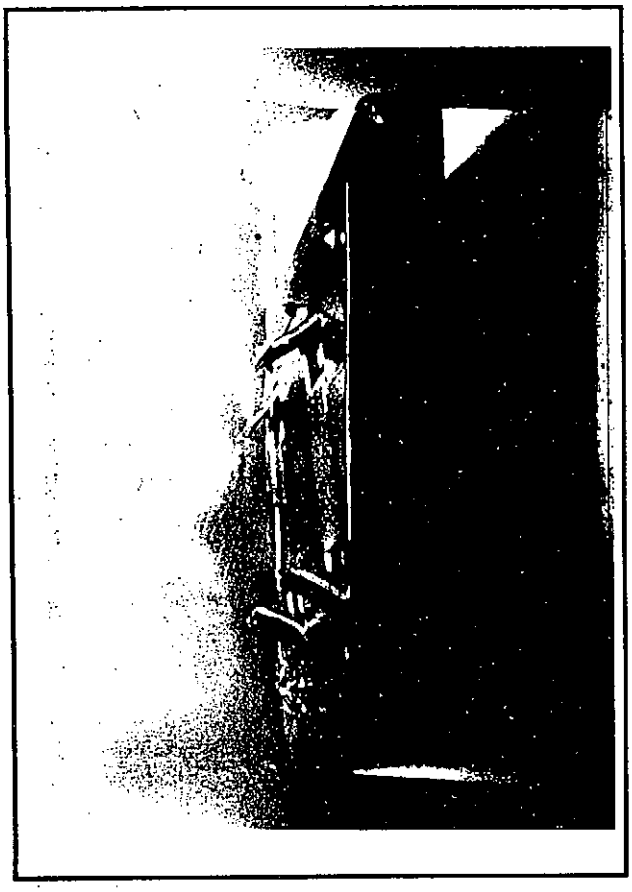

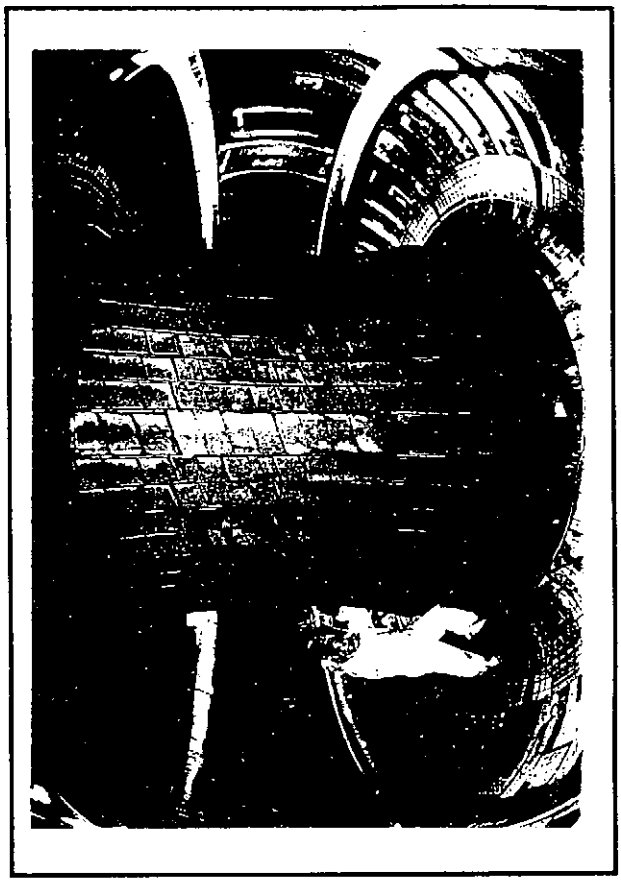

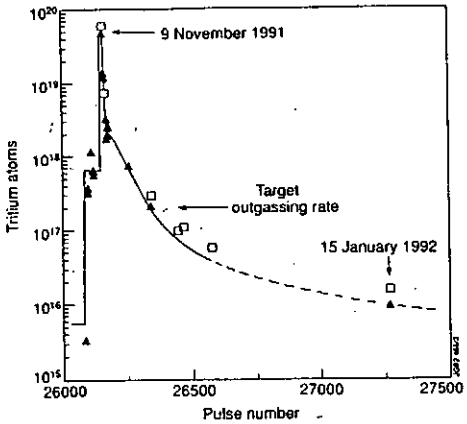
9 November 1991
Target
outgassing rate
15 January 1992
Tritium atoms
Pulse number
26000
26500
27000
27500

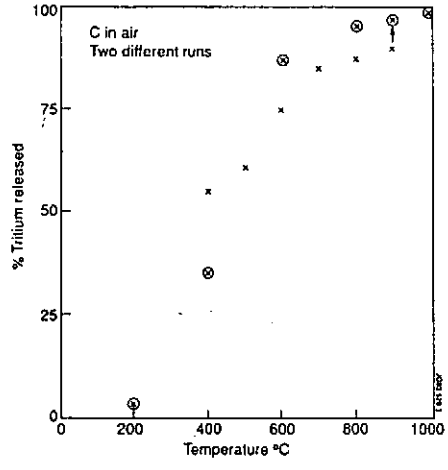
C in air
Two different runs
% Tritium released
Temperature °C
0
25
50
75
100
200
400
600
800
1000

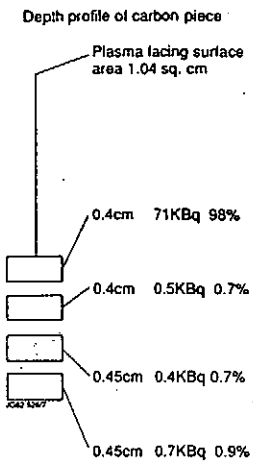
Depth profile of carbon piece
Plasma facing surface
area 1.04 sq. cm
0.4cm 71KBq 98%
0.4cm 0.5KBq 0.7%
0.45cm 0.4KBq 0.7%
0.45cm 0.7KBq 0.9%

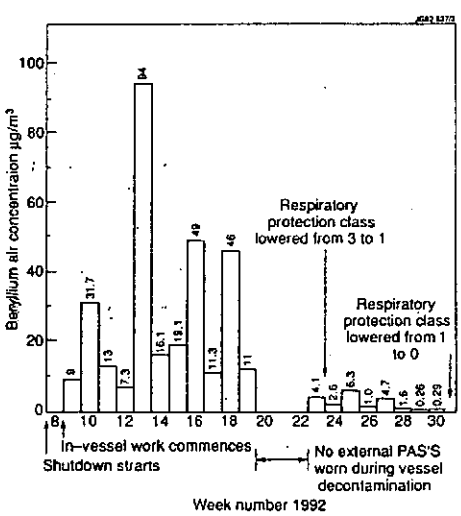
Beryllium air concentration µg/m³
100
80
60
40
20
0
9
31.7
13
7.3
94
16.1
18.1
49
11.3
46
11
4.1
2.6
6.3
1.0
4.7
1.6
0.26
0.29
8
10
12
14
16
18
20
22
24
26
28
30
Respiratory protection class lowered from 3 to 1
Respiratory protection class lowered from 1 to 0
In-vessel work commences
Shutdown starts
No external PAS'S worn during vessel decontamination
Week number 1992

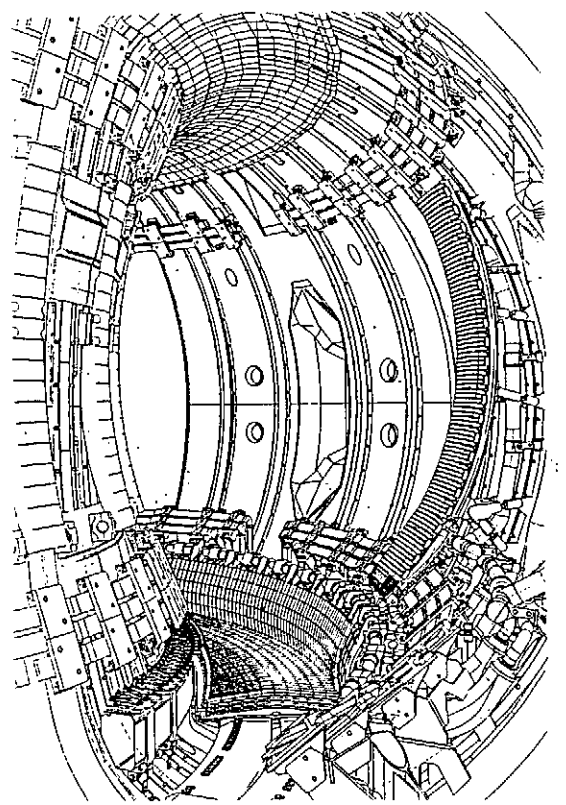

MATERIALS AND LOADS

Loads

NORMAL

50 MW m^{-2} Peak
15 MW m^{-2} Sweeped

DISRUPTION

15 MJ Deposited within 100 μs

Materials

Mark I:
Inertia Cooled Beryllium
Inertia Cooled Carbon Fibre Composite

Mark II:
Beryllium Brazed to Hypervapotrons
(Directly Cooled Beryllium?)

Walls:
Fine Grain Graphite
Carbon Fibre Composite
Beryllium

New JET pumped divertor target plate design

Power handling capability:

20 MW for 3-4s including sweeping.

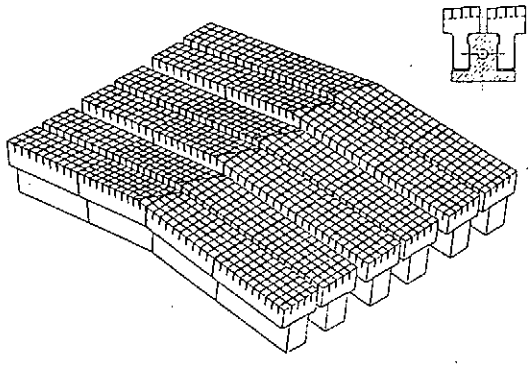

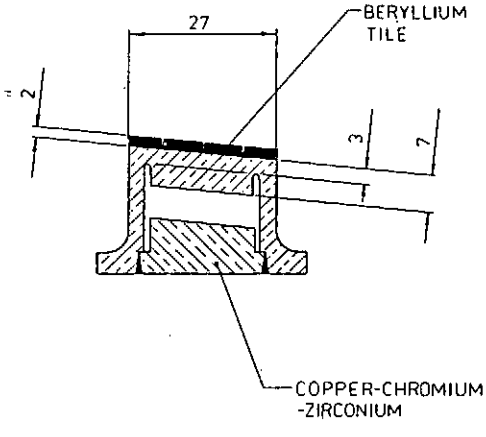

HYPER VAPOTRON SECTION

TEST FACILITIES

ION BEAM FACILITY

Total Power	8	MW
Peak Power Density	240	MWm^{-2}
Maximum Pulse Length	20	s
Beam Energy	80	keV
Modulation (on/off)	0.1/0.3	s minimum
Species	H, D, He	
Shielding (Concrete)	2	m
Possibility to Test Beryllium		

JET TOKAMAK

Tests in Realistic Conditions in Thermonuclear Grade Plasmas

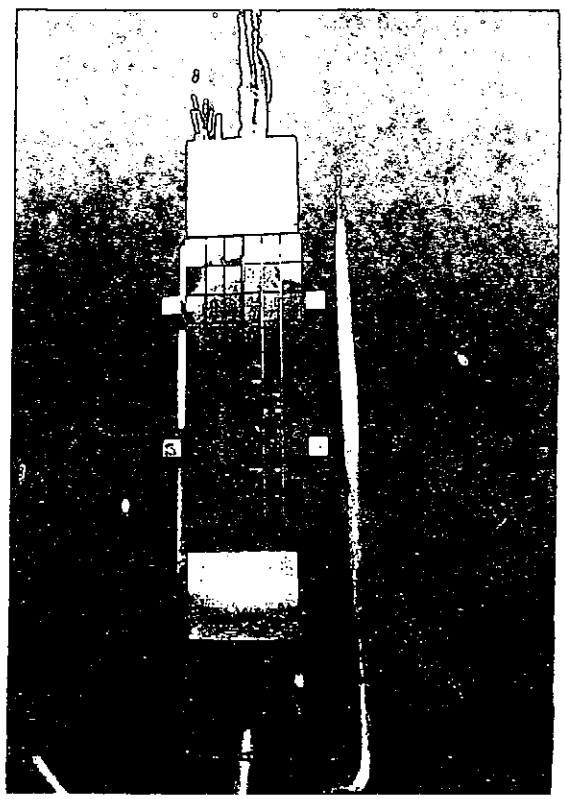

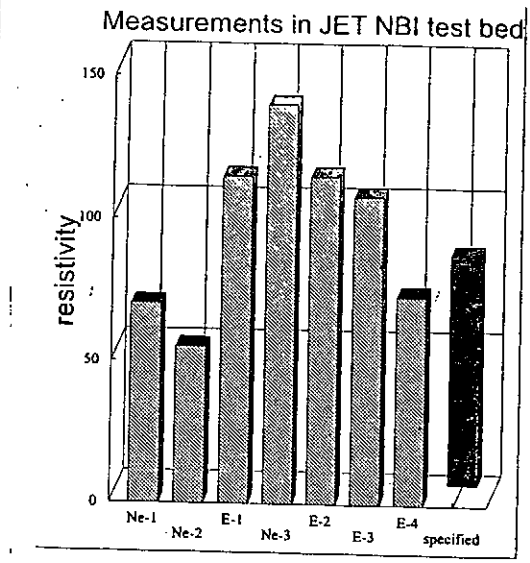

JET

SUMMARY

To Contribute to Materials Development for Future Machines it is Mandatory to Have **Access to a Powerful Tokamak** Because Only the Operational Experience Allows for the Identification of Problem Areas

JET is in an Unique Position to Evaluate the Performance of Materials in Thermonuclear Grade Plasmas

A Suite of Facilities is Available

- Modelling
- Assessment of Magnetic Forces
- Ion Beam testing
- Test Inside JET With Relevant Plasmas

Future Activities Include

- Validation of Open Divertor Geometry for High Density Operation at Large Connection Length
- Development of Joining Techniques for Cu-Be
- Development of Berylliumcarbide Fibre Composites
- Development of Directly Cooled Beryllium
- Validation of the Developed Materials and Related Techniques inside JET

Overview for Presentations from Japan Side in JPN-US Workshop P196, 11/17-19, 1992, Kyushu Univ.

Japanese Studies on HHFC and PSI

Tomoaki Hino and Toshiro Yamashina

Department of Nuclear Engineering, Hokkaido University
Sapporo, 060 Japan

In this Japan-US workshop P196, from Japan side thirty presentations are scheduled. The numbers of the sessions are as follows :

PFC and PSI in Large Devices	: 5
Developments of HHFC/Divertor and Enegy Deposition	: 11
PFC and PSI Studies in Laboratory	: 9
Tritium Inventory and Handling	: 2
Neutron Damage	: 3

The construction of LHD has been progressed on schedule. For the LHD divertor, the HHFC has been tested now and the boronization experiment has been initiated for the reduction of oxygen in the LHD plasma.

In JT-60U, several B4C materials have been tested and the degree of the damage has been evaluated. First boronization was carried out and the result showed large reduction of $\overline{Z}$ eff.

For ITER divertor, JAERI group and numerous Japanese industries have very aggressively developed the brazing component. The heat clcle test showed no significant damage after 1000 shots with the heat load of 20 MW/m2.

In the laboratories, one of major researches for erosion and retention is on boron coated material and boron mixed material. In this workshop, the session of tritium inventory and handling is newly included for the preparation to DT discharge. The results on neutron damage on graphite in Japan is also reviewed.

Japanese Studies on HHFC and PSI

T. Hino and T. Yamashina
(Hokkaido University)

Presentations in P196

- PFC and PSI in Large Devices 5
- Developments of HHFC/Divertor and Energy Deposition 11
- PFC and PSI Studies in Laboratory 9
- Tritium Inventory and Handling 2
- Neutron Damage 3

– Total 30 –

HINO-1

PFC and PSI in Large Devices

Present Status of LHD

O. Motojima

Target : $n\tau_E T$ Close to Breakeven

Schedule:

1994 ~ Installation of Vac. Chamber

End of 1996 Constructed

Major R&D Issues:

Super Conductor

Divertor with Active Cooling

Heating

Power Supply

Control System

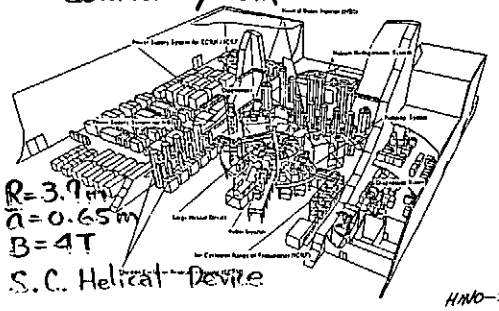

R = 3.9 m
a = 0.65 m
B = 4T
S.C. Helical Device

HINO-2

PFC and PSI in TRIAM-1M

M. Yoshida

Mo Limiter, SS Chamber

Al Probe → Impurity Dep. Rate
Relation with n_e

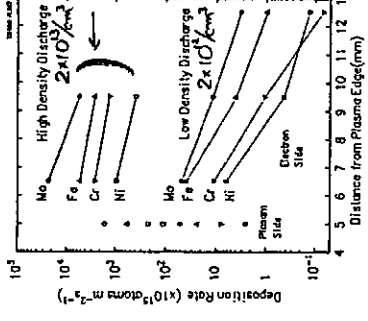

Impurity deposition rate on the plasma and the electron drift sides as a function of the distance from the plasma edge, measured with thin-foil Al collector probe specimens introduced to the scrape-off layer of TRIAM-1M. The deposition rates during high density ($\sim 2\times10^{13}$/s) and low density ($\sim 2\times10^{12}$/s) discharges are compared.

HINO-3

PFC Development in JT-60U

T. Arai

B4C Coated CFC → Exposed to 360 Shots
(Conversion : 50-200μm) (170 NBI shots
(CVD, Plasma Spray : 150μm) (Heat Flux ≤ 5 MW/m²)

No Melting, No Peeling in Flat Region
Edge Region : Melting, Peeling (Plasma Spray)

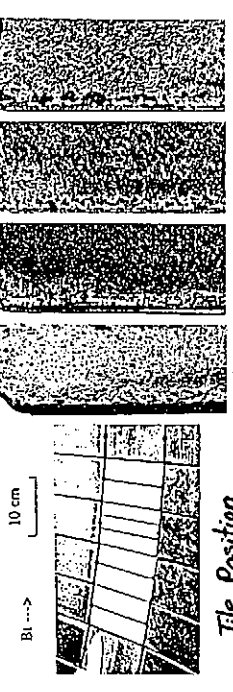

HINO-4

Boronization of JT-60 Using Decaborane M. Saido

Decaborane $B_{10}H_{14}$: Easy Handling
(H. Sugai, Nagoya Univ.)
Joul Heating After First Boronization

Z_{eff} : 3.5 → 1.8
(O : 3.6% → 0.5%)

Hydrogen Recycling in JT-60U H. Nakamura

Lower Baking Temp. → Low Recycling
He TDC → Reduction of Recycling
Low Recycling Condition
(H mode
Hot Ion Temp (38 keV)

He Ash Simulation Experiment Using He Beam Fueling

HINO-5

Developments of HHFC/Divertor

HHFC Development and Runaway Electron Analysis in JAERI M. Akiba, K. Nakamura, T. Kuroki

JAERI: ITER Divertor, First Wall
JT-60U Tiles

ITER Divertor

Saddle Type: 1D CFC + Helical Cu Tube

Heat Load Test (JEBIS)
No Major Damage for 1000 Shots
(20 MW/m², 30 sec)

JT-60U Divertor

B_4C/CFC → 10 MW/m², 5 sec
Melting: Enhanced by Thick Coating

HINO-6

Runaway Electron Analysis During Disruption

EGS4 Code
300 MeV
0.5° → Divertor
Energy Deposition in Cu
≃ 20 MeV/cm

HHFC Test for LHD Divertor Y. Kubota

CFC-Cu Brazing Mater. → Heat Cycle Test
(CX2002U
8 m/s Flow)
(10 MW/m², Period ~ 40s
Active Cooling Teststand)
Temperature Change: Measured up to ~2400 shots

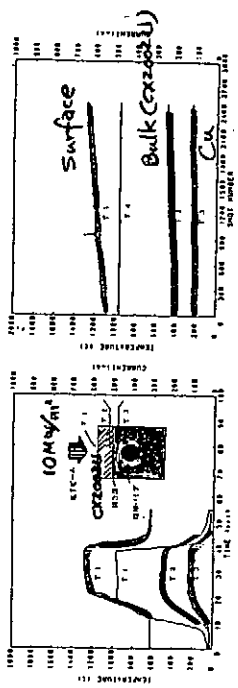

HINO-8

C-B-Ti Material

H. Shinno

Hot Pressed C-B-Ti Mater.
→ Low Z, B Contained

XRD Structure : TiC, TiB_2, Graphite

Thermal Diffusion: Comparable with TiC, TiB_2

Thermal Shock :

Mater. with high ratio of TiB_2/TiC showed better property.

HINC-9

PFC Development in Japanese Industries

Kawasaki H. I.

S. Yamazaki

Mockup Structure (JAERI)

Cylinderical Monoblock Type (LHD)

The mid-size divertor mockup.

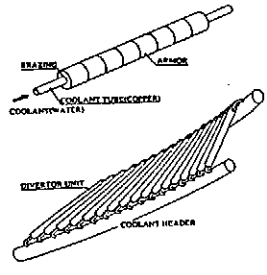

Concepts of the LHD divertor plate

HINC-10

Mitsubishi (MAPI, MHI)

K. Ioki

Conductively Cooled First Wall (ITER)
→ Carbon Sheet

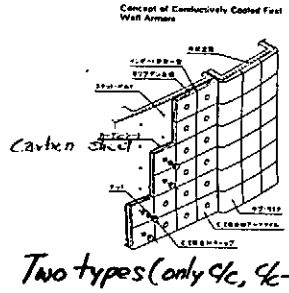

Two types (only C/C, C-Mo Brazed) are tested

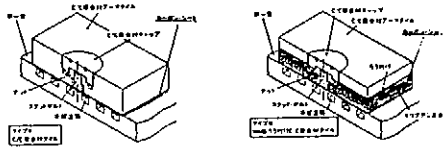

HINC-11

Hitachi, A. Shipenaka

C/C-OFCu Brazing Structure will be tested with 20MW/m²

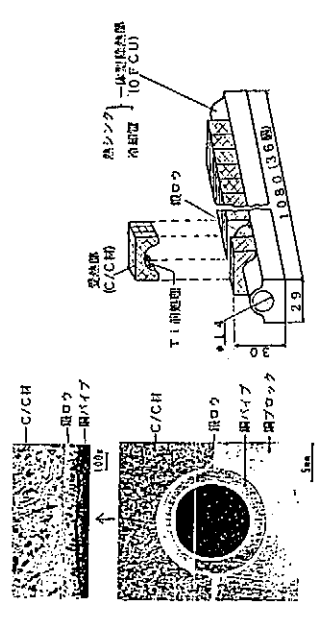

HINC-12

Toyo Tanso

T. Matsuda

- $\begin{pmatrix} CX\,2002U \\ IG\text{-}430U \\ IG\text{-}110U \end{pmatrix}$ - $\begin{pmatrix} Cu \\ Mo \end{pmatrix}$ Brazing Materials for LHD
- Fe-Cu Brazing Filler
  → Columnar growth of Fe/Cu/C phase
- Bending Strength : Const. less than ~600°C

HINO-13

Toshiba Corp.

K. Kitamura

- Graphite-Cu Brazing Material for ITER Divertor
- Residual Stress : Examined both by experiment & analysis

HINO-14

PFC and PSI Studies in Laboratory

Boronization Experiment in NIFS

N. Noda

Surface Modification Teststand

$(B_2H_6 + He)$ Glow
↓
O_2 Glow
↓
(O Adsorption
RGA
Surface Analysis

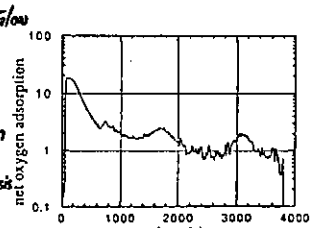

Boronization Experiment Using Decaborane

H. Sugai

$(B_{10}H_{14} + He)$ Glow
↓
Film Uniformity
(DC Glow
Pulsed Discharge

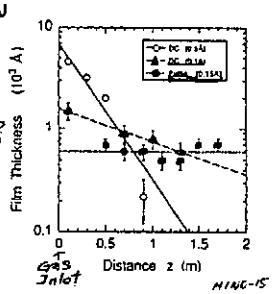

HINO-15

Net Erosion Observed in PISCES

A. Sagara

- Excess of Net Deposition
  ↑
- Deposition by Chem. Sputtered Carbon in vicinity of sample

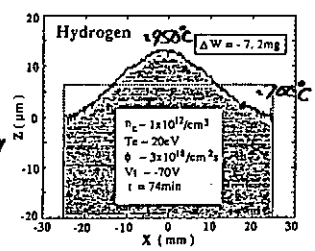

Erosion of Metal Mixed Graphite due to Hydrogen Ion

T. Hino

- V mixed graphite enhanced erosion at temp. ≥ 1000°C
- V evaporation rate is very large.

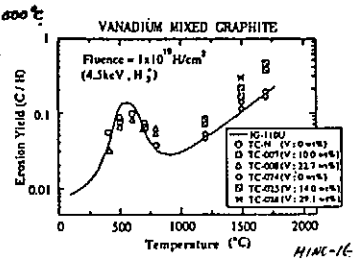

HINO-16

Hydrogen Recycling and Inventory. K. Morita

- Mass Balance Eq. for Recycling of DT Discharge
- Discussed : Isotope Effects
  Reaction Coefficients

HINO-17

Deuterium Retention of B4C Coated CFC. Y. Gotoh

- Peak Temp : 200°C Lower
- CD_4 Formation : much reduced

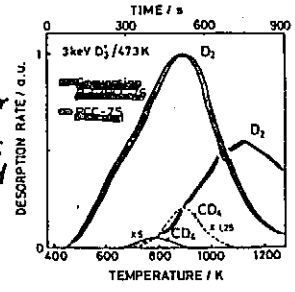

Hydrocarbon Release from Graphite M. Yamawaki

- Comparison between Model and experiment

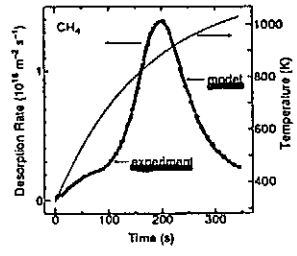

HINO-18

Hydrogen Solubility in Graphite H. Atsumi

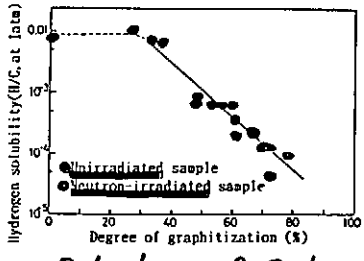

Deuterium Retention of Carbon Contained Cu S. Amemiya

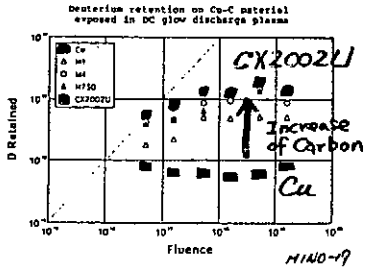

HINO-19

Tritium

Deuterium Permeation Behavior K. Okuno

- Incident Energy Dependence
- Temperature Dependence
  ↓
- Ion Driven Permeation Mechanism in Mo

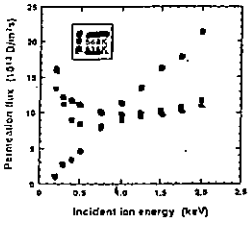

Incident ion energy dependence of IDP flux for deuterium implanted into pure molybdenum (thickness:5x 10⁻³m; incident flux:6.37x 10¹⁸D⁺/m²s)

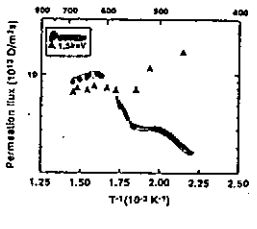

Permeation flux of deuterium implanted into pure molybdenum (5x 10⁻³ m; 6.37x 10¹⁸ D⁺/m²s)

HINO-20

Points to be Taken Care in T Experiment

M. Nishikawa

Interaction of T with
- Pipe Material
- Catalysis
- Adsorbants

HINO-21

Damage

Neutron Irradiation Effect on Thermal Conductivity

T. Maruyama, M. Iseki

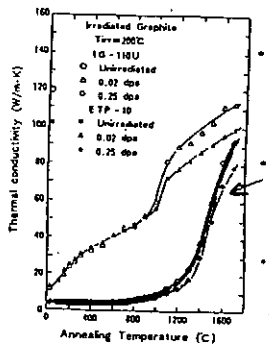

Post-irradiation annealing and the thermal conductivity of neutron-irradiated fine-grained isotropic graphites IG-110 and ETP-10.

- T.C. largely drops in case of low temp. (200-450°C).
- Recovery is difficult in case with dose more than 0.1dpa.
- Boron mixing enhances reduction of T.C.

HINO-22

Material Damage due to Hydrogen Ion

T. Muroga

Low Energy Hydrogen Ion → Mo, Al

Structure Change → TEM

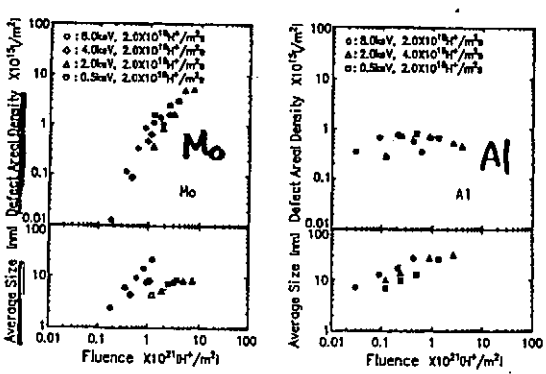

HINO-3

Session 2: PFC and PSI in Large Devices

THE DIII-D DIVERTOR DEVELOPMENT PROGRAM

by

L. SEVIER

Presented at
Japan-U.S. Workshop P196
High Heat Flux Components and
Plasma Surface Interactions for Next Devices
Fukuoka, Japan

NOVEMBER 17-19, 1992

GENERAL ATOMICS

THE DIII-D DIVERTOR DEVELOPMENT PROGRAM

L. Sevier
General Atomics Company
San Diego, California, USA

The DIII-D tokamak has a "D" shaped cross-section with a major and minor radius of 0.67 and 1.67 m respectively. DIII-D is capable of producing various plasma discharges including inside and outside wall limiter discharges, and single or double null diverted discharges. The divertor can be electrically biased. The DIII-D device is currently being upgraded with 100% graphite tiled vessel walls and a cryopumped divertor.

The objective of the DIII-D Divertor Development Program is to develop and implement a divertor design that solves the "divertor problem" by providing significant dispersal of plasma energy flow prior to it reaching the divertor surface. This solution will ease the divertor heat removal and reduce surface erosion from excessively hot impinging plasma.

The DIII-D Divertor Development Program will proceed through three phases. The first phase, the Advanced Divertor Program (ADP), will complete the on-going DIII-D plasma boundary and research program. This phase will employ the electrically biasable divertor ring now installed in DIII-D and an in-vessel cryopump to study electrical biasing, baffling, pumping, and gas and impurity injection on divertor performance and particle and impurity control. These studies will obtain data to support both the ITER divertor design and the design of the follow-on DIII-D radiative divertor and actively cooled divertor installations.

The second phase of DIII-D Divertor Development and Research will be the Radiative Divertor Program (RDP), in which the physics basis of radiative power dispersal and divertor plasma cooling will be demonstrated in an inertially cooled double-null divertor configuration that is optimized for radiative power dispersal. The RDP will focus on divertor physics studies and obtaining data for the ITER design.

The third phase of the Divertor Development and Research will be the Actively Cooled Divertor Program (ACDP), in which the radiative divertor solution will be demonstrated with actively cooled hardware suitable for steady state operation. This installation will enable DIII-D to extend its pulse length to 60 seconds with up to 38 MW input power and conduct research on time scales much longer than the current relaxation time scale and at the particle-wall equilibrium time scale.

GENERAL ATOMICS

DIII-D DIVERTOR PROGRAM STRATEGY

TOKAMAK DEVELOPMENT PATHS FOR DIVERTOR SOLUTION

CHOSEN PATH:

Power Dispersal and Plasma Cooling

Reduction of Peak Heat Loads and T_e

OTHER PATH:

Special Materials and Special Cooling

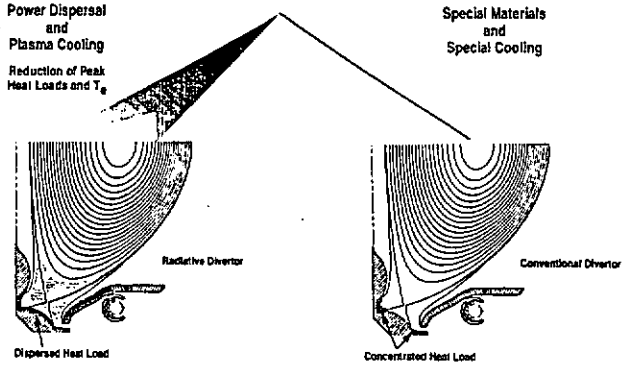

GENERAL ATOMICS

DIII-D CAPABILITIES ALLOW A WIDE RANGE OF RESEARCH AND TECHNOLOGY ISSUES TO BE ADDRESSED

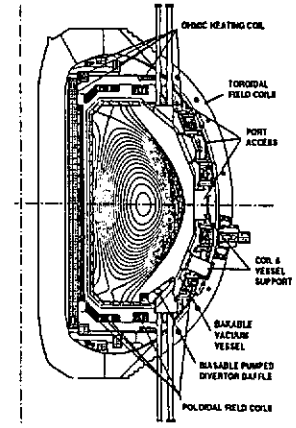

	Present	Proposed
Major radius	1.67 m	
Minor radius	0.67 m	
Maximum toroidal field	2.2 T	
Available OH flux	1.2 V-sec	
Maximum plasma current*	3.0 MA	3.5 MA
Neutral beam power (80 keV)	20 MW	20 MW
RF power (60 GHz)	2 MW	
RF power (110 GHz)		10 MW
RF power (30–120 MHz)	2 MW	8 MW
Current flattop (divertor at 2 MA)	5 sec	10 sec (60 sec at 1 MA)

*Divertor operation; Limiter operation of 3 MA achieved.

GENERAL ATOMICS

THE DIVERTOR PROBLEM

Issue	ITER CDA Problem	Our Line of Solution
High peak heat flux	20MW/m²	Power dispersal via radiation and charge-exchange $q < 3$ MW/m²
	Divertor sweeping (thermal fatigue)	Eliminate
	Braze technology	Lower peak q produces higher reliability and makes lower temperature materials possible
Plate erosion	Localized at strikepoint	Disperse particle flux
	High T_e at plate	Lower with radiation
	Disruption erosion	Use sacrificial material or cushion with radiation
Tritium inventory	Carbon	Lower peak q makes other materials possible
	Steam production from water on high T surfaces	Possible use of helium gas coolant
Large pump ducts	Open, swept geometry neutron leaks	Smaller ducts via neutral pressure buildup

BEST DIII-D PLASMA PERFORMANCE

(6-1-92, not simultaneous)

Average plasma toroidal beta, $\langle\beta_T\rangle$	11%
Central electron temperature, T_e (0)	7 keV
Central ion temperature, T_i (0)	17 keV
Line average electron density, $\bar{n}_e$	1.4×10^{20} m^{-3}
Total plasma energy, W	3.7 MJ
Plasma energy confinement time, τ_E	0.4 seconds (with 4 MW)
Confinement product, $n_e(0)\tau_E$	0.39×10^{20} m^{-3} seconds
Thermonuclear triple product, $n_D(0)T_i(0)\tau_E$	2×10^{20} m^{-3} keV seconds
H-mode duration	10.3 seconds
Peak heat flux on divertor	5.3 MW/m²

GENERAL ATOMICS

D_2 INJECTION WAS EFFECTIVE IN REDUCING HEAT FLUX ON THE DIVERTOR TILES WITH LITTLE DEGRADATION IN PLASMA STORED ENERGY DURING THIS ELMING H-MODE ($\nu_{ELM} \approx 100$ Hz)

D_2 Injection (Solid), Reference Shot (Dashed)

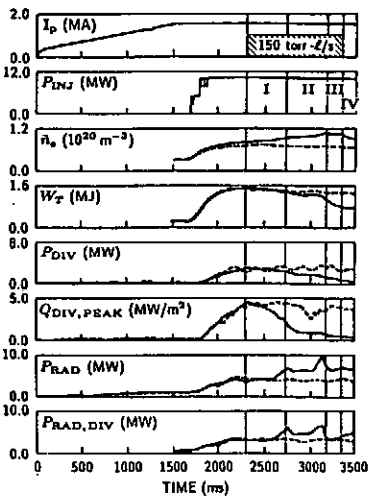

GENERAL ATOMICS

DIII-D DIVERTOR DEVELOPMENT PROGRAM

- Supports ITER and TPX and the divertor needs of machines beyond ITER (DEMO, reactor)
- The ongoing Advanced Divertor Program (ADP) is developing the tools and the database on divertor biasing and pumping for use in future optimized divertor designs
- The proposed Radiative Divertor Program (RDP) will develop a physics solution to the divertor problem of reducing peak heat loads and divertor erosion
- The later Actively Cooled Divertor Program (ACDP) will develop a technology solution to the problem of safe, maintainable, active cooling of a divertor structure

GENERAL ATOMICS

DIII-D LONG RANGE PROGRAM FACILITIES CAPABILITIES

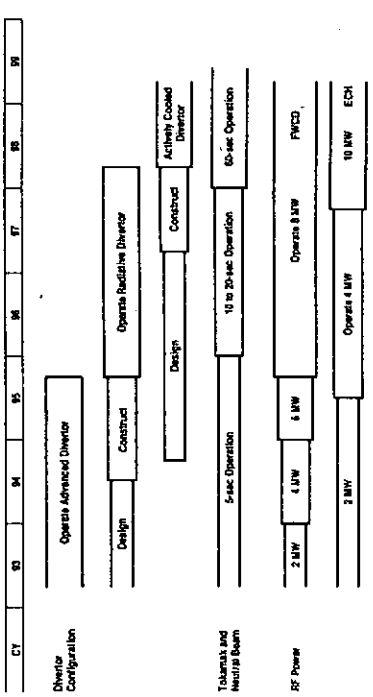

GENERAL ATOMICS

ADVANCED DIVERTOR PROGRAM (ADP)

- Current divertor and first wall
  - Graphite coverage over 31 m^2 (40%) of first wall and divertor
    - Inertial cooling
    - Copper foam metal interface layer (tile to vessel)
  - Open divertor (flat)
  - Biasable toroidal ring electrode
  - Toroidal gas baffle
  - Boronization
- 1993 ADP upgrade
  - 100% graphite tiles on all walls
    - Existing tiles cleaned by B_4C grit blasting
    - Copper foam metal interface layer replaced by Grafoil
  - Cryopump (50,000 ℓ/s capacity) under toroidal gas baffle

GENERAL ATOMICS

ADVANCED DIVERTOR STRUCTURE

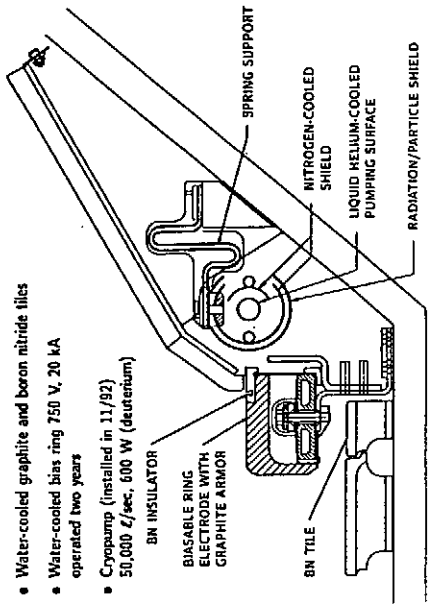

- Water-cooled graphite and boron nitride tiles
- Water-cooled bias ring 750 V, 20 kA operated two years
- Cryopump (installed in 11/92) 50,000 ℓ/sec, 600 W (deuterium)

GENERAL ATOMICS

DIVERTOR PUMPING

ORNL

Large pressure buildup in the pumping plenum

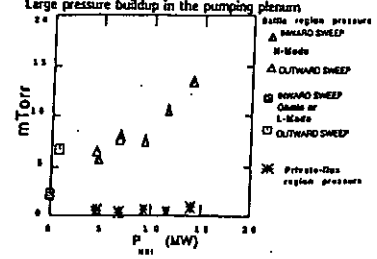

DIVERTOR BIAS

- Principal application: Use of $\vec{E}\times\vec{B}$ drift to guide plasma into pumping ducts
  - Plasma temperature increased with density control
  - Possibility of "electric" sweeping instead of magnetic sweeping
  - Can shift the in-out heat flux asymmetry.

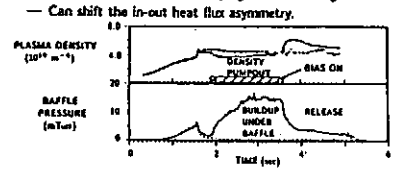

GENERAL ATOMICS

THE RADIATIVE DIVERTOR

- Basic idea is to radiate the power flowing in the divertor channel to a large area of structure
  - Desire nominal <3 MW/m^2
- Features of a radiative divertor
  - Impurity seeded radiation, probably trace high Z noble gases
  - Strong fuel ion flow in the divertor channel to entrain the impurities and hold them near the divertor plate
    - Radiation is from divertor plasma, not the SOL or main plasma
  - Tight fitting mechanical structure around divertor channel to confine neutrals and maximize recycling flux amplification.
  - Possible use of forced recirculating flow to increase fuel flow and entrainment
  - Dissipation of $\geq$90% of the power flow in radiation. The flowing plasma is extinguished in gas.
  - Large volume divertor plasma.
  - Radiation to a large area.
  - Particle flux also spread out. Colder particle flux hitting surfaces.
  - Smaller pumping ducts with high pressure buildup.
  - No divertor sweeping
  - Enhanced helium exhaust opportunities.

GENERAL ATOMICS

PROPOSED RADIATIVE DIVERTOR

Double-null, 17 m^2 divertor surface area,
Operational modes: radiative, ergodized, non-radiative

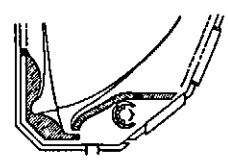

Radiative Divertor Program RDP (10 Second Pulse)	Actively-Cooled Divertor Program ACDP (60 Second Pulse*)
380 MJ/shot	2000 MJ/shot (60 sec)
Inertially cooled Forced convection cooled support	Actively cooled
High conductivity C-C composite used in high heat flux area, remainder is graphite	Bonded graphite tiles
Four point biasing Twelve toroidally biased segments (lower section)	Four point biasing Twelve toroidally biased segments (lower section)

*Material selection (graphite, beryllium, tungsten)

GENERAL ATOMICS

DIII-D RADIATIVE DIVERTOR (TRIANGULAR OPTION)

Equilibrium Properties

$\kappa_a = 2.00$ $\delta = 0.80$
$I_p = 2.0$ MA $B_T = 2.0$ T
$q_{95} = 3.1$ $\beta_T = 4.9\%$

Features

1. Tight baffling, structure conforms to flux surfaces
2. Pumping with cryopumps
3. Large radiating volume with "stubby" divertor
4. Four point divertor biasing
5. Plasma-aided ergodization
6. Shield plasma

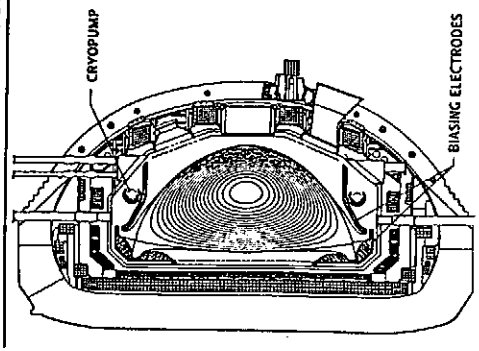

GENERAL ATOMICS

DIII-D RADIATIVE DIVERTOR (SLOT OPTION)

Equilibrium Properties

$\kappa_a = 1.69$ $\delta = 0.32$
$I_p = 1.5$ MA $B_T = 2.0$ T
$q_{95} = 3.0$ $\beta_T = 3.6\%$

Features

1. Slot-like structure to confine neutrals
2. Strike points on outer sections to encourage helium enrichment in the duct
3. Removable center section
4. Pumping of either inboard or outboard legs
5. Biasing possibilities

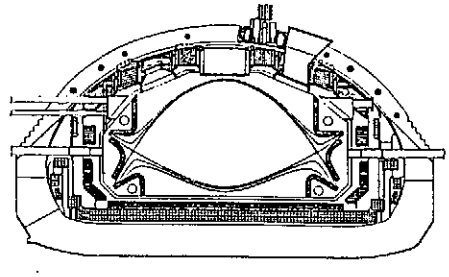

GENERAL ATOMICS

ACTIVELY-COOLED DIVERTOR PROGRAM

- Work with/through ITER technology R&D to develop solutions
  - — Helium cooling to eliminate steam safety issue
  - — Clamped tiles for easy maintenance
  - — Mono-block beryllium to eliminate brazing
  - — Advanced hypervapotrons (water cooling)
  - — Improved graphites
- Design for full power (38 MW) for 60 seconds
- Physics objectives
  - — Revisit the full list of divertor isssues with a divertor whose surface is maintained at a constant temperature
  - — Explore advanced tokamak regimes for times = 2-3 "wall times". Approaches steady state.
- Technology objectives
  - — Demonstrate cooling methodology
  - — Show ability to handle required heat loads for 60 seconds
  - — Show practical tokamak engineering
    - Problem of vast numbers of coolant leads
    - Maintenance of PFC tiles
    - Disruption/halo current survivability
    - Thermal expansion of system

GENERAL ATOMICS

DIII-D ACTIVELY-COOLED ITER DIVERTOR TESTING

Configuration	SN or DN
First wall	Graphite
Divertor	Graphite or Be
Sweeping	Can
Pumping	Yes
Biasing	Yes
Heating power (MW)	38
NBI	20
ECH	10
ICRF	8
Pulse length (sec)	60
R (m)	1.67
Figures of merit	
Power P/R	12-23
Surface area of plasma (m^2)	60
Average P/A leaving plasma (MW/m^2)	0.6
Peak power flux on plate (MW/m^2)	12
Stored energy (MJ)	7
Disruption energy flux (MJ/m^2)	2.5-25 (avg-sample)
Integrated divertor plate test	H gas
Peak heat flux (MW/m^2)	12
Pulse length (sec)	60
Number pulses	750/month
Erosion predicted	~5 microns

GENERAL ATOMICS

DIVERTOR-TARGET EROSION MEASUREMENT

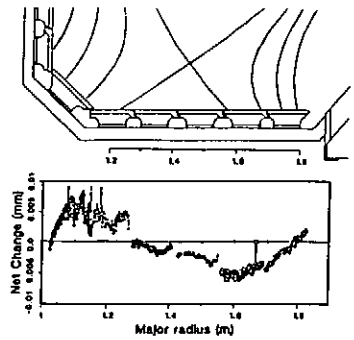

- Surface profile was measured before and after exposure (9 months)
- Startup and rampdown on inner wall, away from divertor
- With 60 second pulses, this fluence could be produced in about two weeks running

  ⇒ Whole new tile assemblies could be erosion tested about one every four months.

GENERAL ATOMICS

THE BEHAVIOR OF THE RADIATIVE DIVERTOR WILL INFLUENCE THE SELECTION OF FUTURE DIVERTOR MATERIALS

- Lower peak heat flux
  - — Use of lower melting temperature materials (beryllium)
- High density, low temperature plasma in the divertor region
  - — Lower sputtering (carbon, beryllium, tungsten)
- Bias sustained plasma shielding
  - — Use of high atomic number materials (W)

GENERAL ATOMICS

DIMES SYSTEM DESIGN AND 1993 EXPERIMENTAL PLAN

PRESENTED BY: C. WONG

JAPAN/U.S. WORKSHOP P196
ON
HIGH HEAT FLUX COMPONENTS AND
PLASMA SURFACE INTERACTIONS FOR
NEXT DEVICES

NOVEMBER 17–19, 1992
KYUSHU UNIVERSITY
FUKUOKA, JAPAN

Paper 3-1 # 2 - Abstract - Nov. 1992

DIMES System Design and 1993 Experimental Plan

Presented by Clement Wong - General Atomics - U.S.A.

The Divertor Materials Evaluation System (DIMES) program is evolving from the phase of building the sample changer mechanism to the phase of doing experiments. The sample changer operation was successfully tested in late October 1992. While operating in high vacuum, a DIMES sample can be delivered from the pit of the DIII-D machine to the bottom divertor of the machine in ~ 3 minutes. Sample exposure experiments will be performed in Feb. of 1993 when DIII-D is operational after the present venting period. Samples can be changed overnight. This schedule is controlled by the required pump down time of about 6 hours for the DIMES system.

Different DIMES samples have been prepared by SNL-L. These include, ATJ graphite reference sample, ATJ graphite with buried Si marker, ATJ graphite with protrusion, (i.e, shaped surface in order to enhance the reception of surface power) and ATJ graphite with Si insert. B_4C coated Russian graphite sample is also available.

In coordination with the operational schedule and practice of DIII-D, two groups of experiment will be performed in CY93. They are the erosion/redeposition, and disruption experiments. Modeling results obtained by ANL indicates that ~ 100 nm of erosion can be obtained from Si from one high power plasma shot. This is larger than the 10 nm thickness change that can be measured by RBS. Similarly, a well placed disruption on shaped sample can deliver an energy density of 1 - 10 MJ/m^2 which is in the range of 3-12 MJ/m^2 as specified in the ITER-CDA design.

DIMES PROGRAM
KEY COLLABORATORS AND STRUCTURE

• Sample supply and control, material characterization, in-situ measurement, planning	R. Bastasz, SNL-L
• Advanced diagnostics	D. Buchenauer, SNL-L
• Erosion/redeposite modeling	J. Brooks, T. Hua, ANL
• Disruption modeling	D. Ehst, A. Hassanein, ANL
• Disruption simulation	J. Gahl, UNM, J. Gilligan, NCSU
• Solid target boronization	Y. Hirooka, UCLA
• Russian sample materials and coatings	O. Buzhinskij, Troitzk; I. Mazul, Efremov
• DIMES experiment coordination	C. Wong, GA (acting)
• Mechanical design	R. Junge, T. Colleraine, GA
• Diagnostics	P. West, GA; D. Hill, LLNL
• DIII-D support	A. Kellman, J. Luxon, T. Petrie, and others, GA
• FUNDED BY	U.S. DOE/OFE, M. COHEN

DIMES
(DIVERTOR MATERIAL EVALUATION SYSTEM)

- A material sample changer mechanism that allows the exposure of instrumented material sample from one to a few shots in DIII-D* and overnight sample changeout.
- Relevant ITER concerns on material net erosion, tritium retention, disruptions, and material transport will be addressed.
- Ex-situ measurement techniques are available; in-situ measurement capabilities are being developed.

*Can be exposed to a single discharge or a series of discharges under selected plasma conditions at the DIII-D bottom divertor.

DIII-D ELEVATION AT 150°

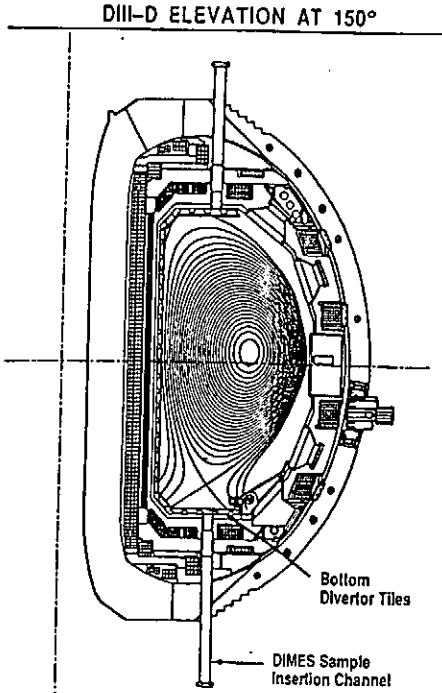

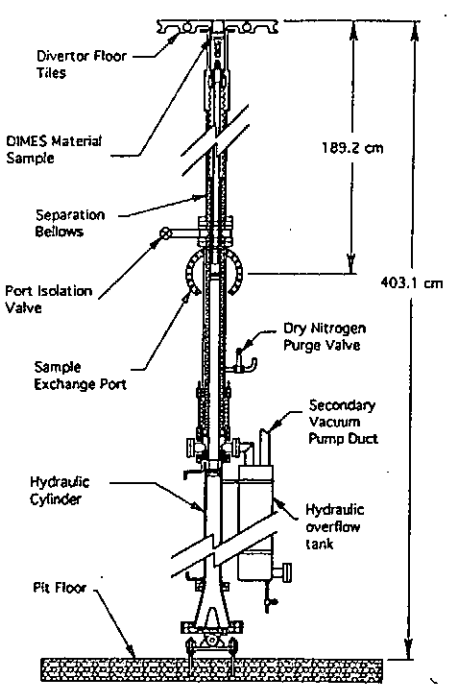

DIMES Mechanical System

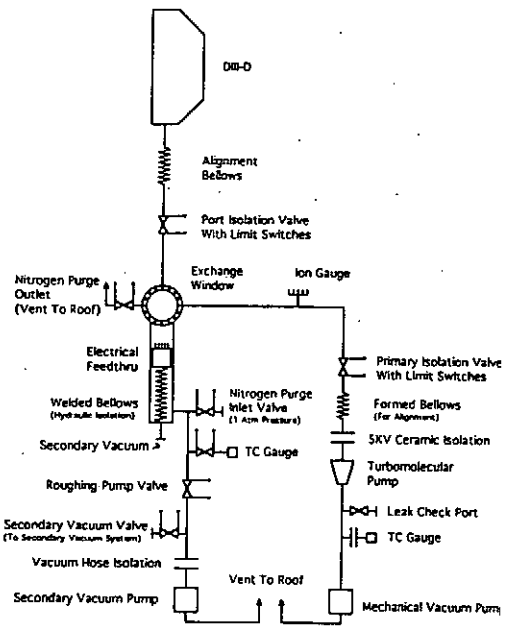

DIMES PRIMARY VACUUM P&ID

DIMES SAMPLE CHANGER SYSTEM SCHEDULE

Hydraulic Cylinder Operation Testing	Completed
DIMES Mechanical System	Installed
Testing	
Mechanical	Completed
Vacuum	Completed
Tile Alignment	11/16/92
Control System	
Design	Completed
Installed	By 12/4/92
Diagnostic Wiring	
Internal	Completed
External	Need to Design
DIMES Hydraulic System	Completed

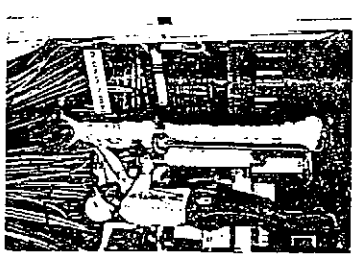

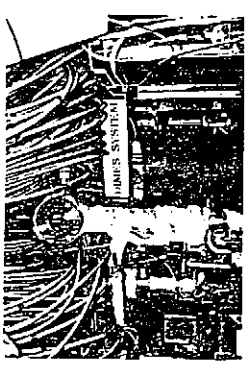

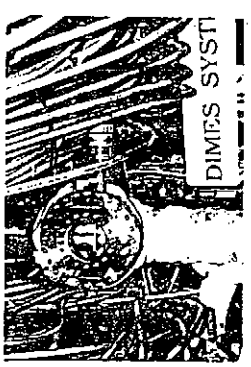

DIMES FY1993 PROGRAM SCHEDULE

- Sample changer operational in vacuum 10/23/92
- 1993 experiments coordination workshop at GA 10/29/92
- First short exposure experiment 2/93

1993 EXPERIMENTS OBJECTIVES (IN COORDINATION WITH THE 9 to 12 WEEK RUN PERIOD OF DIII-D)

Perform:

- Erosion/redeposition experiments on different sample and coating materials.
- Disruption experiments.
- Particle energy characterization experiments.

DIMES SAMPLE DIII-D OPERATIONAL REQUIREMENTS

- Exposed material to be examined and approved by DIII-D Vacuum Committee
- Samples must outgas less than 10^{-7} Torr-ℓ/sec in 10^{-6} Torr vacuum
- Samples must be outgassed at 1000°C for 2 hr before exposure

DIMES SAMPLE CHANGER OPERATIONAL CHARACTERISTICS

- Sample changeout is overnight
- 6 hr pumpdown time after sample changeout (possibly shorter)
- In-situ temperature up to 350°C
- Minimum exposure one shot

Experiments can be performed as passive, piggy-back, or dedicated runtime experiments

DIMES DIAGNOSTIC WIRE CAPABILITIES

10 DIAGNOSTIC WIRES TOTAL (SHIELDED)

- 2 wires for type E thermocouple
- 2 wires for 20 gauge (5 amp/500 V DC, 8 sec max)
- 6 wires 24 gauge (2 amp/500 V DC, 8 sec max)

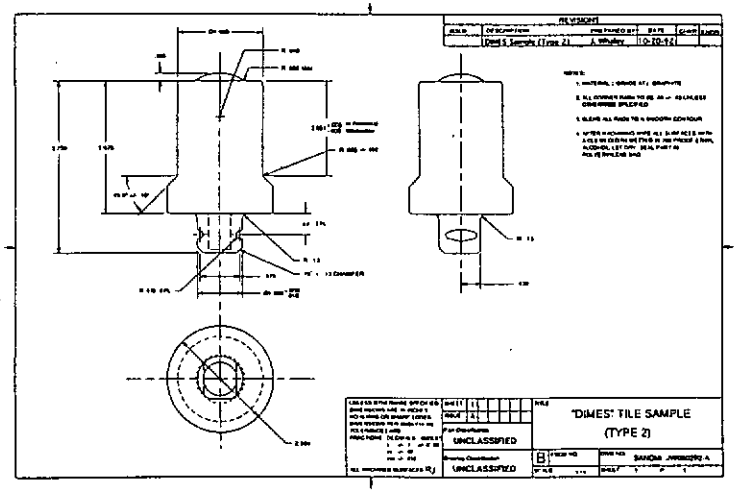

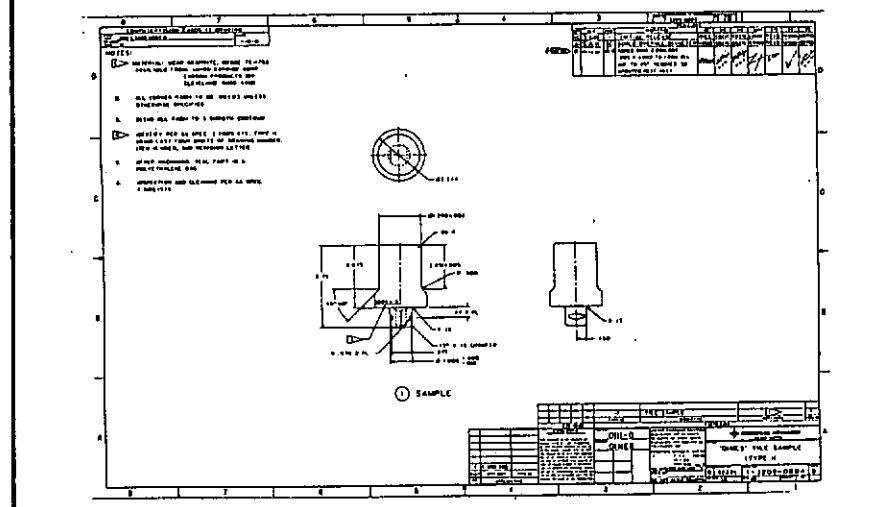

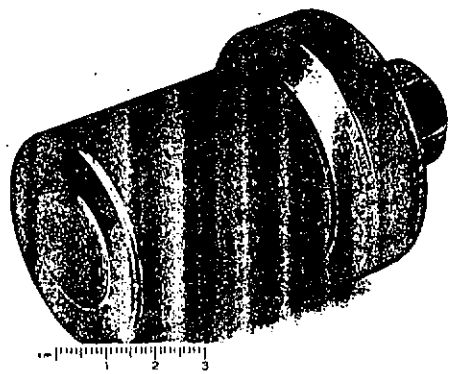

GENERAL ATOMICS

Available DIMES samples

- Standard sample: ATJ graphite.
- Erosion/deposition sample: ATJ graphite with buried Si marker.
- Disruption sample: ATJ graphite with protrusion.
- Particle collector sample: ATJ graphite with insert.
- B_4C coated graphite samples from Russia

More Surface Analysis Techniques

- Nuclear Reaction Analysis (NRA)

  10^{-1} monolayer sensitivity for various low Z elements (e.g., H, D). Effective probe depth is 10–1000 nm. Depth profiling possible via energy loss measurements.

- Secondary Ion Mass Spectrometry (SIMS)

  10^{-5} monolayer sensitivity for most elements. Effective probe depth is about 1 nm. Depth profiling possible with ion beam sputtering.

- Low-Energy Ion Scattering (LEIS)

  10^{-4} monolayer sensitivity for most elements. Effective probe depth is one atom layer.

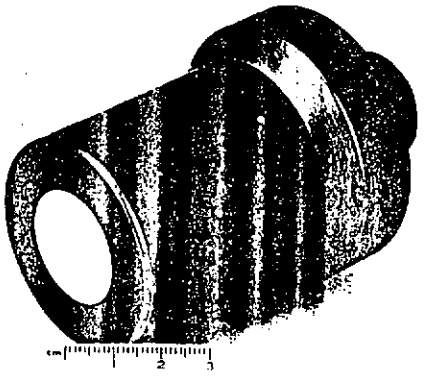

EROSION AND REDEPOSITION EXPERIMENT SENSITIVITY

- Rutherford backscattering spectrometry on Si implant can measure change of ~10 nm.
- Estimated erosion on Si surface from DIII-D plasma is ~10 nm.
- We will have to put the plasma separatrix intersection on the DIMES sample surface.

Surface Analysis Techniques

- Auger Electron Spectroscopy (AES)

  10^{-1} monolayer sensitivity for elements with Z>3. Effective probe depth is about 2 nm. Depth profiling possible with ion beam sputtering.

- Scanning Electron Microscopy – Energy Dispersive X-Ray analysis (SEM–EDX)

  Surface imaging with element identifcation for Z>10. Effective probe depth is about 1000 nm.

- Rutherford Backscattering Spectrometry (RBS)

  $10 - 10^{-4}$ monolayer sensitivity for elements with Z>2. Effective probe depth is about 10 nm. Depth profiling possible from energy loss measurements.

GENERAL ATOMICS

DIII-D ADVANCED DIVERTOR FLEXIBILITY

GENERAL ATOMICS

DIII-D CAPABILITIES ALLOW A WIDE RANGE OF RESEARCH AND TECHNOLOGY ISSUES TO BE ADDRESSED

	Present	Proposed
Major radius	1.67 m	
Minor radius	0.67 m	
Maximum toroidal field	2.2 T	
Available OH flux	12 V-sec	
Maximum plasma current*	3.0 MA	3.5 MA
Neutral beam power (80 keV)	20 MW	28 MW
RF power (60 GHz)	2 MW	
RF power (110 GHz)		10 MW
RF power (30–120 MHz)	2 MW	8 MW
Current flattop (divertor at 2 MA)	5 sec	10 sec (60 sec at 1 MA)

* Divertor operation; Limiter operation of 3 MA achieved.

GENERAL ATOMICS

BEST DIII-D PLASMA PERFORMANCE

(6-1-92, not simultaneous)

Average plasma toroidal beta, $\langle\beta_T\rangle$	11%
Central electron temperature, T_e (0)	7 keV
Central ion temperature, T_i (0)	17 keV
Line average electron density, $\bar{n}_e$	1.4×10^{20} m^{-3}
Total plasma energy, W	3.7 MJ
Plasma energy confinement time, τ_E	0.4 seconds (with 4 MW)
Confinement product, $n_e(0)\tau_E$	0.39×10^{20} m^{-3} seconds
Thermonuclear triple product, $n_D(0)T_i(0)\tau_E$	2×10^{20} m^{-3} keV seconds
H-mode duration	10.3 seconds

DISRUPTION EXPERIMENTS WITH DIMES

1. Study of disruption effects on materials from a diverted plasma

   Needs:

   - Control of induced disruption events
   - Characterization of disrupted plasma, vapor shield
   - Characterization of material surface before and after disruption
   - Modeling

2. Characterization of disrupted plasma as inputs for disruption simulation experiments.

GENERAL ATOMICS

MAJOR DISRUPTION

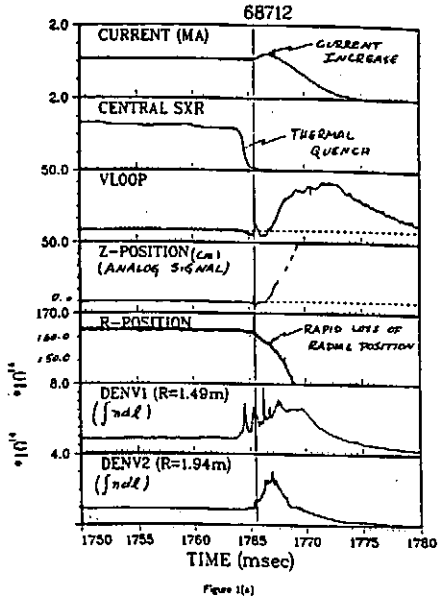

Figure 1(a)

TYPICAL DIII-D PARAMETERS

	Normal	Disruption
I_p	1 to 3 MA	—
Gas	D2, He	—
Paux	0 to 20 MW	—
n_e	10^{13} to 10^{14} cm^{-3}	10^{13} to 5×10^{14}
T_e	1 to 5 keV	5 to 100 eV
T_i	1 to 17 keV	?
W	1 to 4 MJ	—
SOL current	<5 kA	<0.2 I_p (600 kA)
Power/Area (divertor)	1 to 6 MW/m^2	—
Energy/Area (divertor)	—	0.1 to 1 MJ/m^2
— with elevated DIMES		1 to 10 MJ/m^2
Field line angle	1 to 5 deg	?
Current decay time		>4 msec
Thermal quench time		>0.2 msec
n_e (SOL)	10^{13} to mid 10^{14} cm^{-3}	
T_e (SOL)	10 to 70 eV	

(ITER CDA has energy density of 3 to 12 MJ/m^2)

GENERAL ATOMICS

EXTENSIVE EDGE DIAGNOSTICS ON DIII-D

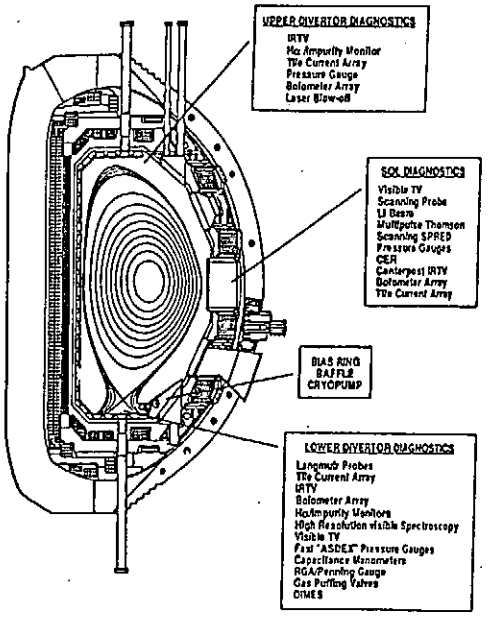

DIMES SCHEDULE

Nov. to Dec. 1992	Complete DIMES changer details
Nov. 1992 to Jan. 1993	Practice sample exchange
	Prepare diagnostics, CCD, and optical spectroscopy
	Initiate net erosion calculation
	Initiate disruption calculation
Nov. 1992 to May 1993	Preparation of special disruption samples
2nd week of Jan. 1993	DIMES experiments preparation meeting
Feb. to Sept. 1993	Perform boronization, erosion, and disruption experiments in coordination with DIII-D operation and experimental plan

DEUTERIUM RETENTION IN TFTR

M. Caorlin, M. Ulrickson

Princeton University Plasma Physics Laboratory,
James Forrestal Campus,
PO Box 451, Princeton, NJ 08543, USA.

ABSTRACT

The Tokamak Fusion Test Reactor is scheduled to begin operation with deuterium and tritium plasmas in 1993. Stringent tritium inventory limits will affect the machine operation. Tritium in-vessel retention is one key parameter in determining operational schedule and procedure. In particular, tritium retention will have to be periodically monitored and cleanup intervals will have to be interspersed with normal machine operation.

The current knowledge on deuterium and tritium retention in TFTR is based on several years of operation with deuterium plasmas and on laboratory tests carried out at SNL with TFTR material components. This body of information is summarized here and retention estimates are given. Deuterium is mainly retained in a thick codeposition layer on the bumper limiter tiles. The average retention scales linearly with the deuterium (or tritium) fuelling and increases with the average neutral beam power. An average deuterium retention factor of 0.44 ± 0.15 has been determined for beam-fuelled discharges over a five year period.

Removal of the codeposited layer by means of He/O glow discharges is also addressed.

Implications for the D-T phase are discussed and suggestions for near future work are outlined.

DEUTERIUM RETENTION IN TFTR

by
M. Caorlin, M. Ulrickson

Princeton University Plasma Physics Laboratory

PSI/HHF Japan-US Workshop P196,
Kyushu University, Fukuoka,
November 17-19, 1992.

CONTENT

1. INTRODUCTION

- TFTR tritium inventory limits (5 g on-site, 2.5 g stored, 1 g in-vessel).
- Tritium in-vessel retention affects
  1. Tritium input (number of shots)
  2. Tritium cleanup frequency and duration

⇓

NEED TO *PREDICT* TRITIUM RETENTION.

2. RETAINED DEUTERIUM DISTRIBUTION IN TFTR.

- Codeposited layer on tiles mainly
- Average buildup rate is 40 Å/shot
- Four-year average: wall 32 %, BL tiles surface 49 %, gaps between BL tiles 19 %
- Poloidal and toroidal distribution

3. LONG-TERM D RETENTION IN TFTR.

- Retention scales linearly with deuterium input.
- Long- vs short-term retention; short-term matters for weekly predictions prior to DT phase.
- Long-term average retention factor is 0.44 ± 0.15.
- Modelling needs short-term retention data.
- No data available for TFTR short-term retention.

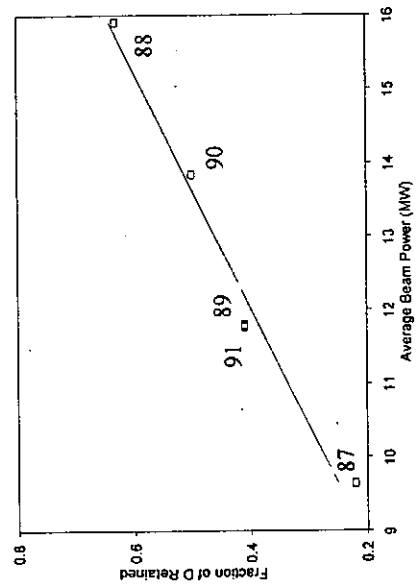

4. RETAINED TRITIUM CLEANUP.

- He/O GDC is the preferred choice to remove the codeposited layer
- Lab tests show He/O GDC gets into gaps
- Measured removal rate is 0.2 Å/s
- Attempted (24 hours) in TFTR
- Drawbacks:
  1. impurity production requires boronization
  2. requires time and resources
  3. side-effects? (e.g. internal hardware)

5. IMPLICATION FOR THE D-T PHASE.

- DT Plan (under revision) requires a total input of 12.4 g T_2
- Total tritium retention would be 5.5 g if no cleanup is performed
- At least 5 cleanups required
- Reasonably short (1-3 days each time) cleanup periods anticipated

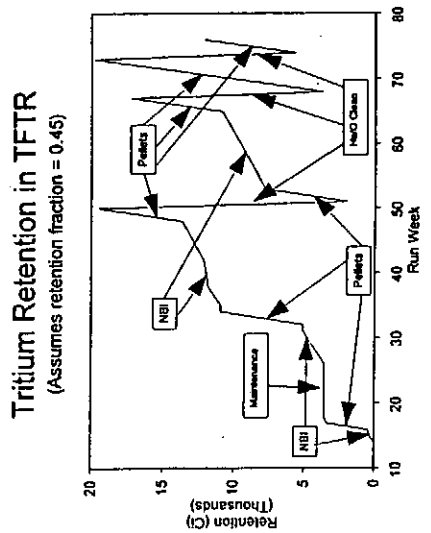

6. FUTURE WORK.

Near future

- Longer *in-situ* He/O cleanup test (5 days)
- *MEASURE* short-term retention, w/o tritium and check cleanup
- Check retention data in trace-tritium experiments

8

7. SUMMARY.

- Deuterium is codeposited on BL tiles mainly
- Non-uniform distribution
- Long-term deuterium average retention factor is 0.44 ± 0.15
- Cleanup periods required to comply with inventory limits
- Cleanup by He/O GDC is current choice

9

Preparation for DT Operation on TFTR

M. Ulrickson
Princeton University

Presented at the US-Japan Workshop
on
High Heat Flux Components
and
Plasma Surface Interactions
held at
Kyushu University
November 17-19, 1992

- Tritium Inventory Management
- Tritium Delivery System
- Tritium Processing

Tritium Inventory Management

- The tritium inventory in the TFTR vacuum vessel must be controlled because of limits on the allowed inventory (see M. Caorlin's talk).
- HeO GDC is the preferred method for T inventory management.
- HeO cleaning has been performed on TFTR.
- Approximately half of the Oxygen used during HeO cleaning is trapped in the torus after the cleaning.
- Significant amounts of elemental H,D are released during HeO cleaning.
- Boronization is required after HeO cleaning to obtain high performance plasmas.
- Approximately 4 HeO cleaning cycles will be required during the TFTR DT run.

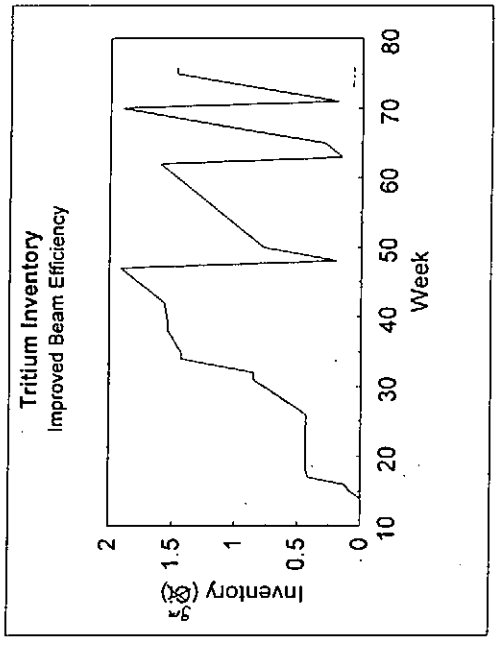

I. Helium/Oxygen Glow Cleaning

- Species Observed

  Hydrogen isotopes (D, HD)

  Water (H_2O, HDO, D_2O)

  Formaldehyde (COD_2)

  Boric Acid (DBO_2)

  Carbon Monoxide (CO)

  Carbon Dioxide (CO_2)

  Oxygen and Helium

- Changes in the yield of various species during the glow

  Deuterium containing species decreased to about 1/2 to 1/4 of the initial values

  Oxygen containing species remained nearly constant (< 20% change)

  Hydrogen partial pressures decreased to about 1/3 of the initial values

Changes During He/O Cleaning

Mass	Partial Pressure Start	End	Ratio
2	1.0E-08	4.0E-09	0.40
3	2.5E-08	6.0E-09	0.24
4	1.1E-05	9.0E-06	0.86
12	2.2E-08	1.8E-08	0.82
14	3.0E-09	2.1E-09	0.70
16	1.5E-07	1.2E-07	0.80
17	2.9E-09	9.0E-10	0.31
18	1.3E-08	3.3E-09	0.25
19	1.6E-08	4.1E-09	0.26
20	2.6E-08	4.9E-09	0.19
22	1.5E-09	8.5E-10	0.57
28	2.1E-07	1.7E-07	0.81
29	2.8E-09	2.0E-09	0.71
30	1.3E-09	7.5E-10	0.58
32	6.5E-07	5.7E-07	0.88
33	5.7E-10	4.9E-10	0.86
34	2.8E-09	2.6E-09	0.93
44	1.5E-07	8.0E-08	0.53
45	1.8E-09	1.2E-09	0.67

Duration 8.3×10^4 s

Correction of the RGA Data to Get Total Amounts of Gas Generated

The total amount of a particular gas species generated during the He/O cleaning is found from

$$Q_i = R_i \, S_i \int P_i \, dt$$

where

R_i = the ratio of the actual pressure to the RGA pressure for mass i

S_i = the pumping speed for mass i

P_i = the partial pressure of mass i

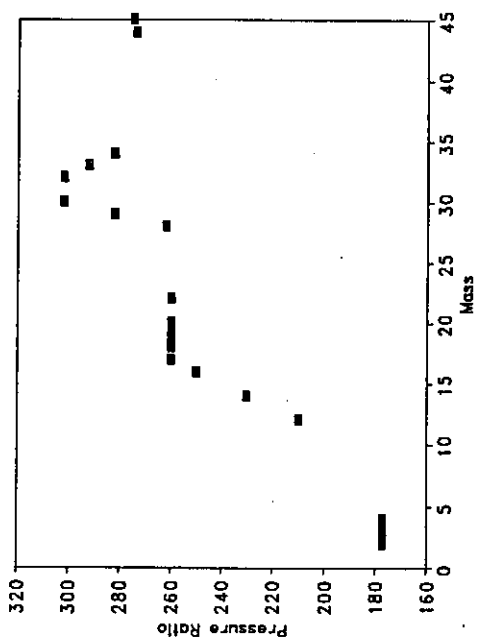

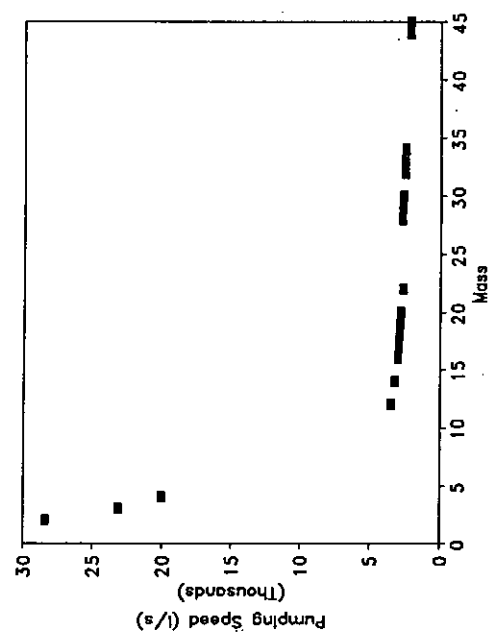

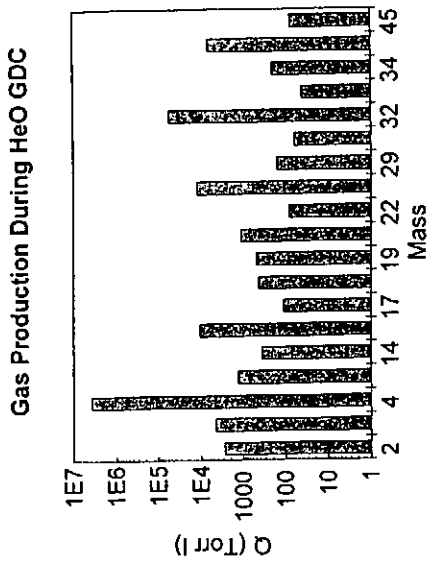

- The Total Amount of Gas Produced

  Integrated the partial pressures of various species from the RGA. $\int P dt$

  Corrected for the pressure ratio due to the differential pumping (Dylla, Blanchard, et.al.) $\mathcal{R}$

  Multiplied by pressure corrected pumping speed for the various species. S

  RESULT:

  3.96 x 10^4 Torr-l of gas were pumped

  3.70 x 10^4 Torr-l was Helium

  1.90 x 10^1 Torr-l was Oxygen

  INPUT:

  3.80 x 10^4 Torr-l of He/O mixture

  Input gas was 10% Oxygen

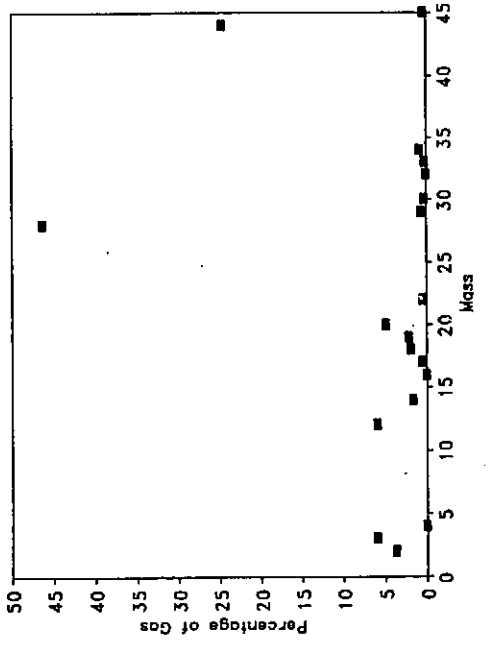

Tritium Delivery System

- The TFTR tritium delivery system consists of uranium beds for storage of T, T gas lines to the torus, NBI, and pellet injector, and gas storage tanks for the used gas.
- The tritium systems are currently in the middle of the required safety reviews.
- Testing of the system with 1000 Ci should begin soon.

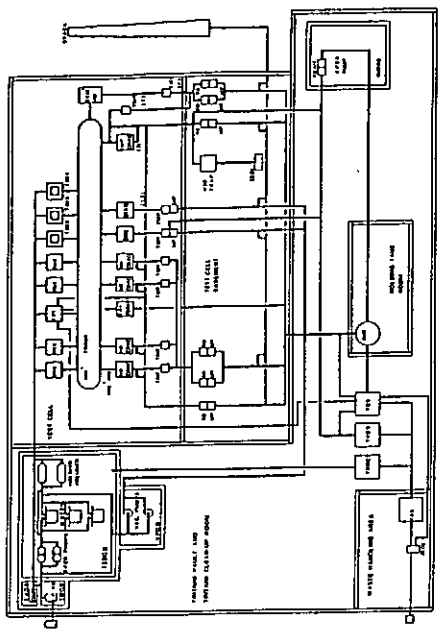

TRITIUM FLOW THROUGH TFTR
FIGURE 8.1

8-3

D-T Plan
Sept. '91

Tritium Processing System

- A low inventory DT reprocessing system is being designed for TFTR.
- This system will permit on-site reprocessing of DT mixtures and reduce the amount of tritium contaminated waste generated.
- The system was developed by the Canadian Fusion Fuels Technology Program (CFFTP).
- The processing system will not be available until CY94.

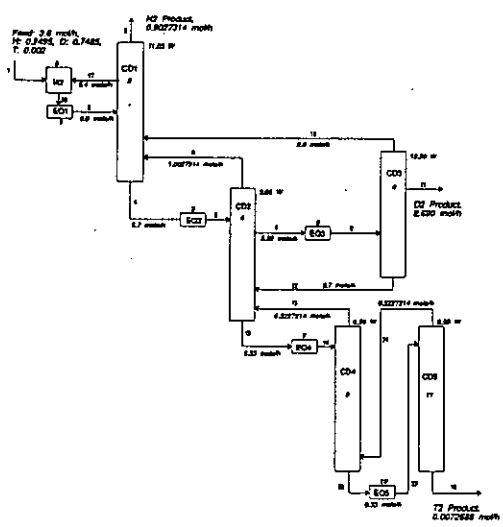

Figure-5: CD Cascade Parameters for Reference Case

22

SUMMARY OF TPS TRITIUM INVENTORY

EQUIPMENT	DESCRIPTION	TRITIUM INVENTORY (Ci)
UB1, UB2, UB3	URANIUM BEDS	1650
A01	GUARD ABSORBER	175
PIPING, VALVES, EXCHANGERS	--	23
TOTAL		1848
CD1	CRYO-DISTILLATION UNIT 1	189
CD2	CRYO-DISTILLATION UNIT 2	682
CD3	CRYO-DISTILLATION UNIT 3	227
CD4	CRYO-DISTILLATION UNIT 4	829
CD5	CRYO-DISTILLATION UNIT 5	2404
PUMPS, EQUILIBRATORS, PIPING	--	233
TOTAL CD		4564
TOTAL ESTIMATED INVENTORY		6412

The estimated inventory in the TPS is shown in Table 5.

TABLE 5

SUMMARY OF TPS TRITIUM INVENTORY

Equipment	Description	Tritium Inventory, Ci
UB1,UB2,UB3	U-Beds (Total of 3)	1650
AD1	Guard Adsorber	175
Piping, Valves, Exchangers in FTS	--	23
Total FTS Inventory		1848 Ci
CD1	CD Column 1	189
CD2	CD Column 2	682
CD3	CD Column 3	227
CD4	CD Column 4	829
CD5	CD Column 5	2404
Pumps, Equilibrators, Piping Valves in CD System	--	233
Total CD Inventory		4564 Ci
Total TPS Estimated Inventory		**6412 Ci**

Cryogenic Refrigeration Units

Four Cryomech cryogenic refrigeration units provide the necessary refrigeration to the five condensers of the CD columns. The Cryomech cryogenic refrigeration unit is a two stage Gifford McMahon (G-M) Cycle Refrigerator. It consists of a cold head and a helium compressor system which supplies clean compressed helium (free of oil, moisture and other gaseous contaminants) at room temperature to the cold head via stainless steel flexible lines. The cold head achieves the low temperatures in the G-M cycle by expanding the high pressure helium to low pressure. This is repeated several times a minute by the action of the rotary valve,

Table-2: Cryogenic Distillation System Parameters

Parameter	CD1	CD2	CD3	CD4	CD5
NTP	100	60	100	25	25
HETP, cm	2.50	2.50	2.50	10.00	10.00
Column ID, cm	2.00	1.20	2.00	0.23	0.23
Column Height, cm	250	150	250	250	250
Pressure, kPa	120	120	125	120	120
Condenser Temperature, K	21.01	24.26	24.41	24.36	25.17
Reboiler Temperature, K	24.27	24.39	24.44	25.19	25.63
Condenser Duty, W	11.03	3.06	13.50	0.50	0.50
Feed Stage(s)	40, 45, 50	20, 46, 58	85	2,24	2
Product Stage(s)	1, 42, 100	1, 15, 50	1, 2, 100	1, 25	1,25

The parameters for the Reference Case, including all the internal flows in the cascade are shown in Figure 5. Similarly, the parameters for the cascade for the Performance Test are shown in Figure 6.

The entire cascade operates in a recycle mode, which is highly advantageous as compared to a cascade (such as the TSTA ISS) with no recycles. Recycles allow concentration profiles to establish themselves naturally throughout the cascade, thus eliminating the need for a complex startup sequence. Furthermore, if normal operation becomes disrupted, feeds and drawoffs can be temporarily suspended until concentration profiles become re-established by normal system reflux. In addition, appropriate valves and connections are provided so that if the feed gas is not available for a temporary period, the product gases can be combined and recycled to the front of the cascade, allowing the entire CD system to be operated in a closed loop. This mode of operation has the advantage that it allows tritium concentration profiles and inventories to be essentially maintained at close to normal values, thus allowing for an immediate resumption of operation upon commencement of normal feed flows. This arrangement also facilitates startup, commissioning and performance testing.

The TFTR CD cascade has five equilibrators, one for the main feed stream to each column. The purpose of the equilibrators is to promote the breakdown of the intermediate species HD, HT, and DT

impurities would freeze out at the operating temperatures of 20-25K in the CD, and would impair or block its operation. Therefore, the Feed Treatment System (FTS) is designed to separate hydrogen isotopes from the inert gas and impurities, and ensure a high degree of recovery.

The FTS is based on once-through purification concept (11,12,13) using a proven and tested Uranium Bed design, is adequately safe (14) and consistent with TFTR operating systems.

The feed gas is withdrawn from the 7 m^3 tank using a metal-bellows pump and sent to the U-Bed system. A Normetex pump is provided in series to be used for evacuating the large tank if feed gas is not available temporarily.

Three Uranium beds (Figure 2) in parallel form the heart of the system. Each U-Bed has 5 kg of uranium metal and is of a design used presently on a Gas Chromatographic System being supplied to KfK in Germany. The KfK beds have been completed and have passed rigorous performance tests at Ontario Hydro research. Each U-Bed is provided with integral inlet and outlet sintered metal filters, heaters and a vacuum jacket. One U-Bed is capable of separating and storing hydrogen isotopes equivalent to 3 hours of feed gas flow (3.59 * 3 * 2 * 238/1.025 = 5000 g U). Therefore, a 3-bed system allows 6 hours for warming up and recovering hydrogen isotopes. Active gas impurities such as water and oxygen will be irreversibly absorbed on uranium (water will decompose releasing hydrogen). Methane and argon will carry through and will be discharged to the TFTR Exhaust Gas Detritiation System. If methane removal is desired on occasion, this can be accomplished by removing hydrogen isotopes from the system on closed loop, and then circulating the inert gas through the U-Beds heated to
400° C.

Each U-Bed is designed to be loaded to a ratio of $UQ_{1.025}$ (where Q represents H,D or T). This is 1/3 of stoichiometric loading, and at this loading it is expected that the exit gas from the U-Bed will contain about 10 to 100 mCi/m^3 which is well within the effluent specification. A tritium monitor is provided at U-Bed outlet to switch beds once the exit concentration reaches a pre-determined value. Integral, redundant heaters are provided within secondary containment of the U-Beds to heat up the beds for hydrogen isotope recovery. An evacuation and helium backfill connection is also provided. During loading and heat-up, the secondary containment is maintained under vacuum.

In order to maintain a steady feed flow to the CD system, each U-Bed is unloaded over a 3 hour period. After 3 hours, the next U-Bed is brought on-line. A flow controller is used to hold the feed flowrate relatively constant. During the initial heating up period, a pressure switch is used to turn on a vacuum pump which is used to draw-off the isotopes. Once the unloading temperature of 400° C is attained, this pump is

3.0 DESIGN DESCRIPTION

3.1 Available Options, Proposed System

FTS Options

In general a number of FTS options are available. Most options were summarized in (6). In addition at least three versions were designed for full sized ITER and NET applications (7), (8) and (9). These have been designed for steady state long term operation of large machines and with the exception of the TSTA system (10), none has been demonstrated.
For the TFTR feed treatment system the emphasis was on proposing a process which is simple, proven, and has low tritium inventory. The TFTR overall operating time is not expected to make the gettering material consumption prohibitive. The impurities in the feed are within 3 * (1~10) = 15 ppm and this is considered acceptable.

Isotope Separation Options

For the isotope separation system the GasChromatographic (GC) hydrogen isotope separation and the Cryogenic Distillation (CD) options were considered.

There are two basic versions of the GC process, namely the carrier gas free GC which has apparently been industrially proven, but this technology is not on the open commercial market. CFFTP is about to build an experimental facility for this concept, however, this technology would not be available in time to be of interest to TFTR. The Helium carrier gas based system would have to be, in terms of total hydrogen gas throughput is 28 times larger and in terms of tritium product flow equal to the unit presently supplied to KfK (see Appendix III). This concept was rejected for the TFTR application because:

a) It would be too large for the available space at TFTR
b) Its tritium inventory, based only on the batch processing time which is in the order of 140 hours, could reach 140 * 3.6 * 0.002 * 60,000 = 60,480 Ci for the reference case 2.2.2.

Cryogenic Distillation (CD) is a proven process and mainly due to the CFFTP development meets the PPPL requirements and consequently is selected.

3.2 Feed Treatment System (FTS) Figure 1.

Feed gas for the CD is available at conditions specified under 2.2.1. Before this gas can be fed to the cryogenic distillation system, all impurities except helium must be removed from the hydrogen isotopes to a very low concentration. Otherwise, the

switched off and unloading continues. As the bed gets progressively unloaded and the hydrogen overpressure reduces, the vacuum booster pump is brought on-line again to complete the unloading phase.

Just prior to regeneration, The U-Bed is isolated and evacuated to remove any free gas. Upon regeneration of a U-Bed, hydrogen isotopes which are essentially pure are liberated. A heat exchanger, to cool the isotopes is followed by the U-Bed regeneration pumps to transfer the isotopes to the Cryogenic Distillation system. However, to remove trace impurities of active gases, a cryogenic adsorber AD1 is provided. This contains a small quantity of molecular sieve and is maintained at a temperature of about 77K by a small flow of liquid nitrogen. If LN_2 is not readily available in the laboratory, the use of an alternative electrically powered refrigeration unit will be investigated during project implementation.

In order to complete the cooldown of a U-Bed within the available period of 3 hours, a slow purge of helium is used through the secondary containment to remove heat from the bed. A small blower, located outside the glovebox, is used for helium circulation in a common circuit to all three U-Beds. A finned-tube heat exchanger outside the glovebox is used to dissipate heat to the room. In this manner, overloading of the glovebox with heat is prevented. In addition, the cooldown time can be significantly reduced in comparison to cooling by natural convection.

The maximum inventory in the FTS is estimated as equivalent to about 3 hours of feed flow, or about 1243 Ci (Figure 3). This inventory can be completely unloaded during a shutdown of the CD.

3.3 Cryogenic Distillation System (CD) Figure 4.

Due to the proprietary nature of the CD4, the **design parameters** for the conventional version of this column are used in the design description of the CD in the following paragraph, namely in the table "Distillation System Design". All other parts of the description equally apply to both the **conventional** and the **proposed** options. The design of the "advanced" and proprietary distillation column will be disclosed to the TFTR personal subject to signing a non disclosure agreement.

The CD system consists of 4 inter-linked columns and has been optimised to meet the TFTR design requirements, while minimizing the tritium inventory. The design has been carried out using Ontario Hydro's FLOSHEET simulator (15) which uses rigorous models to perform process calculations for hydrogen isotope systems. The FLOSHEET simulation results are attached in Appendix II. The cascade is schematically shown in Figure 5 and the corresponding Mass Balance data are in tables in Appendix III (basic case).

The CD columns are operated in the temperature range of about 20-25K. For this reason they are located within a cold box which is held at a pressure of about 10^{-6} torr. The columns are wrapped in many layers of aluminized mylar super-insulation.

Inter-column flows are maintained by Metal-Bellows model MB-111 doubly contained pumps. These pumps are located within a glovebox placed adjacent to the CD cold-box. Catalytic equilibrators are also placed within the same glovebox. In order to minimize heat leakage into the cold-box the lines going out to the glovebox exchange heat with the return lines into the cold-box.

The design calculations for the cascade are based on the performance of conventional columns filled with Helipak-B random packing. The performance of the Helipak-B packing for hydrogen distillation has recently been evaluated at Ontario Hydro Research Division (OHRD). When operated with a superficial vapour velocity of 6.0 cm/s, the Helipak-B packing Height Equivalent to a Theoretical Plate (HETP) is 2.5 cm, and the liquid holdup is 20% by volume.

Basic case 2.2.2

Based on this measured packing performance, the characteristics of the TFTR CD cryogenic distillation columns are summarized in the table below.

Distillation System Design						
Parameter	units	CD1	CD2	CD3	CD4	Total
NTP	-	80	60	80	60	240
HETP	cm	2.5	2.5	2.5	2.5	-
Height	cm	200	150	200	150	700
Col. Diam.	cm	1.79	1.80	2.01	0.58	- -
Max. Vap. Vel.	cm	6.0	6.0	6.0	6.0	-
Liq. Holdup	vol. %	20.0	20.0	20.0	20.0	-
Liq. Holdup	mol/plate	0.028	0.029	0.036	0.003	-
Reb. Liq. Holdup	mol	0.083	0.086	0.107	0.0089	-
Total Holdup	mol	2.295	1.826	2.951	0.186	7.258
T_2 inv.	Ci	128	3046	83	7590	10847
Cond. Duty	W	9.0	11.9	14.0	1.13	36.03
Cond. Temp.	K	21.0	24.3	24.3	24.5	-

From this table one can note that for the tritium inventory resides primarily in CD2 and CD4. For the **conventional option** the inventories in CD2 is 3046 Ci and in the CD4 is 7590 Ci. To meet the 10 kCi tritium inventory target for the system, the tritium inventory of CD4 is in the **proposed option** reduced by using an advanced

undesirable effect of converting some of the T_2 in the feed into DT. This would have a detrimental effect on the tritium inventory.) The FLOSHEET simulation results are also attached in Appendix II, the flowsheet is in Figure 6, and the corresponding Mass Balance data in tables in Appendix III (Turn-down case).

3.4 Refrigeration System (RS)

The refrigeration system is designed around a closed-cycle helium refrigerator based on the Gifford-McMahon cycle. This cold engine is simply a modified Stirling cycle engine, refrigeration is produced by expansion of compressed gas, in this case ultra-pure helium. The important difference between the Giffort-McMahon engine and a normal Stirling engine lies in the fact that the expansion and compression processes are completely separable both thermodynamically and mechanically. This allows for a conventional room temperature helium compression equipment to be used and the expansion pod - the actual refrigerator - can be located remotely from the compressor. The connection between compressor and cold head is provided by a high pressure helium delivery line and a low pressure return line both at room temperature. The cold head consists of a series of gas expansion stages that use high pressure helium that is precooled within the head by high heat capacity heat exchangers. The advantages of this system include:

since the compressor is independent of the cold head - a high speed, efficient helium compressor and low speed expansion pistons in the cold head to reduce wear and vibration cold parts are used.

all valves and seals are at room temperature.

the drive system in the cold head is simple and only deals with low friction parts and small pressure differentials.

easy multistaging - each stage requires only an expansion volume and a displacer (piston) - the helium exhaust and inlet valves are common.

All of these features combine to produce a unit with a high degree of reliability with typical mean-times-between-failures well in excess of 12,000 hours.
The proposed CD system will have four such units, each distillation column will have one dedicated and independent unit.

proprietary column developed by Ontario Hydro. Column CD2 is also a potential candidate for the "advanced" packing if tritium inventory must be as low as possible. This further potential improvement is addressed in paragraph 8.0.

The holdup per theoretical plate for the proprietary column is at least 6.8 times less than for a comparable conventional column. If one assumes a factor of two design margin in calculation of proposed column holdup, it will still have 3.4 times less holdup or 2232 Ci versus 7590 Ci tritium. Experiments to verify the characteristics of an proprietary column of exactly the same diameter and throughput as CD4 will be carried out in the next two months. With only CD4 replaced by the proprietary column, the total tritium inventory of the cascade will be 5489 Ci.

The design philosophy for the TFTR cascade is similar to that for the ITER CD (A. Busigin, et. al, "ITER Hydrogen Isotope Separation System Conceptual Design Description", Fusion Engineering and Design (1990), pp.77-89). The overhead product of the first column CD1 is a tritium free H_2 (with trace HD) stream. Column CD3 produces the D_2 product, and column CD4 produces the T_2 product.

The entire cascade operates in a recycle mode, which is highly advantageous as compared to a cascade (such as the TSTA CD) with no recycles. Recycles allow concentration profiles to establish themselves naturally throughout the cascade, thus eliminating the need for a complex startup sequence. Furthermore, if normal operation becomes disrupted, feeds and drawoffs can be temporarily suspended until concentration profiles become re-established by normal system reflux.

The TFTR CD cascade has four equilibrators, one for the main feed stream to each column. The purpose of the equilibrators is to promote the breakdown of the intermediate species HD, HT, and DT to produce H_2, D_2 and T_2. The equilibrators use a small amount of Pt on alumina catalyst and are operated at room temperature.

Turn-down case 2.3.3

In addition to the reference design (case 2.2.2) two additional cases were examined:
- the turn-down case 2.2.3 and a
- total reflux case.

In both instances it was concluded that, as long as the CD4 bottom tritium concentration is 99.7 %, the tritium inventory is virtually unchanged from the reference design case. This is explained by the reality that in the reference case the CD4 bottom product flow is already low that the column operates at near total reflux conditions.

For case 2.2.3 (Figure 6) the feed is mixed with the output stream from Equilibrator EQ5 (which is a calculation tool but which is not supplied with the equipment) and fed into CD4. (Mixing upstream of EQ4 is also possible, but the this would have the

3.5 Drain and Purge Operation

A standard requirement for any isotope separation system is the ability to rundown and purge the system for purposes such as for shut-down for maintenance etc. In this design the available $7m^3$ collection tank is proposed to carry out this function. The intent is prior to a scheduled shut down to run the CD for as long as necessary to remove as much tritium as possible. Subsequently the system would be shut down, pumped out by the pump provided and purged into the collection tank. The use of the FTS getter beds for of-specification CD content rundown or as an emergency fast rundown could also be considered.

Present Status of LHD Project

O.Motojima
National Institute for Fusion Science
Fro-cho, Chikusaku, Nagoya 464-01, Japan

This year 1992 FY is the third year of LHD project. We report the present status of the construction of LHD apparatus. Our major activities are concentrated on the engineering design, research and development, and practical construction. The construction schedule is on schedule and progressing. Construction of the building is under progress. On-site fabrication and assembly are scheduled to start in April 1994.

We are almost completing the final engineering design. At the same time, we are pursuing to complete the necessary research and development (R&D) items, especially R&D for superconductor. Several parts of the major components have been initiated to be fabricated. The construction of the main experimental building has also begun. In the following, we explain the present status of each item.

1. DESIGN OF LHD

Currently, LHD construction is at the final stage of engineering design phase. The LHD Design Group (LOB Group) of NIFS is responsible for R&D, and engineering design based on R&D data. To start the construction of the lower part of the inner vertical field coil, the engineering design has been completed as a stand-alone component (no interface). Construction of the winding machine for the helical coil has begun. Engineering design of the major parts, i.e. helical coils, supporting structure, etc. are still progressing. However, it is reaching a final goal. Therefore, arrangements for material acquisition have been begun for the necessary components.

2. R&D PROGRAM

R&D activities on superconductors, vacuum components, power supplies, and control systems etc. are being pursued. Construction of superconducting material and test coil has been completed, and the final Liquid Helium cooling tests are being performed on various test components. Low Temperature Experiment Building was completed by the end of 1990, and the research staff is moving gradually to the new site. A test facility for developing vacuum components has been completed in the Low Temperature Experiment Building, and is under full operation. Main purposes of R&D are the development of advanced technology based on new ideas and positive confirmation of performance. A great deal of technical knowledge is obtained as expected. A large contribution has been made especially in the field of superconductor research. (1) Development of stable large current conductor, (2) Development of large magnet, (3) Development of refrigeration technology, (3) Clarification of superconductor characteristics, (4) Accumulation of coil control technology, etc.

3. PLANNING OF EXPERIMENTAL PROGRAM

Detailed planning of the experimental program has begun, providing for the commencement of the experiments in April 1997. The major objective of this activity is put on the advanced physics understanding, improvement of the accuracy predicting plasma parameters, and establishment of concrete operational scenarios. The major subjects are transport, MHD (high β), heat and particle exhaust with divertor, confinement improvement, steady-state operation, and D-D experiment. One more important objective is to establish analysis methods for experimental data. The arrangements for the necessary components of the experiment (e.g., Plasma production and control, fueling, heating, diagnostics) has begun.

LHDの特徴

(1) 基本スペック

(2) 設計目標

R = 3.9 m
a_p = 0.975 m
a_c = 0.65 m.
A_p = 6
ℓ = 2
m = 10
γ_a = 1.25
α = 0.1
B_0 = 3 T (4 T ; OBJECTIVE)
V_p = 30 m^3
P_H = 20 MW
NbTi

1. PHYSICS EXPERIMENTS EXTRAPOLATABLE TO FUSION CONDITION
   HIGH $n\tau T$, HIGH T, HIGH β
2. CURRENTLESS STEADY PLASMA PRODUCTION
   DIVERTOR EXPERIMENT
3. COMPLEMENTARY TO TOKAMAK APPROACH
4. CONTRIBUTION TO FUSION TECHNOLOGY

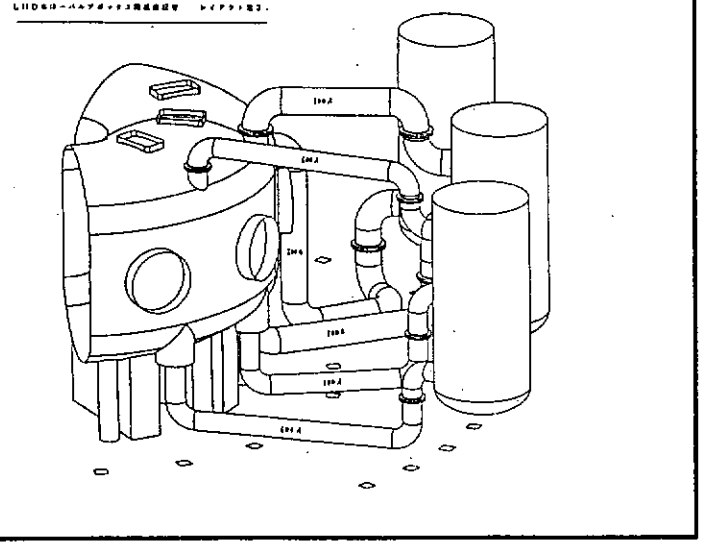

0071

Current Direction of NIFS

Acceleration of LHD Construction
(1) 1992FY, 3rd year of 7 Year Project
(2) Completion of Final Engineering Design
(3) Initiation of Fabrication of Major Components(from 1992)
  Poloidal Coils (until 1994)
  Lower Half of Cryostat (until 1993)
  Helical Coil Fabrication Machine (until 1993)
  Lhe Refrigerator (until 1993)
(4) Acceleration of R&D
  SC (Conductor, Feedthrough, P Coil Test, etc.)
  Power Supply and Control System
  First Wall Material and Cooling System
  Plasma Heating Equipment (Negative Ion Source, Gyrotron, etc.)
(5) Planning of LHD Experiments from 1997
  Transport, MHD, Divertor, Steady State Experiment, etc.
(6) Construction of Buildings and Facilities
  Major Experimental Building (1994, March)
  Computer Center (1993, February)
  SC Research Building (Completed)
  Heating System R & D Building (Completed)

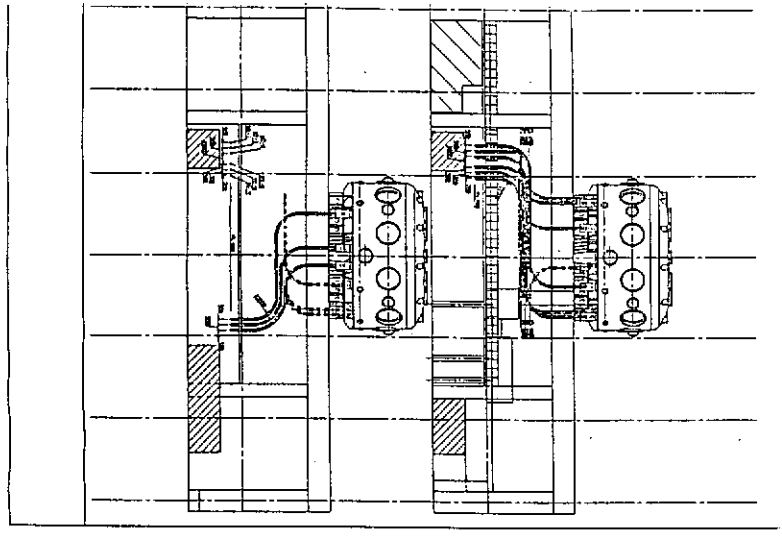

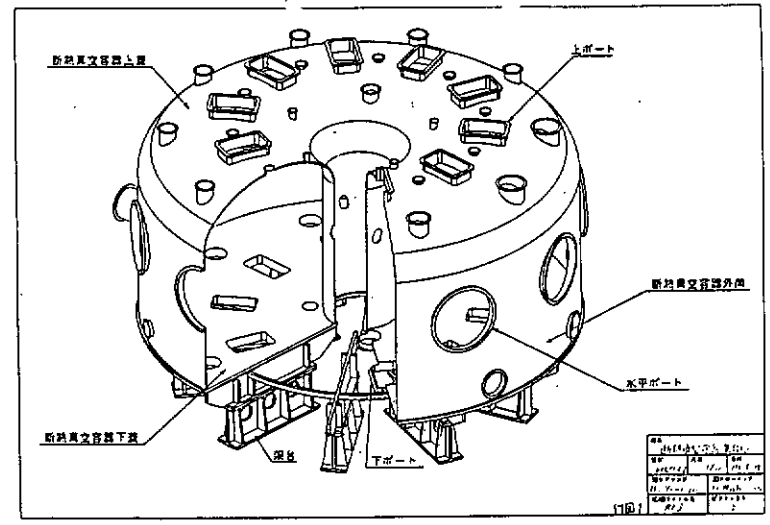

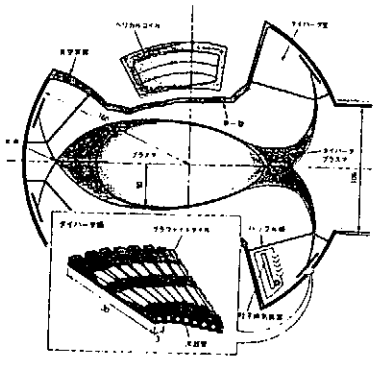

大型ヘリカル装置ポロイダル断面図

Heating Power

Radiation Loss

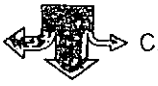

CX Loss

Divertor

Heating Power	ECRH	10 MW	(10s)
		3 MW	(cw)
	NBI	20 MW	(10s)
	ICRF	9 MW	(10s)
Plasma Volume	20 ~ 30 m^3		
			Total(MW)
Max. Heat load on the Divertor Plates	5 MW/m^2	(10s)	20
	10 MW/m^2	(5s)	>30
	0.75 MW/m^2	(cw)	3
Max. Heat Load on the First Wall	0.2 MW/m^2	(10s)	20
	0.015 MW/m^2	(cw)	3

SUMMARY

(1) Construction of LHD is progressing on schedule.
(2) Presently at the final stage of engineering design. Design activities are carried out by the LHD Design Group (LDG Group) at NIFS.
(3) R&D of essential components of the superconducting coils is at its final stage. A large amount of technical knowledge has been obtained and a large contribution has been made to the area of superconducting research. R & D on heating systems have been started also in Toki site.
(4) Fabrication has been started on several components (PF Coil, winding machine, tower cryostat).
(5) Orders on other components (e.g., other PF coils, He liquefier, coil power supplies, cooling system) will be placed shortly according to the construction schedule.
(6) Construction of buildings is under progress.
(7) On-site fabrication and assembly in Toki site are scheduled to start in April 1994

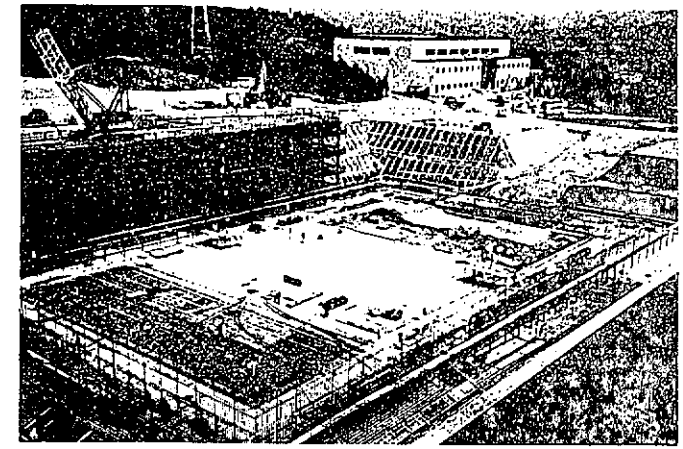

大型ヘリカル装置計画完成予想図

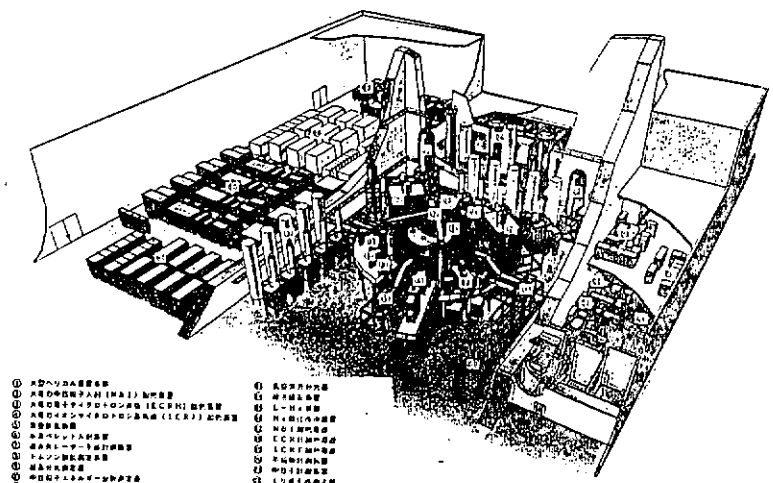

Plasma Facing Components and Plasma-Surface Interactions in TRIAM-1M

Naoaki Yoshida and the Fusion Material Group of RIAM

Research Institute for Applied Mechanics, Kyushu University, Kasuga, Fukuoka 816, Japan

ABSTRACT

On the superconducting high-field tokamak TRIAM-1M at Advanced Fusion Research Center at Research Institute for Applied Mechanics(RIAM), Kyushu University, ultra-long pulse operation longer than one hour has been achieved by a lower-hybrid current drive. Analysis of damage of Mo limiters of TRIAM-1M used for such long pulse discharges and the relevant PFC and PSI studies are being carried out at RIAM.

(1) Damage of Mo limiters and its influence on plasma

Powder metallurgy Mo(99.95%) was used for poloidal limiters and heavy damage due to high heat loading was observed. Brittle fracture occurred along crystal grain boundaries and the cracks expanded by the repeated thermal loading. It is expected that the formation of the cracks leads to the reduction of heat transfer and thus enhances melting and evaporation of the limitors. Suppression of embrittlement is one of the key issues of high-Z materials for plasma facing components.

Mo impurities ejected from the molten surfaces of the limiters often unstabilized long pulse plasma discharge at high density ($10^{13}cm^{-3}$). In order to estimate the critical heat loading which unstabilized plasma, heat loading experiments with the electron beam high heat flux simulator were carried out. In the case of heat loading at $50MW/m^2$ for 30s, melting of Mo is limited only at the surface, if the active cooling is enough. Judging from the experience of TRIAM-1M, the heat loading at this level or lower

does not cause severe problems for plasma confinement. By heat loading above 60MW/m^2, not only the vapor of Mo but also molten droplets of Mo are ejected severely and the vacuum of the chamber gets worse very much. Damage of the Mo at this condition corresponds well with that of "Mo blooming" in JT-60 and ejection of Mo droplets during high density operation at TRIAM-1M. It should be emphasized that the critical heat flux mentioned above would be lowered by the formation of cracks due to repeated thermal stress.

(2) Development of low-Z and high-Z coating technique

Wire explosion spraying method is applicable for repair of low-Z and high-Z coating of PFC on the spot in a torus. This spraying can be performed in atmosphere on a substrate at room temperature without any sophisticated equipments and yield high condensed coatings in a second with the strong adhesive strength. It was demonstrated that TiC and W-Re coatings on a plate of austenitic stainless steel showed very high thermal shock resistance.

(3) Microstructural change of PFC by neutral H

By using the corrector probe transfer system attached to TRIAM-1M atomistic damage in plasma facing materials by energetic plasma particles was detected and the results were compared with those of hydrogen ion irradiation experiments. From the comparison of the density and the size of the radiation induced defect clusters it was estimated that the hydrogen neutrals at 0.5-2keV with a flux of 1.5-3x10^{18}H/m^2s cause displacement damage during long pulse discharge of TRIAM-1M (I_p=23kA, $\bar{n}_e$=2x10^{18}/m^3). This unexpected heavy damage would change material properties at and near the surface and control the behavior of hydrogen in PFC.

PLASMA FACING COMPONENTS AND PLASMA-SURFACE INTERACTIONS IN TRIAM-1M

Naoaki Yoshida

Research Institute for Applied Mechanics,
Kyushu University

- PFC and PSI relevant studies at RIAM -

(1) Performance of Mo-limiters in TRIAM-1M
  *material damage
    - problems of Mo as high heat flux components
  *influence on plasma

(2) Development of low-Z and high-Z coating
  *wire explosion spraying method

(3) Microstructural change of PFC by neutral H

Japan-US Workshop P108 (Nov.17-19,1992, Kasuga)
"High Heat Flux components and Plasma Surface Interactions for Next Devices"

Plasma Facing Components of TRIAM-1M

*Wall: 304SS

*Poloidal Fixed Limiters:
PM-Mo(powder metallurgy)
grain size: 40 micron
purity: 99.95%
sintering: 1800 °C

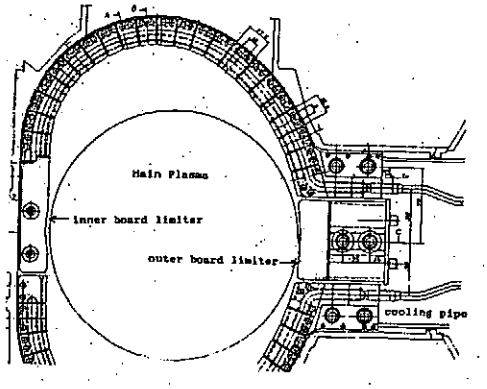

Damage of Inner Limiter(#3, 1991.6)

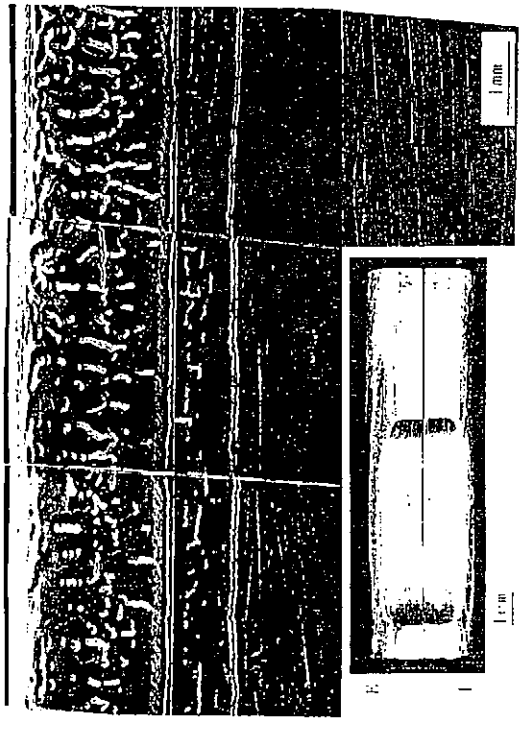

Damage of Mo-Limiter(#1, 1991.6)
Inner Limiter, E-Side
* Cracking at the grain boundaries (brittle fracture)

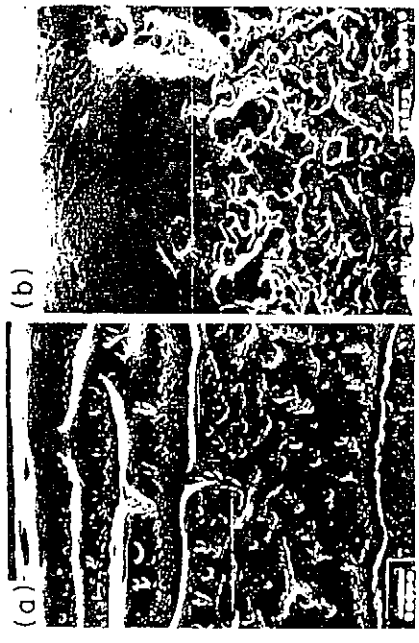

Cross Section of Mo-Limiter(#1,1991.6)
Inner Limiter, L-side

- Formation of cavities under the surface
  -- reduction of heat transfer
  -- enhancement of melting and evaporation
- Brittle fracture should be prevented.

Damage of TiC/Mo divertor plate in JT-60 due to
large heat concentration at the edge

STRESS DUE TO HEAT LOADING

(W. Wang)

PROBLEMS OF PM-Mo FOR HIGH HEAT FLUX COMPONENTS

*Embrittlement
  Heat loading (and ion(O,N,H) bombardments)
    -recrystallization and grain growth in surface layer
    -embrittling at grain boundaries
    -If DBTT > R.Temp
      easy cracking by thermal shock

* Cracking
    -reduction of heat transfer
    -enhancement of melting, evaporation and further cracking

COUNTERMEASURES FOR EMBRITTLEMENT

*High purity EBM-Mo

*Mo-Re alloy

*Addition of strong oxide-, nitride- and carbite-forming elements acting as scavengers
  Ti, Ce, Th

*Operation above DBTT

TIME VARIATION OF PLASMA PARAMETERS AND OTHERS DURING LOW DENSITY DISCHARGE ($2X10^{12}cm^{-3}$)

*Concentration of Mo is almost constant during long pulse discharge(0.2%)

*Mo has no bad effects on the discharge.

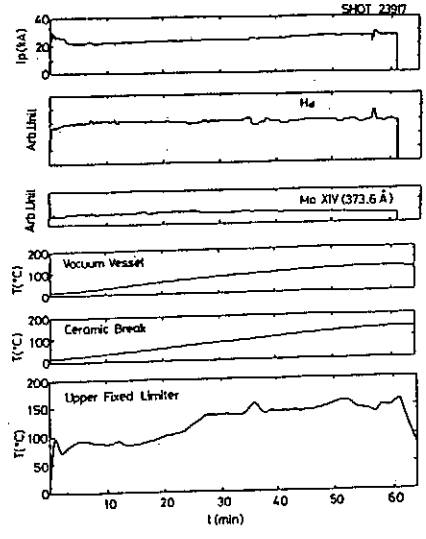

8

Tangential TV Images of Plasma
(shot 26325, $\bar{n}_e$=2.5-7x$10^{12}cm^{-3}$)

*Molten droplets were often ejected from the outer limiters (t>27s)

*At this condition, concentration of Mo in the core plasma increases two to three times and plasma becomes unstable.

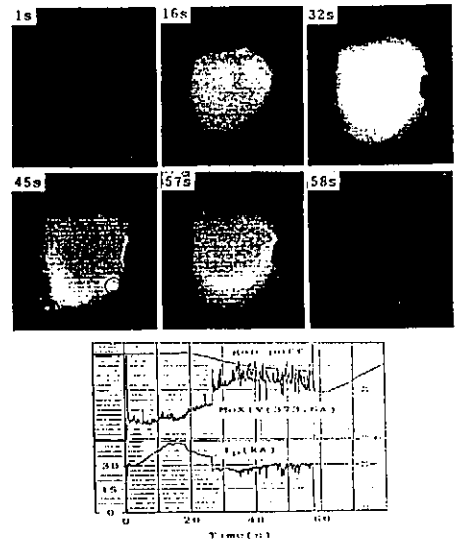

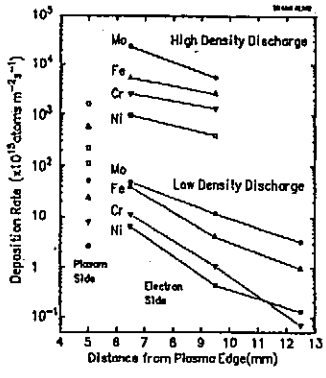

Fig. 1 Impurity deposition rate on the plasma and the electron drift sides as a function of the distance from the plasma edge, measured with thin-foil Al collector probe specimens introduced to the scrape-off layer of TRIAM-1M. The deposition rates during high density ($\sim 2x10^{19}/m^3$) and low density ($\sim 2x10^{18}/m^3$) discharges are compared.

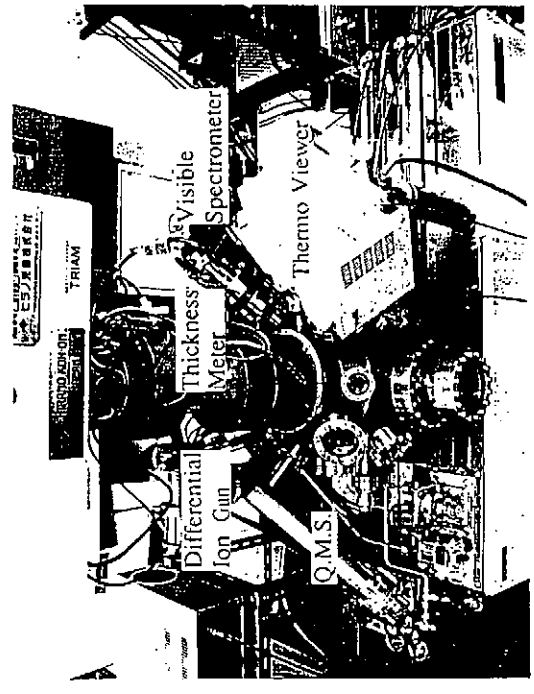

Electron Beam High Heat-Flux Simulater

Effects of Heat Loading on PM-Mo

--electron beam bombardment for 30s--

(1) No Effects
(13MW/m^2, Max. Temp.=1092°C)
*no melting,
*no significant evaporation

(2) Evaporation
(21.3MW/m^2, Max. Temp.=1584°C)
*evaporation starts.
*surface becomes rough.

(3) Surface Melting and Moderate Evaporation
(49.1MW/m^2, Max. Temp.=2606°C)
*melting and recrystallization of thin surface layer
*moderate evaporation
-- small weight loss

(4) Ejection of Droplets
(62.8MW/m^2, Max. Temp.>2783°C)
*strong evaporation
*ejection of molten droplets
*large weight loss

-increase of Mo impurity during high density discharges in TRIAM-1M

-"Mo blooming" in JT-60

WIRE EXPLOSION SPRAYING METHOD

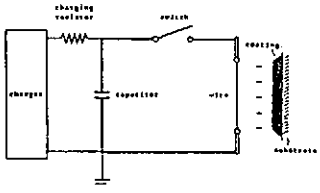

Fig.1 Basic cricuit and equipments for wire explosion spraying.

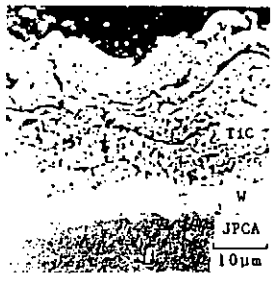

Fig.3 Sectional microstructure of TiC/W/JPCA (at 200 Torr).

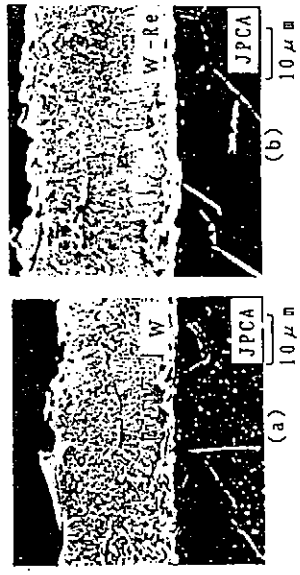

Fig.2 Sectional microstructures of W/JPCA(a) and W-25Re/JPCA(b). (etched)

Comparison of Microstructure Formed in TRIAM-1M and H^+ Ion Irradiations

*Discharge condition of TRIAM-1M
I_p=23kA, $\bar{n}_e=2\times10^{12}/cm^3$
t_j=628s+674s

*Irradiation condition of H ions
Irr. temp.=300K
Ion energy=0.5, 2, 4 and 8keV
Ion flux=3-8x$10^{18}H^+/cm^2s$

Estimation of hydrogen neutrals formed in low density long pulse discharge in TRIAM-1M

Energy: 0.5-2keV
Flux: 1.5-3x$10^{18}H/m^2s$

Molibdenum

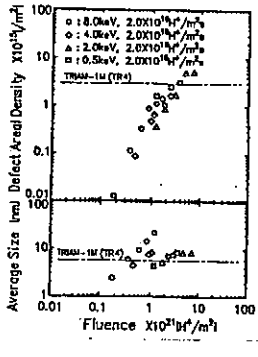

Aluminium

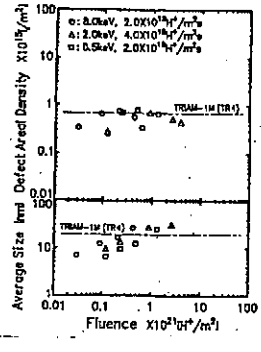

Japan-US Workshop on High Heat Flux Components and Plasma Surface Interactions for Next Devices
November 17-19, 1992 Kyushu Univ.

Development and Experiences with JT-60U Plasma Facing Components

presented by T. Ando
JT-60 Facility Division II
JAERI

SUMMARY

In the framework of R&Ds on boronized carbon-based materials for application to JT-60U, the in-pile test of B_4C-overlaid CFC divertor tiles has been performed. The B_4C-overlaying methods are CVR(Chemical Vapor Reaction)-conversion (50~200 μm), CVD-coating (~150 μm), and LPPS-coating (~150 μm). The results show that almost all B_4C layers were melted at tile edges due to high heat concentration, excepting incidentally shadowed edges. However, exfoliation of CVR-conversion B_4C layer was not observed. Some coating layers were exfoliated at tile edges. These edges should be shaped beforehand to have a slight slope to reduce the local high heat flux. CVR-conversion B_4C graphite tiles were also installed in the first wall region and exposed to JT-60U plasma. The edges of these tiles were also melted, but B_4C layer of ~100μm thick still remains after one-year operations. From view points of the life of B_4C-overlaid CFC/graphite, ~100 μm thick layer is considered to be allowable. Detailed analyses of the removed tiles are planned. One complete poloidal row of outboard divertor tiles (125 units) and selected part of the first wall tiles (150 units) are replaced during this vent (Nov. ~ Dec. '92) by using CVR-conversion B_4C ones.

In the post-experiment observation in this vent, very shallow erosions were observed on the divertor tiles which have not been shadowed sufficiently, and were located at the outboard striking point in low X-point, low density and high power operations in this year. Erosion patterns show clear toroidal periodicity due to field ripple effect, which means that the heat flux is enhanced in the toroidal direction in the case that poloidal field perpendicular to the divertor plate is so small that the field line is significantly affected by the ripple of toroidal field coils.

In collaboration with SNL (US-Japan collaboration: PL-112), beta backscatter analysis has been successfully carried out during this vent (Nov. '92) in order to examine deposited metals on the plasma facing tiles.

Feasibility studies on actively-cooled divertor plate for JT-60U is underway and heat load tests using JEBIS are scheduled for the next FY.

Japan-US Workshop on High Heat Flux Components
and Plasma Surface Interactions for Next Devices
November 17-19, 1992 Kyushu Univ.

Development and Experiences with JT-60U Plasma Facing Components

presented by T. Ando
JT-60 Facility Division II
Japan Atomic Energy Research Institute

Contents:

Operation History of JT-60U in 1992

Calendar	Operation Status	Major Events
1991 Nov.	Regular Maintenance Shutdown Air Vent	<- US-Japan Workshop at Santa Fe <- Installation of B_4C-overlaid Tiles for In-pile Test
Dec.		
1992 Jan.	Exp.	In-pile Test of B_4C-overlaid Tiles Ip~4 MA, P(NBI)~20 MW x 2 s C~6 %, O~4%, Z_{eff} ~4-5 for n_e~2×10^{19} m^{-3}
Feb.		
March	Air Vent	<- Removal of B_4C-overlaid Divertor Tiles <- Clean-up of First Wall due to Falling-off of Schutter plate
April	Exp.	S_n~2×10^{16} s^{-1} in High-β_p Plasma, Ip~1.2 MA No metal impurities , comparable to Exp. in Feb.
May	Regular Maintenance	
June	Exp.	Ip~4 MA, P(NBI)~25 MW x 2 s
July	Air Vent	<- Heat Load Test (JEBIS) of CVR-B_4C Tiles with Thicker Layer (~1 mm) <- Installation of Boronization System <- First Boronization
Aug.	Exp.	S_n~2.8×10^{15} s^{-1}, Ti(0)~38 keV for High-β_p Plasma
Sep.		<- Second Boronization S_n~2.2×10^{15} s^{-1}, Ti(0)~32 keV for H-mode Plasma
Oct.		C~5%, O~1-2% , Z_{eff}~3-4 for n_e~2×10^{19} m^{-3}
Nov.	Regular Maintenance Shutdown Air Vent	<- Beta-backscatter Measurement of Tile Surface <- US-Japan Workshop at Fukuoka
Dec.		<- Installation of CVR-B_4C Tiles <- Installation of In-vessel Tubes (6:upper, 6:lower) for Boronization Gas Feed Lines
1993 Jan.	Exp.	
Feb.		

In-pile Test of B_4C-overlaid Tiles in JT-60U

- B_4C-overlaid CFC
  - Improve surface characteristics of CFC without substantial degradation of its superior thermal performance
  - Modification of surface layer
- JT-60U In-pile Test
  - Examine material behavior under interactions with actual divertor plasma
- Materials Tested
  - CVR (Chemical Vapor Reaction) conversion 50~200 μm
    $2B_2O_3+7C \rightarrow B_4C+6CO$ at~2000°C
  - CVD coating ~150 μm
  - LPPS coating ~ 150 μm (Julich)
- Installation
  - Divertor outboard/inboard regions

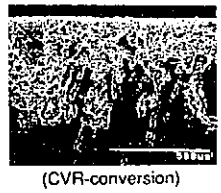

(CVR-conversion)

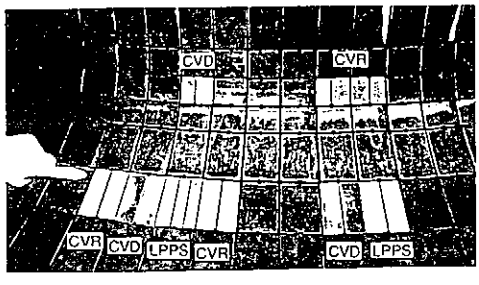

In-pile Test of B_4C-overlaid Tiles in JT-60U (continued)

- Operation Conditions
  - Periods Jan. ~ March 1992
  - Total No. of discharges 360
  - No. of NB-heated discharges 172
  - Heating power ~20 MW x ~2 s
  - Divertor heat flux ≤ 5 MW/m^2(flat surface)
- Results
  - Melting of B_4C at tile edges
    - one order higher local heat flux
    - need to slope slightly (heat flux concentration factor≤ 2)
  - Coatings exfoliated at edges
  - Inboard test tiles covered with sooty carbon deposition (off-trace until March), but with glossy one in Nov.
  - CVR-conversion prefarable for high heat flux tiles

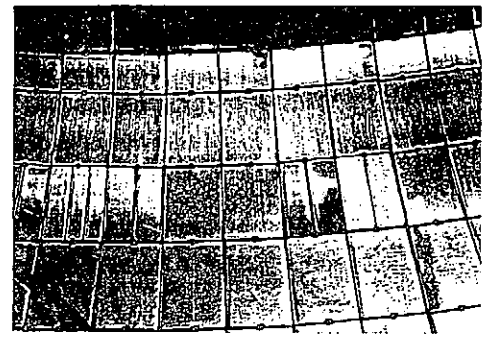

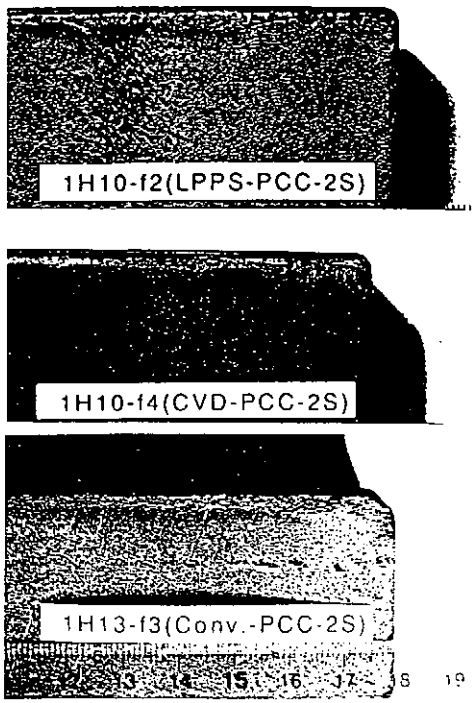

Post-experiment Observation of PFC in Nov. 1992

- Divertor Plate
  - Toroidally periodic, shallow erosion mainly on tile row:e (see figure:outboard strike point in low X-point, low density and high power operations)
  - Carbon powder under the divertor plate (possibly due to sparks in non-controlled discharges)
- First Wall
  - No visible significant damage for graphite tiles
  - Melting of backing plates in large ripple region around outboard ports
- B_4C (CVR-conversion) First Wall Tiles - another in-pile test-
  - Melting at tile edges without exfoliation (B_4C layer remained after one-year operations)
- LH Launcher
  - Melting and deposition of metals on surrounding plasma facing tiles

P-O: Middle point between toroidal coils

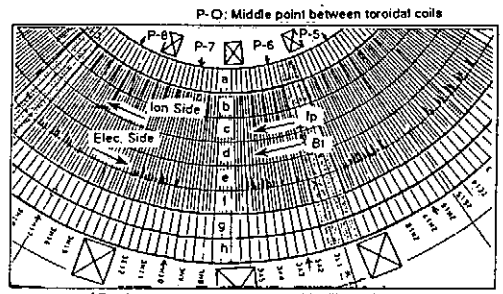

(Erosion patterns are exaggerated for illustration)

Plans for the Vent (Nov. ~ Dec. 1992)

- Install CVR-conversion B_4C tiles
  - ~ 100 μm thick — Divertor 125 units (outboard: row f) with slope at edges (1/50 see fig.); First wall 150 units (around large ports)
  - ~ 500 μm thick — Divertor (1 unit), First wall (1 unit)
  - Different grades — CFC PCC-2S, MFC-1, MCI-felt II; Graphite PD-330S, ETP-10, STP-60

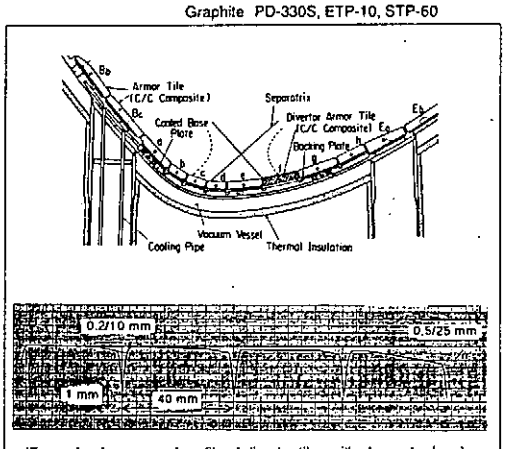

(Example of measured profile of divertor tiles with slope at edges)

Plans for the Vent (Nov. ~ Dec. 1992)

(continued)

- **US-Japan collaboration PL-112 (SNL-JAERI)**
  In-situ analysis of deposited metals by beta backscatter measurement (Oct. 30 ~ Nov. 12, completed)
  Divertor — all tiles (1000 units) + detailed profiles
  First wall — six toroidal sections

- Sampling of redeposited layer on graphite tiles and carbon powder for residual tritium analysis
- Remove several tiles for surface analysis, retention and outgas measurements
- Install probes (rogowski coils) under four divertor tiles for measurements of SOL current during disruptions
- Rearrange Langmuir probes on divertor tiles (15 poloidal points)
- Rearrange thermocouples for calorimetry of divertor tiles (20 poloidal points)

Plans for R&D on Actively Cooled Divertor for JT-60U

- Heat Removal Performance
  - 10 MW/m^2 x 10 s, 5 cm width
  - Surface temperature ≤ 1000 °C
  - Achieve quasi-steady state of plasma-facing surface temperature
- Feasibility Studies
  - Collaboration with NBI Heating Laboratory
  - Supported by Makers' design and analysis
  - View points
    electromagnetic force during disruptions,
    supporting method within the limited space,
    heat transfer capability for the present flow conditions
- Heat Load Test by Using JEBIS
  - Scheduled for the next FY

End of Vu graphs

Japan-US Workshop on High Heat Flux Components and Plasma Surface Interactions for Next Devices,November 17-19,1992 Kyusyu University

Recycling of Hydrogen Isotopes and He Ash in JT-60U

Hiroo Nakamura

Department of Fusion Plasma Research
JAERI,Naka Fusion Research Establishment

Summary

In this talk, experimental results on particle recycling in JT-60U are presented. Objectives of JT-60U are confinement and steady state studies. For both studies, controle of recycling is important issue. Because JT-60U is all graphite machine, careful wall conditioning is necessary. Wall conditioning methods are disruptive discharge cleaning, He-plasma discharges cleaning,Taylor type discharge cleaning,glow discharge cleaning. Recently, boronization is also used. In addition to these methods, low wall-temperature operation is also used. In 1992, optimization of TDC and GDC have been done. In evaluating recycling before and after the boronization, thermal desorption of JT-60U vessel has been done. Due to reduction of wall recycling by TDC,GDC,boronization and low wall-temperature, plasma performance made significant progress.

Recycling of Hydrogen Isotopes and He Ash in JT-60U

Hiroo Nakamura and JT-60 team
JAERI

Japan-US Workshop P196 on High Heat Flux Component and Plasma Surface Interactions for Next Devices
Kyusyu University,Fukuoka
Nov.17 - 19,1992

- Contents -

- Wall Conditioning and Wall Temperature
- Deuterium Recycling in H-mode and High βp Discharges
- Thermal Desorption Data of JT-60U Vessel before and after Boronization
- Summary and Plan

* In this talk,results on He ash is not presented. Experiment has been done in October 1992. He beam was injected into ELMy H-mode discharges. Data analysis is now under way.

Objectives Of JT-60U Experiments

Confinement studies
H-mode (ITER)
high βp (bootstrap, SSTR)
high energy particle transport
rotation

Steady-state studies
-Impurity and divertor control
,current drive(bootstrap, LH),
disruption control

JT-60 Upgrade

start of operation: March 1991

	JT-60	JT-60 Upgrade(achieved)
Ip	3.2MA	6MA (5MA)
gas	H, He	D
NB	26MW	40MW (30MW)
LH	10MW	10MW (2.5MW)
IC	3.1MW	5MW (3.6MW)

JT-60U device

R=3.4 m, Aspect ratio~4
ellipticity~1.4 or 1.7, triangularity<0.1
graphite wall / CFC for divertor tiles
High B_T Max. =4T at the vessel center
Ripple loss of fast ions

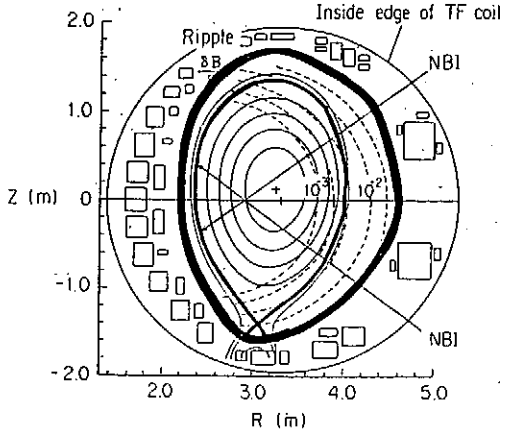

Wall Conditioning in JT-60U

Reduction of recycling and impurities by wall conditioning is one of key issues to obtain good confinements.

- He TDC (Taylor Discharge Cleaning)
  - Low pressure $10^{-4} \sim 10^{-3}$ Pa
  - Interval time 1~5 min
- He GDC
  - Low pressure 0.02~0.06 Pa
  - Higher current 10 A
  - lunch & Dinner GDC., Over night GDC
- Low wall-temperature
  - ~100°C during experiment
  (Week-end ~300°C baking)
- Boronization (Decaborane, $B_{10}H_{14}$)
  → Saido-san (Previous talk)
  → Prof. Sugai (This afternoon talk)

Effect of Wall Temperature on Mass Intensity and Particle Recycling (pre-boronization)

Low temperature operation is effective to reduce residual gas intensity and particle recycling.

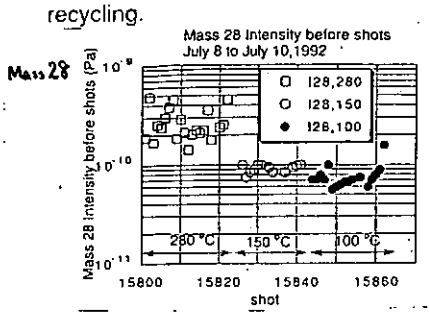

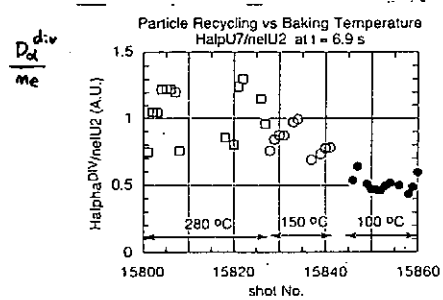

Progress in confinement performance

	High β_p mode	H-mode
$T_i(0)$ (keV)	38	33
$n_d(0)T_i(0)\tau_E$ (m^{-3}keVsec)	4.4×10^{20}	2.5×10^{20}
S_n (n/sec)	2.8×10^{16}	2.3×10^{16}
Q_{DT}	~0.31	~0.15

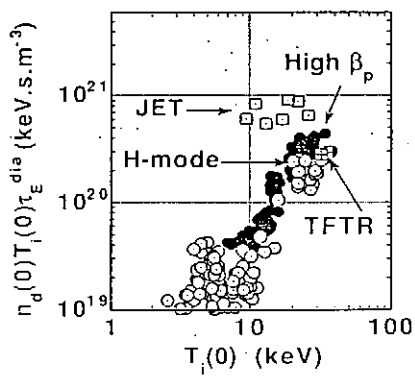

Particle Recycling of High βp Discharges before and after boronization

(3 week after 1st-BZN)

B_T = 4T

OH phase, Ip=1-1.3MA, Apr & Aug.'92

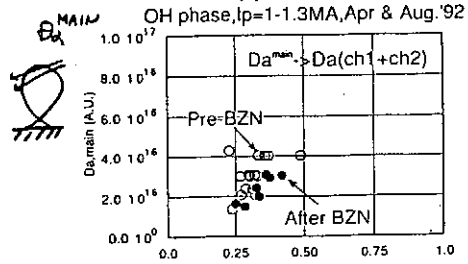

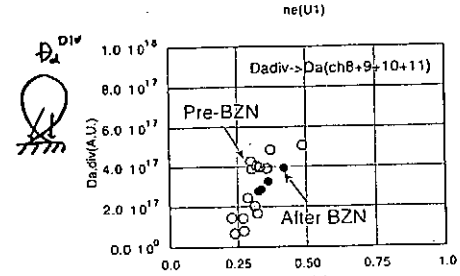

- Low ne target plasma
  Pre-BZN → He TDC between shots
  After-BZN → No He TDC between shots

Particle Recycling of H-mode Discharges before and after boronization

H-mode phase

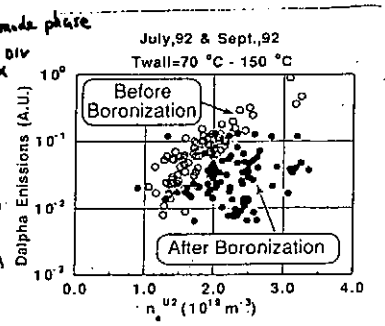

- Before BZN
  B_T = 2~3T
  I_p = 1.5~2MA
- After BZN
  B_T = 4T
  I_p = 3~4MA

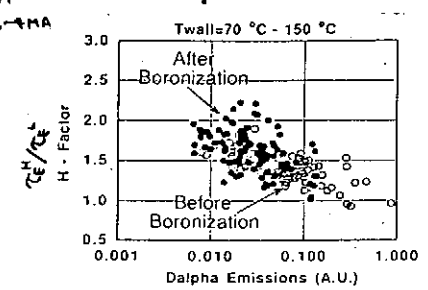

Vessel Baking after Friday Final Shot
Pre-Boronization
(September 7,1991)

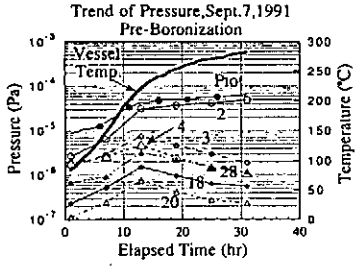

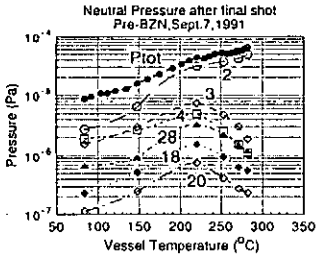

Vessel Baking after Friday Final Shot
2nd Boronization
(September 4 to 7,1992)

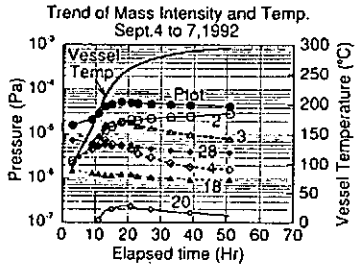

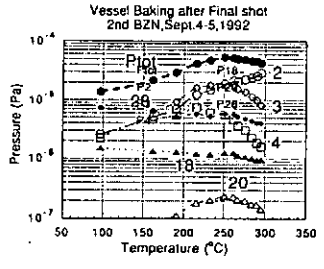

Comparison of D2 Pressures
between pre-and after-BZN

D2 pressures after BZN,are higher than pressures before BZN. This suggests that boronized wall absorbed much deuterium than graphite wall.

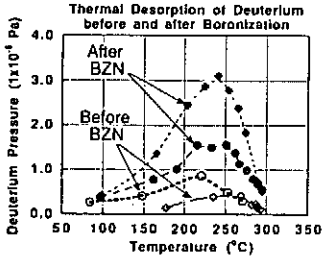

$$(P_{D_2} = P_{m/e=4} + \frac{1}{2} P_{m/e=3})$$

More data analysis is necessary to estimate deuterium pumping capability of boronized wall.

Future plans

1993 : -Step-up of wall conditioning
----uniform boronization
-High power heating- 40MW
-LHCD with two launcher-10MW
-Investigation of SOL and divertor
-Theory and simulation analysis

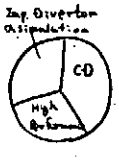

1994: -Installation of negative ion beam injection
-NBCD experiments
-Behavior of α particles (d-^{3}He)

In progressing of plasma performance, systematic studies between tokamak and laboratory experiment become more and more important.

US-Japan Workshop P 196 on High Heat Flux Components and Plasma Surface Interactions for Next Devices, Kyushu University, Fukuoka, November 17-19, 1992

Initial Boronization of the JT-60U Tokamak by Using Decaborane

Presented by M. Saidoh
Department of Fusion Facility, JAERI

Decaborane-based boronization system has been installed in the JT-60U tokamak. Decaborane ($B_{10}H_{14}$) is not explosive and less toxic than diborane, which is conventionally used for in-situ boronization in tokamaks. Decaborane is solid at room temperature and decaborane vapor can be easily obtained by heating to about 110 ℃ (vapor pressure at 110 ℃ is 4 kPa.). This system provides a passive safety by maintaining subatmospheric pressure of decaborane vapor throughout the system. Another advantage of the decaborane-based boronization is short delivery lines (shorter than 20 m), since safety features of decaborane allow installation of decaborane container near the JT-60U vacuum vessel.

Two sessions of boronization (July 30 and September 1, 1992) have deposited films about 30 nm and 46 nm average thickness, respectively. The average wall temperature of JT-60U vessel during boronization was 300 ℃. Characteristics of boronized wall and plasma performance after boronization are following.

(1) Purity of boron film was high.
(2) Hydrogen concentration in the film was 10%.
(3) Oxygen (0.3%) was reduced by an order of magnitude for OH-plasmas resulting in $Z_{eff} \sim 2$, while for NB heating plasmas Z_{eff} was 3, the major contributor being carbon (5%).
(4) Particle recycling flux was reduced by a factor of 2-3 for NB heating plasmas and energy confinement was improved.
(5) Boronization enabled reliable operation at lower densities than were previously possible.
(6) Boron films in the present experiment were toroidally nonuniform: thickness ranging from 150 nm near the injection port to 3 nm.

Further improvement, such as increase of decaborane injection ports, is planned to coat the first wall by boron film with a better toroidal uniformity. Furthermore the combined use of boronized graphite tiles with a good thermal conductivity for armor tile application and wall conditioning of in-situ boronization will be more effective to maintain the boronized surface over long-term operations.

US-Japan Workshop P 196 on High Heat Flux Components and Plasma Surface Interactions for Next Devices, Kyushu University, Fukuoka, November 17-19, 1992

Initial Boronization of the JT-60U Tokamak by Using Decaborane

Presented by M. Saidoh

Department of Fusion Facility
Naka Fusion Research Establishment
Japan Atomic Energy Research Institute

Plan of Talk

1. Objectives
2. Decaborane($B_{10}H_{14}$) based boronization system and process
3. Properties of boron coated films (deposition probe analysis)
4. Plasma impurity and particle recycling after boronization
5. Summary

Major Contributors

1. JAERI: N. Ogiwara, T. Arai, H. Hiratsuka, T. Koike, M. Shimada, Y. Neyatani, M. Shimizu, H. Ninomiya, H. Nakamura, R. Jimbou, T. Sugie, A. Sakasai, N. Asakura
2. Nagoya University: M. Yamage, H. Toyoda, H. Sugai
3. General Atomics: G. L. Jackson

Objectives of boronization

* Reduction of oxygen and carbon
* Reduction of particle recycling flux

Features of JT-60U PFC

* Divertor plates are made of carbon fiber composite tiles
* Complete coverage of the first wall by graphite tiles

Decaborane-based boronization system

* Decaborane ($B_{10}H_{14}$) is not explosive, less toxic than diborane and solid at room temperature.
* Decaborane vapor can be easily obtained by heating to 110 ℃ (vapor pressure at 110 ℃ is 4 kPa).

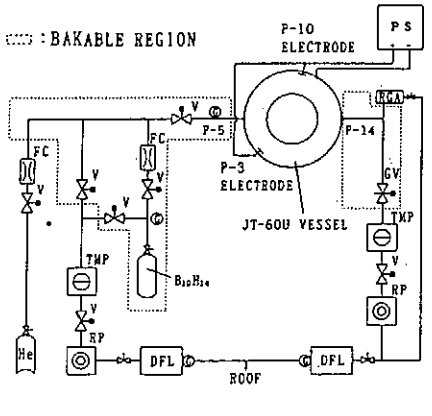

* Present system provides a passive safety by maintaining subatmospheric pressure of decaborane vapor throughout the system and also short delivery lines (less than 20 m).

Boronization process

* Vapor of decaborane is continuously fed into a helium glow discharge, where the decaborane decomposes into boron and hydrogen and ionized borons are accelerated towards the wall resulting in the boron deposition on the first wall.

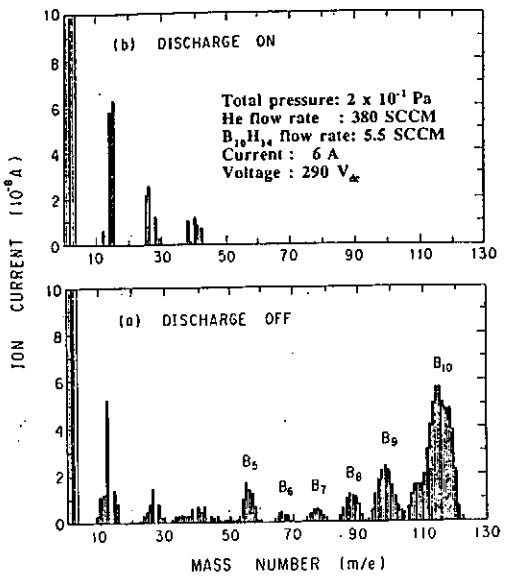

Boronization process

* Decaborane decomposes into boron and hydrogen in the glow discharge so that mass signal of H_2 increases to nearly the same level as that of He.

  This can be explained by taking into account of the number of decomposed hydrogen.

* The fact that hydrogen concentration in the boron film is low (10%) clearly indicates that decomposed hydrogen can be effectively pumped out.

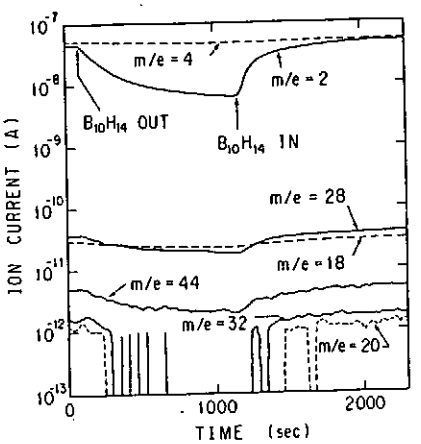

Deposition probe analysis

* Probe samples are located at two positions in JT-60U.
* 15 g of decaborane is processed in 10 hours, depositing 46 nm(average thickness) of boron layer onto the first wall.
* Boron films are toroidally nonuniform: thickness ranging from 150 nm near the injection port to 3 nm.

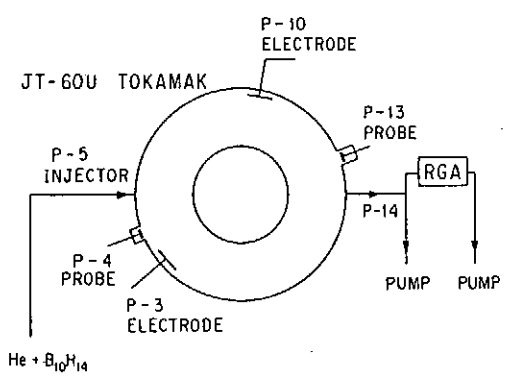

* Two sessions of boronization (July 30: 10 g, Sept. 1: 15 g) have been carried out.

Deposition probe analysis

* Polished Mo and polished/as-received graphite are used as probe samples.
* Polished graphite shows smooth surface with many pores, while as-received graphite shows rough surface.

As-received | Polished

x 200

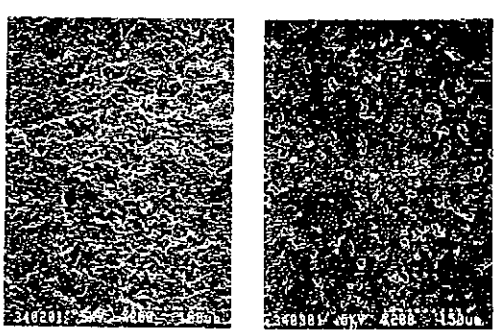

Distribution of coated boron

* Boron films are toroidally nonuniform.

Assumptions:
(1) Boron films are distributed at a center of injection port.
(2) Distribution follows an exponential form.

* Mean free path, λ, is obtained to be 2.75 m.

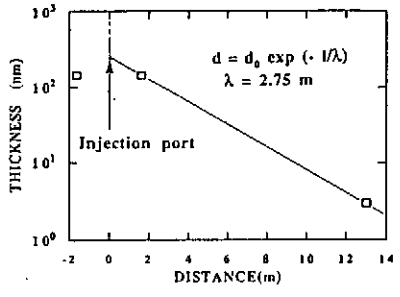

Properties of boron coated films

* Pure boron film is deposited during boronization.
* Hydrogen concentration in the film is 10%.
* The boronization effects in the tokamak should be taken into account of surface roughness.

Method:
#AES + Ar-sputter
(B, C, O, Mo)

#NRA (H)
$^{15}N + H = {}^{12}C + {}^{4}He + \gamma$-ray (4.43 MeV)

Probe sample:
Graphite
Moly.

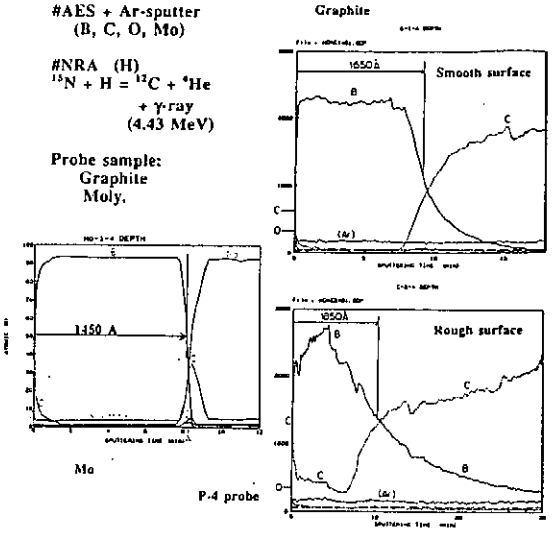

Properties of boron coated films

* Hydrogen concentrations are obtained by means of nuclear reaction analysis(NRA):

$^{15}N + H = {}^{12}C + {}^{4}He$ + gamma-ray(4.43 MeV)

* Hydrogen concentration is 10%.

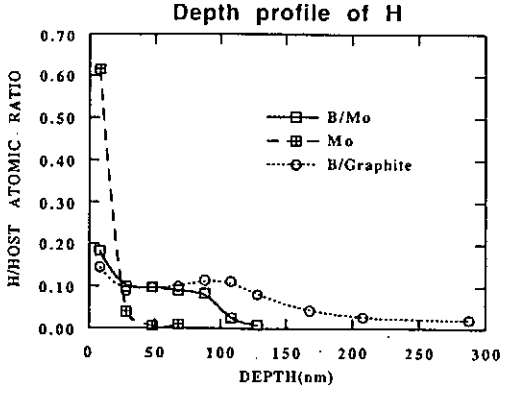

Z_{eff} and impurity level (OH discharge)

* Oxygen is reduced by an order of magnitude resulting in $Z_{eff} \sim 2$.

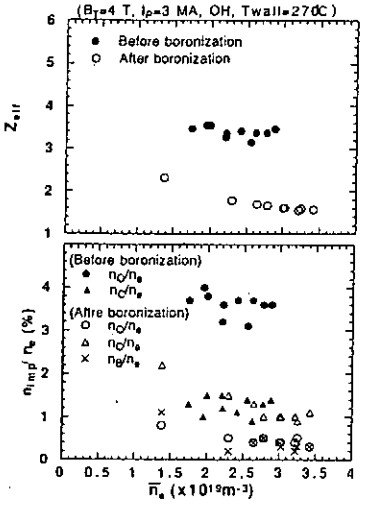

Z_{eff} and impurity level (OH discharge)

- Boronization has a capability of impurity reduction as the same level as previously attained after ~ 200 discharges and additional wall conditioning procedures, such as D_2/He Taylor-type discharge, He glow discharge etc..

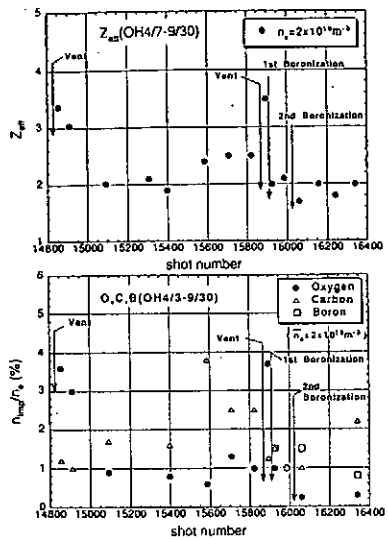

Z_{eff} and impurity level (NB heating discharge)

- 2nd boronization is more effective for oxygen reduction than 1st boronization, but prominent oxygen reduction is not observed.
- The major contributor to Z_{eff} is carbon.

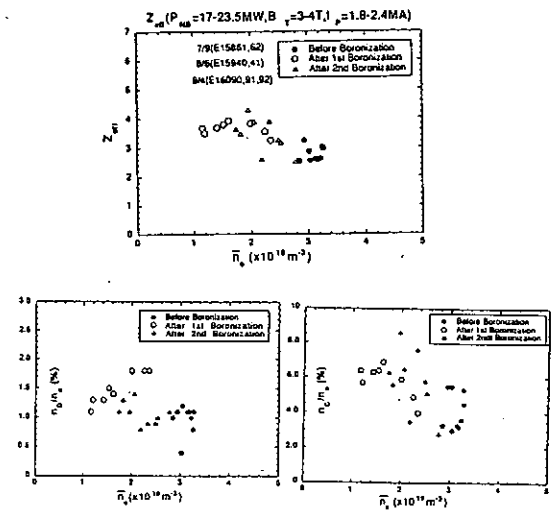

Particle recycling

- Boronization combined with subsequent wall conditioning reduced particle recycling flux for both OH and NB heating plasmas.

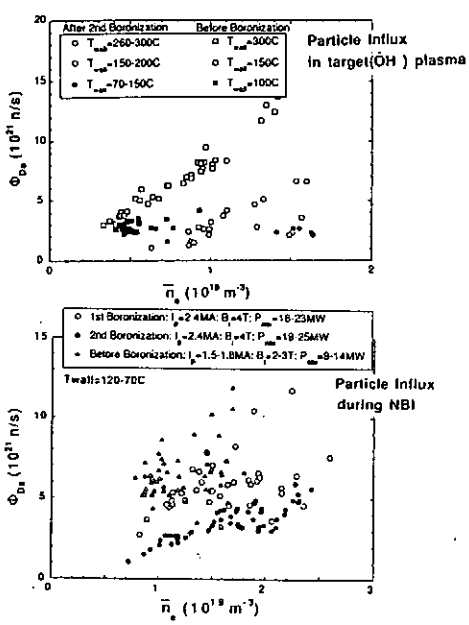

H/(H+D) ratio in plasmas

- In case of decaborane-based boronization, reduction of H/(H+D) ratio can be easily attained so that it is not necessary to use deuterated decaborane for boronization in order to avoid a dilution of fuel particles in D_2 discharge.

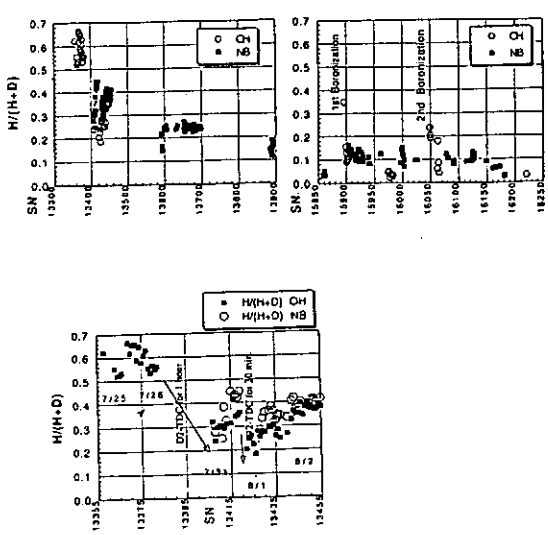

Summary

* Decaborane-based boronization produced boron film free from carbon and with 10% hydrogen.
* Present boronization were effective for oxygen reduction during OH discharges but not during NB heating.
* The major contributor to Z_{eff} was carbon.
* Present boronization were effective for reduction of particle recycling flux during both OH and NB heating discharges.
* Deposited boron films were toroidally nonuniform.
* Present results indicate that a deposition of thicker boron film with a better toroidally uniformity is required in order to improve plasma properties.

** Increase of decaborane injection ports is planned to coat the first wall by boron film with a better toroidal uniformity.

** The combined use of boronized graphite tiles for armor tile application and wall conditioning of in-situ boronization will be more effective to maintain the boronized surface over long-term operations.

Session 3: Developments of HHFC/Divertor and Energy Deposition

PLASMA FACING COMPONENT DEVELOPMENT AND HIGH HEAT FLUX TESTING AT SANDIA NATIONAL LABORATORIES

PRESENTED BY
ROBERT T. MCGRATH

JAPAN/US WORKSHOP P196
17-19 NOVEMBER, 1992
KYUSHU UNIVERSITY
FUKUOKA, JAPAN

PLASMA FACING
COMPONENT DEVELOPMENT
AND
HIGH HEAT FLUX TESTING
AT
SANDIA NATIONAL LABORATORIES

PRESENTED BY
ROBERT T. MCGRATH

JAPAN/US WORKSHOP P196
17-19 NOVEMBER, 1992
KYUSHU UNIVERSITY
FUKUOKA, JAPAN

A brief overview of SNL activities in FY92 will be presented:

I. PFC Design and Fabrication
   - The Phase III actively cooled Pumped Limiter for Tore Supra
   - New Armor Surfaces for the Advanced Limiter Test-II on TEXTOR
   - SNL contributions to the Advanced Divertor Program on DIII-D

II. High Heat Flux Testing and Materials Development

III. Disruption Studies

Tore Supra Phase III Limiter

Sandia, ORNL, Centre d'Etudes Nucleaires (Cadarache)

Sandia Staff

Richard Nygren	Robert McGrath
Jon Watkins	Tom Lutz
Joe Koski	Ben Tafoya
Jimmie McDonald	Chuck Walker
Greg Dale	Mike Hosking
Pat Hubbard	Frank Dempsey

TORE SUPRA PUMP LIMITER

Tore Supra Parameters

• Major radius	2.4 m
• Minor radius	0.7 - 0.8 m
• Plasma Current	1.0 - 1.7 MA
• Pulse length	30 - 60 S
• Toroidal field (superconducting magnets)	4.5 T
• RF heating (first phase)	
ICRH	6 - 9 MW
LH	8 MW
• Neutral beams	8 MW

SNL Phase III Activity Cooled Pumped Limiter For Tore Supra

Armor Material	PG and CFC
Heat Sink Material	OFHC Copper
Armor Attachment	Ti Cu Sil
Coolant	Water
– Flow Rate	7 m/s (central tubes) 10 m/s (leading edge tubes)
– Pressure	4.2 MPa
– CHF enhancement	Twisted tapes (leading edge tubes)
Surface Area Heated	60 cm X 60 cm
Pumping Slot Location	2.5 cm behind LCFS
Peak Heat Flux (steady state)	30 MW/M^2
Total Power Removed (steady state)	2.0 MW

Tora Supra Actively Cooled Pumped Limiter Development

- Materials Selection
- Establishment of a detailed CHF data base for the parameter range of interest
- Development and HHF testing of armor/coolant braze technology
- Plasma Engineering
  - Detailed analysis of power deposition vs particle exhaust
  - Pumped limiter system design for the entire machine
  - off normal event analysis - heat loads, RA electrons, eddy current forces
- Diagnostics Systems Design and Fabrication
- Limiter Head, drive mechanism & pumping system design and fabrication

Sandia National Laboratories

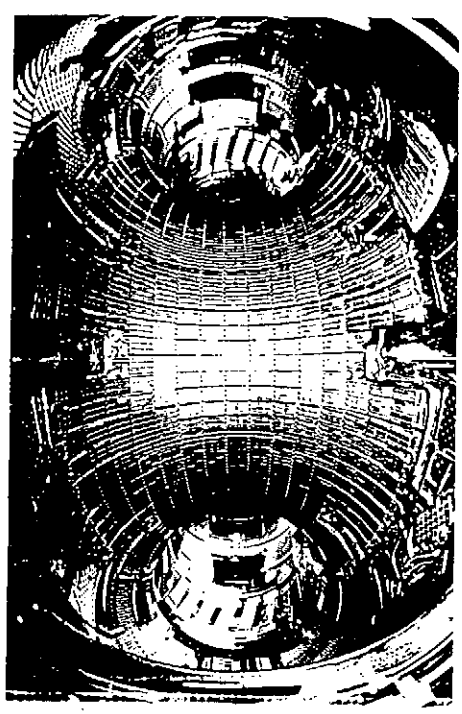

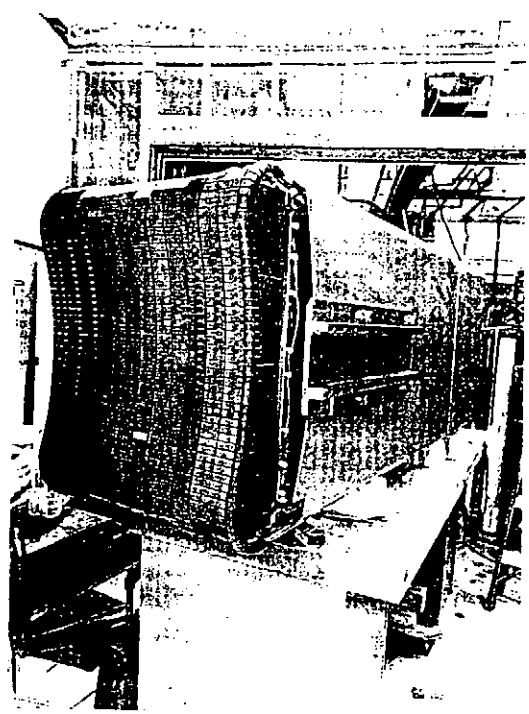

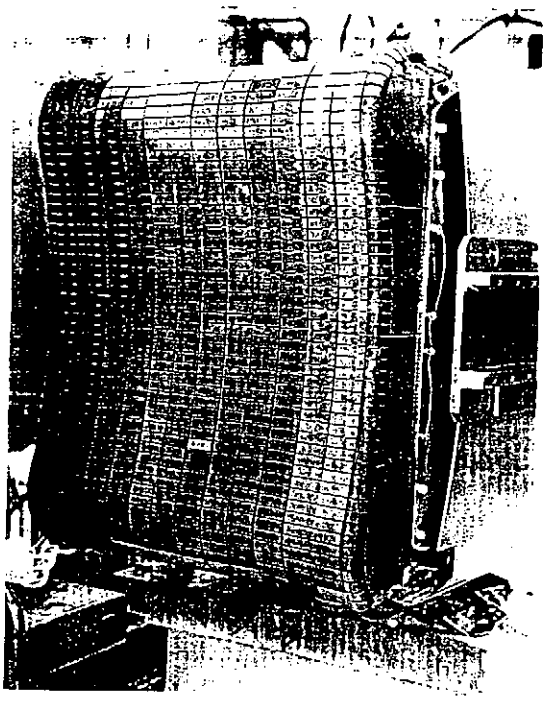

New Design of ALT-II* Armor Tiles
for Upgraded TEXTOR Operation

- In 1993 TEXTOR will begin operation with 10 s discharge and 8.0 MW total heating.
- The deposited energy onto ALT-II will be 400% greater than the original design specifications.
- The ALT-II armor tiles have been redesigned
  - Power deposition profiles have been optimized
  - Tile mass and thermal inertial capacity increased by the minimum amount possible
  - Particle exhaust optimized (Radial tile thickness = 20 mm)
  - Power peaking due to blade mis-alignment has been minimized.

* The ALT-II Program on TEXTOR is a continuing collaboration between KFA, NIFS, and the US/DOE/OFE

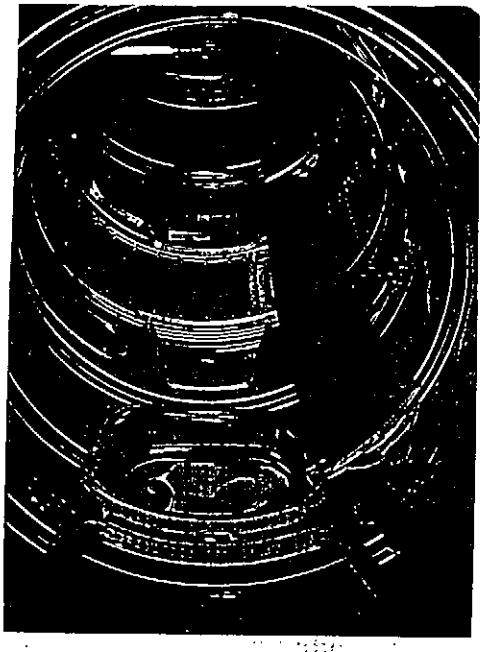

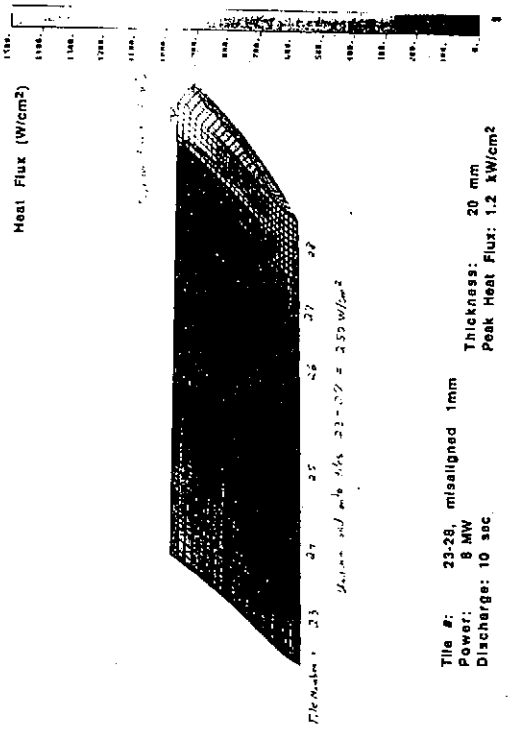

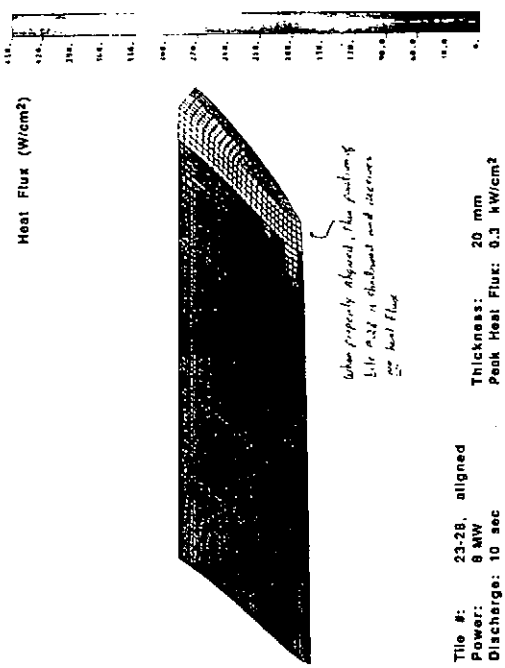

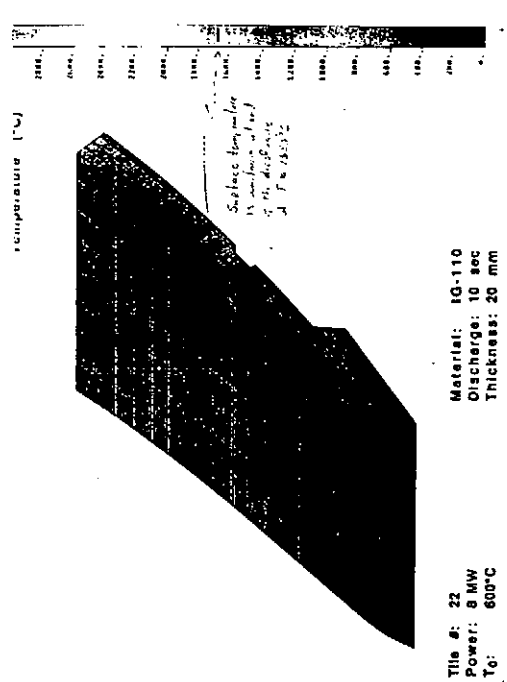

Optimization of New ALT-II Armor was acheived through

- Careful measurement of the boundary layer plasma conditions.
- Detailed analysis using 3D, time dependent heat transfer calculations with anisotropic material properties.
- Judicious material selection

Armor Tile Materials

– Tiles 7-13 and 16-22	IG-110
– Tiles 2-6 and 23-27	APG
– Tiles 1, 14, 15, 28	RG-Ti91 or CFC (TBD)

SNL contributes significantly to the DIII-D Advanced Divertor and Boundary Layer Physics Programs

- Fast Reciprocating Langmuir probes - design, fabrication and operation
- Divertor Floor Langmuir probe arrays - design, fabrication, and operation
- Divertor Materials Evaluation System (DIMES) (see presentation by C. Wong (GA) this meeting)
- Boundary Layer Plasma Analysis
  - Gaseous Divertor Operation & Impurity Transport
    - NEWT-1D - R. Campbell (SNL)
    - NEWEDGE (2D) D. Knoll (INEL) & R. Campbell (SNL)
  - Disruption Run Away Electron Generation
    - Tokdyn - R. Russo (SNL)

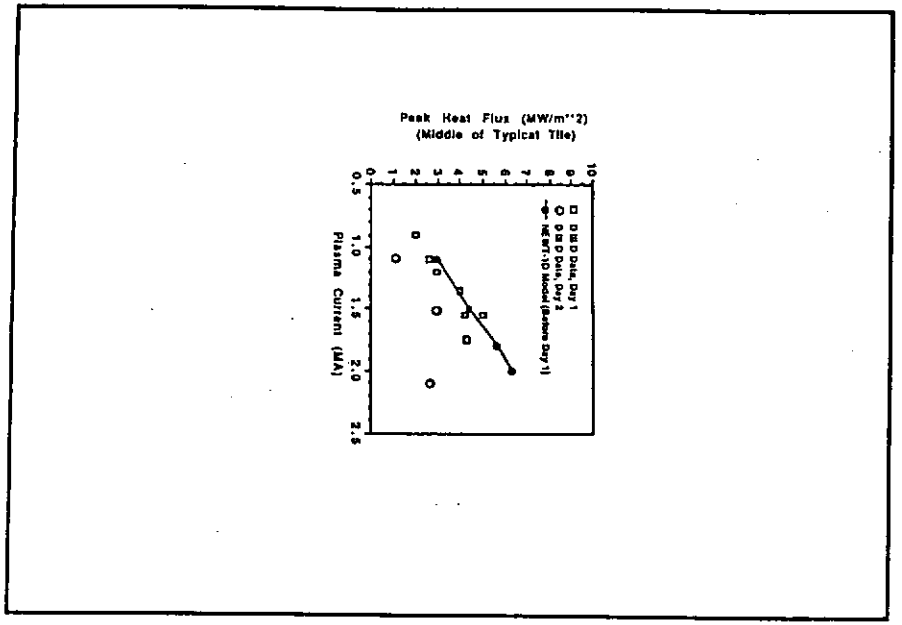

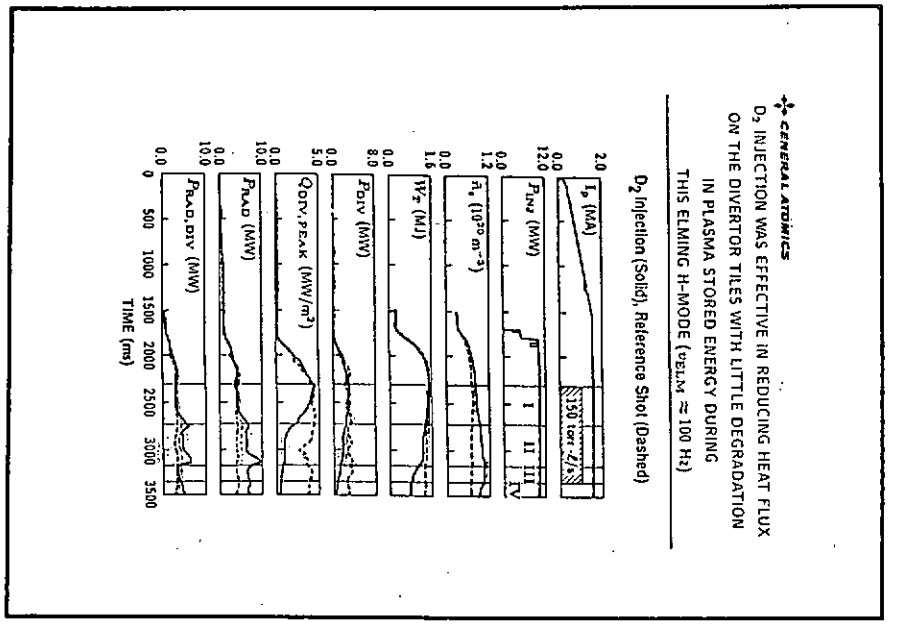

Gas Target Divertor Simulation on D III-D

- Examined Deuterium Puffing on D III-D (Similar to Shot 73786)

n_{sep}=2 x 10^{19}m^{-3}
$T_{e,sep}$=$T_{i,sep}$=150 eV
R_{recy}=0.98
α_{recy}=0.95

Full Plate-to-Plate Calculation
(No Assumption on Slot Throat Boundary Conditions)

Various Grids: 32x8, 64x16, 128x32

150-450 torr-l/sec D_2

Puff from Private Region

Pump on Inner and outer walls → Results in Geometry Similar to Slot Divertor

- At highest puff rates, results in quenching of flame front, peak heat loads reduced an order of magnitude.
- In extended volume near plate, T_e<1eV.
- Radiation zone moves toward X-point after puffing (similar behavior observed in D III-D in non-slot configurations) Movie of front migration available.
- Divertor acts like a cross flow heat exchanger.

Important Progress has Been Made with the NEWEDGE Code Under Development at INEL. (D.A. Knoll, P.R. McHugh, R. Campbell)

- Slot divertor calculations in D III-D geometry. Demonstrated thermal quenching, and radiation zone motion toward X-point. (Motion picture available)
- Plans to model Petrie's 73786 "trophy shot" for D_2 puffing.
- Comparison of NEWEDGE and NEWT-1D in slot divertor simulation:

Radiation Zone as Calculated by NEWEDGE

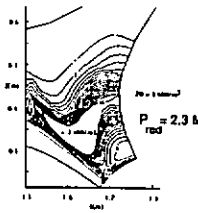

P_{rad} = 2.3 MW

Collapsed Region, Widths of Radiation Zone and Neutral Density are Similar

Profiles for Same Case from NEWT-1D

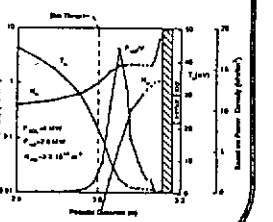

Sandia National Laboratories

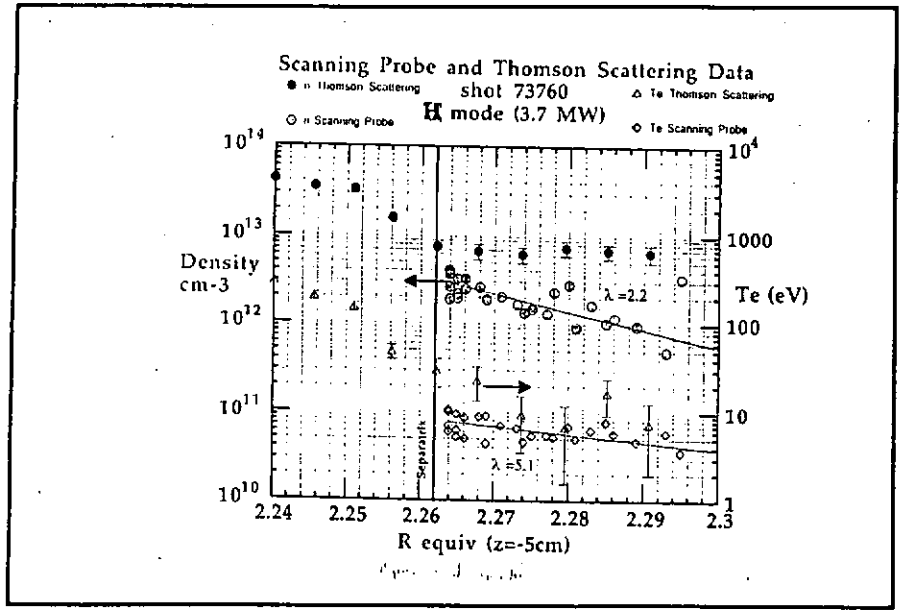
Scanning Probe and Thomson Scattering Data
n Thomson Scattering
shot 73760
Te Thomson Scattering
n Scanning Probe
H mode (3.7 MW)
Te Scanning Probe
Density cm-3
Te (eV)
λ =2.2
λ =5.1
Separatrix
R equiv (z=-5cm)

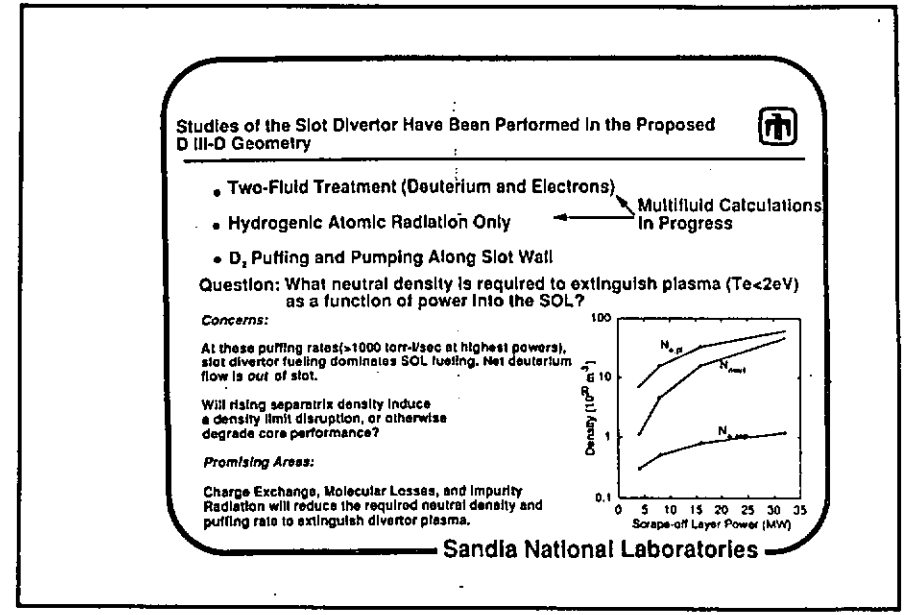
Studies of the Slot Divertor Have Been Performed in the Proposed D III-D Geometry
• Two-Fluid Treatment (Deuterium and Electrons)
• Hydrogenic Atomic Radiation Only
Multifluid Calculations In Progress
• D2 Puffing and Pumping Along Slot Wall
Question: What neutral density is required to extinguish plasma (Te<2eV) as a function of power into the SOL?
Concerns:
At these puffing rates(>1000 torr-l/sec at highest powers), slot divertor fueling dominates SOL fueling. Net deuterium flow is out of slot.
Will rising separatrix density induce a density limit disruption, or otherwise degrade core performance?
Promising Areas:
Charge Exchange, Molecular Losses, and Impurity Radiation will reduce the required neutral density and puffing rate to extinguish divertor plasma.
Density (10^20 m^-3)
Scrape-off Layer Power (MW)
Sandia National Laboratories

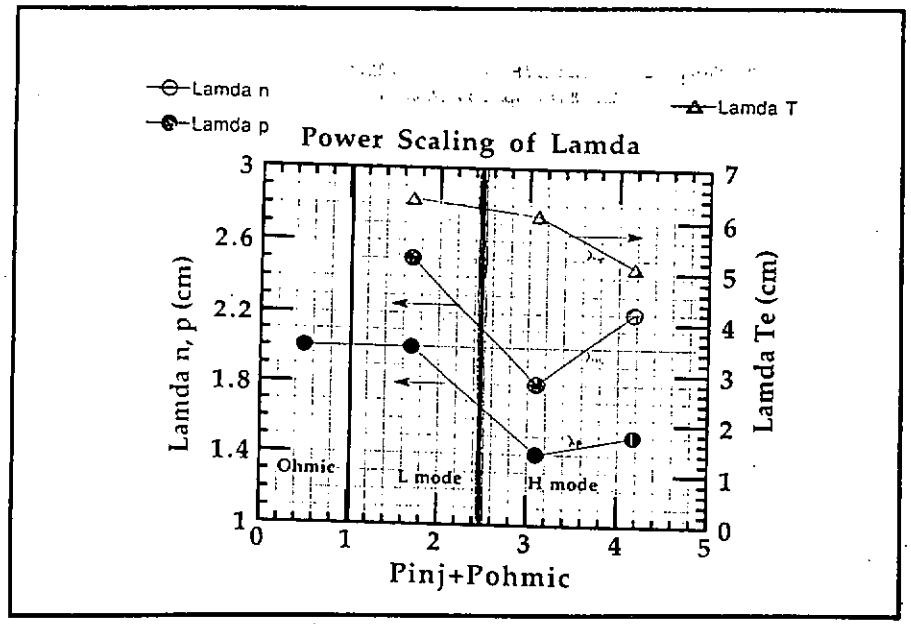
Lamda n
Lamda p
Lamda T
Power Scaling of Lamda
Lamda n, p (cm)
Lamda Te (cm)
Ohmic
L mode
H mode
Pinj+Pohmic

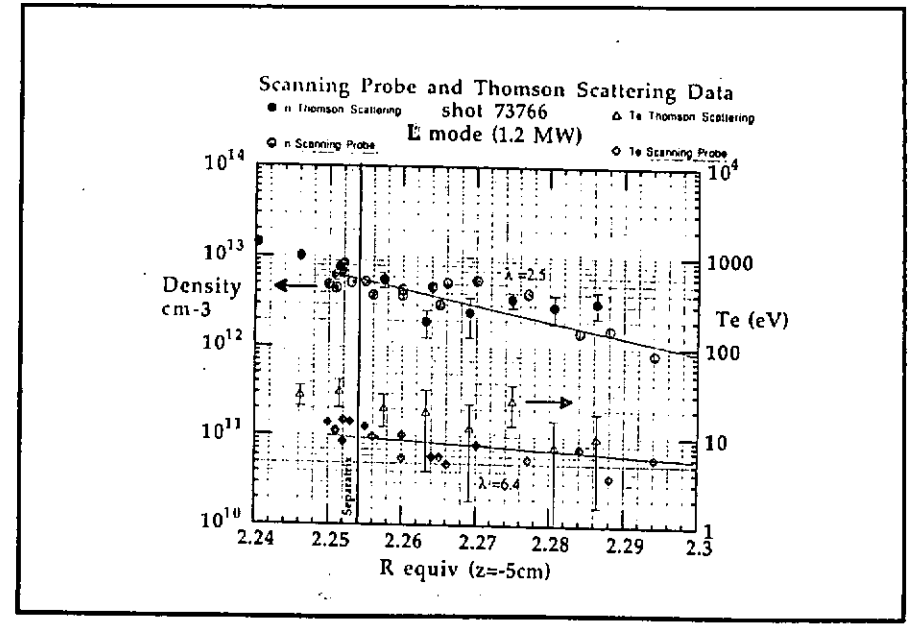
Scanning Probe and Thomson Scattering Data
n Thomson Scattering
shot 73766
Te Thomson Scattering
n Scanning Probe
E mode (1.2 MW)
Te Scanning Probe
Density cm-3
Te (eV)
λ =2.5
λ =6.4
Separatrix
R equiv (z=-5cm)

Runaway Electron Generation

- Plasma temperature drops rapidly (0.1-3 ms) from several keV to a few eV.
- The lower temperature raises the plasma resistance, increasing the loop voltage from less than a volt to several kilovolts.
- The plasma current falls while the collapsing poloidal filed inductively sustains the loop voltage
- Collisional friction forces scale with density and inversely with the 3/2 power of energy. Electrons in the outer radial portions of the plasma become collisionless.
- Collisionless circulating electrons acquire energy equal to the loop voltage each transit and quickly accelerate to MeV energies.
- If a sufficient number of electrons runaway, the high energy, low resistance portion of the current can dominates. The resistance is once again low, the loop voltage small and the current can stabilize at a plateau which is some fraction of the original current.

Sandia National Laboratories

Calculated and Measured Currents for
a) JET Discharge 16165,
b) JET Discharge 18058

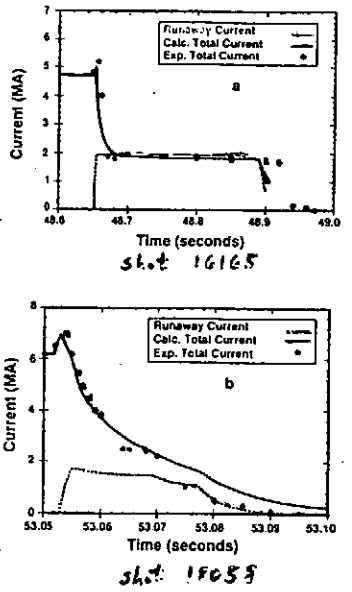

DIII-D Discharge 68768, and d) Discharge 68770.

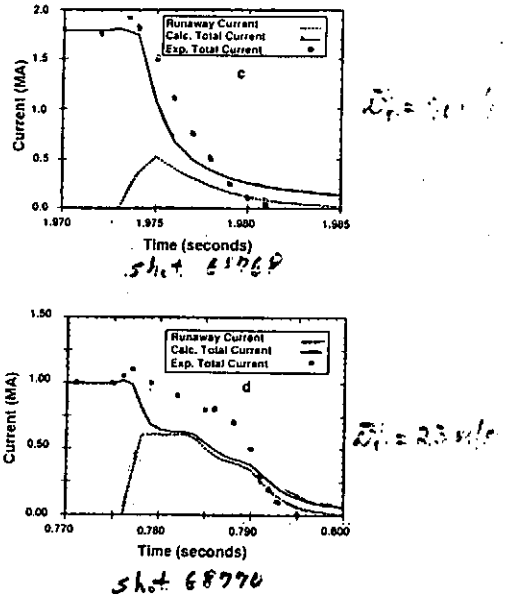

Calculated Current for ITER

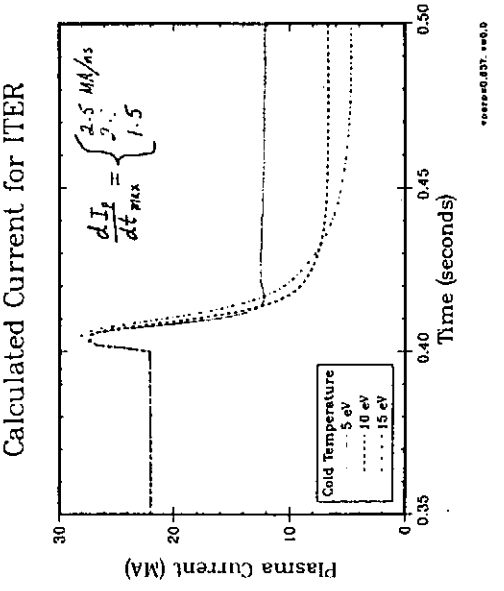

SNL's PLASMA MATERIALS TEST FACILITY

New Systems

- EBTS-1200 - Two 600 kW electron beam guns have been purchased. Installation to begin 7/93.
- Helium gas coolant circuit - Installed and operational.
  - Variable gas temperatures - up to 450°C
  - Peak operating pressure - 4 MPa

High Heat Flux Testing and Materials Development

- CFCs and CFC structures
- Be and Be structures
- Al and Al structures for SSAT/TPX
- CHF enhancement techniques
  - porous coating (Russia / US exchange & SBIR)
  - twisted fins and tapes (Japan / US exchange)
- Helium cooled microchannel heat exchanges (SBIR)

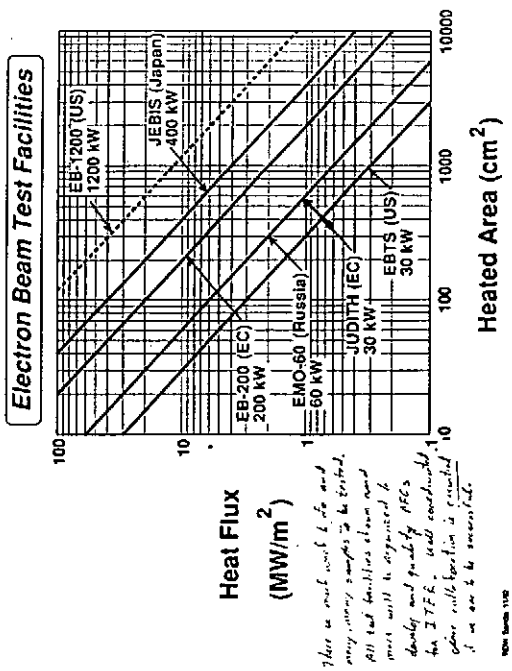

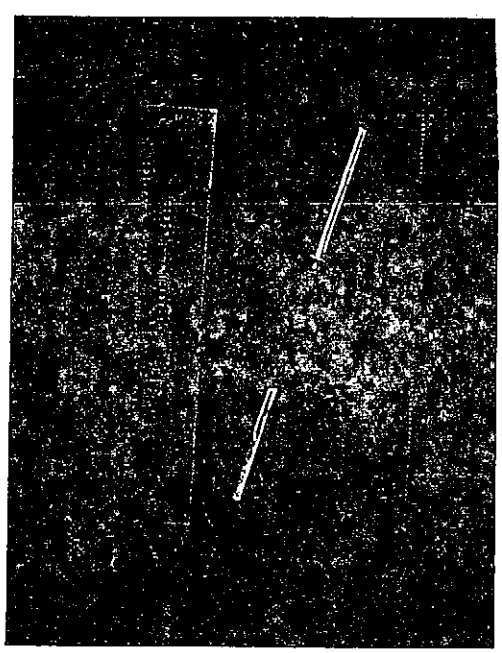

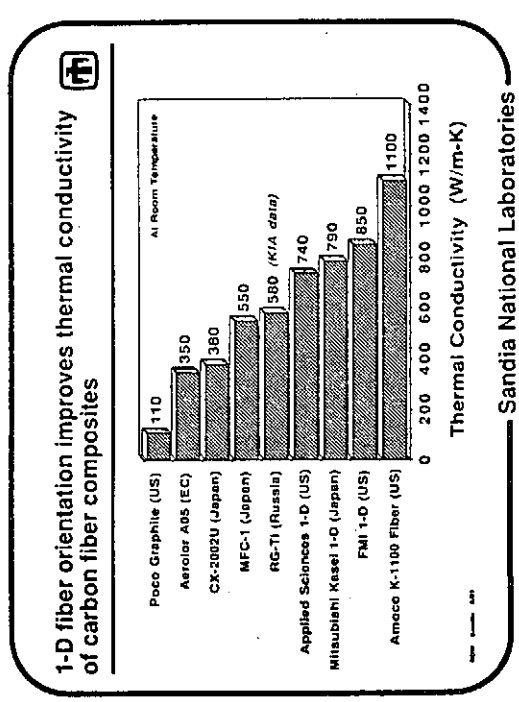

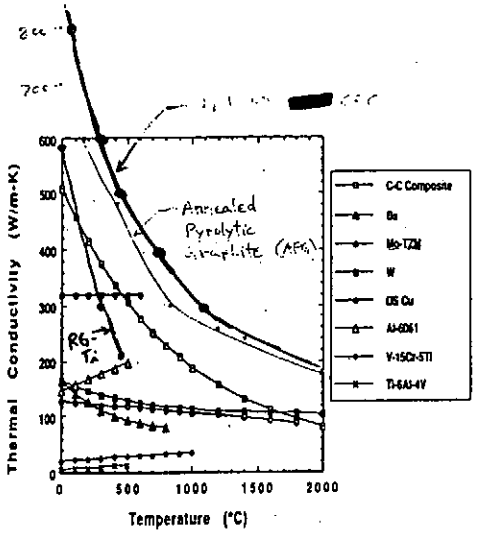

Figure 6. Thermal conductivity of candidate divertor armor and coolant structure materials

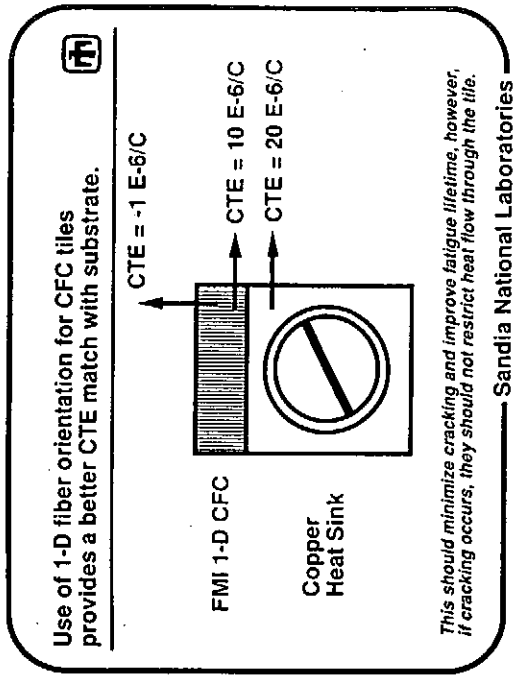

Neutron Damage Degrades The Thermal Conductivity of Graphites!

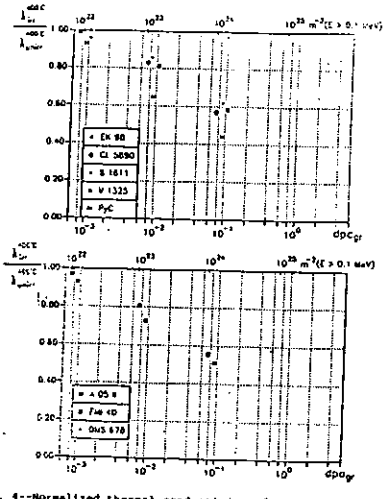

Fig. 4--Normalized thermal conductivity of various carbon materials after neutron irradiation at 400°C and measured at 400°C test temperature

Data provided by KfA Jülich

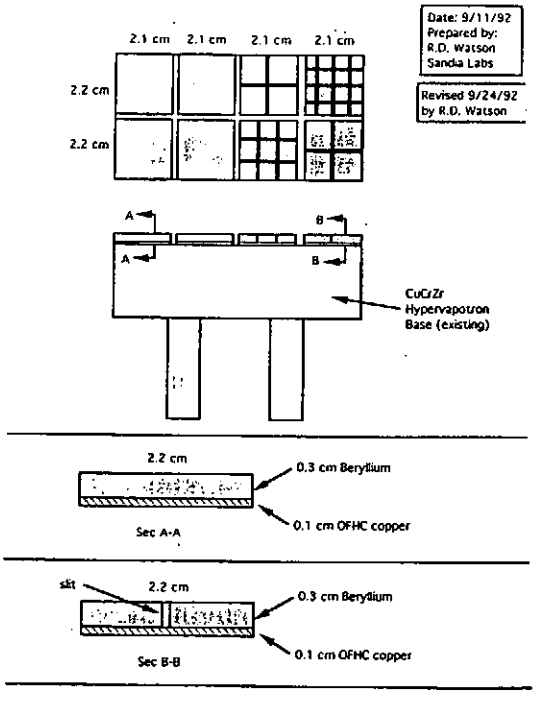

Brush-Wellman

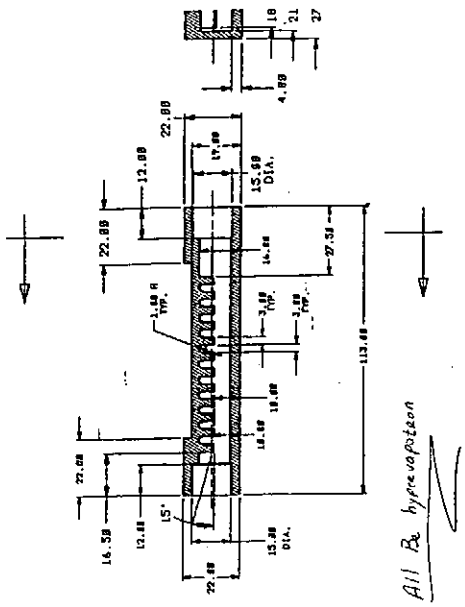

All Be hypervapotron

Beryllium Monoblock Divertor Mockups

Three Samples are being fabricated by Brush Wellman:

1. Slotted surface, 6 mm grid
2. Unslotted surface
3. 90% dense beryllium*

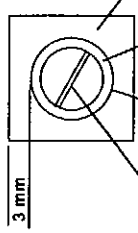

*This may reduce fatigue cracking.

Sandia National Laboratories

Los Alamos National Laboratory

U.S. Beryllium Laboratory for PFC's

- Plasma spraying of beryllium:
  - *vacuum and inert atmospheres*
  - *spherical, low-oxide (.09% BeO) beryllium powder produced by centrifugal atomization*
  - *higher as-deposited densities, ie., better thermal conductivity*
- Joining beryllium to copper:
  - Diffusion bonding
    effects of processing parameters on bond strength
  - Electro-deposition
    pretreatment to improve deposit adhesion
- Mechanical testing of beryllium:
  - *Thermal mechanical fatigue testing up to 800 C - (Gleeble)*

Materials Science and Technology Division

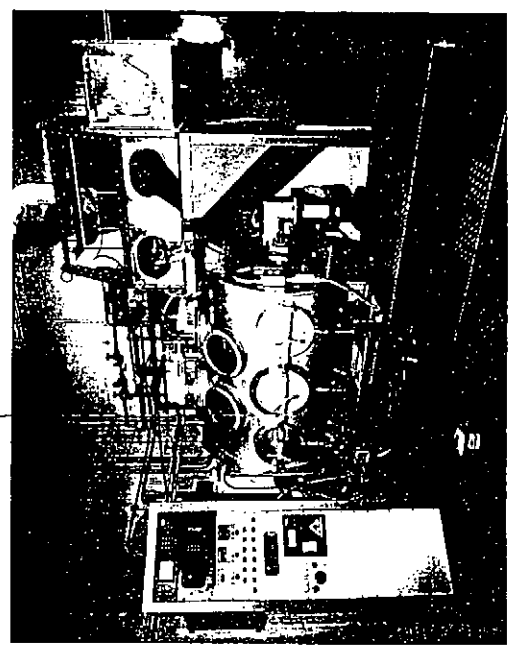

Aluminum divertor mockup e-beam tests

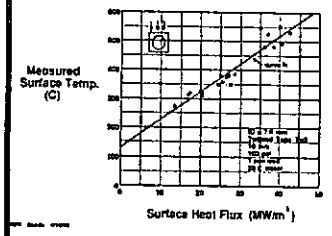

- Bare 6061 aluminum, 1 mm wall
- 30 second shots (steady-state)
- 50 MW/m2 (SS) with no failure
- This exceeds conventional design limits by 10 X.
- 20 MW/m2 & 20,000 cycles with no failure or cracking
- 40 MW/m2 & 1800 cycles caused surface cracking, but no leaks
- Internal corrosion was observed.

Sandia National Laboratories

Significant improvements in plasma sprayed beryllium have been achieved.

- Best density = 87 %
- Best thermal conductivity = 127 W/m-K
  (equivalent to 62% of pure beryllium)
- Heat treatment at 900 °C for 1 hour increased thermal conductivity by an average of 50 %.
- Relatively small variations in the spray deposition parameters have a major impact on thermal conductivity, but not density.
- A new facility at Los Alamos National Laboratory is ready to begin spraying beryllium with low BeO content (0.09%) in July, 1992.

Sandia National Laboratories

R&D GOAL: To develop an ITER-relevant Critical Heat Flux Correlation

Motivation...

Existing CHF correlations are based on data which do not include:

1. One-sided non-uniform heating
2. Very high subcooling
3. High heat fluxes (45-90 MW/m²)
4. Flow enhancement techniques:
   - twisted tape
   - hypervapotron
   - porous coatings
   - internal fins
   - helical wire insert
5. Non-uniform axial heating profile

Beryllium loses its ductility upon neutron irradiation

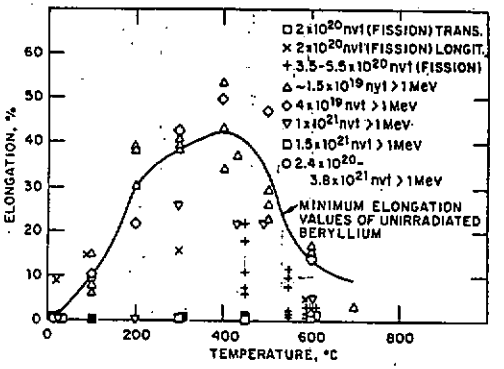

US FED/INTOR

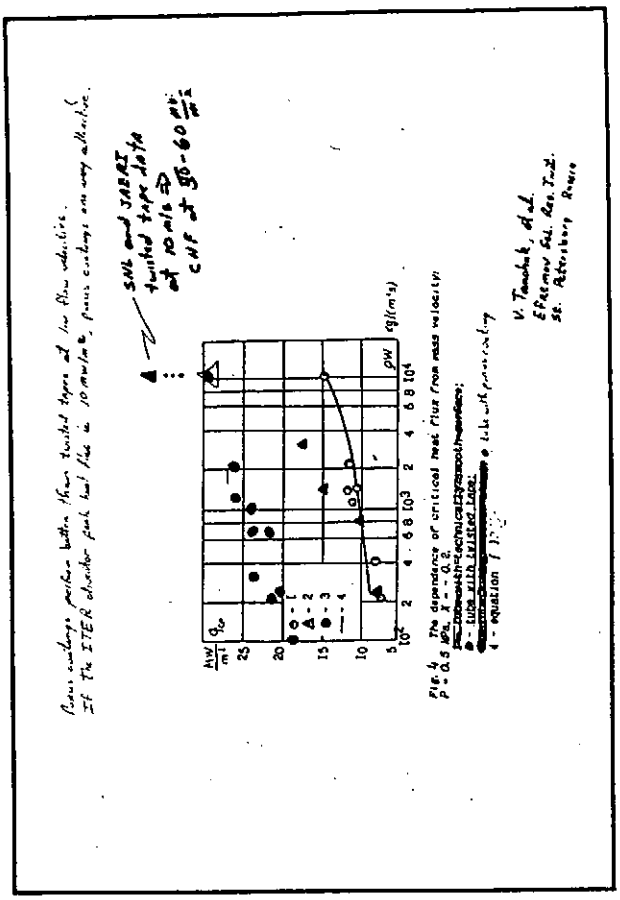

Advantages of Water and Helium Gas Cooling

ISSUE	WATER	HELIUM GAS
Better heat transfer	•	
Lower cost	•	
Lower pressure	•	
Better database	•	
Flexible materials selection	•	
Smaller manifolds	•	
Better safety		•
No corrosion/erosion		•
No critical heat flux		•
No 2-phase flow instabilities		•
Easier bakeout at 350°C		•
Easier tritium recovery		•
Easier cleanup after leak		•
Less neutron effects		•

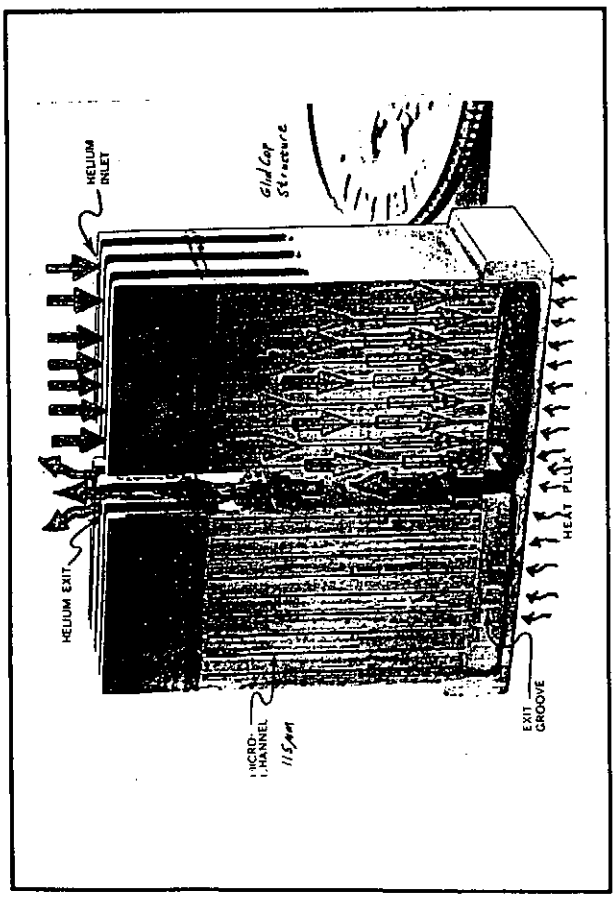

MATERIALS RESPONSE TO DISRUPTION LOADS

- Small Plasma Guns (10-15 MJ/M² on ~ 80 cm²)
  - PLADIS University of New Mexico
  - SIRENS North Carolina State University
- Large Plasma Guns (10-40 MJ/M² on ~1000 cm²)
  - Phillips Laboratories - Albuquerque, NM
  - VIKA, Efremov, St. Petersburg
  - 2MK-200, Kurchatov, Troisk
  - MKT, Kurchatov, Troisk
- Pulsed Plasma - Materials Interactions Modeling
  - A. Hassanein (ANL)
  - J. Gilligan (NCSU)
  - LASNEX (SNL)
- Tokamak Measurements of Material Response to Disruption Loads will be made using the DIMES probe on DIII-D

Plasma Gun Facilities for Tokamak Disruption Simulation

		VIKA	2MK-200	PLADIS	MKT
Location		Efremov, St. Petersburg	Kurchatov, Troisk	University of New Mexico	Kurchatov, Troisk
Power Density	MW/m2	100,000	100,000	100,000	30,000
Pulse Duration	~~88~~ ms	0.1	0.03	0.1	3-100
Energy Density	MJ/m2	12.5	10	10	1.2-6
Particle Energy	eV	10	6,000	10	3,000
Beam Diameter	cm	202	202	5	10

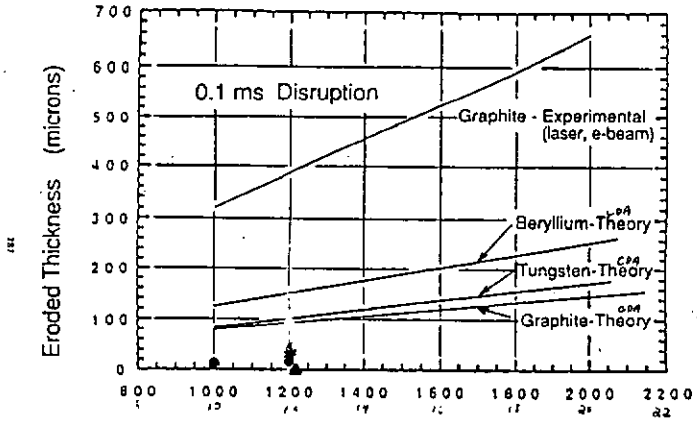

TPX Divertor Design

M. Ulrickson
Princeton University

Presented at the US-Japan Workshop
on
High Heat Flux Components
and
Plasma Surface Interactions
held at
Kyushu University
November 17-19, 1992

- o TPX Mission
- o TPX Machine Configuration
- o TPX Divertor Design
- o Divertor Heat Loads
- o Particle Pumping
- o Erosion

Mission of the Steady State Advanced Tokamak (SSAT)*

Steady State:

- Demonstrate integrated steady-state operating modes near q_{95}=3, β_N=3.0-3.5 %-m-T/MA.
  - Power and particle handling with divertors.
  - Non-inductive current drive.
  - Reliable plasma operation (no disruptions)
  - Steady state technology (S/C magnets, actively-cooled in-vessel components).

Advanced Tokamak:

- Optimize plasma performance → attractive reactor.
  - Goals: τ_E/τ_L>2, β_N>3.5, I_{BS}/I_P→100%.
  - Features:
    - Shaped cross section (κ≈2, δ=0.5)
    - Double null poloidal divertor
    - Deuterium operation
    - High aspect ratio (R/a=4.5)
    - Current profile control

* Also known as the Tokamak Physics Experiment (TPX)

GIIN 09/16/92 - 4

CURRENT SSAT CONFIGURATION WITH DOUBLE-NULL PLASMA

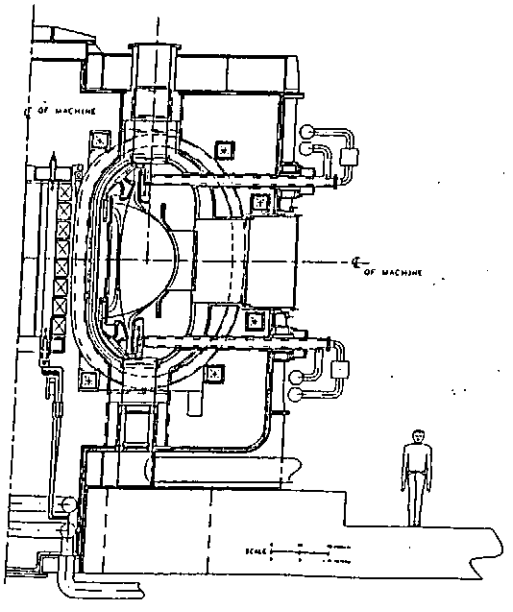

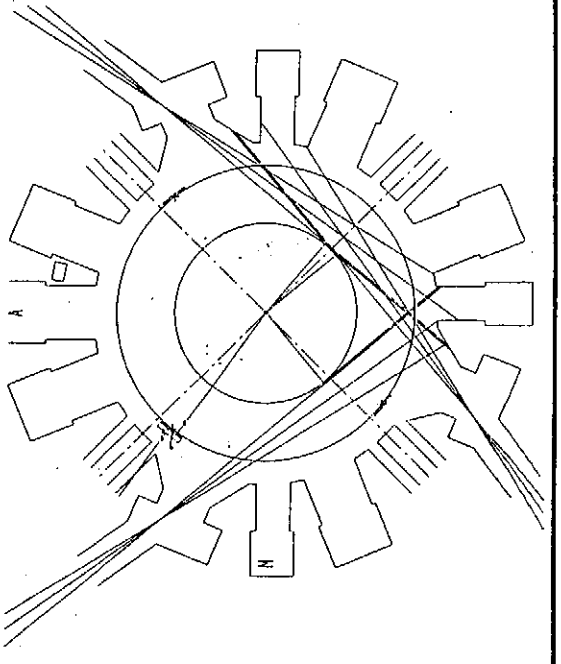

Tokamak Design Features

- Elongated, high-triangularity plasma
- Double-null poloidal divertor (top and bottom pumping)
- Actively cooled PFC's
- Internal passive structure
- Titanium alloy vacuum vessel
- Neutron shield
- Superconducting magnet system
- In-vessel remote maintenance

Machine Parameters

	Reference[1]	Maximum[2]	
Major radius, R_0	2.25		m
Minor radius, a	0.50		m
Aspect ratio, R/a	4.5		
Elongation, κ_x	2.0		
Triangularity, δ_{95}	0.5		
Toroidal field, B_T	3.35	4.0	T
Plasma current, I_p	1.9	2.0	MA
Pulse length	1,000	>>1,000	s
Neutron budget	5×10^{21}		p.a.
Installed heating:[3]			
Neutral beam (Co)	16	32	MW
ICRF	12	18	MW
Lower hybrid	1.5	≥3.0	MW
Electron cyclotron		t.b.d.	

1 Basis for design scenarios
2 Tokamak limits.
3 Initial complement:
NBI: 8 MW
ICRF: 8 MW
LH 1.5 MW

Divertor Design Choices

- High-heat-flux targets plus baffling enables divertor to handle Day 1 heat loads (with reasonable peaking factors) and supports gaseous/radiative target optimization.
- Carbon selected as the baseline material.
  - More forgiving of high plasma temperatures than high-Z. Can switch to high-Z if future developments warrant.
  - Better power handling and more disruption-resistant than beryllium.
- Configuration is being optimized based on a number of factors:
  - Gas isolation
  - Operational flexibility
  - Pumping
  - Diagnostic access
  - Reconfigurability
  - Remote maintenance

Expected Divertor Conditions: Modeling

- Maximum power to divertor (P_{Heat}=30 MW):
  Outer: 7.9±1.8 MW Inner: 2.0±1.2 MW
- Predictions from 2D Scrape-off plasma modeling for "standard" (non-gas-target) divertor operation:
  - B2 Code
  - Outer divertor, χ_e=2 m^2/s, 22° target angle

P_{heat} (MW)	32	18
P_{div} (MW)	8.4	4.7
q_{peak} (MW/m^2)	10.4	6.1
$T_{e,div}$(eV)	54	42
$T_{i,div}$ (eV)	192	127

- Temperature predictions have large error bars, but q_{peak} is more robust to model uncertainties, e.g. in neutral recycling and impurity line radiation.

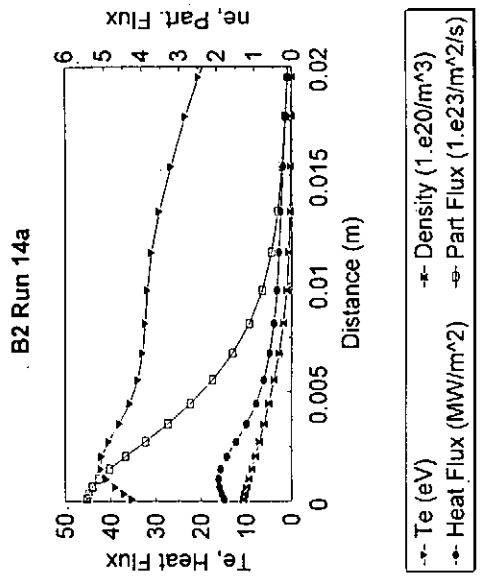

power split
M. Ulrickson
Memo
10/28/92-01

M. Ulrickson
Memo
10/28/92-02

PFC Element No.	Type of PFC	R (m)	as (m)	Area (sq. m)	Bulk Plas Radiation (MW)	Rad from Div Region (MW)	Particle Heat Load (MW)	Ripple Loss (MW)	NB Sh Thr Heat Load (MW)	Total Heat Load (MW)	Peak Heat Flux MW/m2	Average Heat Flux MW/m2
1	Inboard limiter	1.65	0.67	6.85	3.66	0.31				4.37	2.44	0.63
2	Lower Inbd passive plate	1.65	0.35	3.73	0.99	0.17				1.16	0.62	0.31
3	Lower Inbd div target	1.93	0.47	4.78	1.16	1.26	4.22			6.64	15.78	1.41
4	Lower Otbd div target	1.92	0.51	6.15	1.03	1.33	8.51			10.86	4.99	1.76
5	Lower Outbd div target	2.04	0.78	10.00	0.57	1.37	13.92			16.36	15.44	1.64
6	Low Outbd passive plate	2.47	0.58	8.00	2.02	0.40		1.49	0.10	4.00	2.02	0.44
7	Poloidal limiters	2.75	1.19	1.39	0.63	0.08				0.71	4.99	1.40
8	NB Shine thru dumps			1.79	0.63	0.08			2.21	2.92	1.64	1.64
9	Outbd VV, Ports, RF....	2.73	1.19	16.89	6.04	0.36				6.79	0.80	0.40
10	Upper Outbd passive plate	2.47	0.55	9.00	2.02	0.40		1.49	0.10	4.00	2.02	0.44
11	Upper Outbd div target	2.04	0.78	10.00	0.57	1.87	13.92			16.36	15.44	1.64
12	Upper Otbd div target	1.92	0.51	6.15	1.03	1.32	8.51			10.86	4.99	1.76
13	Upper Inbd div target	1.93	0.47	4.78	1.16	1.26	4.22			6.64	15.78	1.41
14	Upper Inbd passive plate	1.65	0.35	3.73	0.99	0.17				1.16	0.62	0.31
	Total			94.67	22.50	11.25	53.30	2.98	2.80	92.82		0.98

Expected Divertor Conditions, cont'd.

- DIII-D power accountability suggests P_{div}/P_{heat} assumed by TPX (60%) may be conservative.
  (But we need to find the missing power and be able to handle it!)
- Summary: heat loads for reference TPX conditions:

TPX Conditions	P_{heat} (MW)	Basis	(q_{peak}) (MW/m^2)	w/ peak. factors
Design	30	Model	9.8	~20
Design	30	DIIID Extrap.	~12	
Day 1	18	Model	6.1	~12

- Temperature expectations for TPX conditions are more uncertain due to model sensitivities and lack of low-density data base.

Divertor Functional Requirements

- Exhaust plasma heat and particle losses:

Conditions	Heat loss	Particle loss
Design	30 MW	$5x10^{21}$ sec^{-1} (75 torr-l/sec)
Day 1	18 MW	$3x10^{21}$ sec^{-1} (50 torr-l/sec)

- Support clean, high performance plasmas.
- Survive at least ~1 year of standard operation.
- Be diagnosable and reconfigurable to support divertor optimization and development.
- Be remotely maintainable.

Divertor Philosophy

- Divertor development is an important part of the SSAT mission.
- Baseline configuration includes baffles to permit optimization of gaseous/radiative target operation from the beginning. This is necessary in order to handle the full heating complement (30 MW).
- However, targets and baffles will be of high-heat-flux design (graphite surface, active cooling) in order to handle Day 1 heating complement (18 MW) under standard operation.

GHN 09/1692 - 10

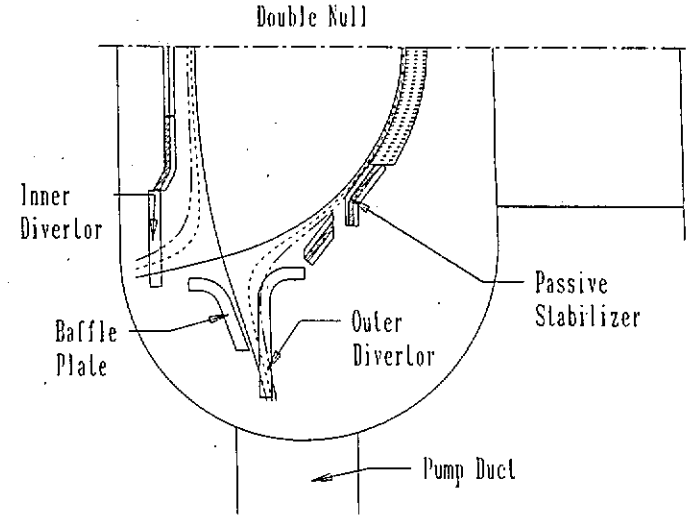

TPX Particle Pumping Requirements

Case	Q gas (part/sec)	Q gas (Torr l/sec)	Q gas (Pa m^3/s)	Expected Pressure (Torr)	Expected Pressure P (Pa)	Pumping Speed S(l/sec)	Pumping Speed S (m^3/s)
Ndotmax	5.603E+21	83.47	11.13	0.001	0.133	83475	83.5
NdotNB (assumes 24 MW NB)	2.782E+21	41.44	5.52	0.001	0.133	41438	41.4
Npelinj (assumes 12 MW NB)	4.213E+21	62.76	8.37	0.001	0.133	62756	62.8
Ngasfuel (efficiency = 0.1)	5.603E+22	834.75	111.29	0.015	2.000	55650	55.6

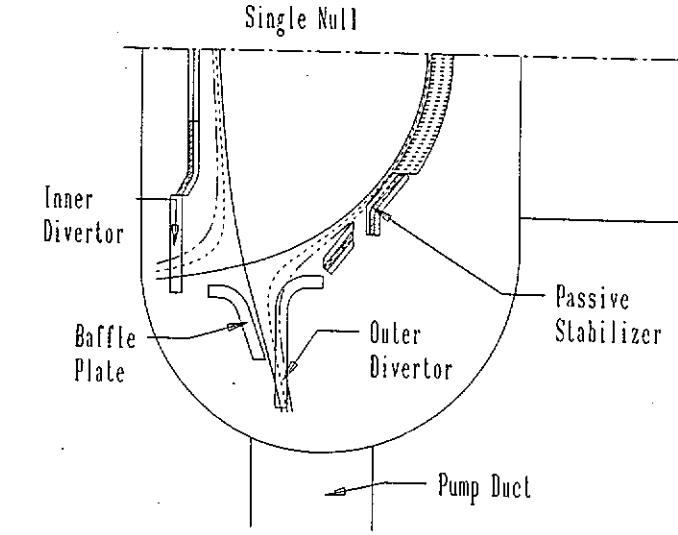

DEGAS Modeling Results

	Per Unit Length	Total (sec^{-1})
Input D^+	3.00×10^{20} /cm/s	4.24×10^{23}
Exiting Atoms	2.58×10^{18} /cm/s	3.65×10^{21}
Exiting D_2	5.46×10^{18} /cm/s	1.54×10^{22}

Recycling coefficient, R = 0.955

Pumping Results

Neutral D_2 density near the duct: 4.0×10^{13} /cm^3

Neutral D_2 Pressure near duct: 1.2 mTorr
0.16 Pa

Total Particle Throughput: 141 Torr l/s
18.8 Pa m^3/s

PRELIMINARY EROSION ANALYSIS
LIFETIME COMPARISONS IN 1000'S OF SEC PER CM
(1 YR = 200,000 SEC OF FULL PERFORMANCE EQUIVALENT OPERATION)

Q-PEAK (MW/M²)	1	10	10	10	10	10
$T_{e_{pk}}$ (eV)	10	20	42	75	150	267
$T_{i_{pk}}$ (eV)	24	48	100	179	357	636
$n_{e_{pk}}$ (10^{14}/cm³)	0.48	1.2	0.4	0.17	0.06	--
CARBON (1200°C)	4505	170	162	164	162	168
BERYLLIUM (800°C)	3154	332	343	509	--	168
MOLYBDENUM (1200°C)	157680	7884	2426	464	RUNAWAY	RUNAWAY
TUNGSTEN (1200°C)	315360	315360	22526	3154	RUNAWAY	RUNAWAY

- ESTIMATES BASED ON PEAK NET EROSION RATES (<1 CM WIDE) AND NEGLECT STRIKE POINT VARIATIONS.
- NUMBERS HAVE SIGNIFICANT ERROR BARS DUE TO UNCERTAIN PLASMA CONDITIONS AND INCOMPLETE MODELS (E.G. IMPURITY TREATMENT).
- DISRUPTION EROSION IS NOT INCLUDED.

HIGH POWER TESTS OF POSSIBLE FIRST WALL MATERIAL FOR JET

presented by H D Falter, JET

1 Main Test Facility

1.1 NB Test Bed Parameters

number of beams	2
power	2x4 MW
Voltage	<160 kV
peak power density	120 MW/m² per beam
pulse duration	≤ 10s
beam particles	H, D, He
shielding	2 m concrete

beam profile (120 kV hydrogen beam)

distance from beam source (metres)	2.48	4.82	6.6	11.2
peak power density (MW/m²)	100	110	100	60
vertical beam width for p>0.8 p_{max} (mm)	240	184	137	135
vertical beam width FWHM (mm)		254	195	270
horizontal beam width (80% / FWHM) (mm)	60/135	94/145		

Vacuum system

length of the beam line (m)	11.2
volume (m³)	90
pumping speed for hydrogen	10^6 4000 l/s
Access port NIB	full cross sect.
Access port Target Tank (m)	1.5

water cooling

highest pressure (bar)	10
pressure head (bar)	6.5
flow (m³/h)	800
temperature (°C)	15 – 50

view graphs: photograph.

page 2

Main JET Neutral Beam Test Bed (rear) and Beryllium test rig (front left). The Be test rigs uses all supplies from the main test bed.

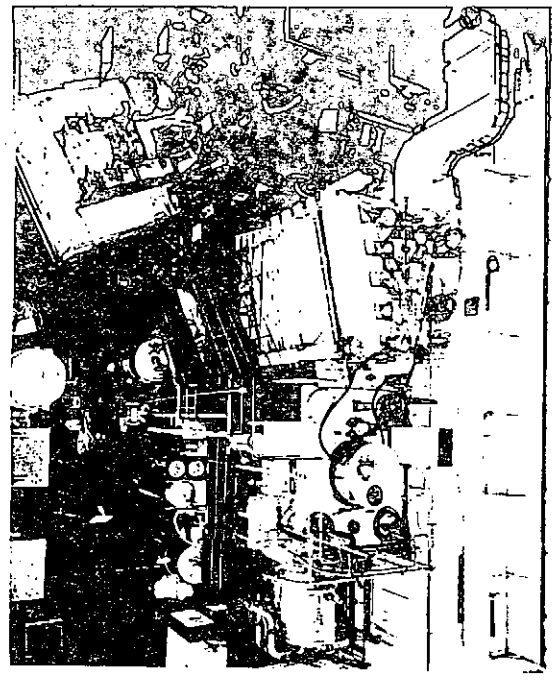

1.2 Tests

1.2.1 Inertial composite graphite tiles

1.2.1.1 Tile material

Material from 4 European, 1 Japanese, and 1 US supplier supplied as part of a tender for material with k>150W/m/k, density > 1.7 gr/cm³ and delivery time of 6 month for 1.5 tons.

1.2.1.2 Test procedure

2 pairs of tiles heated with power densities between 5 and 20MW/m². Surface temperature measured as a function of time with an AGA IR system.

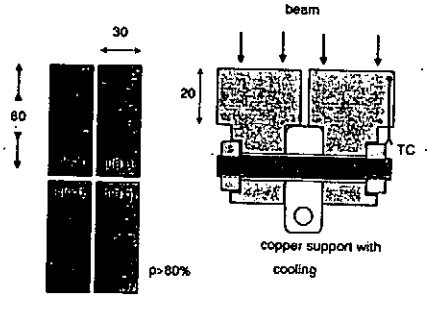

page 4

corrected AGA surface temperatures

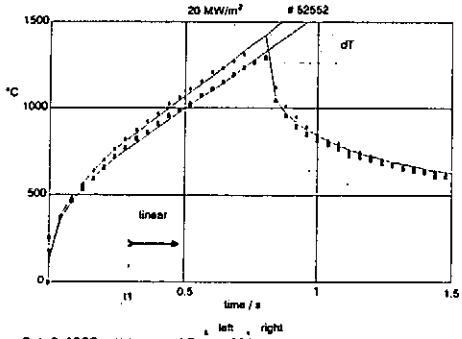

left right

T=A+B×SQRT(t−t0) for t<=t1, & T=A+B×SQRT((t1−t0)+1/2×B/SQRT(t1−t0))×(t−t0) for t>t

left: A=120, B=1300, t0=0, t1=0.3, dT=140, Right: A=120, B=1200, t1=0.3, dT=20

- Temperature rise and temperature decay fit well with $\sqrt{time}$ law for temperatures < 1000°C during the heating phase and for the first second during the cool down.
- A step dT of the order of 100 °C has to be assumed at the beginning of the heating and cooling phase. This step could be caused either by stray light from the beam plasma or from the temperature difference between fibres and graphite matrix.
- The fitting constant B is proportional to $\sqrt{1/(density \times conductivity \times spec.\ heat)}$

page 5

1.2.1.3 Test Results

- 13 pairs of CFC tiles and 2 pairs of fine grain tiles tested.
- 4 tiles meet the technical specification (k > 150 W/mK).
- The best tile is not available within the time scale of the tender (6 month).
- Comparing the selected tile with the best tile, peak power density is limited to 65% of that obtainable with the best tile for the same pulse duration, or, at equal power densities, the best tile would allow twice the pulse duration compared with the selected tile.
- All tiles withstood the test without damage. Power densities of up to 80 MW/m2 were used for some tiles..

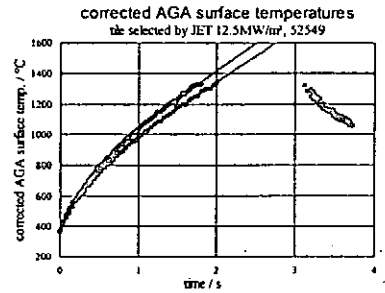

left A=150. B=820. t0=-0.06. t1=1.4 - right: A=150. B=670. t0=-0.06. t1=1.4

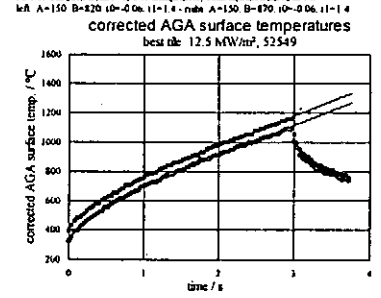

left: A=270. B=430. t0=-0.08. t1=1.3 - right: A=170. B=510. t0=-0.1. t1=1.5

Table of test results.

Resistivity B gives temperature rise T in °K per MW/m² and per second in the range where $T \propto \sqrt{time}$.
For times > t, the temperature rise is linear with time.
dT is the temperature offset used for the fits.
B_{corr} is derived from a later calibration of the surface temperature. The ratio between B and B_{corr} is constant.

<10MW/m²					12.5MW/m²					20MW/m²				
B	Bcorr	t1	dT	test	B	Bcorr	t1	dT	test	B	Bcorr	t1	dT	test
										50		>p	150	1
					47	40	1.3		8	48	41	0.8	110	8
										56		>p	120	1
					111		1	180	2	125		>p	160	2
					86.8		1.7	240	2	104		>p	300	2
					100		1	180	3	108		>p	190	3
					94.4		1.4	120	4					
					92.8		>p	120	3	95		>p	220	3
					72			115	4	98				4
					75	68	1		8	76	63		120/2	8
93		1.2	0	5	100		0.4	100	5					
113		1.3	0	5	115		0.38	150	5					
94.5				6	81.6		0.5	40	6	81		>p	120	6
98.2				8	97.6		0.5	180	6	107		>p	120	6
67		1.9	100	7	71		>p	100	7	70		>p	200	7
73.5		1.6	70	7	83.2		1.3	100	7	84		0.42	180	7
108	94.9	>p	100	9	112	99.2	>p	150/1	9	115				9
91.8	76.6	>p	70/60	9	88	72		160	9	90				9

6 sheet

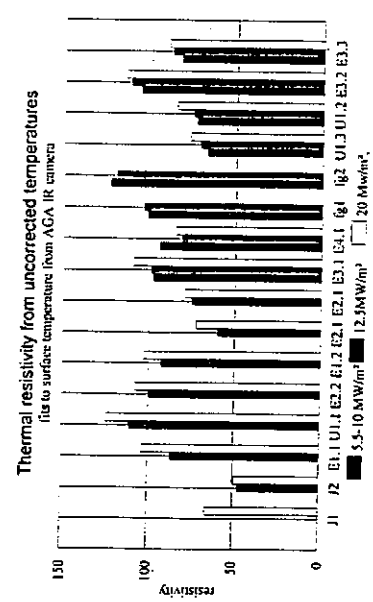

Summary graph for the inertial graphite tile test

1.2.2 Actively cooled CFC tiles

1.2.2.1 Test sections and test procedure

Test sections were monoblocks from NET made from Aerolor CFC brazed onto TZM pipes (2 sections) and TT 20002CX brazed onto glidcop. Two test sections together were exposed to a dc beam for up to 9s.

1.2.2.2 Result

a no deterioration of the tile temperature during the test

b some tiles have higher surface temperatures

c tiles are too small for good measurements with the IR system.

d at excessive tile temperature a clear release of hydrocarbons can be seen

e all tiles were mechanically stable

f the best tile (MF1) and the tile selected for the JET divertor (Dunlop) where tested with power densities of up to 80MW/m² without mechanical damage apart from errosion of the graphite matrix of the Dunlop tile.

tank pressure and temperature for pulse 52995 - 14 MW/m2

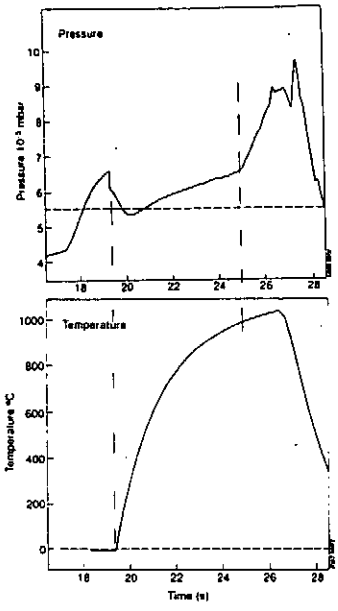

IR and ccd pictures from actively cooled CFC tiles.

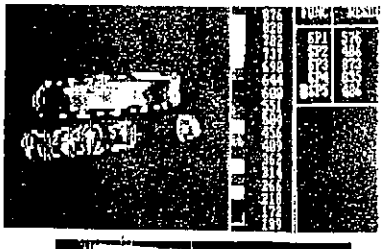

IR camera 440 ms after beam off (viewed from left)

CCD camera 440ms after beam off (viewed from right)

CCD camera 640 ms after beam off (viewed from right side

2 Be test rig

2.1 Test Rig Parameters

Beam:

beam source	modified JET PINI with reduced extraction are
power	<1 MW
peak power density	40 MW/m2
exposed area	200 × 50 mm²
distance from beam source	2m

Vacuum system

Volume	1m³
pumping speed	<1000 l/s (system operated at the pressure of the plasma source)
Access port	400 mm id

2.2 Tests

2.2.1 Inertial Beryllium tiles

2.2.1.1 Test procedure

- Beam with 100 ms on/ 150 ms off
- heating to app 1000°C
- two test sequences:

a first test: tiles with larger castellations – cooled to room temperature between pulses

b second test : two tiles from first test plus two tiles with smaller castellations - not actively cooled (300°C before pulse)

2.2.1.2 Material

- S 65 B Berylium from Brush Wellman machined into blocks of 80x32 mm² exposed surface and 20 mm min thickness

2.2.1.3 test result

- first test: Tiles crack at the surface at power densities of 14 MW/m², (3 pulses at higher power density (18 MW/m2] at the beginning). Temperature cycles from 50°C upwards

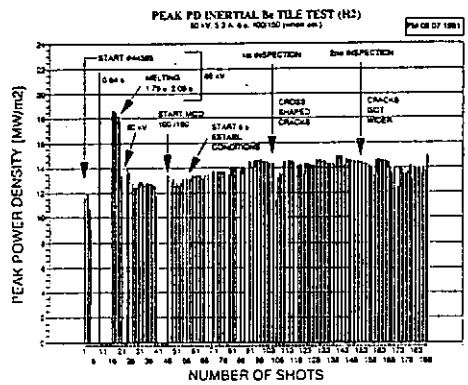

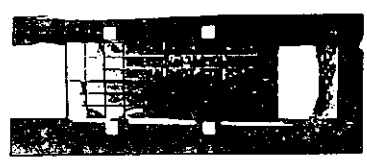

- second test with radiation cooling only and 6x6 mm castellation shows that tiles with smaller castellation are less sensitive to cracks. (tiles cycled between 300 and 900 °C).
- The tiles with large castellations (16x10 mm) perform better than in the first test (cracks at power densities above 20MW/m²)
- Influence of brittle transition for cycling from room temperature has to be further investigated.
- Lateral cracks close to the surface have been observed after the tests on tiles with surface melting. It is unclear whether melting is caused by the cracks or the cracks are caused by surface melting.

statistics of the second test

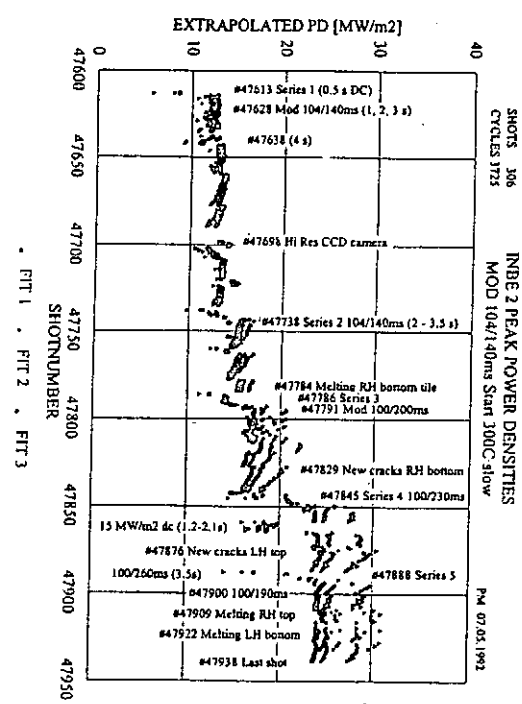

fault sequence during the second test

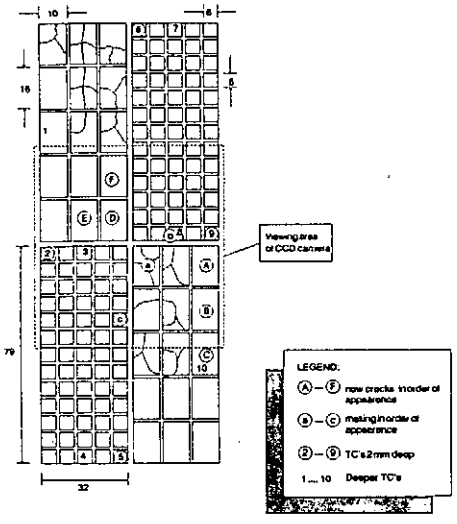

2.2.2 **Beryllium tiles brazed onto CuCrZr**

2.2.2.1 **Materials**

Flat 2 and 3 mm thick Beryllium tiles have been brazed to 27 mm wide CuCrZr base plates. Brazes used were BAg 18 and InCuSOL.

2.2.2.2 **Result:**

a 2 mm thick tiles peform better than 3 mm tiles.

b The limit of 2 mm tiles is 16 MW/m2.

c Castellated tiles fail first. The test has to be terminated as evaporating Beryllium does not allow stable beam operation.

d Cracks in the brittle intermetallic layer between Beryllium and braze appear to limit the performance.

2.2.2.3 **Present status:**

Braze sequences and surface coatings that avoid the formation of the intermetallic layer are being developed.

Other bonding techniques such as HIPing, diffusion bonding and plasma spraying are also being investigated.

photograph taken after the test.

The numbers give the appearance of faults. The tiles heat up suddenly and start to melt after 1s.

Micrograph showing the crack in the intermetallic layer between Beryllium and braze.

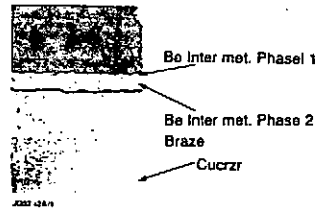

J/US Workshop on High Heat Flux Components and
Plasma Surface Interactions for Next Devices,
Kyushu University, Fukuoka, Japan
Nov. 17 - 19, 1992

Development of Plasma Facing Components for ITER

M. Akiba
JAERI
801-1 Naka-machi, Naka-gun, Ibaraki-ken, 311-01 Japan

This is the overview of the current status of PFC developments at JAERI. Our major efforts have been concentrated to develop high heat flux components for ITER and JT-60U with emphasis on the divertor plate. Basic studies associated with PFC development, such as evaluation of disruptive erosion loss, have also been performed extensively. Recent topics can be summarized as follows:

1. Development of CFC/Cu divertor mock-ups

Several types of bonding interface structures, e.g., flat plate, saddle and monoblock types, have been developed and tested in an electron beam facility of JAERI, JEBIS. The saddle type and monoblock type mock-ups could successfully endured heat loads of 15 ~ 20 MW/m^2, 30s for over 1000 thermal cycles.

2. Heat transfer studies under one-sided heating conditions

Since heat transfer correlations have scarcely existed for the one-sided heating geometry, the establishment of the correlation is necessary to design the divertor plate. JAERI has started heat transfer experiments under the one-sided heating conditions in an ion beam facility, PBEF.

3. Development of divertor support structures

Since the divertor plate will be considerably deformed by incident high heat loads from plasma, it is urgently necessary to develop the divertor support structure which can reduce the deformation. We fabricated 1m-long divertor mock-ups with support structures and have started the heating tests.

4. Development of JT-60U actively cooled divertor plate

Installing water cooled divertor plates has been proposed for JT-60U. We have also been charged in developing the actively cooled divertor plate of JT-60U. We have started the thermal analyses and the evaluation of the magnetic force by disruptions. The fabrication of small mock-ups will be completed by March 1993.

PFC Development at JAERI (continued)

JAERI

- ITER Divertor/First Wall
  - Thermal hydraulics studies
    - Heat Transfer/CHF under one-sided heating conditions
  - Fabrication and testing of the divertor plate
    - Development of divertor support structures
- JT-60U Divertor
  - Evaluation of electromagnetic forces
  - Thermal and mechanical analyses
  - Heating tests of armor materials and divertor mock-ups

NBI Heating Laboratory

Japan-US Workshop on High Heat Flux Components and Plasma Surface Interactions for Next Devices, Kyushu University, Fukuoka, Japan, Nov. 17 - 19, 1992

JAERI

Development of Plasma Facing Components for ITER

M. Akiba
NBI Heating Laboratory
Japan Atomic Energy Research Institute

- Overview
- Recent Topics

NBI Heating Laboratory

International Collaboration

JAERI

- SNL/JAERI
  - CHF
  - Disruption (Plasma Gun)
- UCLA/JAERI
  - Divertor Test at PISCES-B
- NET/KFA/JAERI
  - Divertor Test at JEBIS
  - Heating Test of pre/post-irradiated materials at KFA

NBI Heating Laboratory

PFC Development at JAERI

JAERI

- ITER Divertor/First Wall
  - Material Properties
    - Thermal and mechanical properties (inc. n-irradiation): CFC, Cu, W, bonding structure
    - Evaluation of erosion loss: sputtering, disruption
    - Analytical modeling: disruption erosion, run-away electron damage
  - Joining technology
    - New concepts for CFC joining
    - Tile attachment structures of the first wall
    - Evaluation of joining reliability
      - Divertor small mock-ups (CFC/Cu, W/Cu)
      - First wall small mock-ups

NBI Heating Laboratory

2. Heat Transfer Studies have been performed under the one-sided heating conditions.

JAERI

NBI Heating Laboratory

Recent Topics

JAERI

1. Development of CFC/Cu divertor mock-ups
2. Heat Transfer studies under one-sided heating conditions
3. Development of divertor mock-ups with support structures
4. Development of JT-60U actively cooled divertor plates

NBI Heating Laboratory

3. Heating Tests on Divertor Mock-ups with the Support Structure have started.

JAERI

- Support Structure Concepts
  - Rail Slide
  - Pin Slide
  - Full rigid

NBI Heating Laboratory

1. CFC/Cu Divertor Mock-ups have endured up to 20 MW/m^2, 30 s heat loads for over 1000 thermal cycles.

JAERI

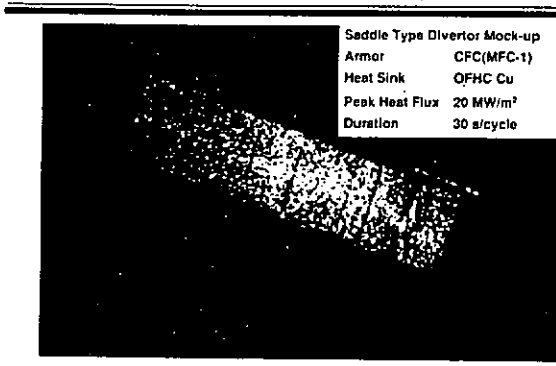

NBI Heating Laboratory

4. The Development of the Actively Cooled Divertor Plates has started for the JT-60U application.

JAERI

- Thermal and stress analyses and the evaluation of electromagnetic forces have been performed on several divertor structures.

Incident Heat Flux: 10 MW/m², 5 s

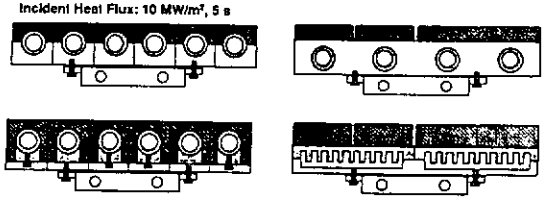

NBI Heating Laboratory

Concluding Remarks

JAERI

- Small scale divertor mock-ups have successfully endured at heat loads of 15 ~ 20 MW/m², 30 s, ~ 1000 thermal cycles.
- Heat transfer experiments with one-sided heating conditions have been performed for smooth and swirl tubes.
- Fabrication and testing of divertor support structures have started with 1m long divertor mock-ups.
- Fabrication of actively cooled divertor mock-ups of JT-60U have started and heating tests will be performed in JEBIS in the middle of 1993.

NBI Heating Laboratory

Japan-US Workshop P196 on High Heat Flux Components and Plasma Surface Interactions for Next Devices, November 17-19, 1992 at Kyushu Univ.

DEVELOPMENT OF FABRICATION TECHNOLOGIES FOR PLASMA FACING COMPONENTS OF ITER/FER AND LHD

Seiichiro YAMAZAKI (Kawasaki Heavy Industries, LTD.)
Masato AKIBA (Japan Atomic Energy Research Institute)
Nobuaki NODA (National Institute of Fusion Science)

Activities on the development of plasma facing components(PFCs) for ITER/FER[1] and LHD[2] are performing in Kawasaki Heavy Industries, LTD.(KHI) in cooperation with Japan Atomic Energy Research Institute(JAERI) and National Institute of Fusion Science(NIFS). We present here the study on the development of fabrication technologies for PFCs, and the manufacture of the mockups.

Vacuum brazing was applied as the fabrication technique of the divertor plates for ITER/FER using high thermal conductive carbon composites(CFCs) as the armor tile and copper as the coolant tube. Various CFCs were brazed to copper using Ti-Cu-Ag as the brazing material. Studies such as microscopic observations and bending tests have been performed to confirm the characteristics of the brazed part. Copper made swirl tube was developed and used as the coolant tube of the divertor. Some monoblock and flat-plate type mockups of the divertor were successfully fabricated using the materials and brazing technique. Cyclic heating tests of the monoblock type mockups were performed with a heat flux of 15 MW/m^2 for more than 1000 cycles in the *J*AERI *E*lectron *B*eam *I*rradiation *S*tand(JEBIS). No degradation of thermal response and no damage at the brazing surface were observed after the tests[3]. A sliding rail concept was proposed as the reliable support structure of the divertor plate in consideration of deformation due to the peaked heat load. A one meter long monoblock type mockup was successfully fabricated with the support structure. A high thermal conductive CFC and a copper swirl tube were also used as the armor tile and the coolant tube. The mockup will be tested in JEBIS.

The design and experimental studies on the divertor module of LHD are also being performed, in consideration of the more complicated figure of the module and larger inclination of the field line to the divertor plate. An array of cylindrical divertor units was chosen as the concept of the module. Some small mockups of the unit were manufactured. These mockups are being tested in *R*astering *E*lectron *B*eam Test *A*pparatus(REBA) in KHI and *A*ctive *C*ooling *T*est Stand(ACT) in NIFS.

HIP bonding techniques have been developed for manufacturing of the stainless steel panel including internal rectangular coolant paths of the ITER first wall[1][4]. From the results of microscopic observations, sufficiently high bonding ratios were obtained not only in flat panel but in bending one. The material properties of bonding part were almost same as those of the mother material. Some mockups were fabricated and provided as the test specimens for heating tests in JAERI. A first wall mockup was also fabricated with radiative cooled graphite armor tiles. Ceramic structures were used as the attachment to the substrate to prevent the heat conduction through the attachment. The surface of the substrate was coated with Cr_2O_3 to enhance the heat radiation. It was tested with a heat flux of 0.6 MW/m^2, i.e. the peak heat flux condition of ITER first wall.

REFERENCES

[1] Yamazaki S. et al., to be appeared as Proc. of 17th SOFT, Rome (1992,9)
[2] Noda N. et al., NIFS-190 (1992)
[3] Suzuki S. et al., Fusion Technol. 21 (1992), 1858
[4] Yamazaki S. et al., Proc. 16th SOFT, London (1990), 302

ACTIVITIES (2)

DEVELOPMENT OF DIVERTOR MODULE FOR LHD

NIFS — KAWASAKI

Design and thermo-mechanical and thermal-hydraulic analyses
Study on divertor module configuration and installation
Fabrication of divertor unit mockups and cyclic heating tests

DEVELOPMENT OF FABRICATION TECHNOLOGIES FOR PFCs OF ITER/FER AND LHD

PRESENTED AT
JAPAN-US WORKSHOP P196
ON HIGH HEAT FLUX COMPONENTS AND PLASMA SURFACE INTERACTIONS FOR NEXT DEVICES

November 17, 1992, KYUSHU UNIV.

Seiichiro YAMAZAKI — Kawasaki Heavy Industries, LTD.
Masato AKIBA — Japan Atomic Energy Research Institute
Nobuaki NODA — National Institute of Fusion Science

DEVELOPMENT OF BRAZING TECHNIQUES AND FABRICATION OF SMALL-SIZE DIVERTOR MOCKUPS FOR ITER/FER

Brazing conditions were selected for various kinds of CFC.
- CFCs were brazed to copper materials at ab. 850 C in vacuum
- Ti-Cu-Ag was used as the brazing material.
- Microscopic observations and bending tests were performed.

Swirl tube was developed and used as the coolant tube.
- Stainless steel made twisted tape(twist ratio of 3.5) was inserted into copper tube.

Some monoblock and flat plate types of small-size mockups were successfully fabricated.

Cyclic heating tests were performed in JEBIS test stand with the mockups.

ACTIVITIES (1)

DEVELOPMENT OF PLASMA FACING COMPONENTS FOR ITER/FER

JAERI — KAWASAKI

DIVERTOR :

Design and thermo-mechanical and thermal-hydraulic analyses
Development of brazing techniques with CFCs and copper
Fabrication of small-size mockups and cyclic heating tests
Fabrication of mid-size mockup with support structure
Development of remote surface inspection technologies

FIRST WALL

Design and thermo-mechanical and thermal-hydraulic analyses
Development of HIP bonding techniques of stainless steel panel
Fabrication of mockups and heating tests
Experimental and numerical study on lifetime evaluation

MID-SIZE DIVERTOR MOCKUP FOR ITER/FER MONOBLOCK TYPE WITH SUPPORT STRUCTURE

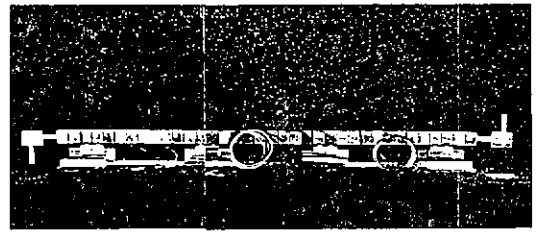

Total length of the mockup is about 1 meter. Sliding rail supports made of stainless steel with a pitch of 250 mm was applied. CFC(CX-2002U) and copper swirl tube were used as the armor tile and the coolant tube.

Kawasaki Heavy Industries, LTD.

SMALL-SIZE DIVERTOR MOCKUPS FOR ITER/FER MONOBLOCK TYPE WITH SWIRL TUBE

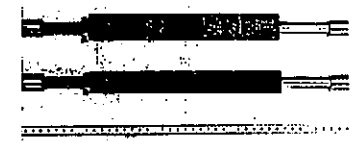

TOP with MFC-1 armor tiles, BOTTOM with CX-2002U armor tiles

No degradation of thermal response and no damage at CFC and brazing surface were observed after cyclic heating tests IN JEBIS, with a heat flux of 15MW/m2 for more than 1000 cycles.
Suzuki S. et al., Fusion Technol. 21 (1992), 1858

Kawasaki Heavy Industries, LTD.

CONCEPT OF DIVERTOR MODULE FOR LHD

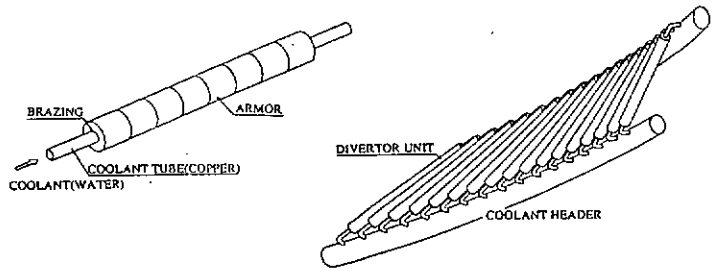

Divertor module is constructed as the array of divertor units with annular carbon armor tiles and a copper coolant tube.
This concept was chosen in consideration of more complicated figure of divertor plate and larger incident angle compared to tokamaks.

Kawasaki Heavy Industries, LTD.

DEVELOPMENT OF SUPPORT STRUCTURES AND FABRICATION OF MID-SIZE DIVERTOR MOCKUP FOR ITER/FER

Sliding rail support structure was chosen in consideration of deformation of divertor plate due to peaked heat load.
Support structure made of stainless steel were attached to a tube with a copper made cylindrical connector.
Excessive residual stress was prevented not to make opening edges at the brazing surface of tile and connector.
The support structure, that has MoS_2 coated and curved contact surfaces, was inserted into a sliding support rail.

A monoblock type mid-size mockup with a length of about one meter was successfully fabricated with the support structure.

This mockup will be tested in JEBIS.

Kawasaki Heavy Industries, LTD.

FIRST WALL MOCKUP FOR ITER/FER (1)
HIP BONDED STAINLESS STEEL COOLING PANEL INCLUDING CORNER PART

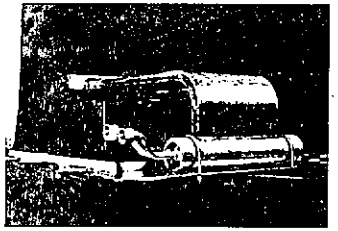

The bonding ratios at not only flat part but corner part were sufficiently high(higher than 95%)[1]. This mockup will be tested in JEBIS to study the thermal stress concentration at the corner.

[1] Yamazaki S. et al., to be published as Proc. 17th SOFT , Rome(1992,9)

Kawasaki Heavy Industries, LTD.

DIVERTOR UNIT MOCKUPS FOR LHD

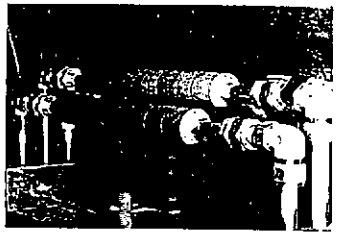

Divertor unit mockups were fabricated with CFCs and isotropic graphite. These mockups are testing in REBA(*R*astering *E*lectron *B*eam Test *A*pparatus)[1] in KHI and ACT(*A*ctive *C*ooling *T*est Stand)[2] in NIFS.

[1] Yamazaki S. et al., Fusion Eng. and Des. 15(1991), 17
[2] Noda N. et al., NIFS-190(1992)

Kawasaki Heavy Industries, LTD.

FIRST WALL MOCKUP FOR ITER/FER (2)
RADIATIVELY COOLED GRAPHITE TILE ARMORED STAINLESS STEEL PANEL

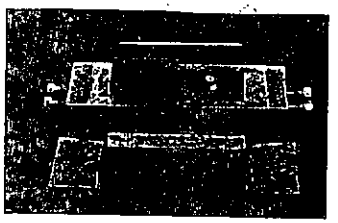

Attachment structures made of ceramic were applied to reduce the heat conduction through the structures. The surface of substrate was coated with Cr_2O_3 to increase emissivity.
No degradation and damage was observed after heating test with a heat flux of 0.6 MW/m2, i.e. the peak heat flux condition of ITER.

Kawasaki Heavy Industries, LTD.

DEVELOPMENT OF HIP BONDING TECHNIQUES AND FABRICATION OF FIRST WALL MOCKUPS FOR ITER/FER

Two HIP bonding techniques,i.e. grooved plate and rectangular tube techniques, were investigated. Sufficiently high bonding ratios were obtained with both ones. Rectangular tube one is more preferable, because it is applicable at the corner(bending) part and able to use no surface treated(as received) material[1].

A first wall mockup with the corner part were fabricated. The bonding ratio at the corner part was sufficiently high as same as the flat part. It will be tested in JEBIS facility.

First wall structure with radiatively cooled graphite armor tiles were designed for the peak heat flux region in ITER. A mockup was fabricated and tested with a heat flux of 0.6 MW/m2.

[1] Yamazaki S. et al., Proc. 16th SOFT , London(1990), 302

Kawasaki Heavy Industries, LTD.

SUMMARY

(1) Activities on plasma facing components development for ITER/FER and LHD are now going on.

(2) The brazing techniques of the divertor plate have been developed for ITER/FER and LHD. Small mockups were successfully fabricated with various kinds of carbon materials and copper tube. They were provided as the test specimens for thermal cycling tests.

(3) A sliding support structure were developed for ITER divertor. A monoblock-type 1 meter long divertor mockup was successfully fabricated with the support structure.

(4)HIP bonding techniques have been developed to manufacture the stainless steel panel with internal coolant paths for ITER first wall. Mockups were successfully fabricated using the techniques.

Kawasaki Heavy Industries, LTD.

R&D OF PLASMA FACING COMPONENTS FOR ITER

Masahiko Toyoda

Mitsubishi Heavy Industries, Ltd.

Kimihiro Ioki

Mitsubishi Atomic Power Industries, Inc.

Masato Akiba

JAERI

Based on the design requirements for the plasma facing components in ITER, design and fabrication studies on the conductively cooled first wall and the divertor plate with sliding support were performed.

Two types of conductively cooled armor have been designed; CFC armor and CFC brazed to molybdenum plate. A first wall test module with two types of full scale first wall armor tile was fabricated and it has been shown experimentally that the conductively cooled first wall can be used at a stationary heat flux of 0.2-0.4 MW/m^2 when neutron irradiation effects on the thermal performance are small. The thermal characteristics of the armor remained unchanged after heat cycles. Stable high-contact thermal conductance was obtained by inserting a graphite sheet between armor tile and first wall.

The sliding support structure with pin rods was designed for the divertor plate. It has been shown by thermal and mechanical analysis that the thermal stress and bending deformation are reduced compared with fixed supports. A divertor test module of 350mm length with sliding supports was fabricated. CFC armor tiles were directly brazed to copper cooling tube. MoS_2 coated pin rods were used for the sliding supports. The heat load test at relatively low heat flux was carried out and it has been demonstrated that the sliding supports work well. A divertor test module of 1000mm length with sliding supports was also fabricated and the heat load test will be performed.

R&D of Plasma Facing Components for ITER

Masahiko Toyoda
Mitsubishi Heavy Industries, Ltd.
Kimihiro Ioki
Mitsubishi Atomic Power Industries, Inc.
Masato Akiba
JAERI

- ◆ Development of first wall
  - ● Conductively cooled first wall armor
    - · Design/Analysis
    - · Fabrication/Test
- ◆ Development of divertor structure
  - ● Development of armor structure
    - · Design/Analysis
    - · Bonding technology of CFC
  - ● Development of slide support
    - · Design/Analysis
    - · Fabrication/Test

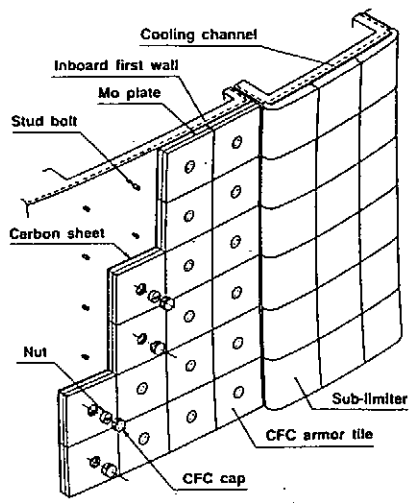

Concept of conductively cooled first wall armors

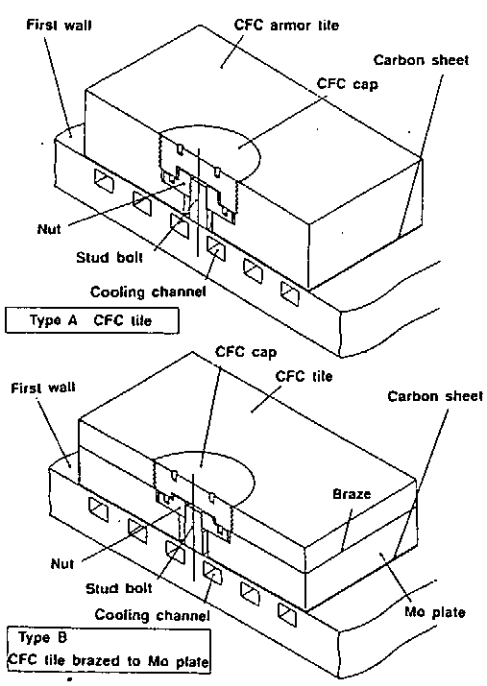

Two kinds of first wall armors designed and fabricated for heat load tests

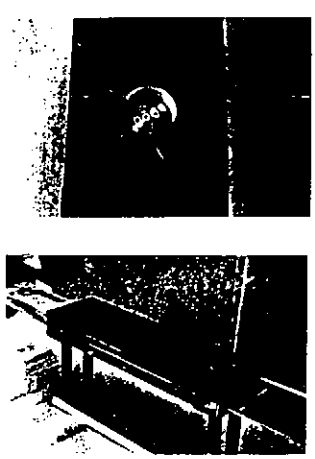

Test module of conductively cooled first wall

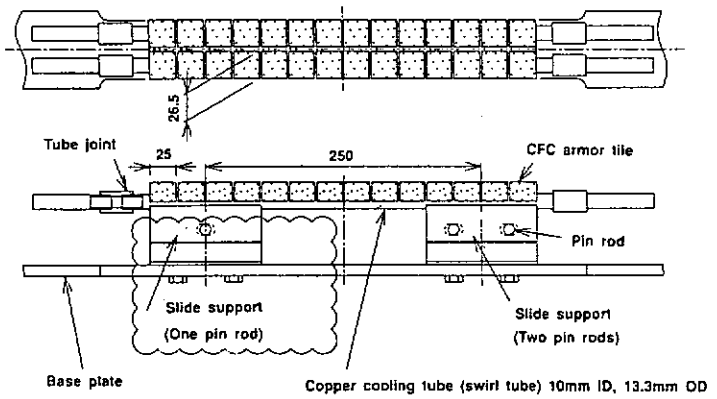

Test module of divertor plate with slide supports

Measured temperatures in first wall armor during heat load tests

Armor	Heat flux	Carbon sheet	Armor temp.	Cap temp.	Estimated a*
Type A	0.2MW/m²	0.2mmt	315°C	758°C	1100W/m²K
Type A	0.2MW/m²	0.6mmt	194°C	722°C	2900W/m²K
Type A	0.4MW/m²	0.6mmt	426°C	933°C	2300W/m²K
Type B	0.2MW/m²	0.2mmt	518°C	898°C	500W/m²K
Type B	0.2MW/m²	0.6mmt	416°C	863°C	700W/m²K

a*: Contact thermal conductance between armor and first wall

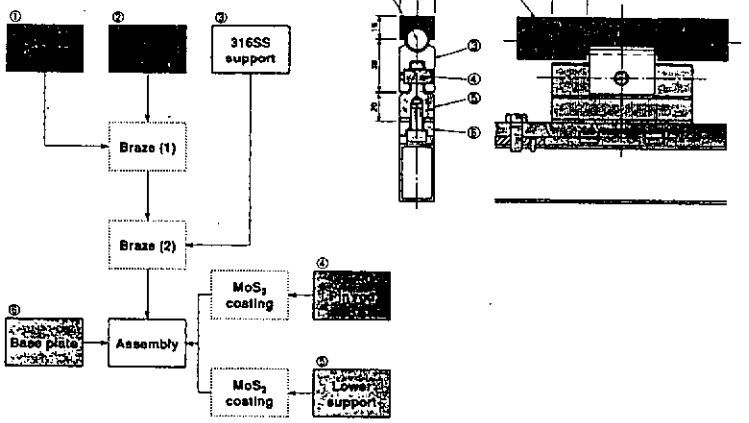

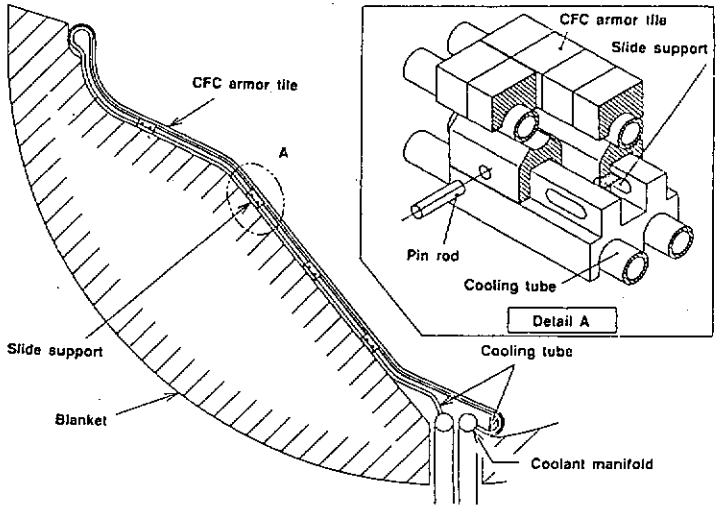

Divertor plate with slide supports

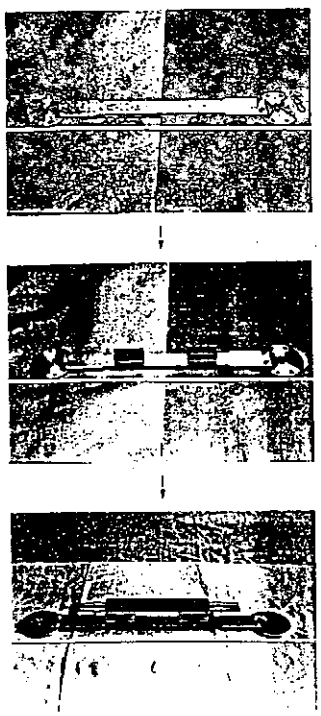

Assembly of the test module

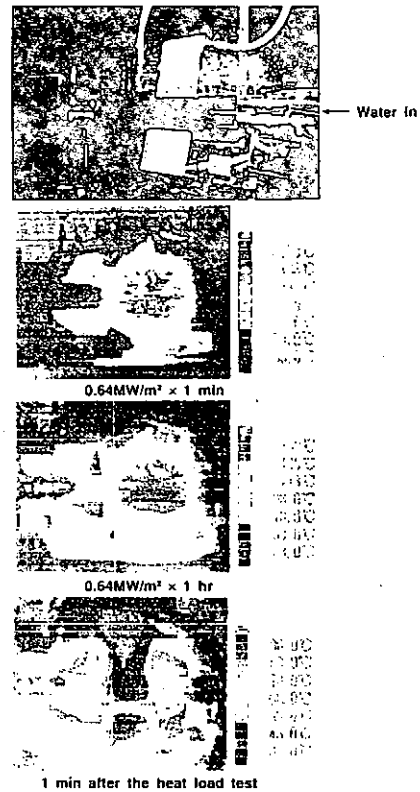

1 min after the heat load test

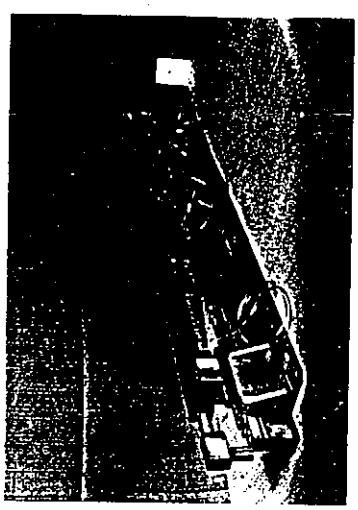

Test module of 1m length divertor plate with sliding supports

Japan-US Workshop P196 on High Heat Flux Components
and Plasma Surface Interactions for Next Devices
Kyushu University, Japan, Nov. 17-19, 1992

Development of a New MFC-1 / W-30Cu Tubeless Flat-Plate Divertor Design

I. Šmid*, M. Akiba, M. Araki, S. Suzuki, M. Dairaku
NBI Heating Laboratory, JAERI

* permanent: Austrian Research Centre Seibersdorf

With MFC-1 armor tiles and a W-30Cu heat sink the presently accepted ITER requirements for the thermal performance of divertor plates can be met:

1100 °C max. surface temperature, at 15 MW/m^2 steady state conditions,
a min. armor thickness of 10 mm, and use of high strength heat sink materials only.

The above materials are characterized and available today.

In the present analysis, the strength of MFC-1 is not exceeded in the brazing process, when joined to W-30Cu. The residual stresses in the critical direction perpendicular ($\perp$) to the fibers stay below 4.0(compr.)/0.4(tensile) MPa. The same is true for a stress analysis with 15 MW/m^2 steady state applied to the top surface: 8.0(compr.)/ 0.4(tensile). Higher thermal stresses are predicted in the heat sink. The peak values, however, never exceed the strength of W-30Cu.

Design: For the present study a minimum armor thickness of 10 mm was chosen. The heat sink consists of one piece only - no additional tube for the coolant water is foreseen. The minimum thickness of the heat sink on top is 1.5 mm. The total width of the armor as well as heat sink is 25 mm.

MFC-1 (1992) is a uni-directional C/C with a high orientation of its pitch-type fibers and a distinct anisotropy of its thermal and mechanical properties in different directions. The thermal conductivity at RT parallel ($//$) to the fibers is a factor of ~ 25 higher than perpendicular ($\perp$) to the fibers. For the elastic modulus and the tensile strength this anisotropy factor is ~ 100. The stresses and temperatures could only be evaluated reliably, if anisotropic thermal and mechanical properties were used in the FEM calculations.

W-30Cu: High strength tungsten-copper composite materials are produced by sintering compacted tungsten powder and subsequent infiltration with liquid copper. Although a good wettability of W with liquid copper occurs, there is (almost) no mutual solid solubility in the W-Cu binary system (therefore it is a composite material, or "pseudo-alloy"), and thus the thermal conductivity in particular of the copper filler matrix is not impaired due to alloying.

FEM Analysis: The finite-element code ABAQUS (Ver. 4-9-1, 1992) was used to predict the residual as well as thermal stresses, and the thermal response at a uniform heat flux to the top surface of 15 MW/m^2, steady state.
Braze solidification at 750°C (i.e. the stress free temperature) was assumed, with subsequent cooling to room temperature, where the residual stresses were taken. The temperature output of the thermal calculation was used as the final condition for the thermal stress calculation. Generalized plain strain elements were used in all stress calculations to account for the stresses in the z-z direction ($//$ to the axis of the coolant tube). The two-dimensional model was constructed with 1454 ^{FLAT} / 1554 ^{BENT} 8-noded isoparametric quadrilateral elements, and a total of 4594 ^{FLAT} / 4906 ^{BENT} node points. Temperature-dependent properties were used for both materials. Anisotropic material properties were used in the case of MFC-1 to account for the orientation of the high-conductivity/high-strength fibers in the y-y direction. A subroutine within ABAQUS was used to calculate the increase in heat transfer film coefficient from simple forced-flow convection to subcooled nucleate boiling, in a self-consistent manner. No twisted tape insert was assumed in the calculations.
Full-size two-dimensional models were applied in the calculations, whereas only one half is presented in the attached diagrams.

Material Properties [1]

	(CX2002U)	MFC-1 (1992)	W-30Cu
Ultimate tensile/compr. /bend. strength (MPa)	35 / 50 / 15 (min.) 50 / 50 / 50 (max)	400 / 215 / 480 (//) 3 / 15 / 5 (⊥)	520
Tensile elongation at RT	--	-	2-3 %
Young's modulus (GPa)	10.7[1], 8.1[2], 3.4[3]	100 (//), 0.8 (⊥)	218
Poisson ratio	0.19	(0.15)	0.3
Melt/sublim. temp. (°C)	3500	3500	1080 (Cu)
Density (g/cm³)	1.67	1.96	14.0
Thermal conductivity, 20°C (W/mK) 300°C	380.0 [1] 240.0 [1]	640.0 (//, 57°C) 442.0 (//)	~ 290.0 276.0
Specific heat at RT (J/gK)	0.71	0.71	0.24
Thermal expansion coeff. (10^{-6}/K)	1.5[1], 1.7[2], 5.8[3]	~ 0.9 (//), 12.0 (⊥)	11.5

[1] data measured, from literature and manufacturer's documentation, respectively; [1], [2], [3] corresponding directions

MFC-1 (1992): uni-directional pitch-type carbon-fiber-reinforced-carbon material, Mitsubishi Kasei, Japan
CX2002U: two-directional felt-type carbon-fiber-reinforced-carbon material, Toyo Tanso, Japan
W-30(wt%)Cu: copper-infiltrated tungsten (pseudo-)alloy, composite material

Development of a New MFC-1 / W-30Cu Tubeless Flat-Plate Divertor Design

L. Šmid*, M. Akiba, M. Araki, S. Suzuki, M. Dairaku

NBI Heating Laboratory, Naka Fusion Research Establishment
Japan Atomic Energy Research Institute
*permanent: Austrian Research Centre Seibersdorf

presented at the
Japan-US Workshop P196 on High Heat Flux Components
and Plasma Surface Interactions for Next Devices
Kyushu University, Japan, Nov. 17-19, 1992

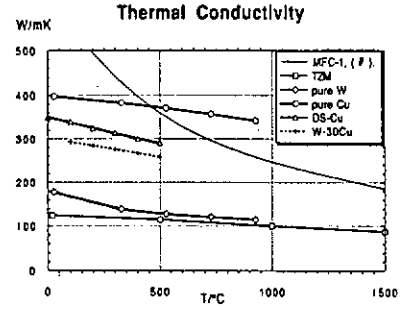

"Accepted" requirements for the normal operation of carbon armored ITER divertor plates:

1000-1100°C max. C/C surface temperature
10 mm min. armor thickness
use of high strength heat sink materials

in addition for the present study

15 MW/m² steady state, uniform to the top surface
10 m/s, 3.5 MPa, 60°C coolant water
no twisted tape

Flat-Plate Divertor: MFC-1 (1992) + W-30Cu; Thermal stresses, temperature and displacement
at a uniform steady state surface heat flux of 15 MW/m² ; coolant: water, 10 m/s, 3.5 MPa, 60°C, no twisted tape.

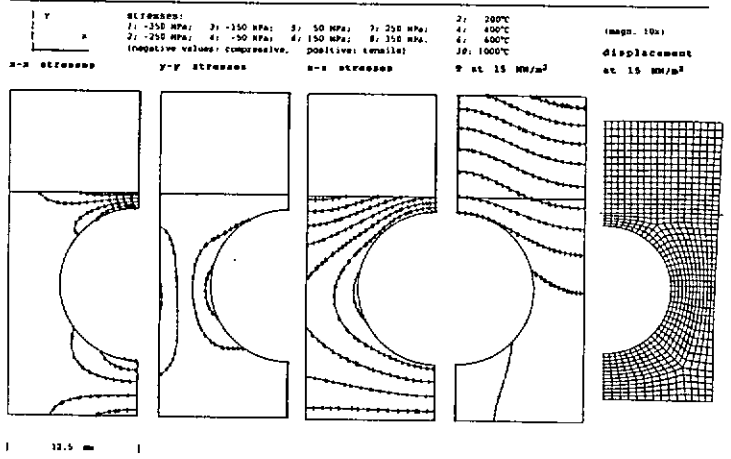

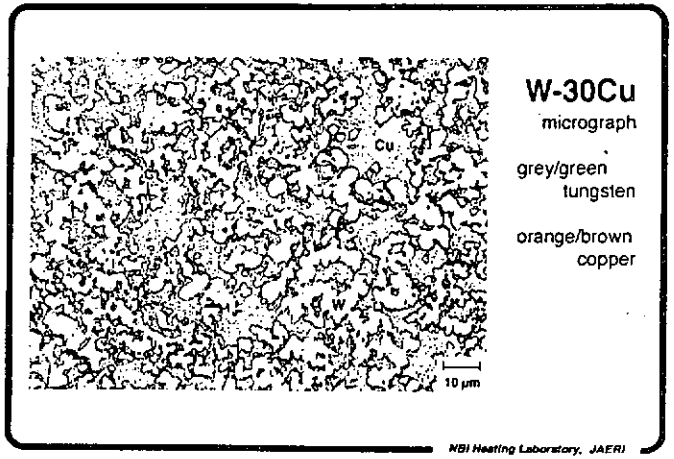

Bent Interface Divertor: MFC-1 + W-30Cu; Thermal stresses, temperature and displacement
at a uniform steady state surface heat flux of 15 MW/m² ; coolant: water, 10 m/s, 3.5 MPa, 60°C, no twisted tape.

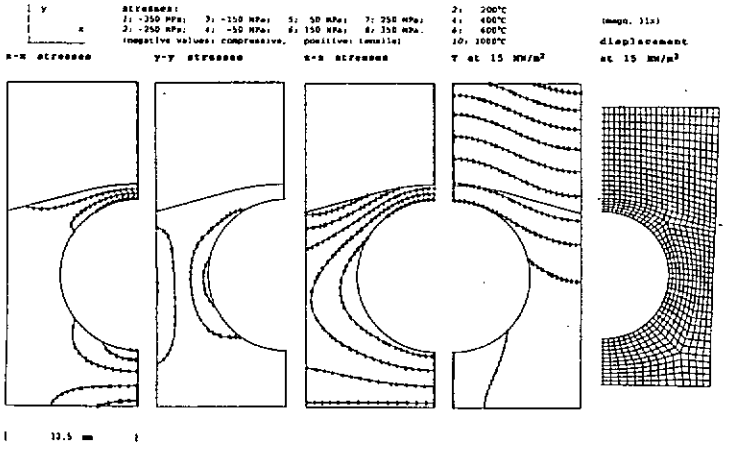

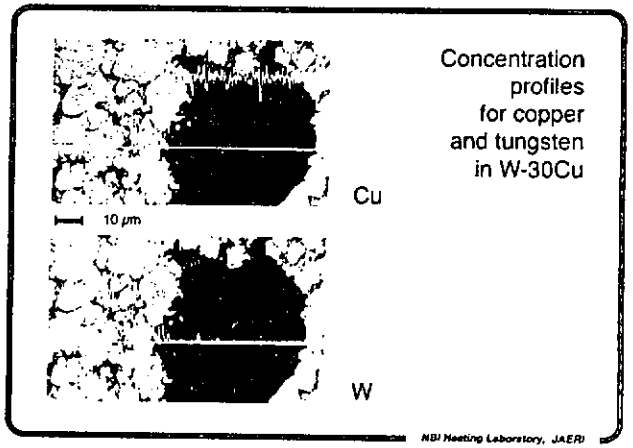

Concluding Remarks:

a new material combination is proposed for the divertor plates of ITER: MFC-1 + W-30Cu

and new design concepts: the tubeless flat-plate design, and the tubeless bent interface design

W-Cu was reported to have good brazing abilities;
there is, however, no experience, with joining to C/Cs;
joining and testing of MFC-1/W-30Cu is under way in JAERI

no degradation of the thermal or mechanical properties of W-Cu will occur due to the temperatures achieved during brazing

only moderate residual and thermal stresses are predicted by FEM

the thermal ITER requirements for normal operation can be met

NBI Heating Laboratory, JAERI

Predicted Stresses (MPa)

		MFC-1 + W-30Cu FLAT-PLATE residual	MFC-1 + W-30Cu FLAT-PLATE thermal	MFC-1 + W-30Cu BENT INTERFACE residual	MFC-1 + W-30Cu BENT INTERFACE thermal
In the MFC-1 armor:					
Peak stresses, in x-x (i.e., ⊥ to fiber dir.)	tensile	0.33	0.38	0.39	0.15
	compr.	*0.01*	*7.4*	*3.9*	*7.6*
Peak stresses, in y-y (i.e., // to fiber dir.)	tensile	8.2	14.	6.5	7.6
	compr.	*0.90*	*8.0*	*8.4*	*12.*
Peak stresses, in z-z (i.e., ⊥ to fiber dir.)	tensile	0.34	0.05	0.34	0.14
	compr.	-	*4.7*	*0.19*	*5.0*
In the W-30Cu heat sink:					
Peak stresses, in x-x	tensile	1.2	261.	23.	255.
	compr.	*4.0*	*197.*	*8.4*	*188.*
Peak stresses, in y-y	tensile	9.6	202.	15.	195.
	compr.	*2.7*	*162.*	*12.*	*157.*
Peak stresses, in z-z	tensile	2.2	278.	6.2	246.
	compr.	*2.1*	*379.*	*5.0*	*301.*

Thermal response at 15 MW/m² steady state

	MFC-1 + W-30Cu FLAT-PLATE	MFC-1 + W-30Cu BENT INTERFACE
Peak temperature (°C)		
on the top surface of MFC-1	1067.	1057.
in the braze & heat sink	546.	455.
tube inner surface	298.	296.
Peaking factor for the heat flux inside the coolant tube	1.28	1.25

High Heat Flux Test of Divertor Materials using ACT

Y. Kubota, N. Inoue, A. Sagara, N. Noda, K. Akaishi, O. Motojima(NIFS)
I. Fujita, T. Hino, T. Yamashina(Hokkaido Univ.)
T. Matsuda, T. Matsumoto, T. Sogabe, K. Kuroda(Toyo Tanso Co. Ltd.)

It is necessary to develop reliable brazing of IG or C/C to OFC(oxygen free copper) for divertor units[1] of LHD. For the purpose, high heat flux tests for some brazing materials have been done by using ACT(active cooling teststand) with a 100 kW electron beam source. Four kinds of brazed samples have been fabricated in Toyo Tanso Co. Ltd. and tested. The samples are namely flat plate type(F/CC, F/IG) and mono-block type(M/CC, M/IG). The brazing technology was reported in the previous workshop in Santa Fe[2]. By observing the thermal responses measured with a pyrometer and two thermo-couples during heat loading, the thermal properties of the samples were evaluated. The results for one shot heat loading and heat cycle tests are as follows,

The surface temperature of the F/CC sample rises with a response time of about 10 seconds and is saturated around 1200 ℃ under a pulse heat load of 10 MW/m^2 . This result is promising for the LHD experiments. On the other hand, the temperature of the M/IG sample reaches 1500 ℃ with very long rise time(>100 s) u nder a heat load as low as 4 MW/m^2 . This is partly because of relatively low t hermal conductivity in the armor compared with the F/CC sample and also becauseo f the mono-block type of geometry. However, the temperature of the M/IG is alsob elow 1200 ℃ at 10 seconds after the beam on, showing that this type is also acceptable for the LHD experiment, especially for a heat load of less than 5 MW/m^2 . To check the thermal fatigue of the brazing region, heat cycle tests have been carried out up to 4100 shots with a heat load of 10 MW/m^2 and water flow velocity of 8 m/s for F/CC sample(No. 1) and 1500 shots with a 7.5 MW/m^2 for two F/IG samples(No. 2 and 3). The surface temperature increased gradually shot by shot for the F/CC sample. This change in temperature may be partly due to heat load change because of the change in background gas pressure, and due to a slight deterioration of the heat transfer coefficient of the brazing layer. However, the temperature did not show such a tendency shot by shot for No. 3 sample of F/IG type by keeping severely the heat load constant. Moreover, no apparent damage on the surfaces and brazing regions of these samples was observed after the test.

References

1)N. Noda et al., NIFS internal report, NIFS-190, (17th SOFT, Rome)
2)T. Sogabe et al., Proc. of US-Japan workshop Q-142, SAND92-0222, P4-148.

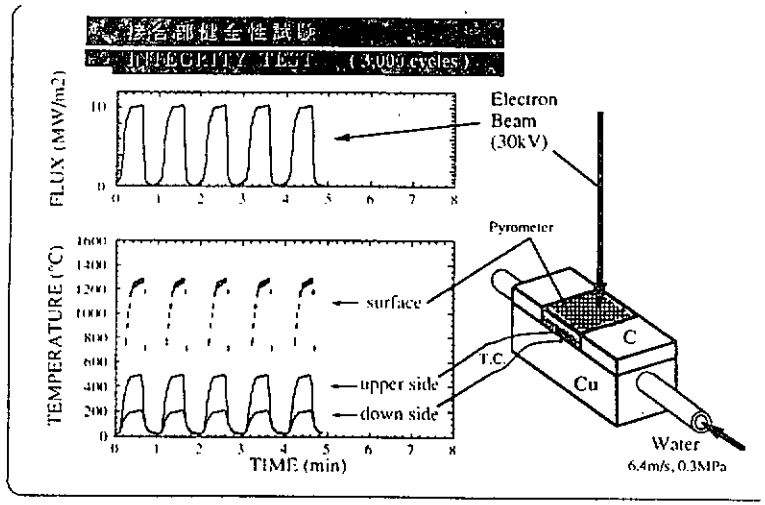

High Heat Flux Test of Divertor Materials using ACT

Y. Kubota, A. Sagara, N. Noda, K. Akaishi, O. Motojima (NIFS)
I. Fujita, T. Hino, T. Yamashina (Hokkaido Univ.)
T. Matsuda, T. Matsumoto, T. Sogabe, K. Kuroda (Toyo Tanso)

* The aim of the tests,

  To develop brazing materials for the divertors of LHD

  ① Surface temperature <1200 ℃

  ② Toughness for cycle heat loads

* The tests performed,

  ① High heat flux test for four kinds of brazing materials

  ② High heat flux cycle tests for three brazing materials

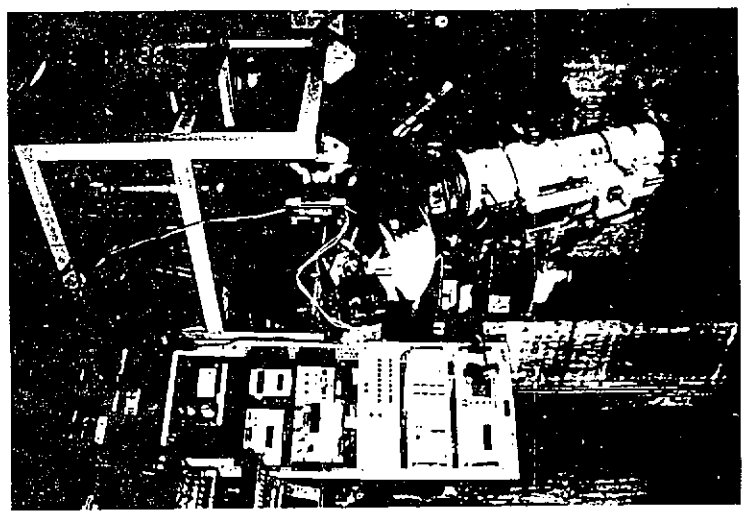

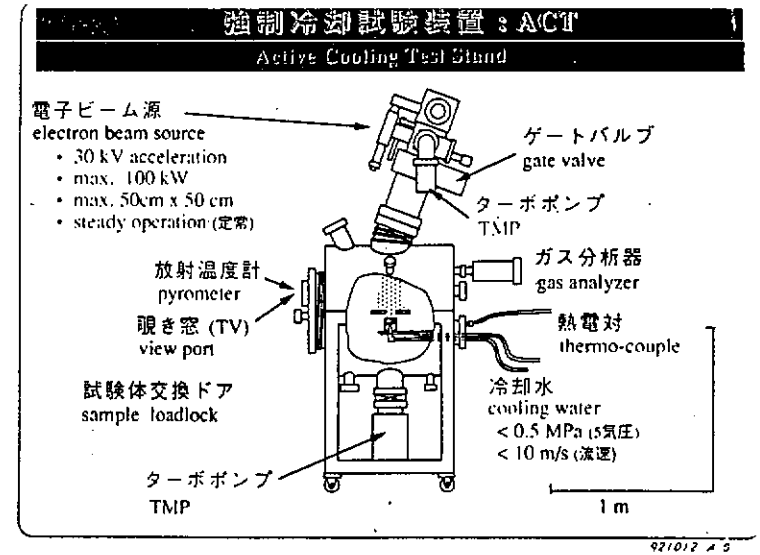

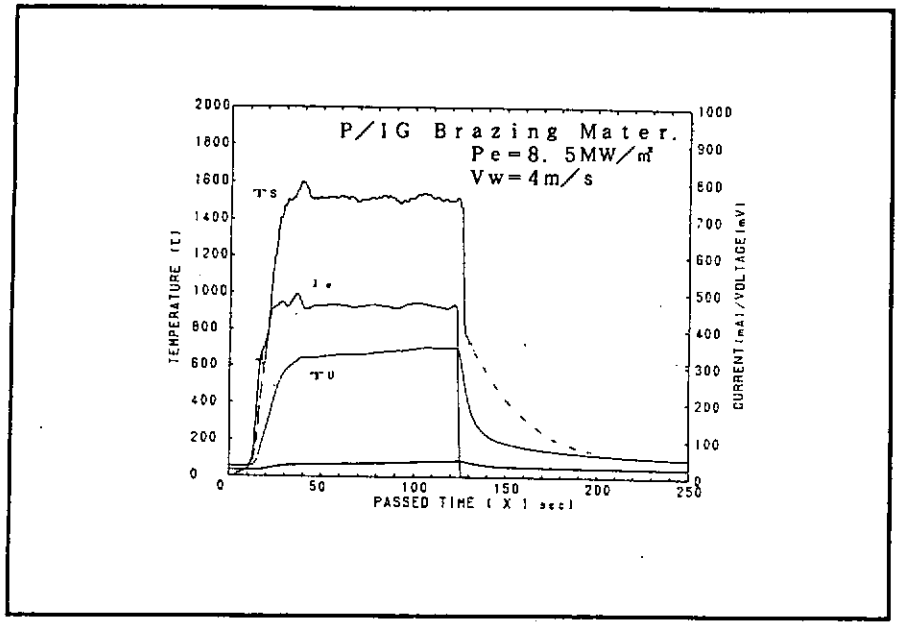
P/IG Brazing Mater.
Pe=8.5MW/m²
Vw=4m/s
Ts
Ie
Tu
TEMPERATURE (t)
CURRENT(mA)/VOLTAGE(mV)
PASSED TIME (X 1 sec)

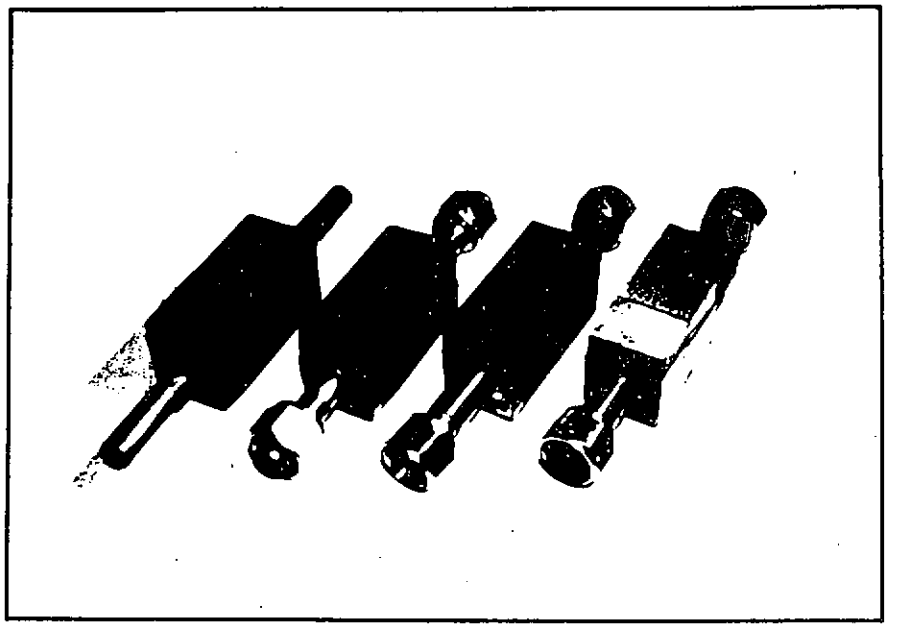

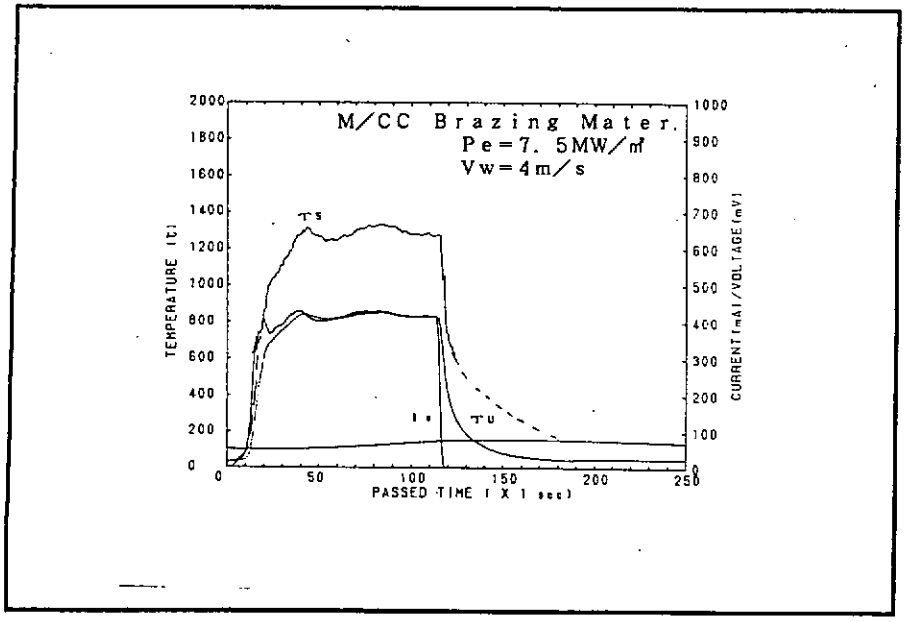
M/CC Brazing Mater.
Pe=7.5MW/m²
Vw=4m/s
Ts
Ie
Tu
TEMPERATURE (t)
CURRENT(mA)/VOLTAGE(mV)
PASSED TIME (X 1 sec)

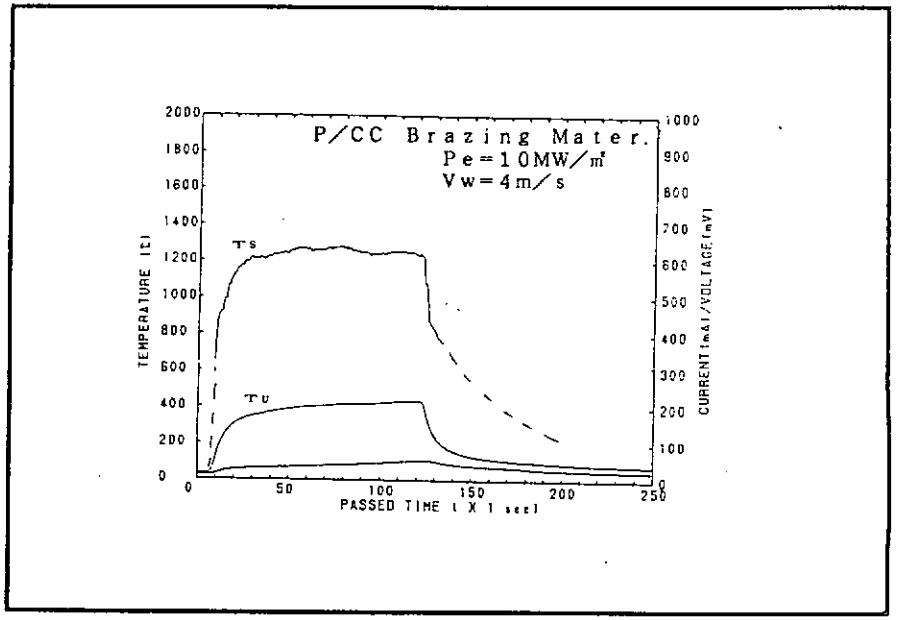
P/CC Brazing Mater.
Pe=10MW/m²
Vw=4m/s
Ts
Tu
TEMPERATURE (t)
CURRENT(mA)/VOLTAGE(mV)
PASSED TIME (X 1 sec)

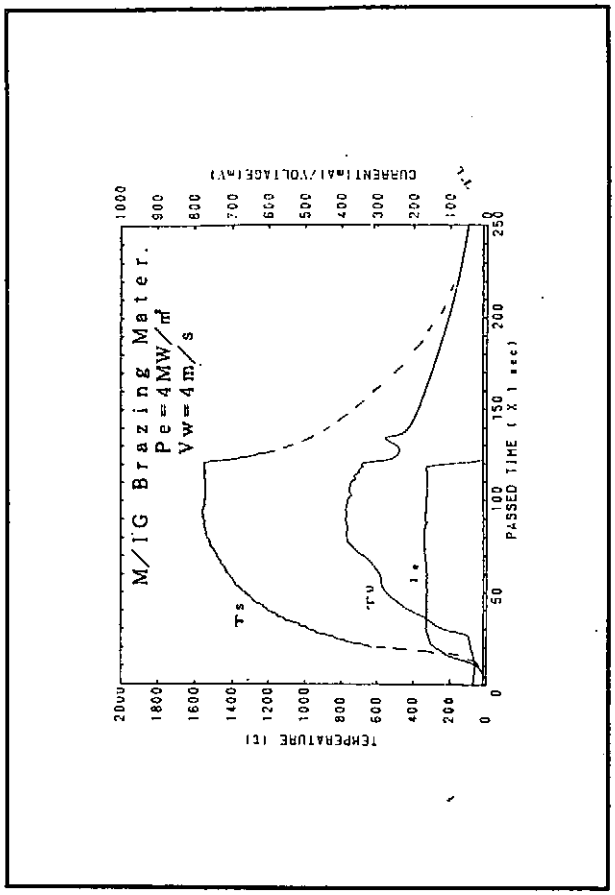
M/IG Brazing Mater.
Pe=4MW/m²
Vw=4m/s
Ts
Tfu
Tfl
TEMPERATURE (℃)
PASSED TIME (X 1 sec)
CURRENT(mA)/VOLTAGE(mV)

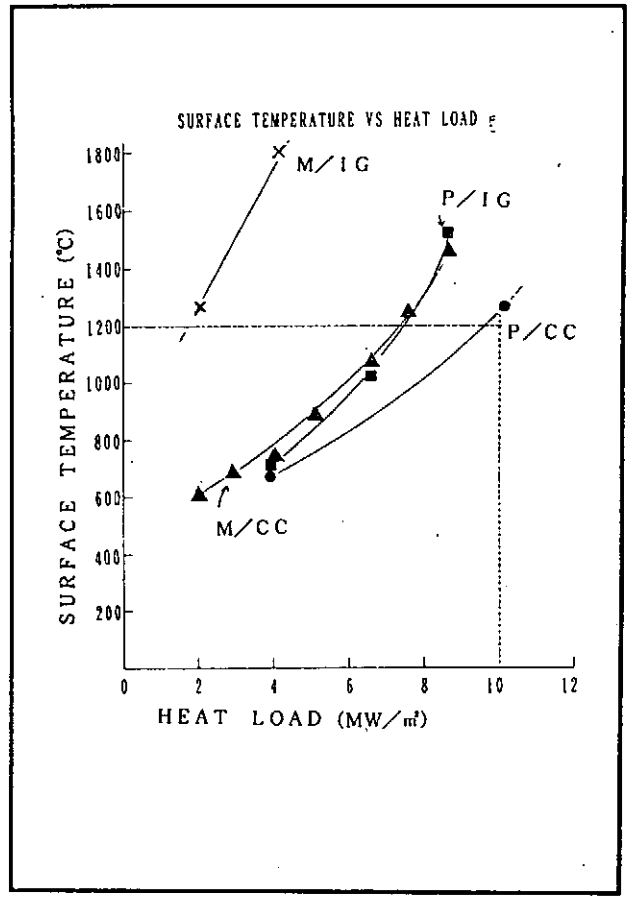
SURFACE TEMPERATURE VS HEAT LOAD
M/IG
P/IG
P/CC
M/CC
SURFACE TEMPERATURE (℃)
HEAT LOAD (MW/m²)

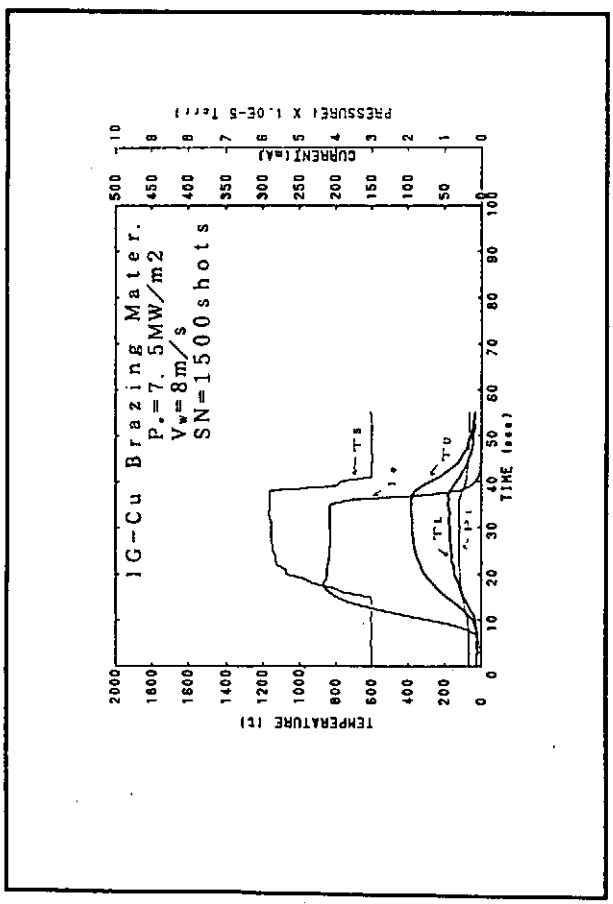
IG-Cu Brazing Mater.
Pe=7.5MW/m2
Vw=8m/s
SN=1500shots
Ts
Tfu
Tfl
TEMPERATURE (℃)
TIME (sec)
CURRENT(mA)
PRESSURE(X 1.0E-5 Torr)

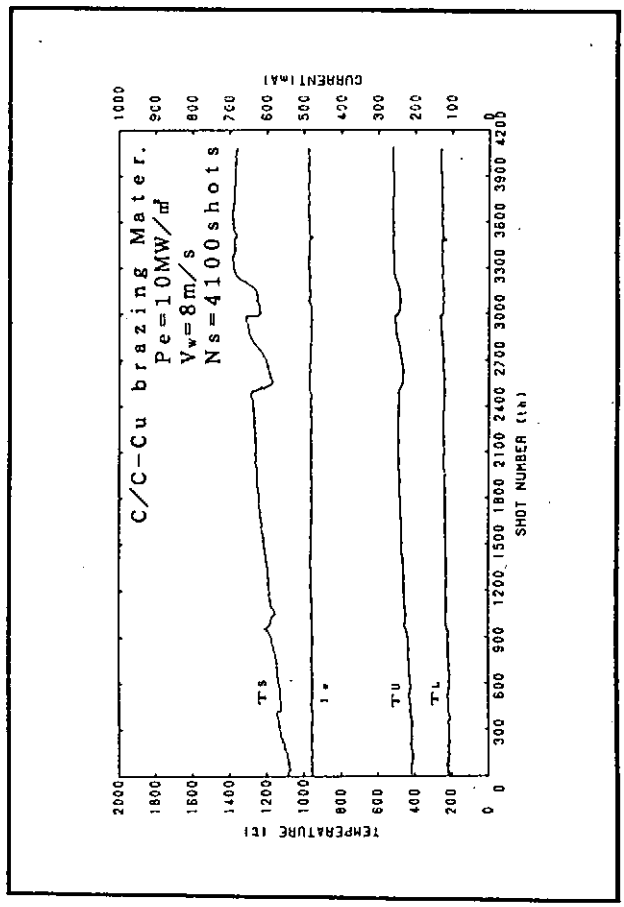
C/C-Cu brazing Mater.
Pe=10MW/m²
Vw=8m/s
Ns=4100shots
Ts
Tfu
Tfl
TEMPERATURE (℃)
SHOT NUMBER (ns)
CURRENT(mA)

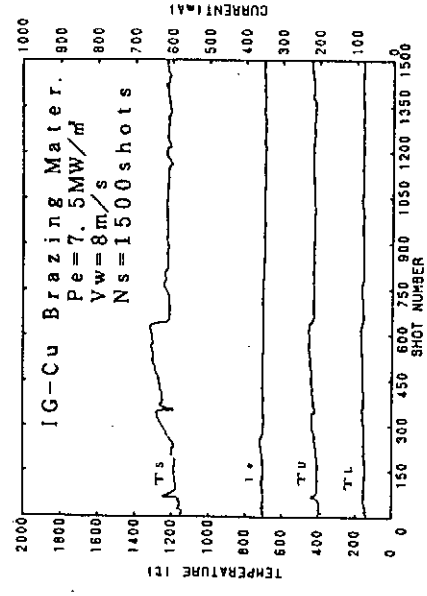

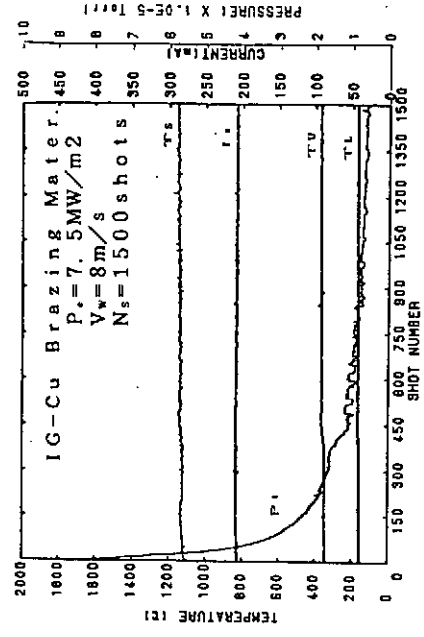

HEAT CYCLE TEST OF BRAZING MATERIALS

No	Name	Type	Total Shot	P (MW/m2)	Result
1	C-Cu	P/C	4100	10	No Damage
2	IG-Cu	P/G	1500	7.5	〃
3	〃	〃	〃	〃	〃

[Note] One Period: 60 sec

Coling Water flow rate: 8 m/s

CONCLUSIONS

1. To perform reliable heat load and heat cycle tests, a feedback control of EBS by target beam current not total current is required.
2. High heat flux tests of four brazing materials have been carried out. The surface temperature of P/CC sample is as low as 1200 ℃ under a heat load of 10 MW/m², which is applicable to the divertors of LHD.
3. The surface temperature of M/IG sample reaches 1500 ℃ with response time of 100 s under a heat load of 4 MW/m². However, the sample is also applicable to the divertor of LHD for 5 sec operation and heat load less than 5 MW/m².
4. Heat cycle tests up to 4100 shots for F/CC sample and up to 1500 shots for F/IG samples have been carried out under 10 MW/m² and 7.5 MW /m², respectively. No damage was observed for them after the heat cycle tests.

PFC Activities at Toyo Tanso

November 17-19, 1992
T.Matsuda,T.Sogabe
T.matsumoto,M.Okada
Toyo Tanso Co.,Ltd.

Abstract

Recently we are studing brazing for plasma-facing compoments. Brazing is carried out by using iron and copper brazing filler metals, and brazed by a mechanism "dissolution and deposit of base metal". The mechanism involves the dissolution of iron in molten copper and subsequent reaction with the graphite, resulting in the growth of a columnar Fe/Cu/C phase. IG-110 and IG-430U (Isotropic graphites) and CX-2002U (CFC) are brazed to copper or molybdenum, or joined to itself. We have prepared some test pieces for the LHD divertor plate that will be tested by ACT facility in NIFS. Soundness of brazing was examined by a simple thermal shock test and by 4- point bending test. 4-point bending test was carried out on brazed specimens with dimensions 6x6x45 (mm) which have brazed joint at the center, under vacuum, at temperature from room temperature to 800 or 1000 deg.C. It was found that strength of brazed materials was maintained at the almost same level of the graphite/carbon material up to 600 deg.C.

SiC coated mirror on isotropic graphite joined with active cooling copper metal is also introduced. This kind of mirror is mainly used for reflecting laser beams. Metal mixed graphite materials has been fabricating including boron, titanium and vanadium. Boronized CFC materials are now developing. Some physicsal properties and air oxidation behaviours are presented.

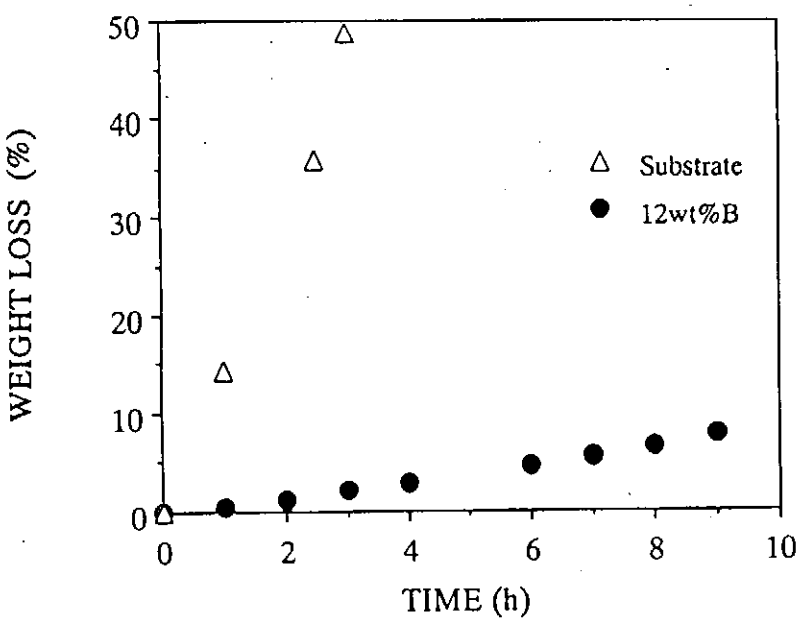

Fig.1 Weight loss of boronized CFC (12wt% boron) due to the reaction with air at 800°C.

Table of Contents

Development of Carbon Material Brazed with Metal and PFC Activity at Toyo Tanso

T.Matsuda, T.Sogabe, T.Matsumoto and M.Okada
Toyo Tanso Co.,Ltd.
(presented by T.Matsuda)

Japan-US Workshop P-196
November.17-19,1992 Kyushu University

Brazing Method

1. A technique named as "dissolution and deposit of base metal" was employed to braze a plasma facing component with metal.
2. Physical properties of PFC used in this study...
   IG-430U(isotropic graphite)
   CX-2002U(CFC)
3. Region for PFC-Mo-Cu brazing

Project Background

1. Carbon and graphite materials have superior thermal properties which ideally suit them for use as plasma facing components in major fusion devices.

2. For magnetic fusion devices such as the Large Helical Device (LHD) and the International Thermonuclear Experimental Reactor (ITER), the development of active cooling for plasma facing components is seen as inevitable.

3. Modifing graphite materials is increasingly important for improved erosion yield, T-retention and so on.

Evaluation of Brazed Components

1. Characterization of brazed zone
2. 4-point bending test (PFC-Mo)
3. Thermal shock test (PFC-Mo-Cu)
4. High-heat load test in ACT (PFC-Mo-Cu)

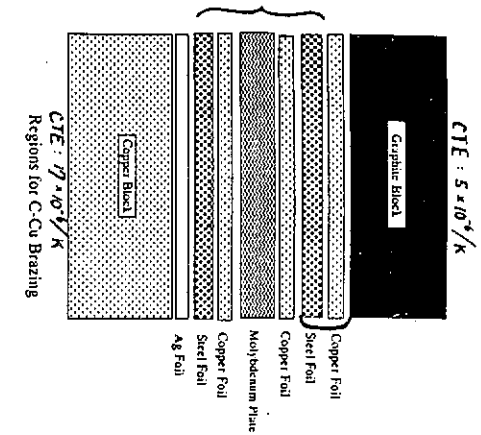

EVALUATION OF BRAZING COMPONENTS

(1) Interface of PFC - Mo Brazing

(Graphite - Cu - Fe - Cu - Mo)

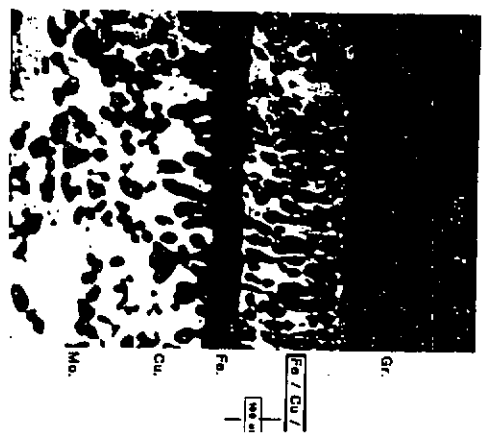

Table 1 Physical Properties of IG-430U and CX-2002U

Name	IG-430U	CX-2002U	
		◂▸	◂▸
Type	Isotropic Graphite	CFC(Felt Type)	
Density (Mg/m^3)	1.82	1.70	
Bending Strength (MPa)	54	54	-
Compressive Strength (MPa)	83	61	64
Young's Modulus (GPa)	11		
Thermal Conductivity (W/(mK))	139	325	186
Coefficient of Thermal Exp. (10^{-6}/°C)	4.4	1.8	5.8

TYPE I

NIFS

ACT : Active Cooling Test Stand

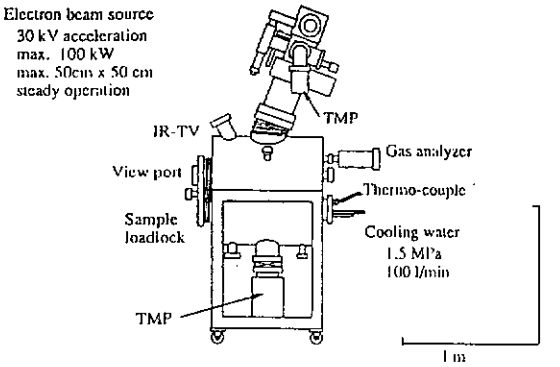

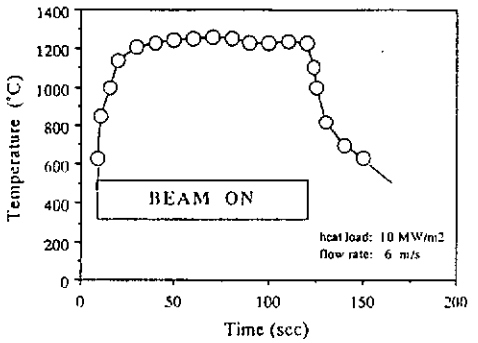

Surface temperature of CX-2002U (Flat-plate Type)

NIFS

Test pieces for the LHD divertor plate

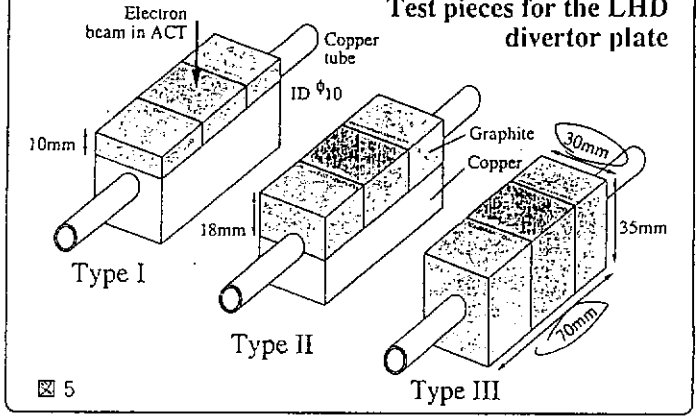

図 5

Recent Development for Plasma Facing Component

1. Boronized Graphite
2. Boronized CFC
3. Boronized Target Material
   (UCLA and Tokamak de Varennes collabolation)

June 11, 1992
TOYO TANSO CO., LTD
RED Section

Properties of bulk-boronized graphites

Material	GB-100	GB-101	GB-103	GB-110	GB-120
Boron conc.(wt%)	0	1.0	3.1	10.9	22.2
Bulk density (Mg/m³)	1.80	1.79	1.85	1.82	1.75
Shore hardness	64	64	67	70	58
Bending strength (MPa)	37	38	44	56	56
Compressive str. (MPa)	100	78	104	137	159
CTE(10^{-6} K) (RT~400℃) // direction	5.7	5.5	5.3	4.9	4.6
Specific res.(μΩ·m)	10.8	8.9	9.1	15.2	25.5
Thermal cond. (W/(m·K)) ⊥ direction	54	48	33	35	33
// direction (laser flash method, RT)	26	29	26	28	23

These values were obtained from each particular block.
They are not guarantee values.

Trial Production Code Name	CXB-006	CXB-007
Type	CFC(Felt Type)	CFC(Felt Type)
Density, (Mg/m³)	1.7	1.7
Boron Conc. (Wt%)	12	3
Thermal Cond.(W/(m·k))	76	116
Bending Strength(MPa)	30	30

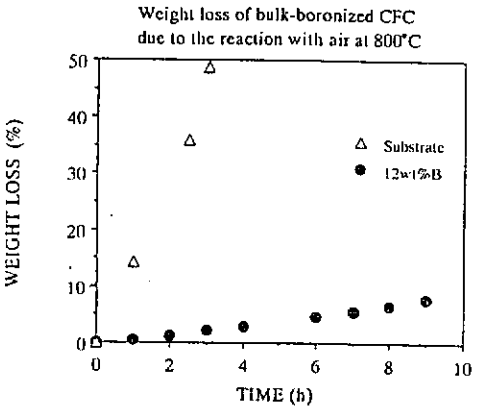

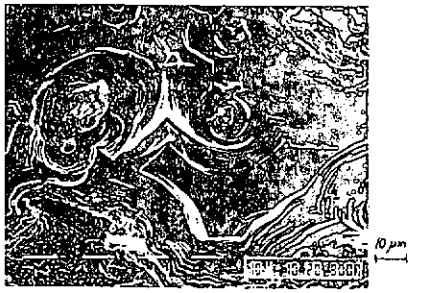

Boronized CFC
(12 wt % B)

Boronized Target

Boron Mapping by XMA

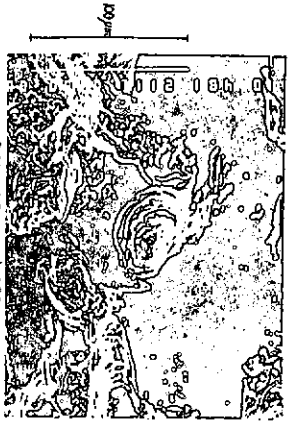

SEM (Boronized CFC)

Summary

1. By the method "dissolution and deposition of base metal', it is possible to braze graphite to copper, with joined areas as large as 30x30 mm. Uniformity of the brazed area is enhanced by using foil filler metals.

2. Flat-plate type C-Cu brazed samples, which were prepared as an application for divertor plate in LHD, showed excellent stability on surface temperature in ACT.

3. Bronized graphite and boronized CFC are also developed for PFC. They can be considered as the material for brazing.

Development of Plasma Facing Components in Toshiba
- Optimal Configuration of Graphite-Copper Bonded System -

Kazunori Kitamura
Heavy Apparatus Engineering Laboratory, Toshiba Corporation
2-4, Suehiro-cho, Tsurumi-ku, Yokohama, 230 Japan

The carbon-fiber-composite(CFC)/copper heat sink and tungsten-copper bonded systems have received consideration for use as a divertor plate in an engineering design activities of the International Thermonuclear Experimental Reactor(ITER)(1). Some bonded features such as a monoblock-type and saddle-type structures are proposed to enhance the thermal and mechanical performance.

Residual stress due to thermal expansion mismatch will have a significant influence on its performance. Thus, a knowledge of the residual stress in the divertor plate with the bonded armor is of great importance. Especially, a normal stress component to bonded interface at the edge needs to be reduced because it is considered to be one of possible driving forces for the interfacial failure.

The residual stresses that developed during cool down of test specimens with tungsten disk brazed to copper heat sink were measured by the strain gauge method and compared with those by thermoelasto-plastic FEM analysis(2). Good agreement was obtained for both residual stress and displacement even when the creep effect of the copper heat sink was neglected in the analysis. The analytical method was consequently confirmed to be reasonable.

The residual stresses on three types of graphite-copper bonded structures such as a flat-type, monoblock-type and saddle-type ones were compared from the calculation to be 44 MPa, 7 MPa and 13 MPa, respectively. Therefore, the saddle-type structure was found to be best in the view of the mechanical integrity, in addition to the standpoints of the fabrication and maintenance.

In addition, the residual stresses around the interface edge in the C/Cu saddle-type structures with wedge angles of 45° to 135° were also examined. As the results, an optimal bonded configuration of the saddle-type structure was found to have the wedge angle of about 60° for the least value of the residual stress.

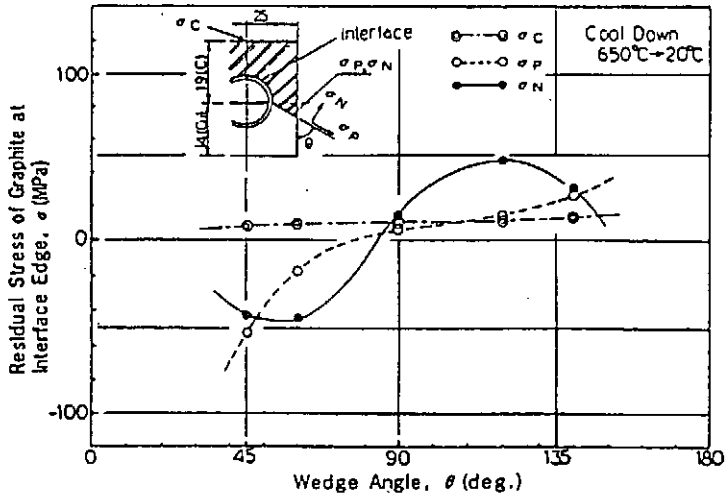

Fig. Influence of Wedge Angle at Interface Edge on Residual Stress

References

(1) T. Kuroda et al., ITER plasma facing components, ITER documentation series no. 30, IAEA, Vienna, 1990.
(2) K. Kitamura et al., Experimental and analytical studies on residual stress in the tungsten-copper duplex structure for a divertor application, Fusion Engng. and Design 18(1991)173-178.

Development of Plasma Facing Components in Toshiba Corp. —Optimal Configuration of Graphite/ Copper Bonded System—

Kazunori Kitamura

Heavy Apparatus Engineering Laboratory,
Toshiba Corporation,
2-4, Suehiro-cho, Tsurumi-ku, Yokohama,
230 Japan

Japan-US Workshop P-196
Nov. 17-19, 1992
Kyushu Univ., Fukuoka, Japan

TOSHIBA

TOPICS

- Introduction
- Comparison of experimental and analytical results of W/Cu duplex structure test specimens on residual stresses that developed during cooling of the joint from brazing temperature.
- Analytical studies on residual stress in C/Cu bonded systems.
  - Comparison of flat-type, monoblock-type and saddle-type bonded structures.
  - Optimal configuration of saddle-type C/Cu bonded structure.
- Summary

TOSHIBA

Mechanical Assessment of Bonded System

- Critical Issues
  - Microcrackings around interface edge.
  - Debonding of armor from heat sink and cooling tube.
- Mechanical Strength of Bonded Interface
  - Evaluation of residual stress around the bonded interface, especially of normal stress component to the interface at the edge (developed during cool down from brazing temp.)
  - Investigation of thermal stress field of bonded structure (induced by cyclic heat loads)

TOSHIBA

- Comparison of experimental and analytical results of W/Cu duplex structure test specimens on residual stresses that developed during cooling of the joint from brazing temperature.

TOSHIBA

W/Cu DUPLEX STRUCTURE WITH STRAIN GAUGES

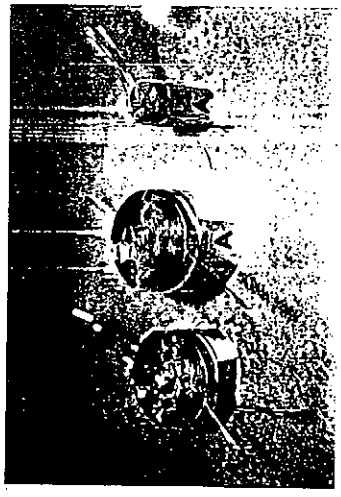

DIAMETER φ30 DIAMETER φ30 DIAMETER φ12.5
Cu THICKNESS 10mm Cu THICKNESS 20mm Cu THICKNESS 20mm

TOSHIBA

AXIAL RESIDUAL DISPLACEMENTS ON TUNGSTEN TOP SURFACE

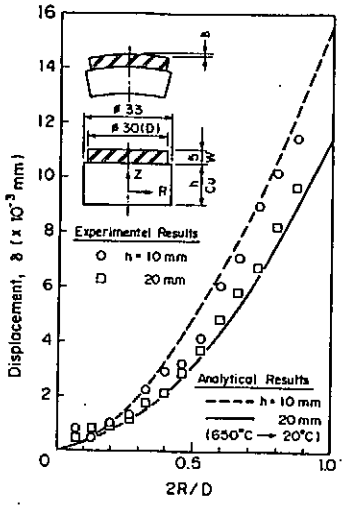

TOSHIBA

RESIDUAL STRESSES ON TUNGSTEN TOP SURFACE

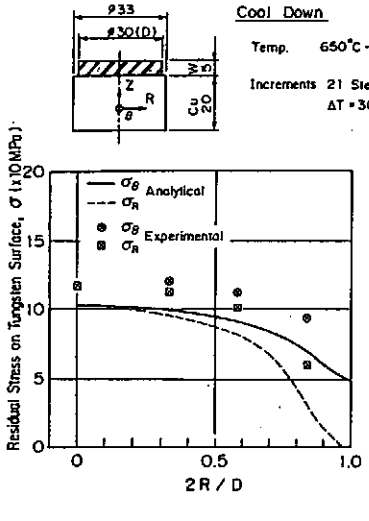

TOSHIBA

RESIDUAL STRESSES ON TUNGSTEN SIDE SURFACE

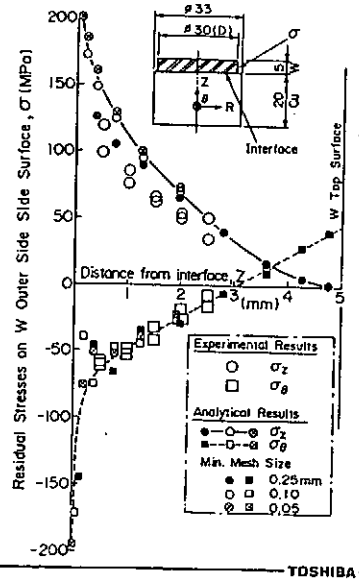

TOSHIBA

- Analytical studies on residual stress in C/Cu bonded systems.
  - Comparison of flat-type, monoblock-type and saddle-type bonded structures.
  - Optimal configuration of saddle-type C/Cu bonded structure.

TOSHIBA

Thermomechanical properties of isotropic graphite and annealed OFCu

	T °C	λ W/m·K	C MJ/m³K	E GPa	ν	α 10⁻⁶/°C	σ0.2 MPa	Et Gpa
Iso. Gra.	20	135	1.31	9.3	0.18	4.7	----	----
	300	116	2.51	9.4	0.18	5.1	----	----
	500	92	2.93	9.8	0.18	5.3	----	----
	800	69	3.28	10.3	0.18	5.6	----	----
	1200	53	3.68	10.8	0.18	6.0	----	----
	1600	47	3.83	11.4	0.18	6.5	----	----
	2000	40	3.93	12.2	0.18	6.9	----	----
Ann. OFCu	20	391	3.39	83.4	0.33	15.4	26	Fig.1
	200	372	3.83	73.6	0.33	16.6	20	
	400	359	3.81	68.7	0.33	18.3	16	
	600	355	3.97	61.8	0.33	20.0	13	
	800	350	4.10	58.9	(0.33)	21.6	7.5	

λ: thermal conductivity, C: specific heat, E: Young's modulus, ν: Poisson's ratio, α: coefficient of thermal expansion, σ0.2: 0.2% proof stress, Et: work hardening slop.

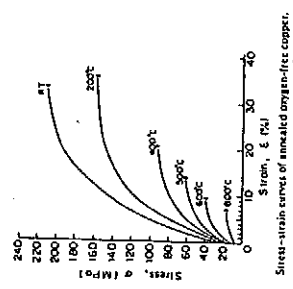

Stress-strain curves of annealed oxygen-free copper.

TOSHIBA

Three Types of C/Cu Bonded Systems

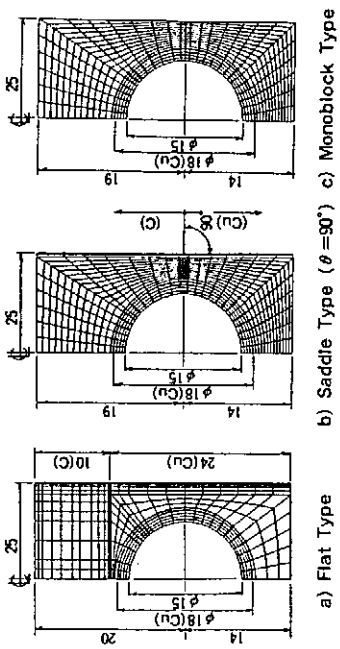

TOSHIBA

Comparison of Three Types of C/Cu Bonded Systems

		Flat-type	Saddle-type (θ=90°)	Monoblock-type
Fabricability		Easy	Possible	Difficult
Maintenability		Easy	Possible	Difficult
Residual stress after brazing, σ (MPa)	σ_C	14	9	1.5
	σ_P	−10	−7	−20
	σ_N	44	13	7

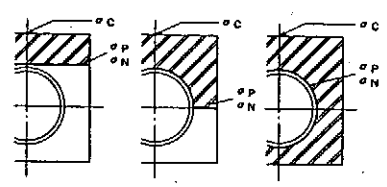

σ_C : Max. stress on C Top surface
σ_P : Max. parallel stress to bonded interface
σ_N : Max. normal stress to bonded interface

TOSHIBA

Saddle-Type C/Cu Bonded Structures with Different Wedge Angles at Interface

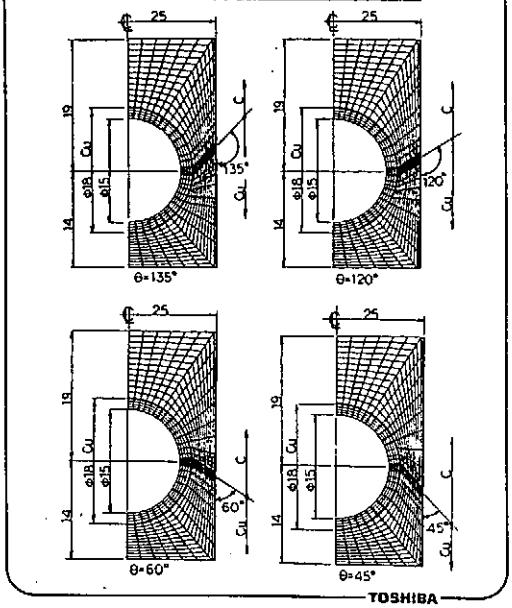

TOSHIBA

Influence of Wedge Angle at Interface Edge on Residual Stress

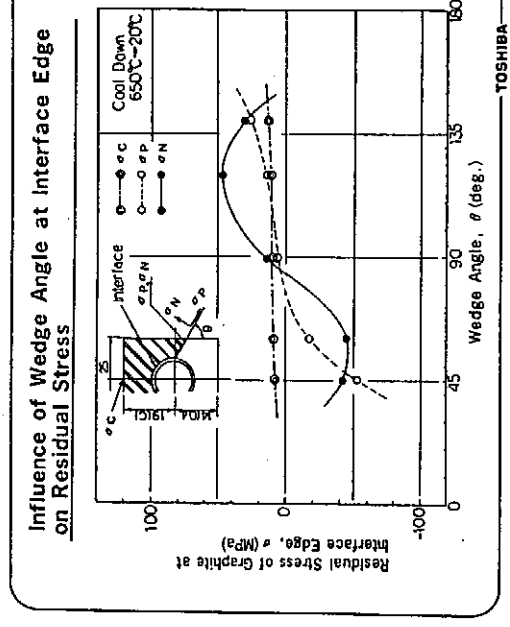

TOSHIBA

Summary

Analytical studies on residual stress around the interface edge of W/Cu and C/Cu bonded structures were performed to assess their mechanical integrities.

- Good agreement was obtained for both residual stress and displacement between experimental and analytical results of W/Cu test specimens.
- Residual stress on three-types of C/Cu bonded structures such as flat-type, monoblock-type and saddle-type ones were compared from the calculation to be 44 MPa, 7 MPa and 13 MPa, respectively and saddle-type one was found to be best in the views of mechanical integrity, fabrication and maintenance.
- Residual stresses at the interface edge in C/Cu saddle-type structures with wedge angles of 45° to 135° were also examined. As the results, optimal configuration of the saddle-type structure was found to have the wedge angle of 60° for the least value of the residual stress.

TOSHIBA

Future Work

- Measurements of residual stresses on C/Cu(CFC/Cu) bonded test specimens by the strain gauge method and comparison with those by thermo-elasto-plastic FEM analysis.
- Thermal fatigue tests of C/Cu(CFC/Cu) bonded structures using electron-beam test facility to verify the optimal bonded configuration.
- Optimization study of W/Cu bonded system.

TOSHIBA

Behavior of Carbon-Boron-Titanium Materials under High Heat Load

H. Shinno, M. Fujitsuka and T. Tanabe (Nat. Res. Inst. for Metals),
T. Shikama (Tohoku Univ.),
A. Ono and T. Baba (Nat. Res. Lab. of Metrology)

Carbon materials with high thermal conductivity are used as protection wall materials of nuclear fusion facilities. And a boronization of surfaces of the carbon materials is going to improve a plasma confinement performance. However, thicknesses of the boronized layers are limited by a relatively low thermal conductivity of B_4C and lives of the boronized layers due to erosion will be shortened. In this experiment, C-B-Ti materials have been examined to increase allowable thicknesses of boron containing layers and to increase the lives of the protection wall materials by improving thermal conductivities of the layers.

Samples were fabricated by an uniaxial hot press and following sintering or HIP process from powders of graphite, boron and titanium. The sintering temperature was 2273K and the HIP process was conducted at a pressure of 196MPa and a temperature of 2273K. The samples were 30 mm dia. and 1 ~ 3 mm thick. Also a functionally-gradient-material was fabricated in which chemical composition changed stepwise along the thickness direction.

Characterization of the samples were performed by an X-ray diffraction, an X-ray microanalysis, a density measurement and an measurement of thermal diffusivity. Thermal shock resistances of the samples were compared using an electron beam apparatus. The electron energy was 40 ~ 50 eV and the beam current was 100 ~ 200 A and the beam diameter was 18 mm. Neutron irradiation was also performed by JMTR. Neutron fluences were 2.34×10^{20} n / m^2 (thermal) and 3.9×10^{19}n / m^2 (fast). The duration was 48 days and the irradiation temperature was 623K.

The X-ray diffraction revealed that the samples were composed of TiC, TiB_2 and graphite. Thermal diffusivities of the samples were close to those of TiC and TiB_2, and increased with increasing TiB_2/TiC ratio. Thermal shock tests showed that resistance against cracking increased with increasing graphite content and TiB_2/TiC ratio. Thermal shock resistances of the functionally-gradient-material was greater than those of any materials of the constituent layers. After neutron irradiation, swelling was observed due to helium produced by (n, α) reaction of B^{10} in the C-B-Ti materials.

Behavior of Carbon-Boron-Titanium Materials under High Heat Load

H. Shinno, M. Fujitsuka and T. Tanabe
(NRIM)

T. Shikama
(Tohoku Univ.)

A. Ono and T. Baba
(NRLM)

Sample Preparation

Table Chemical Composition and crystal structure of the compounds.

Specimen No.		Composition (at.%) C	B	Ti	X-ray diffraction intensity ratio TiC(200)	TiB_2(101)	graphite (002)
1		12	38	50	1	0.70	0
2		24	26	50	1	0.33	0
3		35	13	52	1	0.18	0
4		20	29	45	1	1.12	0
5		31	34	35	1	0.63	0.07
6		35	35	30	1	3.75	0.12
7*	layer1	26	29	45	1	1.12	0
	layer2	31	34	35	1	0.63	0.07
	layer3	35	35	30	1	3.75	0.12

* Gradient material

High heat load testing

heat source:	electron beam (a hot hollow cathode gun)
electron energy:	40~50 eV
electron current:	100~200 A
beam diameter:	18 mm
duration:	< 5 s

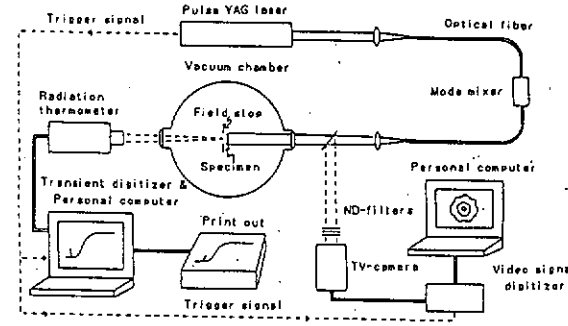

Table Heat-load shock resistance of the compounds.

Specimen No.	Heat load of crack initiation (MW/m²)
1	<38
2	<14
3	<17
4	<23
5	23~29
6	~30
7	>34

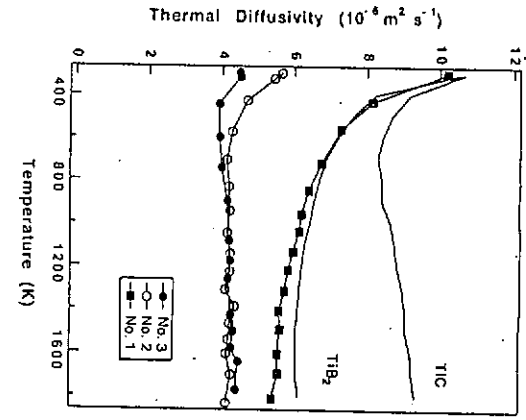

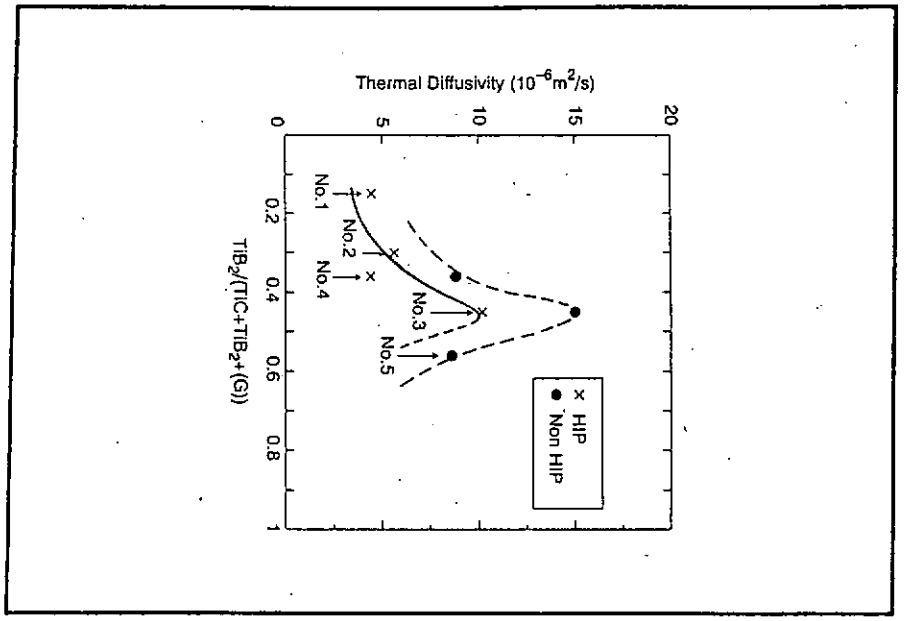

table Chemical composition, crystal structure and density of the compounds

Specimen No.	Composition (at.%)			X-ray diffraction			TiB_2 weight ratio	Density (g/cm^3)
	C	B	Ti	TiC	TiB_2	G*	$TiB_2/(TiC+TiB_2+G)$	
1	35	13	52	o	o		0.15	4.65
2	24	26	50	o	o		0.30	4.71
3	12	38	50	o	o		0.45	4.51
4	26	29	45	o	o		0.36	4.86
5	35	35	30	o	o	o	0.55	4.35

*) G: Graphite

Neutron irradiation

facility:	JMTR
neutron fluence:	2.34×10^{20} n/m² (thermal)
	3.9×10^{19} n/m² (fast)
temperature:	623 K
sample size:	3.5 mm dia., 2~3 mm thick
irradiation duration:	48 full power days

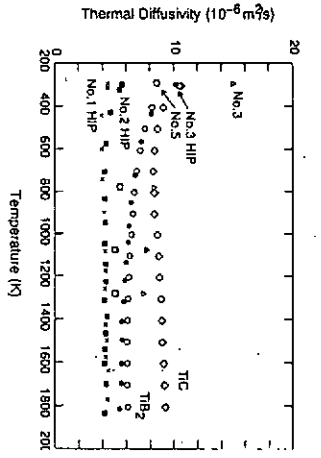

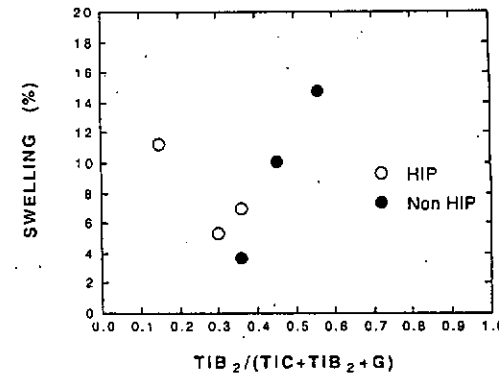

Summary

1. Resistance to thermal shock fracture increased with increasing graphite concentration and TiB_2/TiC ratio.

2. Resistance to thermal shock fracture of a functionally gradient material was higher than that of any material of the constituent layers.

3. Thermal diffusivity increased with increasing TiB_2/TiC ratio.

4. Thermal diffusivity was decreased by a HIP treatment.

5. Swelling was observed in neutron irradiated C-B-Ti materials.

C/C-OFHC Brazing Structure

A. Shigenaka, S. Kajiura, Y. Ozawa, *H. Okamura, *H. Miyata,
*Y. Gotoh and **S. Sakurai

Hitachi Works, Hitachi Ltd., *Hitachi Research Lab., Hitachi Ltd.
**Mechanical Engineering Research Lab., Hitachi Ltd.

Abstract: The divertor system for ITER must withstand static peak power loads in the range of 15 to 30 MW/m². In view of the high heat loads, the divertor plate armor (C/C) has to be brazed to the heat sink (OFHC) with high reliability. On the other hand, the area of ITER divertor is 200m² and more than 100,000 divertor plates will be needed. This means not only development of reliable brazing technique but also development of brazing structure which can mass-produce is an important subject.

Figure 1 shows cross section of the saddle type divertor test module and microstructure of the brazing layer. The upper part of the test module is made of C/C and the lower part is made of OFHC. Ti included Ag-Cu eutectic brazing sheets are used for the vacuum brazing. By means of optimizing heat condition of the brazing reaction, quantity of the brazing sheets and the gaps between C/C and OFHC, a good brazing test module which withstand the static peak power loads of 20MW/m² (which was tested in JAERI) has been made.

Figure 2 shows schematic of the saddle type divertor mock-up. The mock-up has the length of 1m and 32 pieces of the C/C armor tiles are brazed on the heat sink. The heat sink is made of OFHC hollow conductor in order to minimize the brazing part of the mock-up and to simplify the manufacturing process. Using the same materials for the jig of this mock-up, distortion of the mock-up could be kept away as small as possible.

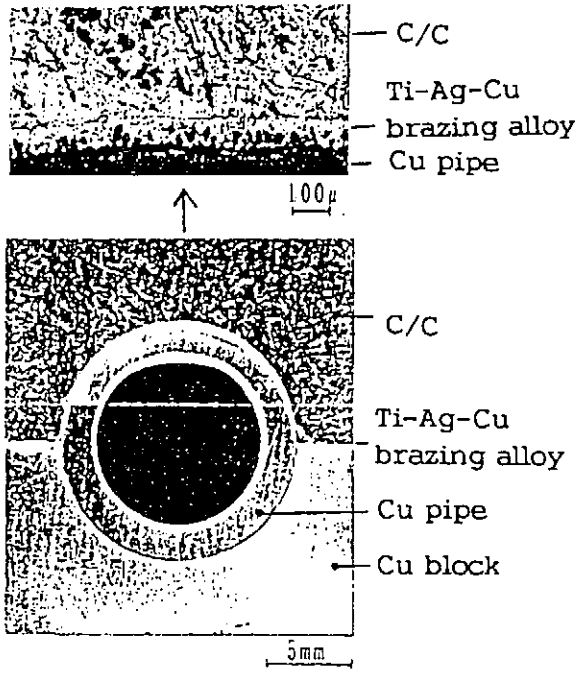

Fig.1 Cross section of the saddle type divertor

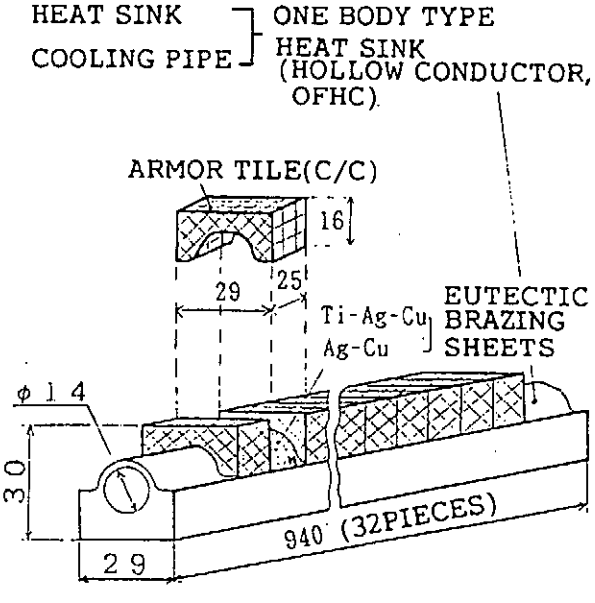

Fig.2 C/C-OFHC brazed divertor test module.

C/C-OFHC BRAZING STRUCTURE

A. Shigenaka, S. Kajiura, Y. Ozawa, *H. Okamura, *H. Miyata, *Y. Gotoh and **S. Sakurai

Hitachi Works, Hitachi Ltd.,
*Hitachi Research Lab., Hitachi Ltd.,
**Mechanical Eng. Research Lab., Hitachi Ltd.

Background

The divertor system for ITER :
(1) Static peak power load is 15-30 MW/m .
(2) Number of divertor plates is >100,000 .

Subjects

(1) Divertor plates must be brazed to the heat sink.
(2) Mass-producing technique is needed for such a system.

Objectives

(1) Development of C/C-OFHC brazing technique.
(2) Development of brazing structure suitable for mass-production.

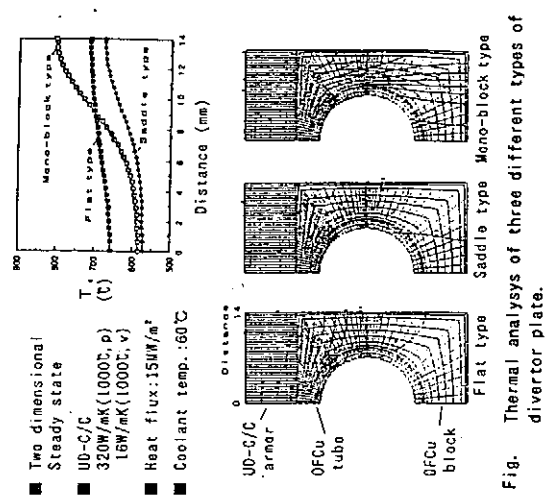

Fig. Thermal analysys of three different types of divertor plate.

STRUCTURE	FLAT TYPE	SADDLE TYPE	MONO-BLOCK TYPE
COOLING CHARACTERISTICS	△	○	○
MANUFACTURING	○	×	×
IN-SITU MAINTAINABILITY	△	×	×

○:GOOD/EASY △:MEDIUM ×:BAD/DIFFICULT

Fig. Brazing structures and their characteristics of divertor

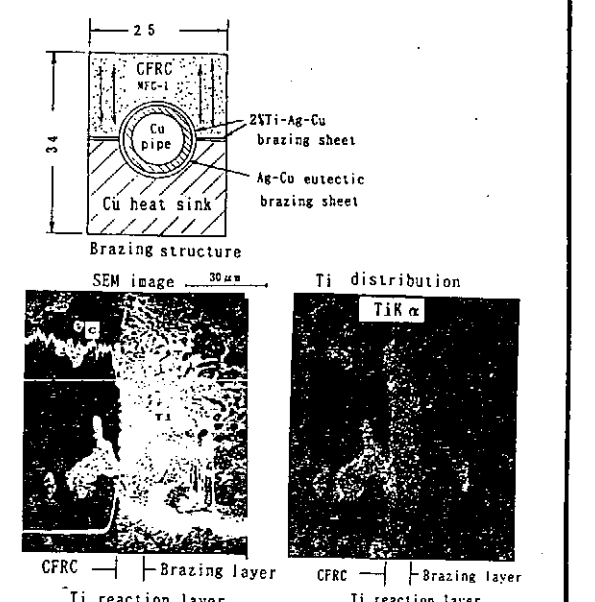

Fig. Brazing structure and bonding mechanism of Divertor test module

CFC/OFHC brazed divertor test module.

(a) Divertor test module

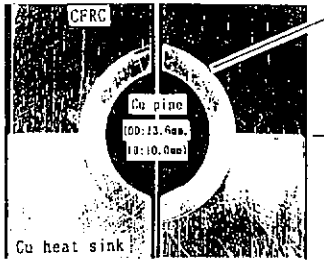

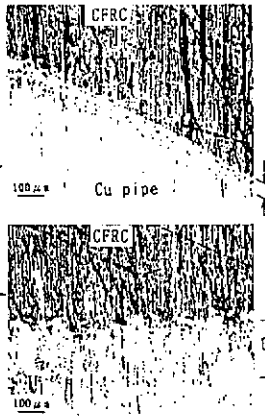

(b) Cross section of Divertor test module (c) Microstructure of brazing layer

Fig. Divertor test module and microstructure of brazing layer

TABLE PARAMETERS OF THE IRRADIATION SYSTEM

PARAMETERS	VALUES
POWER	20 Kw
ACCELERATION VOLTAGE	20 kv
BEAM CURRENT	1 A
DURATION	4 ms ~ 3 s
DIMENSION OF THE V.V.	φ610 x 900
DEGREA OF VACUUM	10^{-7} Torr
IRRADIATION AREA	30 x 25 mm^2
DETECTABLE RANGE OF THE TEMPERATURE	200~3000 C°

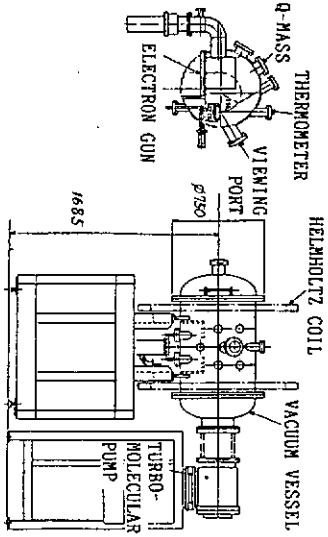

Fig. Electron beam irradiation system.

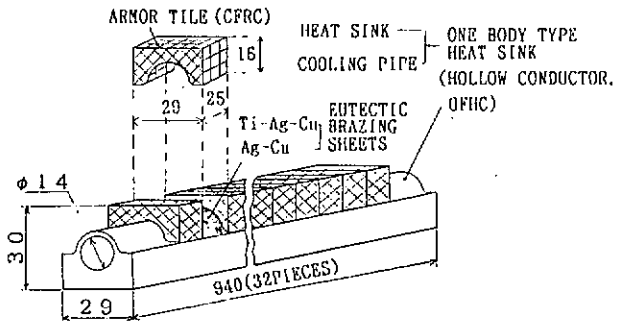

Fig. CFRC/OFHC Brazed divertor test module.

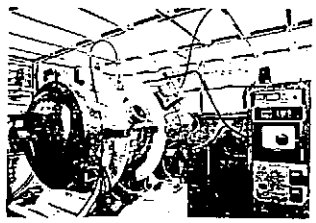

Electron beam irradiation system.

Irradiation test module.

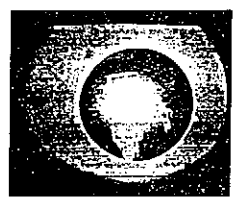

Top view of irradiation test module (15MW/mm²)

Summary

C/C-OFHC brazing structure and bonding mechanism has been investigated for ITER divertor test module.

(1) Saddle type is favorable when UD-C/C is used for the divertor plate.

(2) Using Ti-Ag-Cu brazing alloy, a good brazing divertor test module which withstands the heat load of ITER (20MW/m)has been made.

(3) In order to mass-produce the divertor modules, heat sink made of hollow conductor will be one of the effective suggestion.

J/US WorkShop on High Heat Flux Components and
Plasma Surface Interactions for Next Devices,
Kyushu University, Fukuoka, Japan
Nov. 17 - 19, 1992

High Heat Flux Experiments on B_4C Overlaid Carbon Based Materials for JT-60U Divertor

K. Nakamura
JAERI
801-1 Naka-machi, Naka-gun, Ibaraki-ken, 311-01 Japan

Objectives: B4C overlaid CFC is applicated as some tiles of JT-60U divertor, and more tiles made of B4C overlaid CFC and isotropic graphite are in preparation for JT-60U divertor and first wall. This work is the evaluation on thermal resistivities (exfoliation, melt, crack, etc.) of B4C overlaid CFC under disruption and normal heat loads with JAERI Electron Beam Irradiation Stand (JEBIS) for JT-60U application.

The criterion of B_4C overlaid CFC for JT-60U divertor application:

(1) B_4C overlaid CFC is not exfoliated at disruption heat load, which is estimated ~3MJ/m^2 in a few millisecond in JT-60U.

(2) B_4C overlaid CFC has not significant cracks, exfoliations and melt at normal heat load, which is estimated 10MW/m^2, 5s in JT-60U.

Summary of heating conditions and samples:

Heat Load	550~1600 MW/m^2, 2~5 ms
	5~40 MW/m^2, 5 s
B4C Production Methods	CVR(chemical vapour reaction Method)
	CVD(chemical vapour deposition)
	LPPS(low pressure plasma spray)
Substrate Materials	U-D and 2-D CFC, isotropic graphite
Thickness of B_4C Layers(μm)	100~1300

Results:

(1) The B_4C overlaid CFC produced by CVR show no exfoliations at the disruption heat loads(~3 MJ/m^2), although some small places of bombarded area are melted.

(2) The B_4C overlaid CFC produced by CVR, CVD, LPPS have no failures at the normal heat load(10MW/m^2, 5s) below the average thickness of 400 μm except small weight loss.

High Heat Flux Experiments on B_4C Overlaid Carbon Based Materials for JT- 60U Divertor

Objectives:

Evaluation of the thermal resistivity (exfoliation, melt, crack etc.) of B_4C overlaid carbon based materials for JT-60U divertor application

Criterion of JT-60U Application

1. No exfoliations at disruption heat load (~3 MJ/m^2 in a few millisecond)
2. No significant cracks, exfoliations and melting with normal heat load (10 MW/m^2 , 5 s)

NBI Heating Laboratory

High Heat Flux Experiments on B_4C Overlaid Carbon Based Materials for JT- 60U Divertor

presented by
K. Nakamura

NBI Heating Laboratory
Japan Atomic Energy Research Institute

*H. Ishikawa, T. Ando, K. Sato, K. Yokoyama, S. Suzuki, M. Dairaku, M. Araki, M. Akiba, *S. Ido and Y. Ohara

Naka Fusion Research Establishment, JAERI
*)Saitama University

NBI Heating Laboratory

Heating Conditions and Samples

JAERI

Heat Load	5-40 MW/m^2, 5 s(10 MW/m , 5 s) 550-1600 MW/m^2, 2-5 ms(~3MJ/m^2)
B_4C Production Method	CVR : Chemical Vapour Reaction CVD : Chemical Vapour Deposition LPPS : Low Pressure Plasma Spray
Substrate Materials	2-D CFC (PCC-2S, CC312, CX2002U, MCI-felt) U-D CFC (MFC-1) Isotropic Graphite (PD-330S, PD-600S, HCB-5S1, ETP-10, STP-60)
Thickness of B_4C Layers(μm)	100~1300

NBI Heating Laboratory

Current Activities on PSI in NBI Lab.

JAERI

- ITER Application
  Disruption Heat Load Experiments on U-D and 2-D CFC Materials (~3 MJ/m^2)
- JT- 60U Application
  Disruption and Normal Heat Load Experiments on B_4C Overlaid Carbon Based Materials (~3 MJ/m^2 and 10 MW/m^2, 5 s)
- Basic Studies on PSI(under Preparation)
  Sputtering, Erosion/Redeposition, RES, etc.

NBI Heating Laboratory

Concluding Remarks

JAERI

- The B_4C overlaid CFC produced by CVR show no exfoliation at the disruption heat loads (~3 MJ/m^2), although some small places of bombarded area are melted.
- The B_4C overlaid CFC produced by CVR, CVD and LPPS have no failures at the normal heat loads (10 MW/m^2, 5s) below the average thickness of 400 μm except small weight loss.

NBI Heating Laboratory

Surface observation of B_4C overlaid CFC after disruption heat load (at 550 MW/m², 5ms)

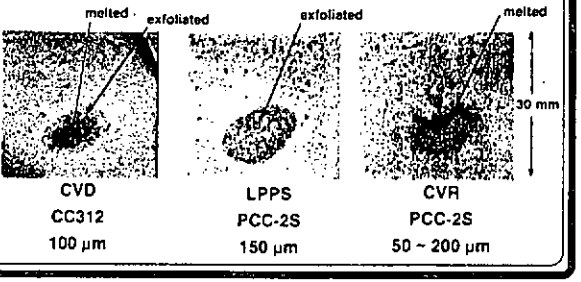

CVD	LPPS	CVR
CC312	PCC-2S	PCC-2S
100 μm	150 μm	50 ~ 200 μm

Plans of Basic PSI Studies in NBI Lab.

JAERI

Materials : Low-Z(CFC, etc.) and High-Z(W, etc.)
Temperature : Room Tem. ~ 1800 °C

- Measurements of Sputtering Yield
  - LSP(Low-Energy Sputtering Test Stand)
    (H,D,He 0.1-1 keV 10^{19}/m^{2}s)
  - SSP(Self-Sputtering Test Stand)
    (W,Mo 0.1-10 keV 10^{17}/m^2 s)
- Evaluation of Erosion/Redeposition
  - Divertor Plasma Experiment Stand
    (H,D,He 5-500 eV 10^{23}/m^2 s)

NBI Heating Laboratory

Surface observation of B_4C overlaid CFC after normal heat load (at 10 MW/m², 5 s)

CVR	CVR	CVR
PCC-2S	PCC-2S	PCC-2S
150 ~ 400 μm	200 ~ 600 μm	400 ~ 800 μm

EVALUATION OF ENERGY DEPOSITION DUE TO RUNAWAY ELECTRONS

Presented by Tomoaki KUNUGI
Reactor System Laboratory, JAERI

Japan-U.S. Workshop P196 on High Heat Flux Components
and Plasma Surface Interactions for Next Devices
November 17 - 19, 1992, at Kyushu University

ABSTRACT

We have been investigated the energy deposition due to runaway electrons using the EGS4(Electron Gamma Shower, ver.4) code. We have done the evaluation of the energy deposition in the PFC without a magnetic field.

In the present study, we are trying to evaluate the effects of the magnetic field for a simple divertor model and three types of the ITER divertor models.

For the simple divertor model, as the incident energies and angles of the runaway electrons increased the effects of the magnetic field decreased. No inclination effects of the magnetic field appeared.

For the ITER divertor models, we found the high energy deposition inside the water and coolant tube due to the magnetic field. Because of the deep penetration of the runaway electrons due to the magnetic field, the deposited energy in the copper structure increased.

These results suggest to us that we need to improve the divertor material and its structure against the impacts of the runaway electrons.

SIMULATION MODELS

- Simple Divertor Model
- ITER Divertor Models

EVALUATION OF ENERGY DEPOSITION DUE TO RUNAWAY ELECTRONS

Presented by Tomoaki KUNUGI

Reactor System Laboratory, JAERI

Japan-U.S. Workshop P196 on High Heat Flux Components
and Plasma Surface Interactions for Next Devices
November 17 - 19, 1992, at Kyushu University

- Simple Divertor Model
  - Effect of Incident Angle,
  - Effect of Runaway Electrons Energy,
  - Effect of Inclination of the Magnetic Field.

OBJECTIVES

We have been investigated the energy deposition due to runaway electrons using the EGS4 code. We have done the evaluation of the energy deposition in the PFC without a magnetic field. In the present study, we are trying to evaluate the effects of the magnetic field for a simple divertor model and three types of the ITER divertors.

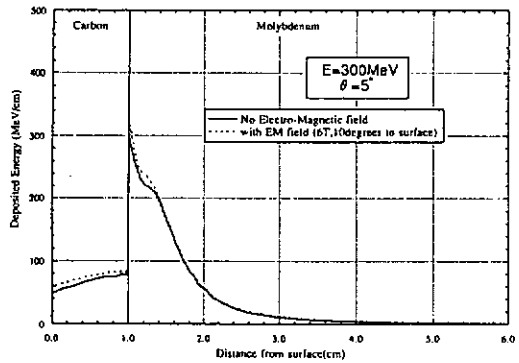

Fig. Effect of Magnetic field (6T) to the Deposited energy on C:10mm + Mo:50mm Layer. Incident Angle=5degree, Energy=300MeV

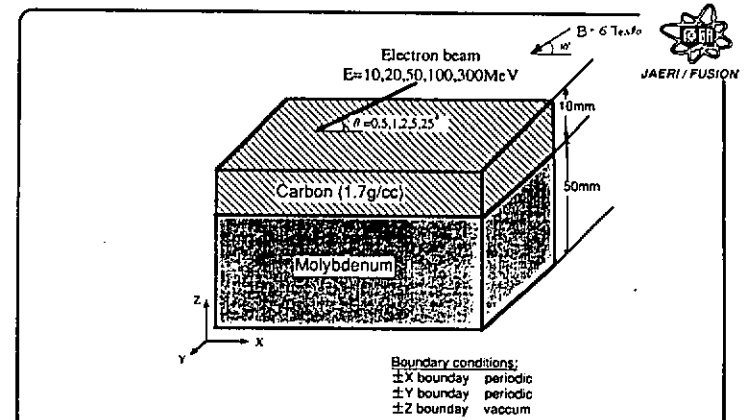

Fig.1 Calculation model
10mm thick carbon and 50mm thick molybdenum infinite area layers.

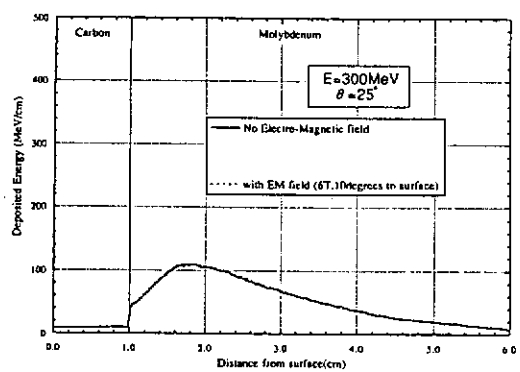

Fig. Effect of Magnetic field (6T) to the Deposited energy on C:10mm + Mo:50mm Layer. Incident Angle=25degree, Energy=300MeV

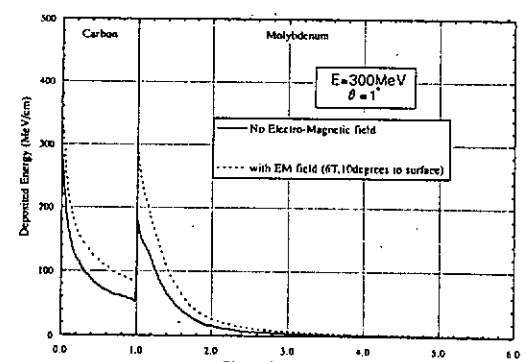

Fig. Effect of Magnetic field (6T) to the Deposited energy on C:10mm + Mo:50mm Layer. Incident Angle=1degree, Energy=300MeV

Peak Deposited Energy Ratio in Molybdenum Layer

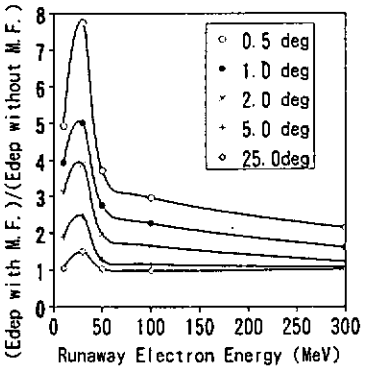

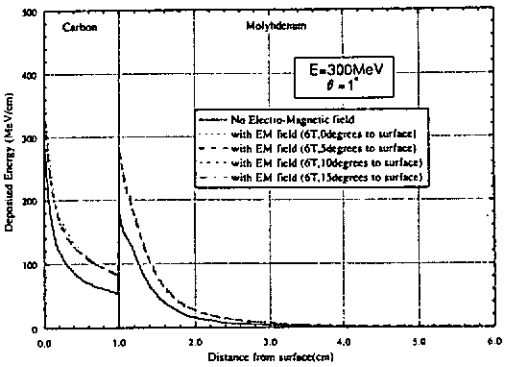

Fig. Effect of Magnetic field direction to Deposited energy , Incident Angle=1degree, Energy=300MeV

Effect of Inclination of Magnetic Field

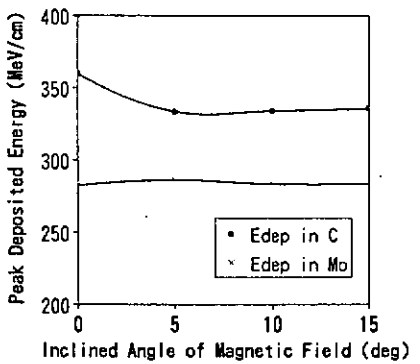

Peak Deposited Energy Ratio in Carbon Layer

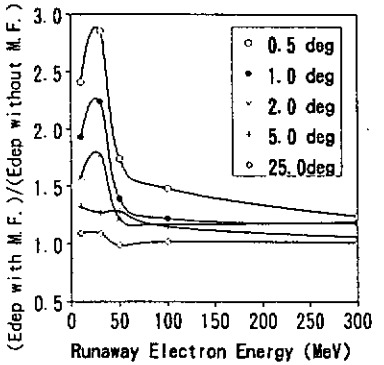

- ITER Divertor Models
  - Effect of Magnetic Field,
  - Effect of Divertor Configurations.

Fig. EGS-4 model for the calculation of energy deposition from runaway electrons on various types of divertor targets

Energy deposition distribution in ITERdivertor target type A
(with 6T Magnetic field)

Fig. Energy deposition distribution in ITERdivertor target type A
(with 6T Magnetic field)

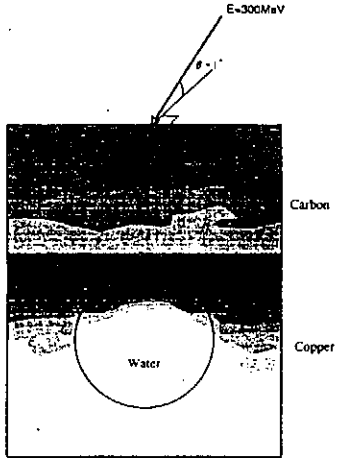

Energy deposition distribution in ITERdivertor target type B
(with 6T Magnetic field)

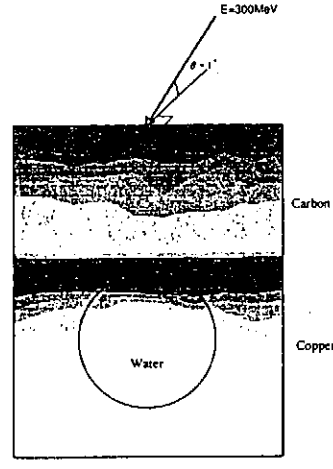

Fig. Energy deposition distribution in ITERdivertor target type B
(no Magnetic field)

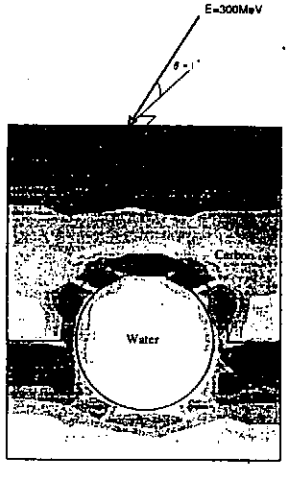

Energy deposition distribution in ITERdivertor target type C
(with 6T Magnetic field)

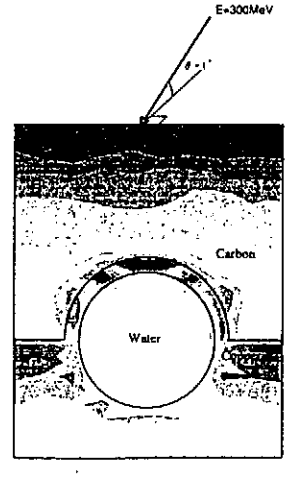

Fig. Energy deposition distribution in ITERdivertor target type C
(no Magnetic field)

Table 1
Peak deposited energy densities for three types of ITER divertor targets

Type	Peak deposited energy density on Copper structure (MeV/cm)	
	with EM field*	no EM field
A	280.8± 13.4	169.3±10.8
B	282.8± 4.7	167.0± 4.3
C	256.2± 12.4	142.8± 9.5

* Electro Magnetic field above divertor target, 6 Tesra, 10 degree to divertor surface

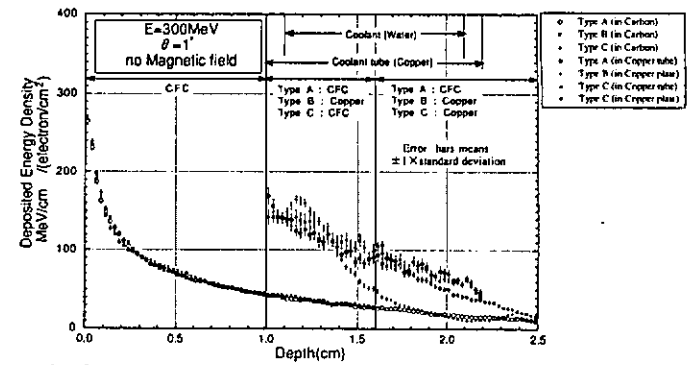

Fig. Deposited energy densities in three types of divertor targets. Incident beam angle (=0.5°, Electron energy (E)=300 MeV, without Magnetic Field.
The deposited energy density is an average of deposited energy per unit volume in each 0.025cm-thick layer.

CONCLUSIONS

- Simple Divertor Model
  - As the Incident Energies and Angles of Runaway Electrons increased the Effects of Magnetic Field decreased,
  - No Inclination Effects of the Magnetic Field on the Peak Deposited Energy appeared.
- ITER Divertor Models
  - High Energy Deposition inside the Water and Coolant Tube Due to the Magnetic Field,
  - Increase the Energy Deposition inside the Copper Structure Due to Deep Penetration of the Runaway Electrons.

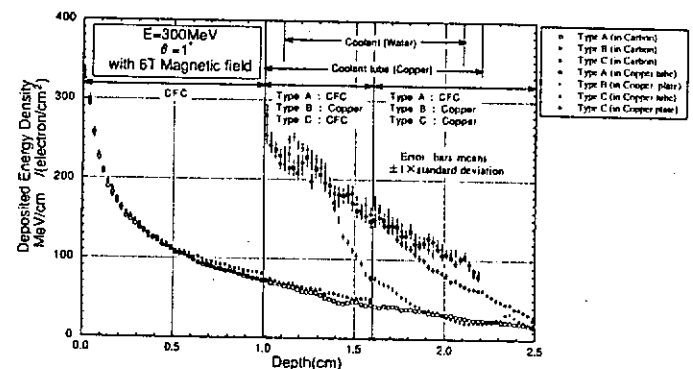

Fig. Deposited energy densities in three types of divertor targets. Incident beam angle (=0.5°, Electron energy (E)=300 MeV, with 6T (10°) Magnetic Field.
The deposited energy density is an average of deposited energy per unit volume in each 0.025cm-thick layer.

The NET Team
A. Cardella

Progress in the EC Technology Programme on Plasma Facing Components

ABSTRACT

This presentation briefly describes the EC programme for the plasma facing components of NET and reports some recent results. The programme consists of specific R&D tasks on the structural materials, the protection materials and the components (i.e. divertor, first wall and sublimiters). A significant progress has been made in the characterization of the selected armuor and structural materials. Divertor and first wall mock-ups have been manufactured and tested in order to demonstrate the basic feasibility of the selected concepts.

PROGRESS IN THE EC TECHNOLOGY PROGRAMME ON PLASMA FACING COMPONENTS

Cardella Antonino

The NET Team
Boltzmann str. 2
D-8046 Garching
Germany

Presented at the

US/Japan Workshop P196 on
high heat flux components and
plasma surface interactions for next devices

Fukuoka, Japan
November 17-19, 1992

The technology programme on plasma facing components for NET is mainly divided in three R&D tasks:

- Structural Materials
- Protection Materials
  - Plasma Wall Interaction
  - Material Characterization and Selection
- Components Development and Testing
  - Divertor
  - First Wall
  - Sublimiter

The Plasma Facing Component Group of NET consists at present of: G. Vieider (Group Leader), A. Cardella, C. Wu, G. Federici.

STRUCTURAL MATERIALS
(Recent Results)

Preliminary results on **TZM** show that the DBTT remains below room temperature after irradiation to 0.3 dpa at 100 °C.

On **Cu-alloys**:
- marked brittleness at 450 °C (typically creep fracture strain < 3%).
- indication of microstructural stability of irradiated Cu-Al_2O_3; only a slight decrease in the mean Al_2O_3 size and density after 750 Mev p-irradiation at 200 °C up to 2 dpa.

On **316L s.a.** and its joining, 18 Mev p-irradiation at <= 450 °C resulted in an increased resistance to crack growth and thus of the fatigue life, but a hold time as low as 20 s causes a reduction of fatigue life due to creep-fatigue interaction

Fatigue life of **316 L EB welds** is not reduced by He implantation at 450 °C up to 1500 ppm but at 600 °C decreases with decreasing frequency, increasing hold time and He content. He embrittlement at creep rupture at 600 °C is large in the base material and in the weld is significant only at >300 ppm.

PROTECTION MATERIALS

On CFC characterisation, the scatter in the results underline the need to address statistical aspects (failure probability) in design with CFC materials.

A development and fabricability study of B_4C or TiC doped CFC materials has started with Hot Isostatic Pressing. Short fibre composites and infiltrated 3D C-fibre [redacted] with densities up to 95% have been achieved. Process control and thermal conductivity have to be optimized.

On coating development, thick (0.4-0.8 mm) plasma sprayed B_4C coatings on 316L substrates were tested at energy density of 2.1 MJ/m^2 in 1.2 ms. Typical values for the depth of the erosion crater are in the range 0.05-0.15 mm, but differences between 1 and 5 shots do not scale linearly.

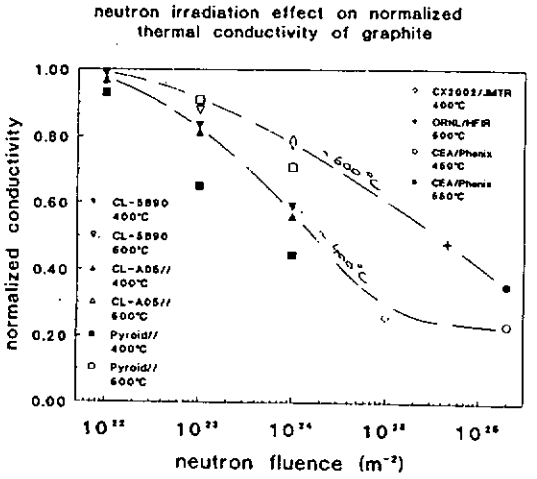

PROTECTION MATERIALS (cont'd)

Gas inclusion and volumetric heating effects complicate direct quantitative analysis, but results indicate that no gross failure of the coating took place.

On high emissivity coatings, thermal cycling tests on 316L type tube specimens with black (oxide) coatings have been finished. No influence of the coatings on tube lifetime was found. Failures occurred, at welds and spot welded thermocouple locations.

The low dose neutron irradiation effect on the thermal conductivity of carbon based materials PyC, S1611, CL5890, and A 05 has been investigated for irradiation temperature of 400°C and 600°C with damage of 0.01 and 0.1 dpa. The neutron-induced degradation in thermal conductivity of fine grain graphites is slightly smaller than that of CFCs, i.e. about 30% at 600°C for 0.1 dpa.

PROTECTION MATERIALS (cont'd)

The first results on dimensional changes in carbon based materials induced by neutron damage have been obtained at 1500°C, and damage range of 1 to 5 dpa.
The results show that the neutron damage did induce shrinkage in graphites, whilst the swelling on the c direction in CFCs may be as high as 28% at 3 dpa. To improve the dimensional, high crystallinity pitch fibres, and high graphitization temperature (3000/3100°C) will be the objective.

The T-retention in first wall and divertor carbon-based armous under normal operation has been assessed for NET/ITER devices. Apart from the potentially large inventory in the neutron damaged bulk of first wall armours, the actual T-inventory is dominated by the tritium that resides in the redeposited carbon films and dust.

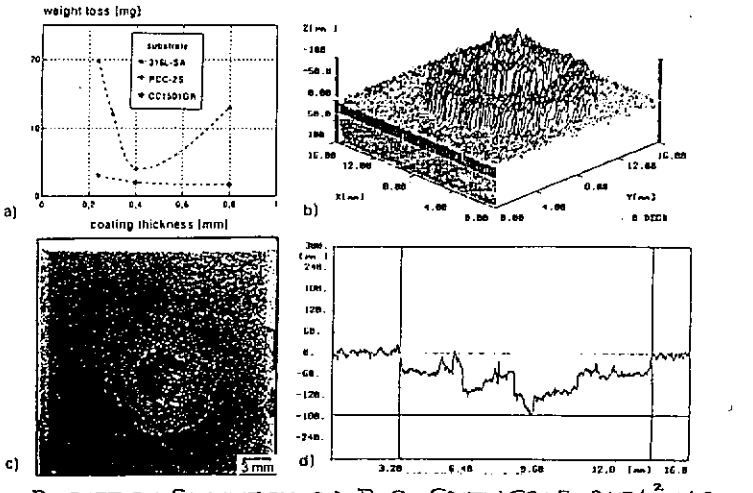

DISRUPTION SIMULATION ON B_4C - COATINGS: $5 \times 2\ MJ/m^2$ IN 1.2ms

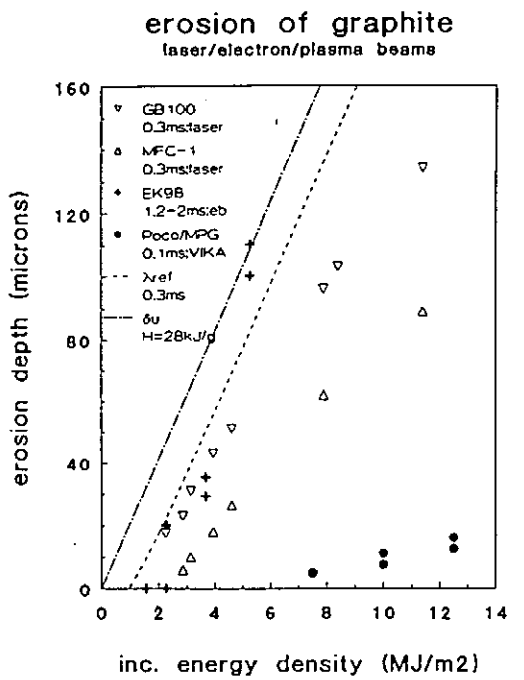

DIVERTOR DESIGN

Two main design concepts have been developed:

- **flat tiles** on metallic rectangular tubes with internal circular bore

- **monoblock** (tube in tile)

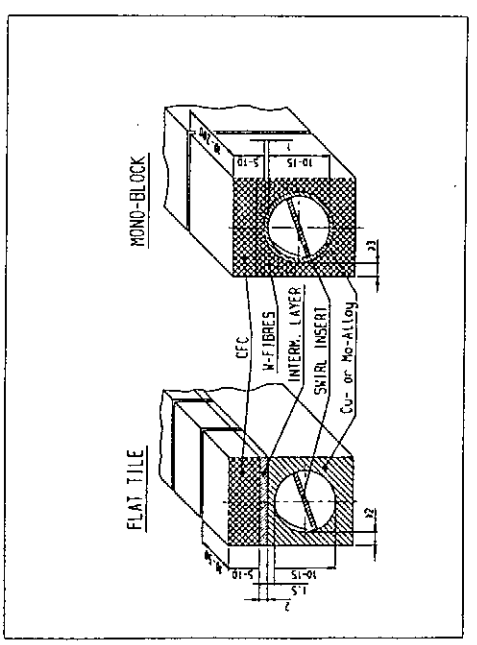

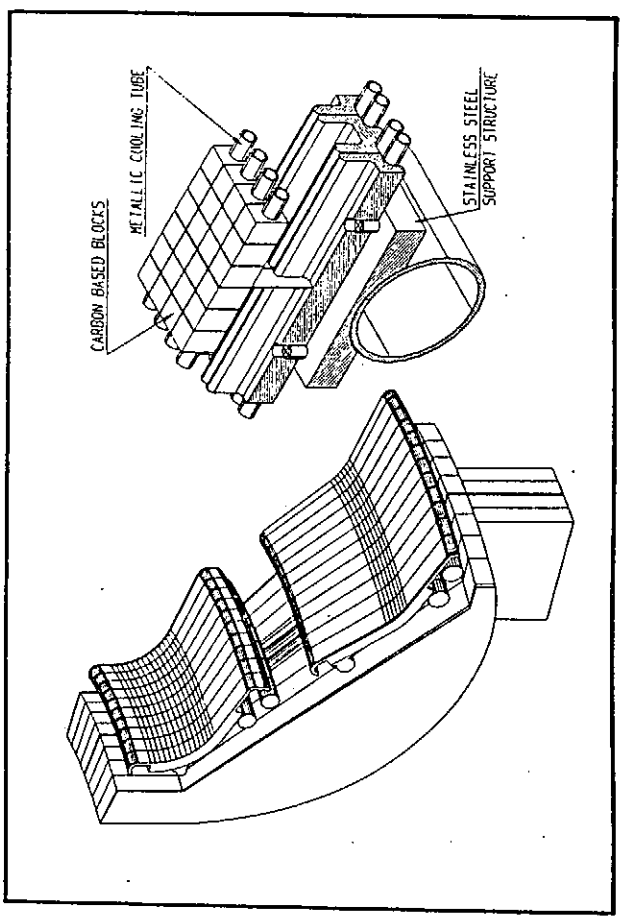

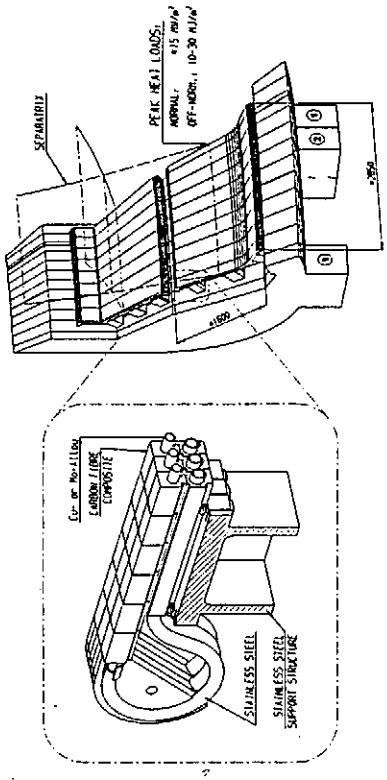

NET DIVERTOR PLATES WITH CARBON COMPOSITE MONOBLOCK

SPECIFIC TECHNOLOGIES

JOINT DEVELOPMENT

- Focus on	CFC on Mo or Cu alloy Brazing and Diffusion Bonding
- Collaboration with	ENEA, CEA, Ansaldo, Metallwerk Plansee, Vide et Traitement
- Armour Mater.	Aerolor A05, Sep Carb N112, Toyo Tanso CX2002U
- Tube Material	TZM, Mo-41Re, Mo, Glidcop

DEVELOPMENT MAIN RESULTS

- Chosen Braze	TiCuSil
- Brazing Temp.	900 - 950 °C
- Technique	Selected by the manufacturer

TESTS ON TRIAL PIECES

- Metallographic Examination
- Shear Tests
- Thermal Shock (heating at 600 °C, quench in cold water)
- Ultrasonic and X rays

DIVERTOR PLATES

- The 200 kW EB facility FE200 for high heat flux testing in Le Creusot France has been commissioned by CEA/Framatome and it is operational since one year.

- 13 actively cooled monoblock mock-ups have been manufactured by ENEA in collaboration with Ansaldo and Metallwerk Plansee. 11 have been tested in Le Creusot and at the NBI test bed of JET. Tiles have resisted to 1700 cycles at 13 MW/m² and additional 1000 cycles at 15 MW/m². Higher fluxes have been reached in single shots.

- 8 flat tile concept mock-ups with TZM tubes have been manufactured by Metallwerk PLansee. 5 have been tested at the Marion NBI facility in KFA Julich.* Tiles resisted to 16 MW/m² in single shots and 1000 cycles at 7 MW/m².

* 1 MOCK-UP HAS BEEN TESTED LAST YEAR IN JET BIS

DIVERTOR PLATES
(cont.)

- 2 flat tile concept mock-ups with glidcop tubes have been manufactured by CEA Cadarache. 1 has been tested in Le Creusot. Tiles have resisted to 16 MW/m² in single shots and 1000 cycles at 14 MW/m²

- Critical heat flux experiments by CEA, ENEA and JET show that 50 MW/m² can be achieved at water interface using the subcooled boiling technique with turbulence promoters.

HIGH THERMAL FLUX TEST STATION FE 200

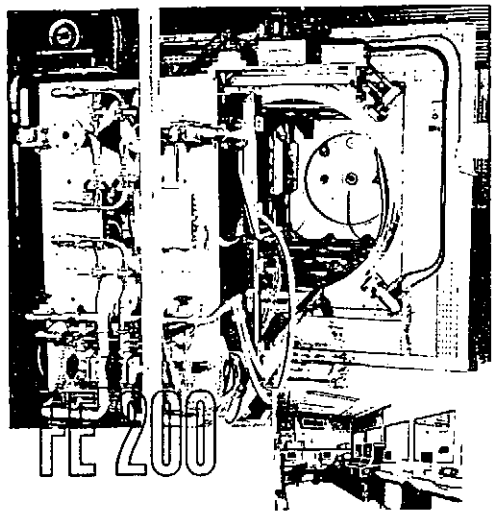

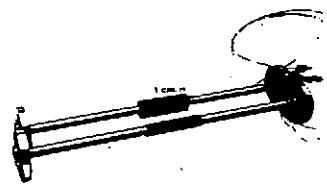

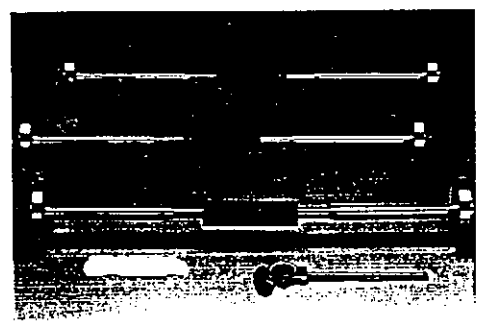

MONOBLOCK DESIGN - MOCK-UPS READY FOR TESTING

DIVERTOR FLAT TILES TESTING

Test Facility	MW/m² Water	MW/m² Inc-Rei	No. Cycles	Surface Temp. °C	Cycle Time ON/OFF sec	Failure at Joint
30 kW El. Beam Sandia	11.20	13.86	1	2300	>50	Yes
-	7.0	7.7	1000	1200	45/45	No
-	8.9	9.0	900	1700	45/45	Yes
-	10.0	12.0	210	2150	45/45	Yes
400 kW El. Beam JEBIS	-	15.9	1	>2800	50	No
- -	-	10.5	1000	2000	35/25	No
-	-	12.5	300	2350	35/25	No
6 MW Ion Beam KFA	10.3	-	26	2200	30/300	Yes
-	-	10.0	376	1950	30/300	Yes

MONOBLOC TESTS

MATERIAL COMB.	MW/m² SCREEN.	N. cycles	MW/m² FATIGUE
AOS/TZM	15	1700 + 1900	13 15
AOS/MoRe	10	-	-
AOS/Mo	13	700	11
*TT/Mo	15	-	-
TT/Mo	15	1000	11
TT/GLIDCOP	16	1000	13

ALL "WATER CALORIMETRY DATA

* TI = Toyo Tanso Ci 2002U

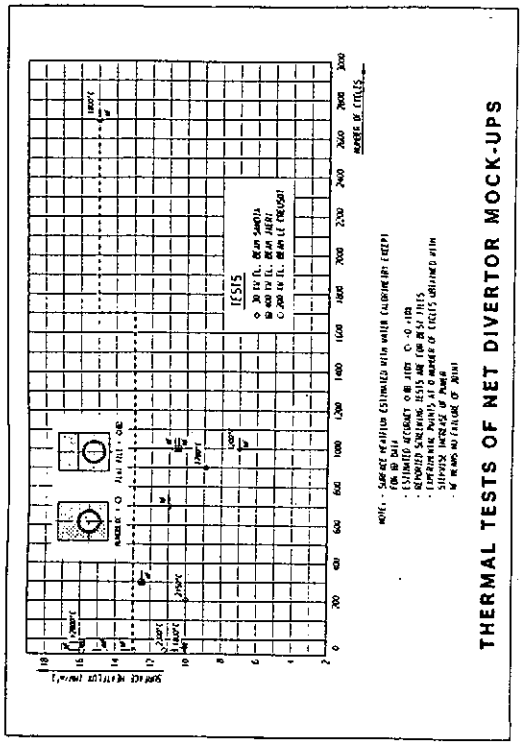

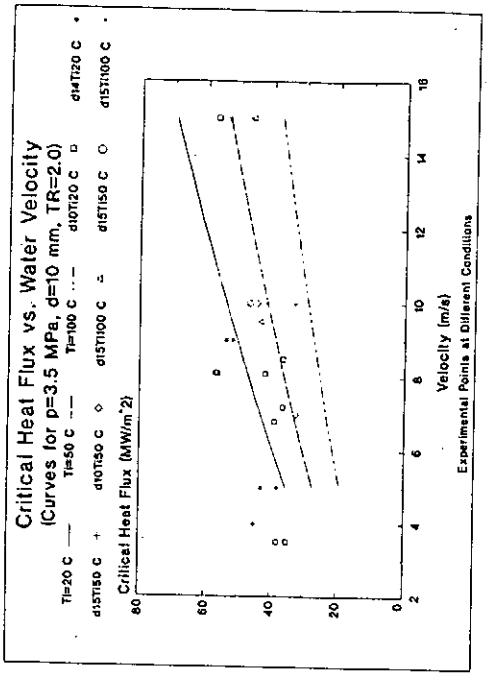

FIRST WALL AND SUBLIMITER

- The new 500 kW facility "Fiwatka" for thermal testing is being commissioned at KFK Karlsruhe.
- Thermal fatigue testing in the 150 kW facility at JRC Ispra on actively cooled mock-ups achieved with 0.5 MW/m² 27 000 and 52 000 cycles without leak but with first cracks.
- A new design concept consisting of a coated FW and sublimiters has been developed.

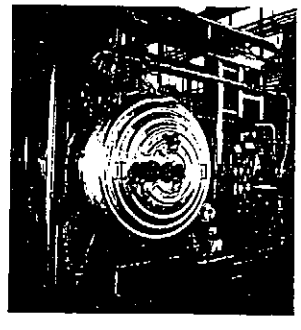

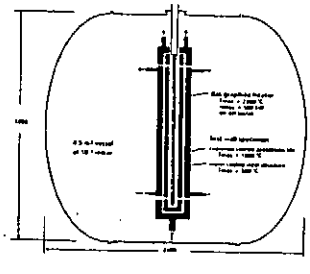

500 KW FIRST WALL TEST KARLSRUHE FIWATKA

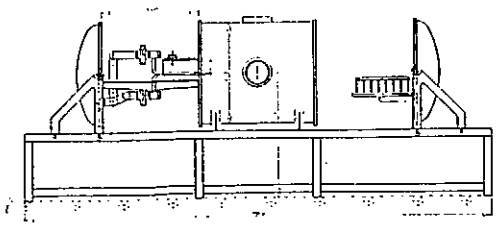

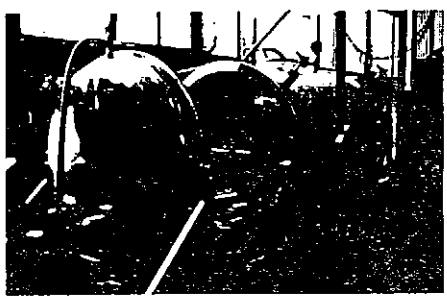

150 KW THERMAL FATIGUE TEST FACILITY AT IRC ISPRA

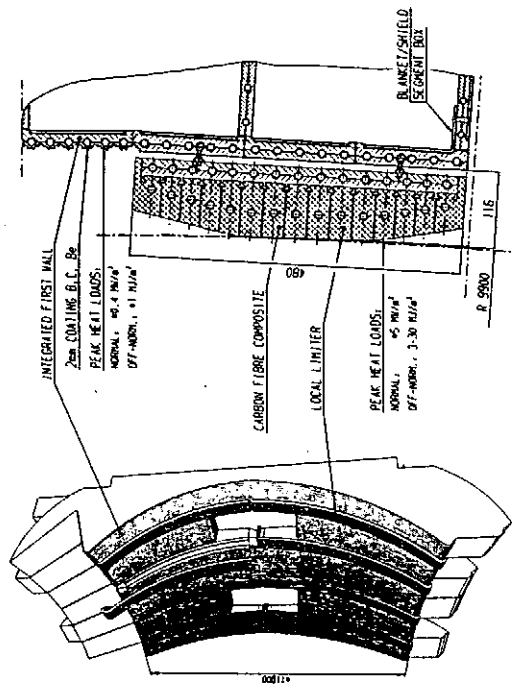

NET OUTBOARD FIRST WALL WITH LOCAL LIMITERS AND COATINGS

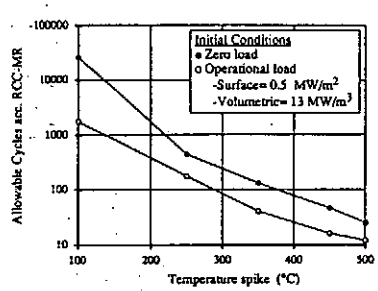

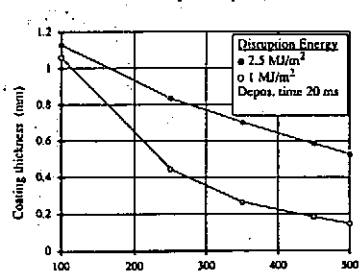

Thermal Fatigue of Steel First Wall by Disruption.

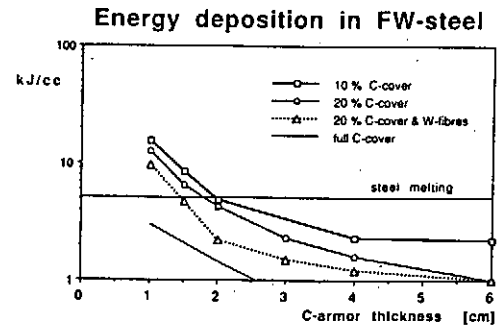

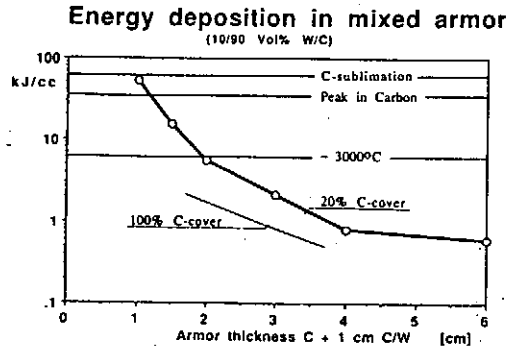

Jülich Divertor Test Equipment (JUDITH)

Construction of an electron beam apparatus for materials testing in the Hot Cells

In the KFA, testing of materials which have been subjected to neutron irradiation is being carried out for the fusion reactor research programme. An electron beam test apparatus is being installed in the Hot Cells of the Institute for Reactor Materials, complementing the test equipment available in Japan, USA, France and GUS. Gamma ray emitting specimens are to be tested under thermal shock, thermal cycling and long-term loading conditions.
The apparatus, built in cooperation with the PTR (Präzisionstechnik Remagen) Company, consists of:

- a powerful electron beam unit;
- a vacuum chamber in which the specimens are placed;
- a number of diagnostic devices with which surface temperature, specimen changes and gas compositions can be measured.

Technical data:	
beam potential	≤ 150 kV
beam current	≤ 400 mA
beam power	≤ 60 kW
pulse duration	≥ 1 ms
pulse increase time	≤ 200 ms
beam defection	± 50 mm in x,y
deflection frequency	≤ 100 kHz
power density	0.06 MW/mm²
specimen dimensions	≤100 x 100 mm²

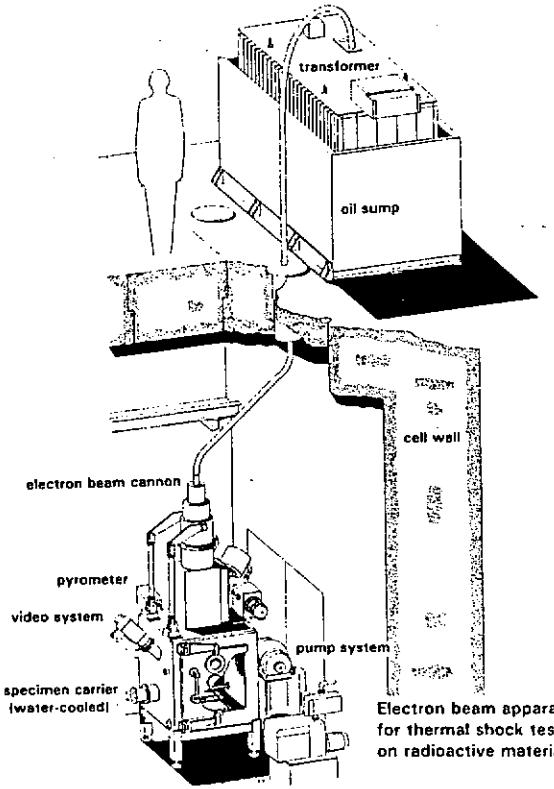

Electron beam apparatus for thermal shock tests on radioactive materials

Jülich Divertor Test Equipment (JUDITH)

Construction of an electron beam apparatus for materials testing in the Hot Cells

In the KFA, testing of materials which have been subjected to neutron irradiation is being carried out for the fusion reactor research programme. An electron beam test apparatus is being installed in the Hot Cells of the Institute for Reactor Materials, complementing the test equipment available in Japan, USA, France and GUS. Gamma ray emitting specimens are to be tested under thermal shock, thermal cycling and long-term loading conditions.

The apparatus, built in cooperation with the PTR (Präzisionstechnik Remagen) Company, consists of:

- a powerful electron beam unit;
- a vacuum chamber in which the specimens are placed;
- a number of diagnostic devices with which surface temperature and specimen changes can be measured.

Technical data:	
beam potential	≤ 150 kV
beam current	≤ 400 mA
beam power	≤ 60 kW
pulse duration	≥ 1 ms
pulse increase time	≤ 130 µs
beam deflection	± 50 mm in x,y
deflection frequency	≤ 100 kHz
power density	60 kW/mm²
specimen dimensions	≤100 x 100 mm²

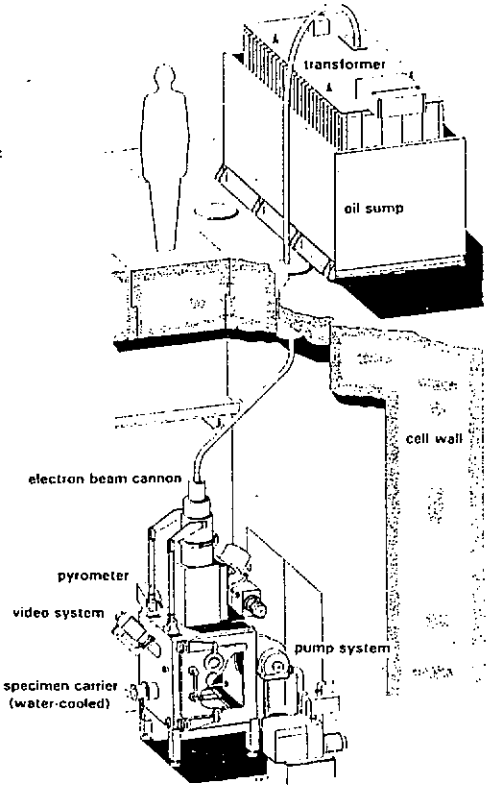

The following diagnostic devices are incorporated for measurement of the surface temperatures and materials changes:

- an infra-red pyrometer for point measurements of temperatures from 200 to 1100°C;
- an infra-red pyrometer for the temperature range 1000 - 3500°C;
- an infra-red high temperature camera with a picture frequency of 25 Hz in video technique for temperatures above 800°C;
- a video camera for visual monitoring of a test;
- thermocouples and strain gauges;
- gas analysis.

In addition the cooling water temperature and flow rate are also measured.

The characterization of the specimen surfaces before and after the test can be carried out with the available metallographic examination techniques in the Hot Cells. In particular, radioactive specimens with activities below 10^6 Bq can be examined in an optical micoscope and specimens with up to 10^7 Bq in a scanning electron microscope.

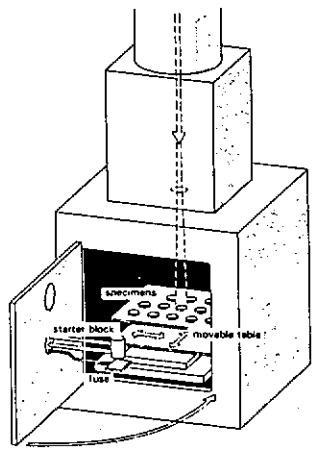

Test setup for small specimens

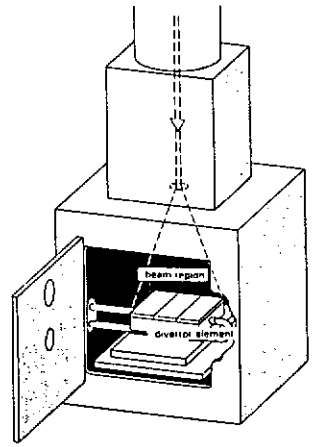

Test setup for divertor element

Short impulses (up to 100 ms) obtain their energy through a charged condenser, the pulse increase and decrease times being 200 μs. For longer pulses, the power input is by means of a high voltage transformer, for which the time constant for the control is increased to 400 ms, in order to avoid induced over-voltages during impulse switching. The setting of the beam parameters can be made either manually or automatically using a programmable control. The automatic control is particularly necessary when a specific series of impulses should be carried out.

A specimen surface of 100 x 100 mm^2 can be scanned because of the beam deflection in the x-y direction. The deflection frequency of up to 100 kHz allows a quasi-areal energy input to be achieved.

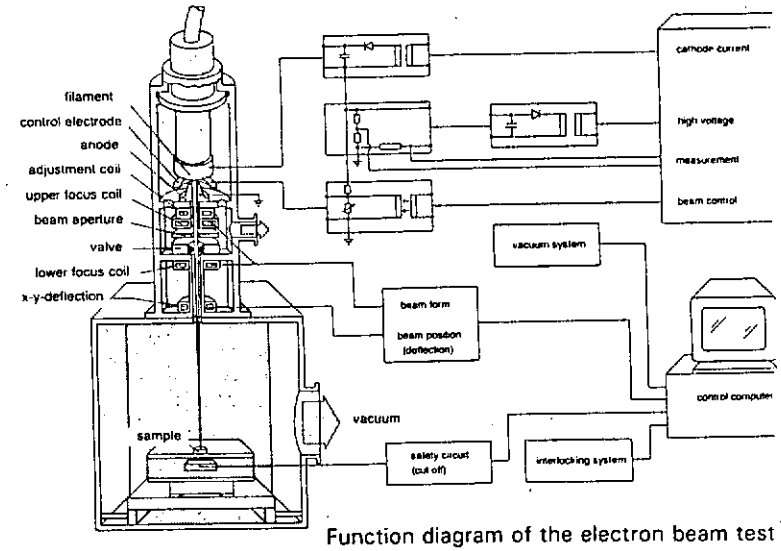

Function diagram of the electron beam test

The vacuum chamber was manufactured in the KFA. It consists of a 430 l cuboid stainless steel container on which the electron beam unit is placed. The wall thickness of the chamber is 25 mm, the base dimensions 800 x 600 mm^2, the height 900 mm.

A door 660 x 660 mm^2 is located on the front side, so that widely different specimens can be positioned in the chamber using the remote manipulators. The specimen holder is mounted on a movable table, allowing the appropriate beam position for each specimen to be set up. Set into the door is a "starter block"; it is a water-cooled copper plate which is used to bring the electron beam up to full power before the specimen surface is examined.

A flange on the side of the chamber can be used for introducing an actively cooled divertor element for examination under the electron beam. The cooling circuit has a flow rate of 5 m^3/h and a pressure of 40 bar, enabling a thermal power of 40 kW to be used in continuous operation.

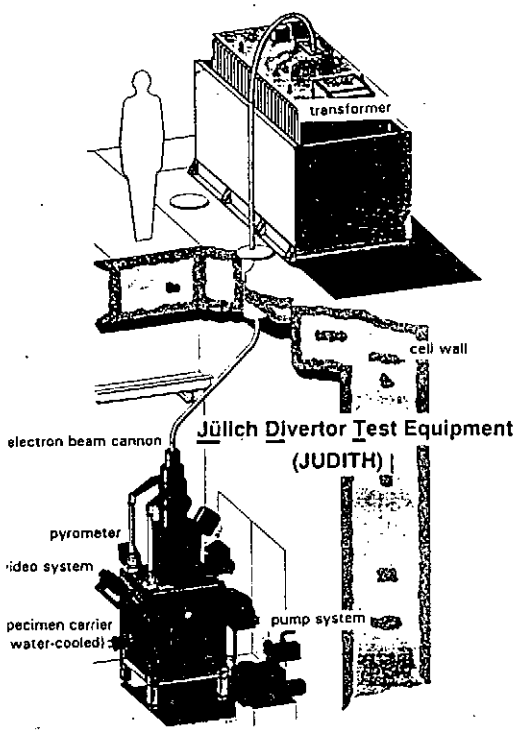

Juelich Divertor Test Facility Hot Cells (JUDITH)

lay-out data:

total power:	60 kW
acceleration voltage:	≤ 150 kV
power density:	< 15 GWm^{-2}
loaded area:	4 mm^2...100 cm^2
beam spot:	focussed or defocussed
scanning frequency:	100 kHz
pulse duration:	1 ms to continuous
beam rise time:	130 µs
x-y-table max. area:	40 cm x 25 cm

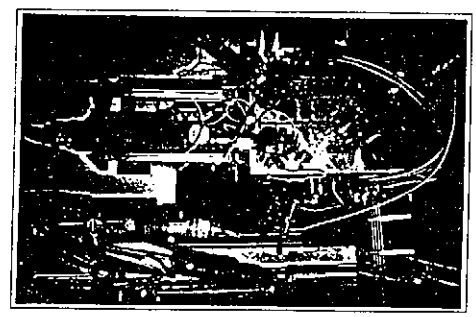

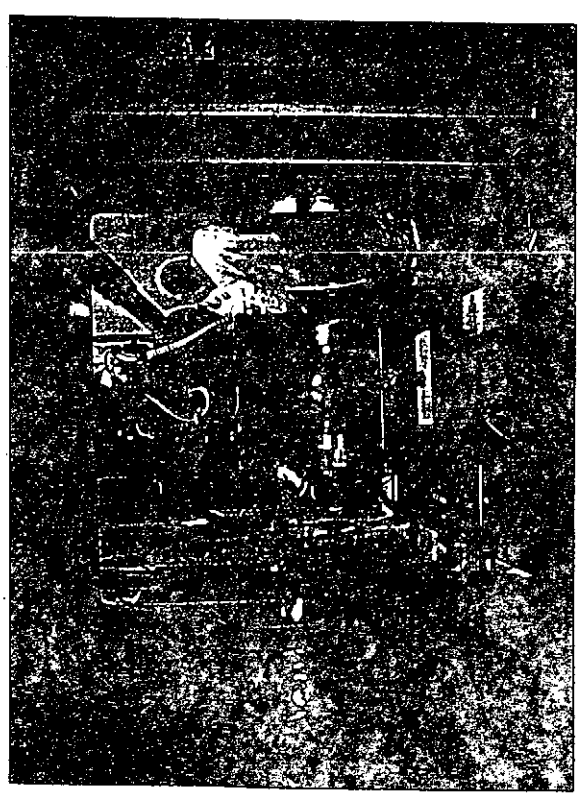

Control- and diagnosticsystems

Controlpanel :
computer for servicefunctions
- Beam control
- Moving of xy-table
- Vacuum system
- Interlock system

Computer with dataloggerfunction
- Temperature (pyrometer, thermocouples)
- Beamparameter (current, profile)
- Cooling circuit (waterpressure, flowrate,temp.)

Infrared imageprocessing
- Camera control
- Evaluation

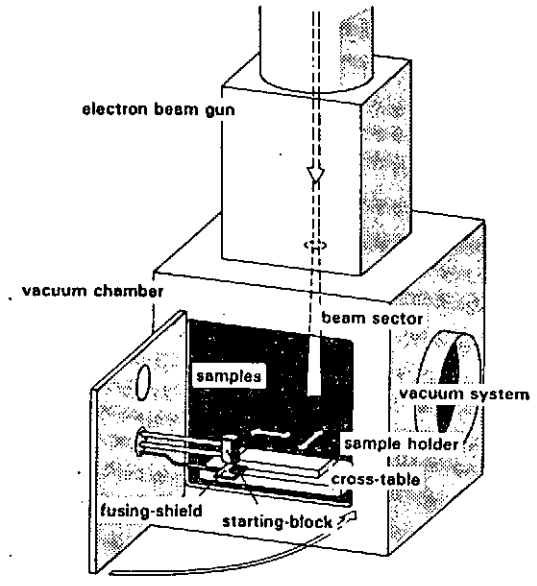

Test Configuration
for small Samples (F = ~ 4cm²)
on Cross-Table

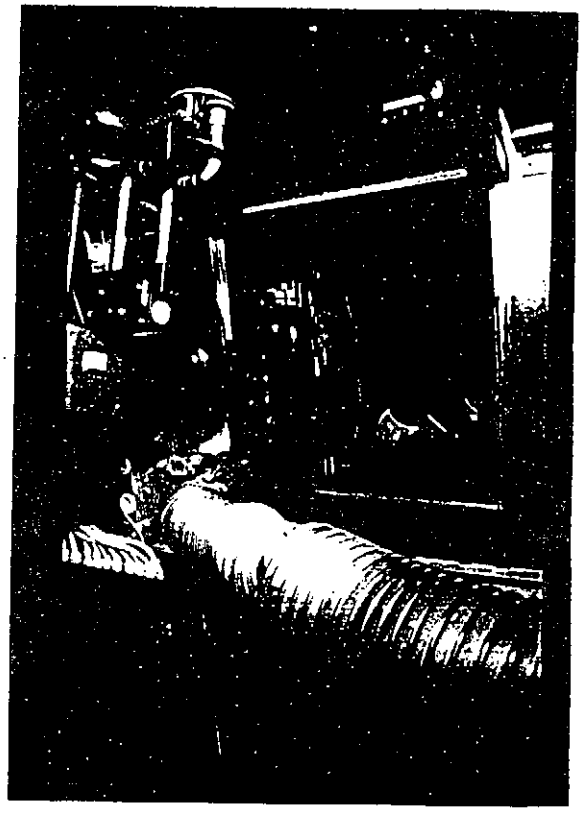

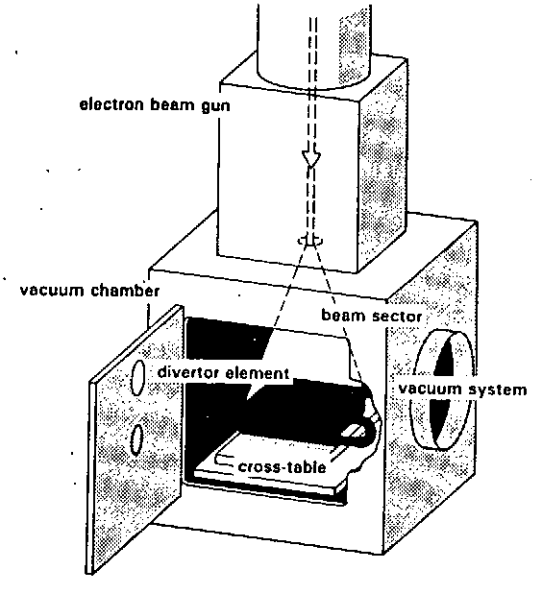

Test Configuration for a fixed and cooled
Divertor Element (F = ~ 30cm²)

Former Experiments in JUDITH

Tests in 1991/92

1. Thermal behaviour of a limitermodule(TEXTOR)
2. Test of a divertormodule (coop.JAERI)
   Thermofatiguetest, Disruption
3. Disruptiontests on different matirials
4. Divertortest with monoblockdesign
   (coop. Efremov-Institute St.Petersburg)
5. Divertortest in comparison to MARION
6. Disruptiontests with boron carbide coatings
   (coop. with General Atomic, San Diego)

0007 25KV X20 1mm WD17

Actively cooled divertor modules

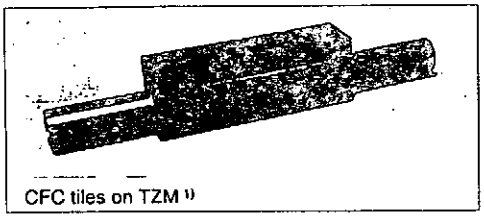

CFC tiles on TZM [1]

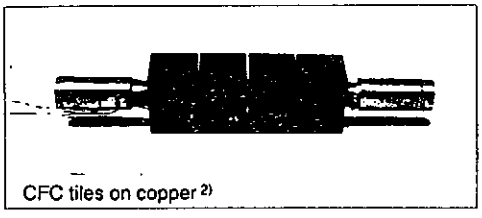

CFC tiles on copper [2]

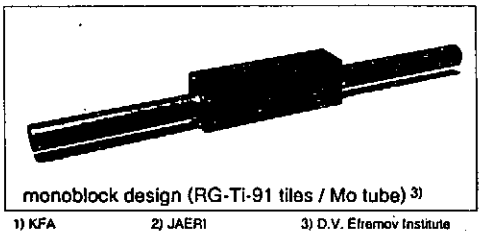

monoblock design (RG-Ti-91 tiles / Mo tube) [3]

1) KFA 2) JAERI 3) D.V. Efremov Institute

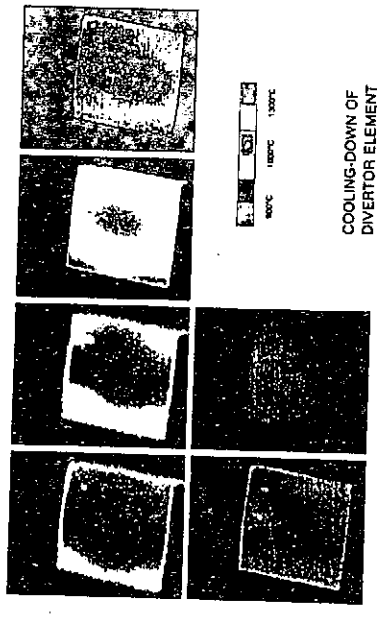

COOLING-DOWN OF DIVERTOR ELEMENT

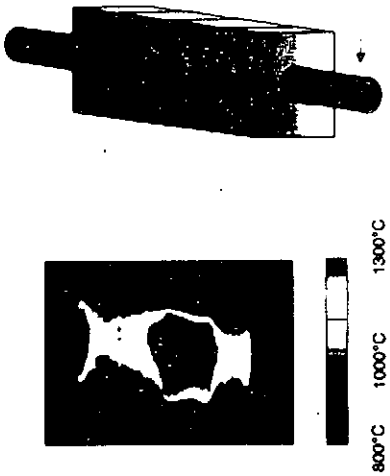

SCREENINGTEST OF A DIVERTOR TEST ELEMENT

Session 4: PFC and PSI Studies in Laboratory

HYDROGEN IN GRAPHITE:

TRANSPORT / REEMISSION / RETENTION

A. A. HAASZ
UNIVERSITY OF TORONTO

1. HYDROGEN TRANSPORT

* Molecule formation due to simultaneous exposure of graphite to H^+ and D^+.
  (S. Chiu and A. A. Haasz, University of Toronto)

2. HYDROGEN REEMISSION

* Atomic reemission of hydrogen from graphite at temperatures > 1000K.
  (D. Franzen, IIP, Garching, Germany; E. Vietzke, V. Philipps and D. Reiter, IPP, KFA Forschungszentrum, Jülich, Germany; A. A. Haasz and J. W. Davis, University of Toronto)

3. HYDROGEN RETENTION

* Effect of graphite structure on H retention at high H^+ fluence.
  (A. A. Haasz, J. W. Davis and S. Chiu, University of Toronto; R. Macaulay-Newcombe and D. A. Thompson, McMaster University)

Haasz, Japan-U.S. Workshop, Kyushu University, Fukuoka, Japan
November 17-20, 1992

1. HYDROGEN TRANSPORT

OBJECTIVES

- To study the mechanisms for:
  - (i) H-transport and recombination in graphite.
  - (ii) The effect of graphite structure on H-transport.
  - (iii) The methane formation process.

EXPERIMENT

- H^+ and D^+ implanted into graphite, either individually or simultaneously (using dual ion beam accelerator).
- Observe reemission of H_2, HD, D_2 and CH_xD_y
- Thermal desorption of H_2, HD, D_2 and CH_xD_y from previously implanted graphite.

Japan-U.S. Workshop, Kyushu University, Fukuoka, Japan
November 17-20, 1992

2

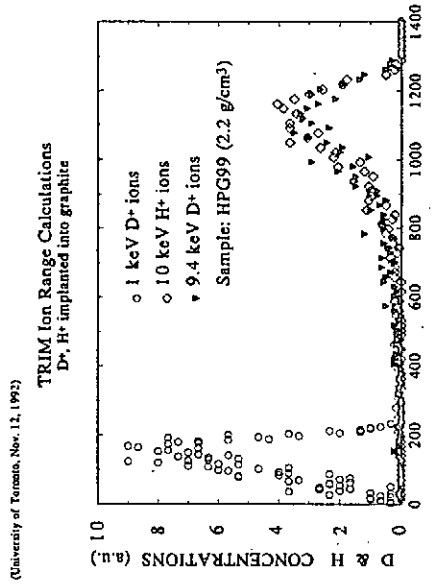

3

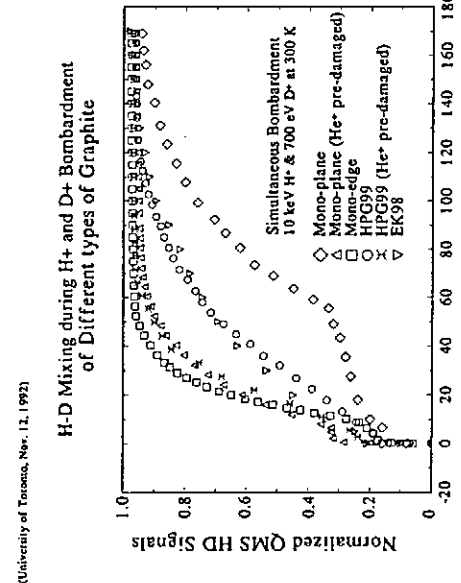

4

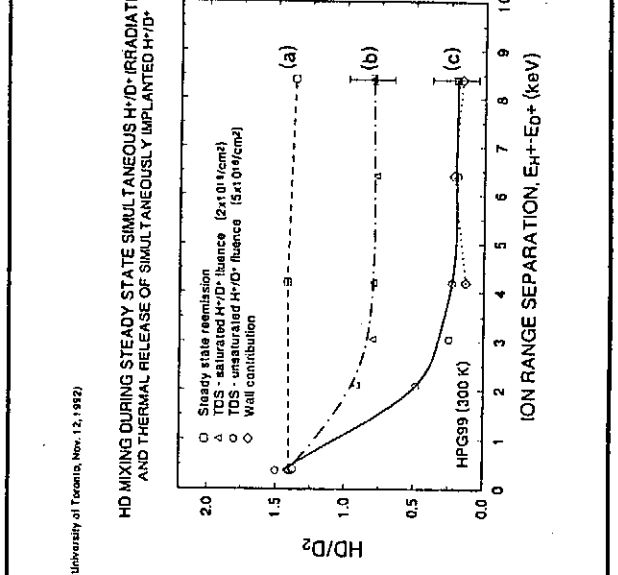

5

Fig. 1 Steady state re-emission signals as a function of sample temperature, for 3 keV D_3^+ ions incident on EK98, USB15 and GB110.

Fig. 2 Atomic H, molecular H_2 and D_2 re-emission during 3 keV H_3^+ bombardment of pyrolytic graphite measured by a line-of-side mass spectrometer. The H_2 and D_2 re-emission have been normalized at 525 K. The atomic H flux values are relative to the H_2 flux. The solid lines represent the result of the model calculation. The error bars correspond to twice the standard deviation for 14 experimental runs.

3. HYDROGEN RETENTION

OBJECTIVES

- To study H retention in graphite as a function of H^+ fluence.
- To investigate the effect of graphite structure on H retention.

EXPERIMENTS

- Graphite specimens were implanted with D^+ to fluences in the range 10^{17} - 10^{21} D^+/cm^2.
- Retained D was measured using Thermal Desorption Spectrometry (TDS).
- For some cases NRA was performed on the back of the specimens.
  (NRA performed at McMaster University)

Davis, Haasz & Wu, J. Nucl. Mater. 176-177 (1990) 742

H- RETENTION AS A FUNCTION OF H^+ FLUENCE

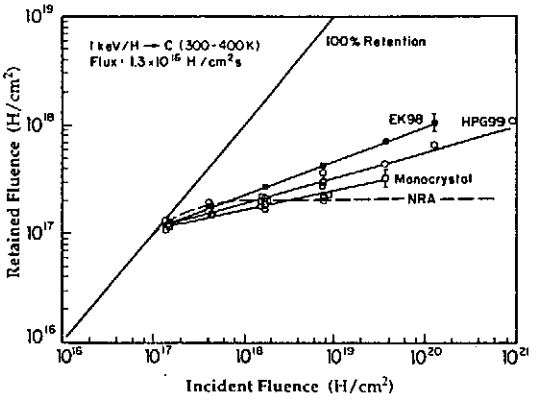

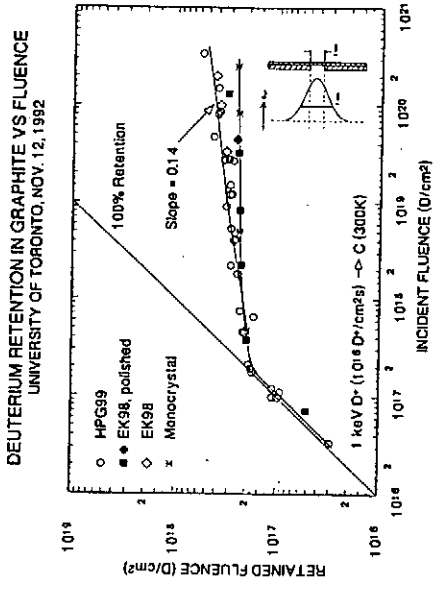

SUMMARY

1. HYDROGEN TRANSPORT

- During steady-state H^+/D^+ ion implantation in graphite, hydrogen diffuses in the form of atoms in the implantation zone.
  - complete mixing of mobile H/D occurs.
  - H recombination occurs throughout the implantation zone, possibly on internal surfaces.
- Methane formation during ion impact occurs at end of ion range (consistent with previous findings by Roth et al/IPP-Garching).
- Post-implantation TDS results show that, in the absence of impacting ions, both H recombination and methane formation occurs locally at the end of ion range.

2. HYDROGEN REEMISSION

- Below 1000K, implanted H/D from graphite is reemitted in the form of molecules.
- Above 1000K, both molecules and atoms are reemitted; the atom fraction increases with increasing temperature, reaching a value of 95% at 1850K.

SUMMARY (continued)

3. HYDROGEN RETENTION

- The amount of retained hydrogen in most forms of graphite increases with increasing fluence, well above the saturation levels observed in the implantation zone.
- The extent of the increase appears to depend on the structure of graphite.
- Proposed Hypothesis: mobile H from the implantation zone, during H^+ impact, diffuses "deeper" into the material and becomes trapped on "internal surfaces."

PROPOSED HYDROGEN TRANSPORT MODEL

- Implantation zone is comprised of two regions:
  - graphite crystallites
  - intercrystalline paths
- Implanted H is initially deposited within crystallites where it may be trapped, or if traps are saturated, it may diffuse to an intercrystalline path.
- During H impact, crystallites are "broken" and new intercrystalline paths are formed.
- During bombardment at low temperature, paths would become covered with enough hydrogen to fill all the traps, resulting in a low activation energy for atom motion.
  ⇒ this would allow for the fast movement of H/D atoms and their isotopic mixing.
- During thermal desorption, the traps on the paths would not be populated, and the motion of atoms would be a slower stepwise diffusion process.
  ⇒ this would allow recombination to occur before mixing.
- The production of methane molecules might occur at trapping sites at "edge of crystallites", where the C+H reactions are dominated by the hydrogen locally implanted in the crystallites.
- Mobile hydrogen in the implantation zone will either recombine (and thus be reemitted) or diffuse "deeper" into the material via inherent "micropaths" where trapping might occur.

ITER Divertor Materials and PFC Technology Development in the PISCES Program at UCLA

Yoshi Hirooka
Institute of Plasma and Fusion Research
University of California, Los Angeles

As part of the US ITER-R&D program, over the last few years the PISCES team at IPFR-UCLA has been assigned to work on the three key areas related to the plasma-facing component development: (1) divertor target materials evaluation and development; (2) new divertor concept development; and (3) high-density, steady-state plasma source development.

One example for the first task is that a new class of material, including bulk-boronized graphite and boronized C-C composite, was developed jointly with Toyo Tanso Inc., Japan in 1989-90, using PISCES-B. Due to its superior erosion resistance, bulk-boronized graphite with 20% boron is being used as the limiter material in the Wenderstein Stellarator AS-7 at IPP, Garching. Also, boronized C-C composites have been used as the boron source for solid target boronization in tokamaks including: TdeV and PBX-M.

As to the new divertor concept development, a major effort has been made to prove and refine the gaseous/radiative divertor concept using PISCES-A. In this linear facility it has been clearly demonstrated that the heat flux to the target plate can be reduced by a factor of 100 in the gaseous divertor mode. As opposed to the design of ITER during the CDA phase, more advanced divertor designs based on the new concept development effort will probably be implemented in the EDA design.

High-density plasma generation is the key capability required for the PFC qualification facilities. By modifying PISCES-B into PISCES-B Mod, the maximum ion flux has been increased to the level relevant to ITER, i.e., of the order of 10^{23} ions/m^2. However, futher requirement has come up to heat ions to about 10-20 eV. Also, the plasma diameter must be enlarged to about 20 cm so as to be able to accommodate a large PFC component. An effort is being made to meet all these requirements with the PISCES-Upgrade facility.

In the presentation at this meeting, the recent efforts in the first task on materials evaluation and development are reviewed with an emphasis to identifying the areas of data need to analyze the erosion and redeposition behavior of materials under high-flux, steady-state, plasma bombardment. In the remainder of this report, the result from

tungsten erosion experiments conducted in PISCES-B will be reviewed.

Tungsten in the form of bulk-material, relatively thick (1 mm) chemically deposited (CVD), and low-pressure plasma-sprayed (LPPS) coatings on molybdenum has been evaluated as a plasma-facing material, focusing on some of the key issues related to the divertor plate design.

(1) Thermal outgassing: Total outgassing quantities up to 1000°C from tungsten materials have been found to be of the order of $10^{17\text{-}18}$ molecules/cm^2, orders of magnitude smaller than those from graphites including C-C composites. Among the tungsten materials tested, LPPS coatings tend to have higher outgassing rates. This is presumably due to the porous structure, necessitating R&D for higher density coatings.

(2) Plasma erosion: Deuterium plasma net erosion rates at 1500°C are basically the same for bulk tungsten, CVD and LPPS coatings. Generally, at ion bombarding energies below 350 eV oxygen-containing impurities (such as H_2O^+) in the deuterium plasma dominate the total erosion rate of tungsten. On the other hand, at low electron temperatures around 5 eV, positive ionization of these impurities is significantly reduced, whereby plasma erosion data basically agree with those estimated for deuterium sputtering. For oxygen, the electron attachment reaction: $O_2 + e \Rightarrow O_2^-$ is dominant at electron temperatures below 10 eV. To ensure this point, more atomic physics data are needed in at these low electron temperatures.

(3) Hydrogen retention: Postbombardment thermal desorption measurements have indicated the deuterium retention quantity in tungsten materials is of the order of $10^{14\text{-}15}$ D-atoms/cm^2, which is considerably smaller than the corresponding data for graphites and C-C composites. Also, it is important to note here that there is no codeposition-driven tritium inventory with tungsten.

(4) Disruption simulation: Disruption-simulated high heat loads up to 6MJ/m^2 have caused microcracks in tungsten materials. As shown in Fig. 3, a strong heat shielding effect has been observed, decreasing the heat transmission factor to about 1%. This is explained by a molten layer protection effect, presumably combined with a mild vapor shielding effect.

Clearly, further effort is needed to improve the fusion-required quality of tungsten coatings. Because of its high probability of redeposition, however, in general tungsten neither causes heavy core contamination nor suffers from severe erosion even with open divertor configurations. Nonetheless, the application of tungsten will be found most viable if a gas target divertor configuration is implemented.

Current activities in the PISCES program

1. Edge-plasma control concept development efforts:
   - *Gaseous divertor
   - *RF ponderomotive force divertor } US-Japan WS (D. Tamano, Tsukuba Univ. in Dec./92
   - *DC-biased divertor
2. Materials and PFC technology development efforts:
   - *Evaluation of high-Z materials (tungsten) - ANL, NCSU, SNLL
   - *Actively-cooled PFC unit test (C-C composites) - JAERI
   - *Be safety facility development - SNLA
   - *Solid target boronization- CCFM (TdeV), PPPL(PBX-M)
3. Plasma facility development efforts:
   - *PISCES-B Mod (discharge power: 40 kW ->100 kW)
   - *ICH R&D in PISCES-A - Nagoya Univ.
   - *High-dens. plasma source R&D (PISCES-Upgrade)

IPFR-UCLA

ITER Divertor Materials and PFC Technology Development in the PISCES Program at UCLA

US-Japan Workshop on PMI-HHF
Kyushu Univ., 11/17-11/19, 1992

Yoshi Hirooka

PISCES Plasma-Surface Interactions Research Program
Institute of Plasma and Fusion Research
University of California, Los Angeles

IPFR-UCLA

PISCES-B Mod in 1992

IPFR-UCLA

Table of Contents

IPFR-UCLA

Table PMI-conditions in PISCES-B Mod. and ITER

PMI-conditions		PISCES-B Mod.	ITER-divertor*
Plasma species		H, D, He Ar, N	D, T, He
Pulse duration (s)		Continuous	200
Plasma density (cm^{-3})		10^{13} (H,D) 10^{14} (Ar)	10^{14} - 10^{15}
Electron temperature (eV)		5-30	10-20
Ion bombarding flux (ions s^{-1} cm^{-2})		up to 3×10^{18} (D-plasma)	4×10^{19} (peak)
Ion bombarding energy (eV)		30 - 300 (dc bias)	60-200
Power load (MW/m^2)		5 - 15 (with dc-bias)	10 - 30
PFC surface temperature (°C)		RT - 1700	1000 (carbon) 1500 (tungsten)
Ionization mean free path for 1st ionization (cm)	C^{++} W	~ 1 ~ 0.02	~ 0.5 ~ 0.01
Neutral pressure (Torr)		up to 10^{-3}	~ 10^{-2}

*From the IAEA document No 30: ITER plasma facing components.
**Physically sputtered carbon

Tungsten for PFCs in ITER ?

Issues are

- ARIES (W)
- C-Mod (Mo)
- TRIAM (Mo)

IPFR-UCLA

Experimental Conditions in PISCES-B

1. Surface temp.: 1500 C
2. Ion bomb. flux: 3-4 x 10e18 ions/sq-cm/sec
3. Bomb. energies: 50 -500 eV
   (D :85%, D2 :10%, D3 :5%)
4. Controlled Oxygen Impurity (OH, H2O ions):
   High impurity conds. (2%, Te >10 eV)
   Low impurity conds. (0.1%, Te < 5 eV)
5. Redeposition: 20 - 40% (calculated from WBC-code)

IPFR-UCLA

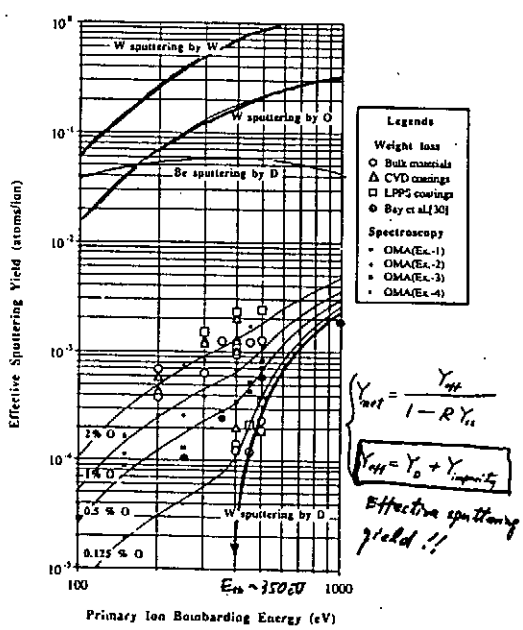

$Y_{net} = \frac{Y_{eff}}{1 - R Y_{eff}}$

$Y_{eff} = Y_0 + Y_{impurity}$

Effective sputtering yield !!

Fig. Tungsten erosion by deuterium plasmas contaminated with trace amounts of oxygen.

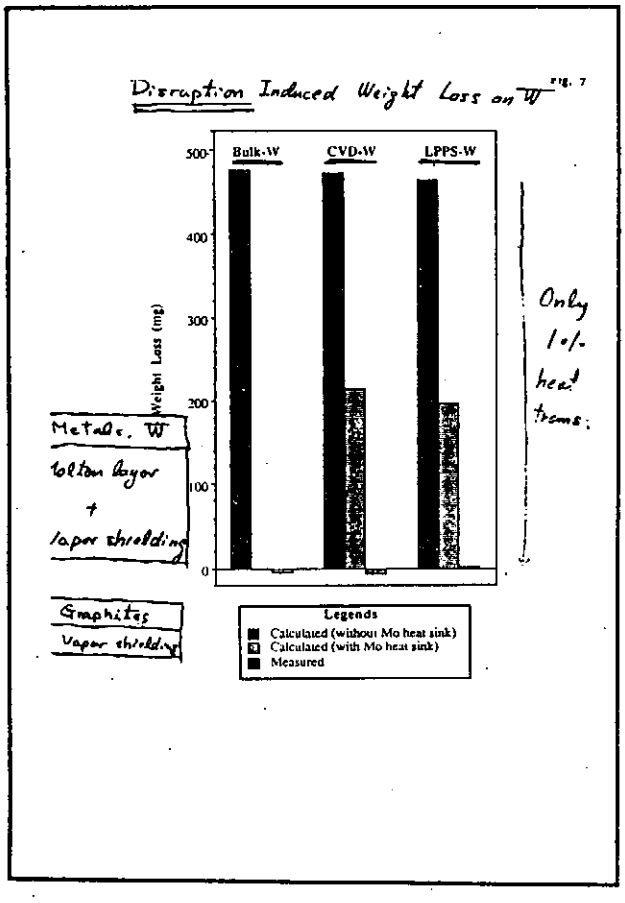

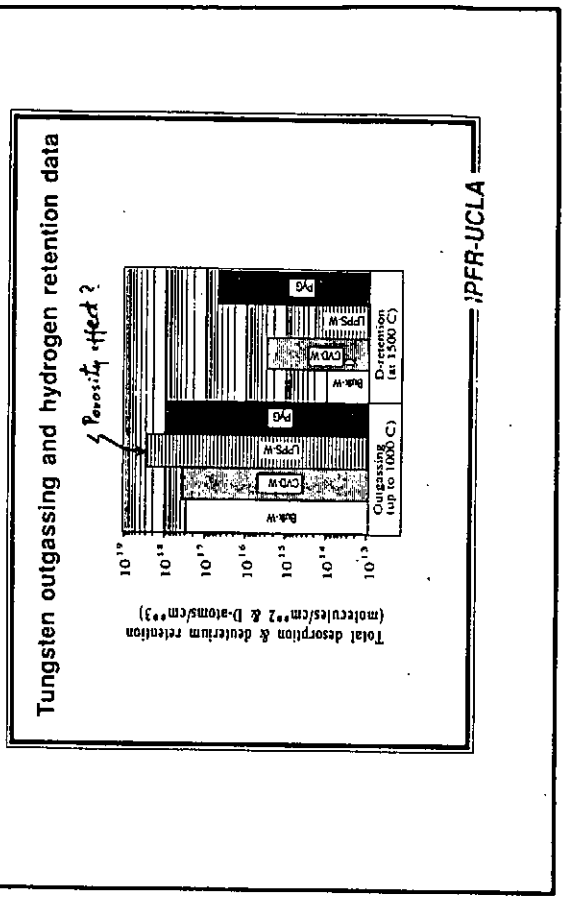

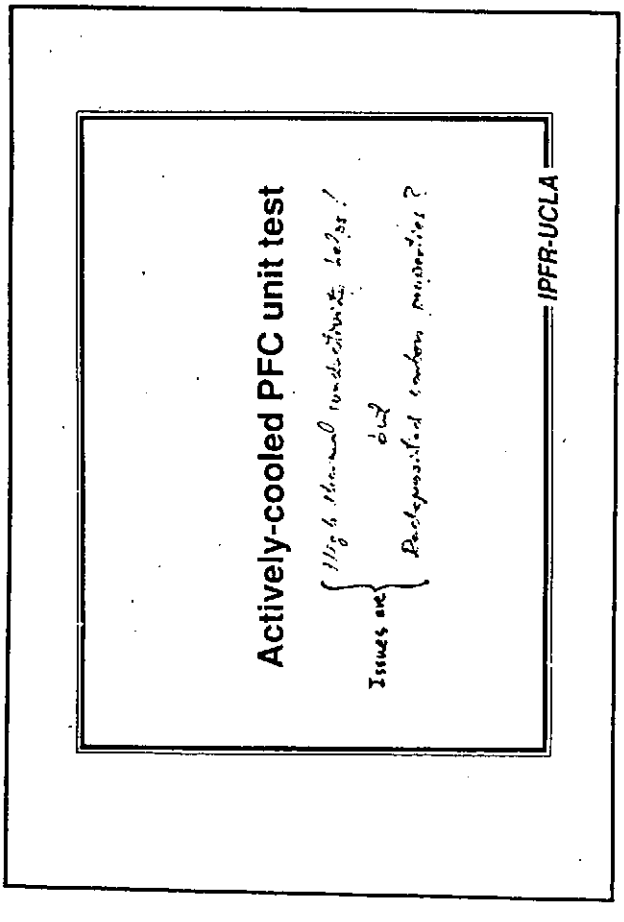

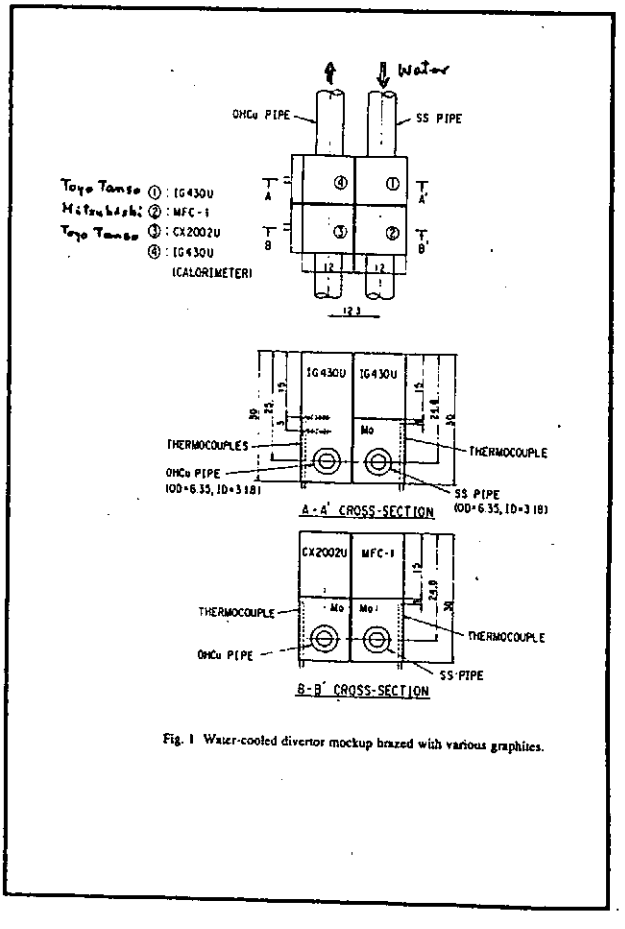

Fig. 1 Water-cooled divertor mockup brazed with various graphites.

Beryllium handling facility for PISCES experiments

1. Major features

*Ultra-clean room for PISCES-B Mod (<0.01μg-Be/m^3)
*High-rate ventilation (4000 CFM) with HEPA-filtered exhaust
*Negative internal pressure
*Double-door limited access
*Operation in full-face, air-supplied resparator

2. Schedule

*SOP reviewed (UCLA-EH&S, SNL, LANL) by: 8/31/92
*Facility conceptual design finished by: 8/31/92
*Detailed design of Be facilities finished by: 12/31/92
*Complete the facilities by: 7/31/92
*On-site safety review (UCLA-EH&S, SNL, DoE) by: 8/31/93

IPFR-UCLA

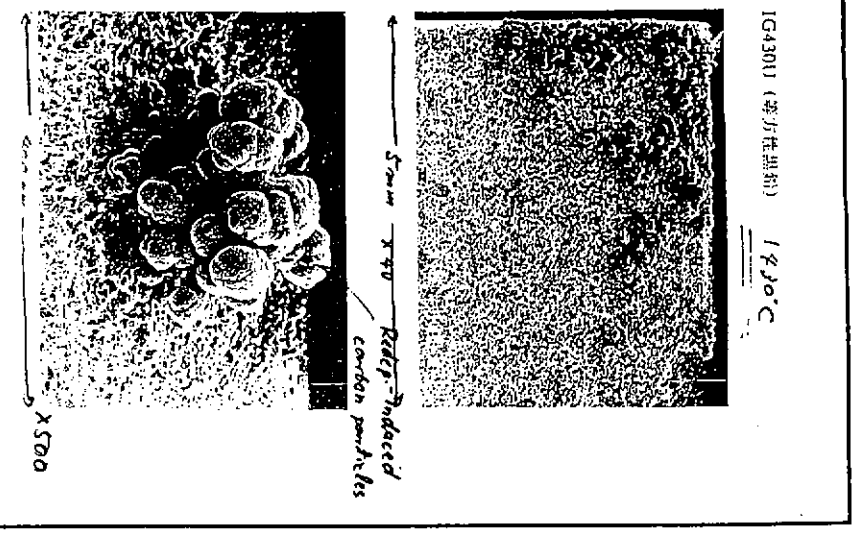

Solid Target Boronization (STB)

STB Target requirements
1. Low thermal conductivity
2. Low heat capacity (Low density)
3. High thermal shock-resistance
4. High boron content

IPFR-UCLA

Beryllium facilities for PISCES

Because
1. P-H. Robut likes Be ? ( )
2. M. Cohen likes Be ? ( )
3. It is fashionable to work on Be ? ( )
4. There is a possibility for Be ( )!!

IPFR-UCLA

Issues on Gas Boronization Techniques

1. Safety
   - Di-borane or tri-methylboron hazard
   - Dedicated machinetime needed (weekend operation)
2. Cost
   - Special gas handling system needed
3. Finite lifetime
   - Erosion of boron coatings, e.g. 2 days in W-AS7
4. Density control
   - He-cond. needed (shorter lifetime for boron coatings)
   - H incorporated in H+B+C coatings!

IPFR-UCLA

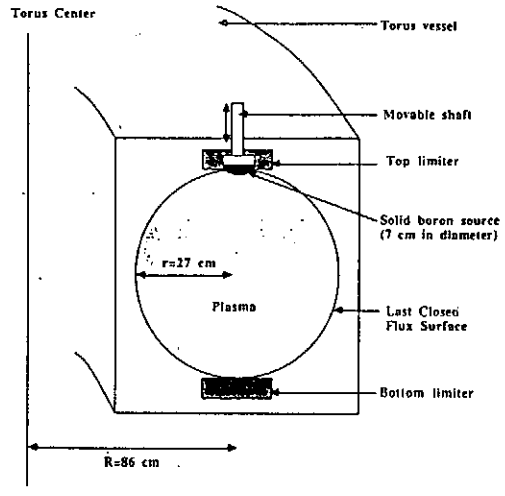

Fig. 3 Schematic illustration of the experimental setup for the STB technique demonstration in the Tokamak de Varennes.

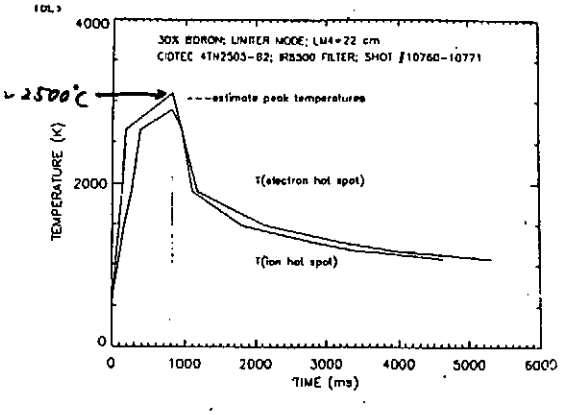

To: Comment #(1)

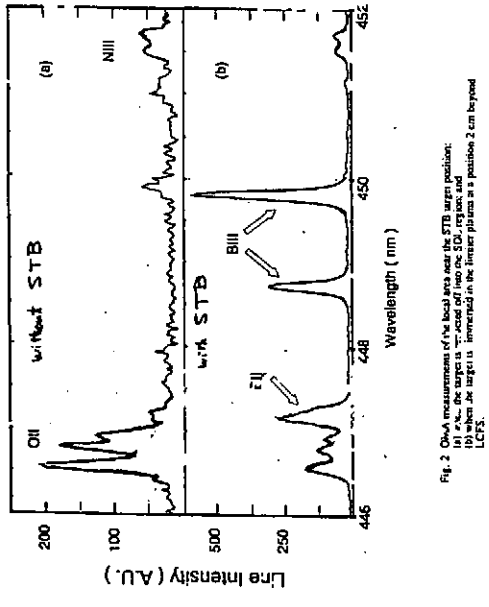

Fig. 2 OMA measurements of the local area near the STB target position:
(a) when the target is "retracted" into the SOL region and
(b) when the target is immersed in the limiter plasma at a position 2 cm beyond LCFS.

Solid Target Boronization in the PBX-M tokamak

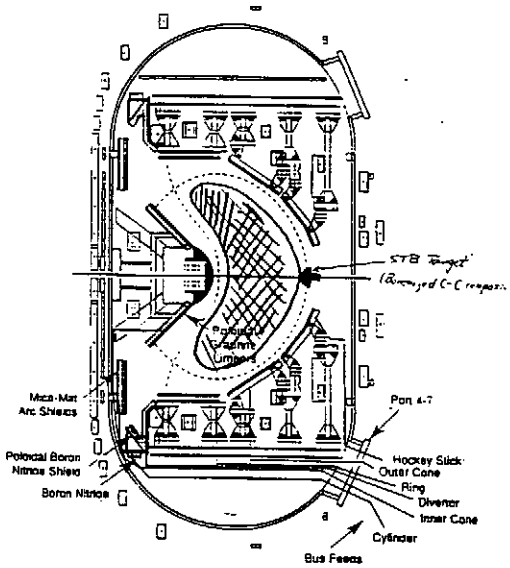

Oxygen and Boron Spectral lines

PROBE - 1 - Visible Region

BEFORE BORONIZATION

A)

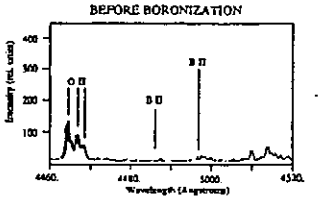

AFTER BORONIZATION

B)

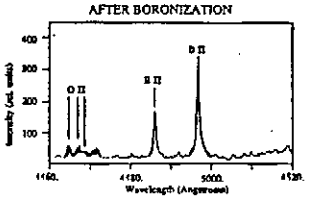

EROSION/REDEPOSITION MODELING AND ANALYSIS ACTIVITIES

Thanh Hua
(with contributions from Jeff Brooks)

Fusion Power Program
Engineering Physics Division
Argonne National Laboratory

Impurity generation and transport codes used for erosion/redeposition analysis are described. Primary applications of each code in the plasma scrape-off region and possible coupling among the codes are discussed. Recent erosion/redeposition analysis activities are reviewed, followed by presentation of key results and comparison with experiments. These include plasma contamination in TFTR, DIII-D divertor tiles erosion/deposition profile, and transport of Mo in PISCES. In general, the agreement between analysis and experiment is very good. Erosion analysis for the JT-60U divertor tiles and DIII-D DIMES experiments are ongoing activities.

Methods for transport calculations of chemically-sputtered carbon are discussed. Finally, the development of a sheath code is introduced. Effects on the sheath potential and heat transmission factor as a result of in-sheath ionization of neutral molecules are presented.

EROSION/REDEPOSITION MODELING AND ANALYSIS ACTIVITIES

Thanh Hua
Fusion Power Program
Argonne National Laboratory

Presented at the Japan/US Workshop P196
November 17-19, 1992, Kyushu University, Japan

Impurity Transport Codes for Erosion/Redeposition

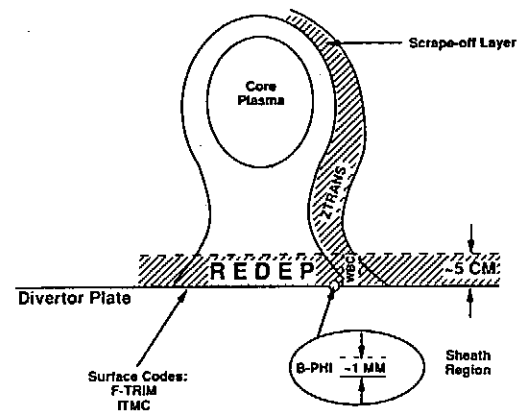

Code	Type
REDEP	Kinetic, Gyro Averaged, Finite Difference
WBC	Kinetic, Sub-Gyro, Monte Carlo
B-PHI	Kinetic, Finite Difference
ZTRANS	Quasi Fluid, Monte Carlo
F-TRIM, ITMC	Binary Collision, Monte Carlo

Erosion Code Verification Activities

- Recent activities: (J. N. Brooks, T. Hua, ANL)
  a. TFTR bumper limiter[1] (with PPPL, SNLL)
  b. DIII-D divertor[2] (with GA, SNLL)
  c. DIII-D DIMES probe (with GA, SNLL)
  d. PISCES - W, MO, B, D^+, Ar^+ exposed target experiments (with UCLA)

Key findings: Good agreement observed between REDEP/WBC analysis and experiment for TFTR plasma contamination, DIII-D divertor erosion, and PISCES data. Critical phenomena identified (e.g., sputtered energy distribution effects).

[1]T. Hua, J. Brooks, 10th PSI paper.
[2]C. Wong et al., 10th PSI paper.

REDEP Analysis for TFTR Bumper Limiter*

- Analysis was carried out for a series of ohmic discharges in TFTR. The Z_{eff} as a result of carbon contamination of the plasma is shown below.

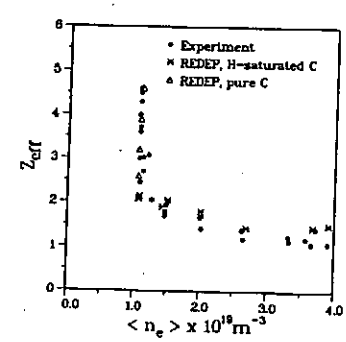

*Hua and Brooks, 10th PSI paper.

REDEP Analysis for DIII-D Graphite Divertor Tiles*

- Divertor tiles were exposed to ~1700 plasma discharges over a nine-month period. Analysis for typical plasma parameters were weighted by the strike point distribution.

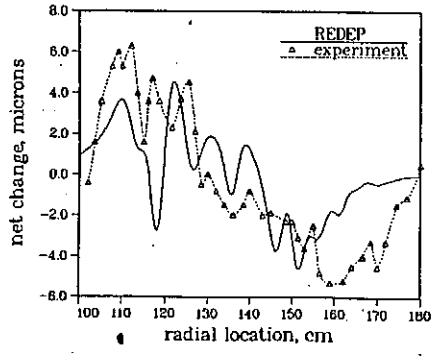

*C. Wong et al., 10th PSI paper.

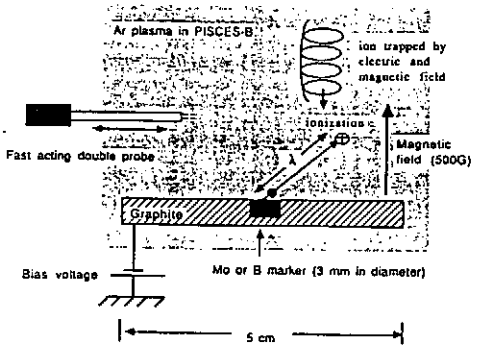

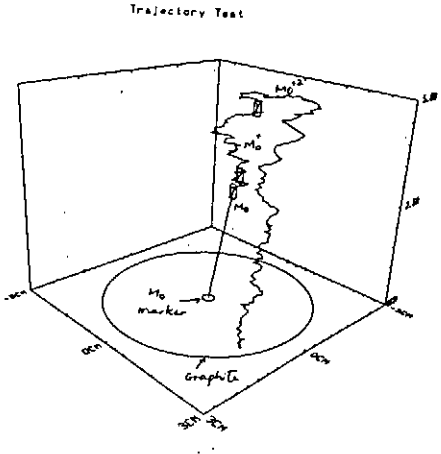

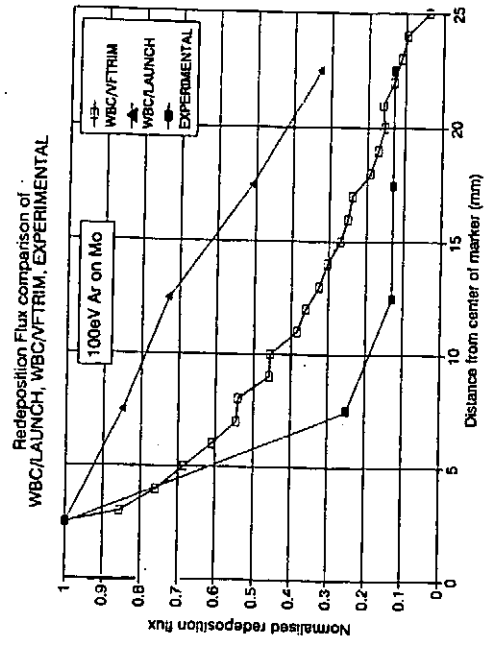

Chemical Sputtering - Carbon Transport

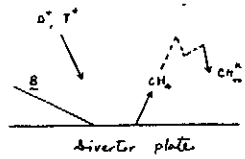

- WBC code used with PPPL-2477 (Ehrhart and Langer) rate coefficients
- -1000 CH_4 molecules launched at random thermal energies
- Particle history terminates upon redeposition or being lost to near-surface region
- CH_4 reflection cascade computed

Electron Impact Collision Processes:

$$e + CH_4 \rightarrow CH_4^+ + 2e \quad (1)$$
$$e + CH_3 \rightarrow CH_3^+ + 2e \quad (2)$$
$$e + CH_2 \rightarrow CH_2^+ + 2e \quad (3)$$
$$e + CH \rightarrow CH^+ + 2e \quad (4)$$
$$e + CH_4 \rightarrow CH_3^+ + H + 2e \quad (5)$$
$$e + CH_4 \rightarrow CH_2^+ + 2H + 2e \quad (6)$$
$$e + CH_4 \rightarrow CH^+ + 3H + 2e \quad (7)$$
$$e + CH_3 \rightarrow CH_2^+ + H + 2e \quad (8)$$
$$e + CH_2 \rightarrow CH^+ + H + 2e \quad (9)$$
$$e + CH \rightarrow C^+ + H + 2e \quad (10)$$
$$e + CH \rightarrow C + H^+ + 2e \quad (11)$$
$$e + CH_4 \rightarrow CH_3 + H + e \quad (12)$$
$$e + CH_3 \rightarrow CH_2 + H + e \quad (13)$$
$$e + CH_2 \rightarrow CH + H + e \quad (14)$$
$$e + CH \rightarrow C + H + e \quad (15)$$
$$e + CH_4^+ \rightarrow CH_3 + H^+ + e \quad (16)$$
$$e + CH_4^+ \rightarrow CH_3^+ + H + e \quad (17)$$

$$e + CH_3^+ \rightarrow CH_2 + H^+ + e \quad (18)$$
$$e + CH_3^+ \rightarrow CH_2^+ + H + e \quad (19)$$
$$e + CH_2^+ \rightarrow CH + H^+ + e \quad (20)$$
$$e + CH_2^+ \rightarrow CH^+ + H + e \quad (21)$$
$$e + CH^+ \rightarrow C + H^+ + e \quad (22)$$
$$e + CH^+ \rightarrow C^+ + H + e \quad (23)$$
$$e + CH_4^+ \rightarrow CH_3 + H \quad (24)$$
$$e + CH_4^+ \rightarrow CH_2 + 2H \quad (25)$$
$$e + CH_3^+ \rightarrow CH_2 + H \quad (26)$$
$$e + CH_2^+ \rightarrow CH + H \quad (27)$$
$$e + CH^+ \rightarrow C + H \quad (28)$$
$$e + C \rightarrow C^+ + 2e \quad (29)$$

Hydrogen Ion Impact Collision Reactions:

$$H^+ + CH_4 \rightarrow CH_4^+ + H \quad (30)$$
$$H^+ + CH_3 \rightarrow CH_3^+ + H \quad (31)$$
$$H^+ + CH_2 \rightarrow CH_2^+ + H \quad (32)$$
$$H^+ + CH \rightarrow CH^+ + H \quad (33)$$
$$H^+ + C \rightarrow C^+ + H \quad (34)$$

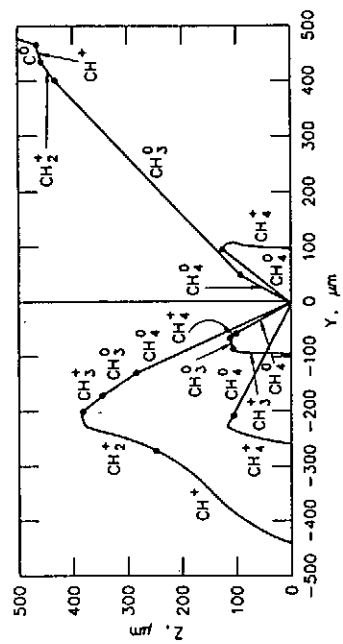

Figure 2. Sample histories of chemically sputtered carbon.

The BPHI Code

- A sheath code recently developed at ANL to simulate plasma flow in the magnetic and Debye sheath regions of the plasma scrape-off layer
- The code computes the sheath potential, distributions of angle of incidence and charge state, in-sheath ionization of neutrals, transport and redeposition of impurities, and total heat deposition at the wall.
- Computational time is ~ 1 CPU minute on the Cray for oblique field angle of 87°.

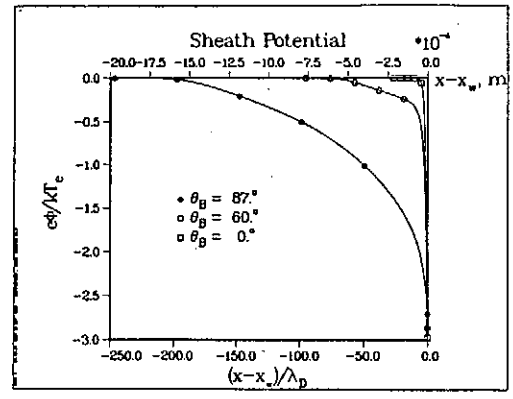

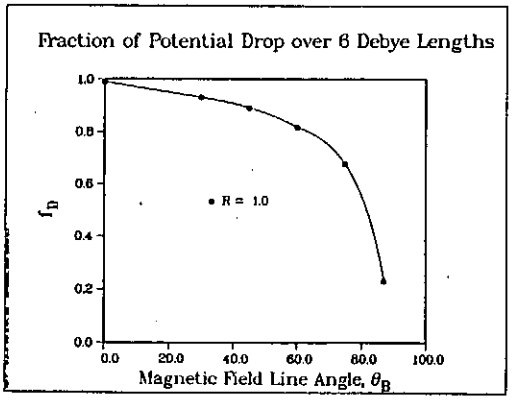

PRELIMINARY ANALYSIS OF H_2 DESORPTION FROM DIVERTOR

- H_2 molecules desorbed from wall with initial thermal energy (~ 0.1 eV) and are ionized within the magnetic sheath via

  $$H_2 + e \rightarrow H_2^+ + 2e$$

- The electrons are drawn into the plasma, H_2^+ are accelerated toward the wall. A fraction of the H_2^+ ions are dissociated before reaching the wall via

  $$H_2^+ + e \rightarrow H^+ + H + e$$

- Effects on sheath potential, heat transmission factor are studied for ion reflection coefficients varying from 0 to 1.
- Results presented here are for a DT plasma with $n_e = 10^{20} m^{-3}$, B = 5T, $\theta_B = 87°$, and $T_i = T_e = 5 - 1000eV$.

R = 0.25

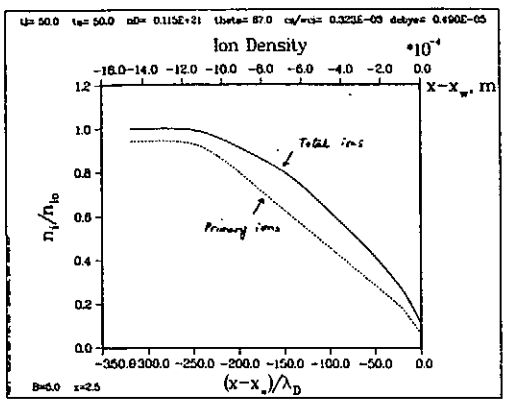

R = 0.25

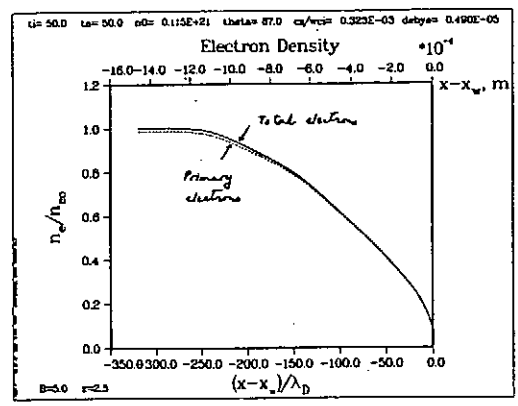

R = 0.25

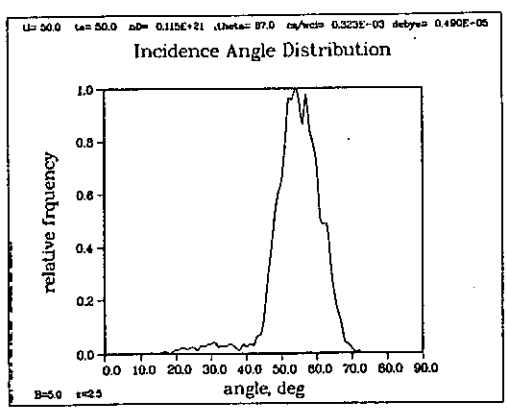

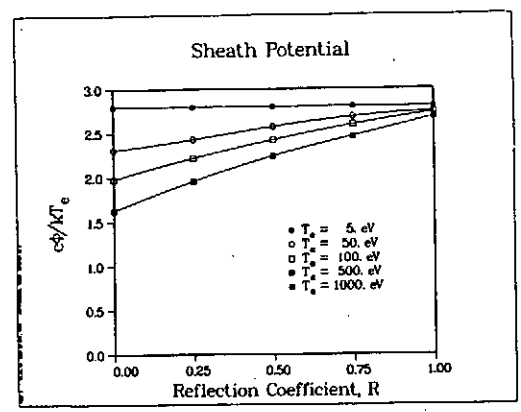

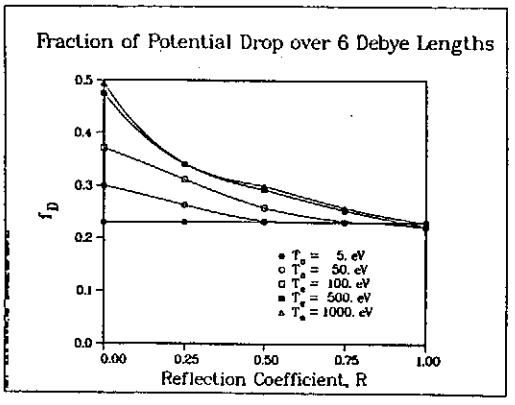

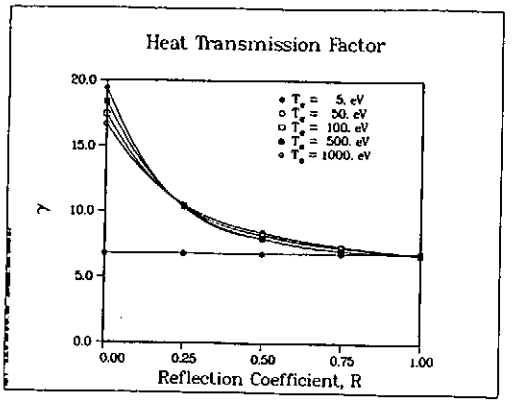

SUMMARY

- Erosion code verification has, to date, been successful. Key erosion and plasma contamination trends have been predicted and explained for tokamaks (TFTR, DIII-D, TEXTOR) and simulation facilities (PISCES). This work has led to improved models and code capabilities.
- Near-term erosion/redeposition modeling activities include: (1) analysis of JT-60U graphite divertor tiles and simulation experiments (with JAERI), (2) analysis of DIMES experiments in DIII-D (with GA, SNL).
- BPHI code results provide improved models for erosion analysis as well as important parameters for divertor design.

Experimental Study on Boronization using SUT

N. Noda, A. Sagara, Y. Kubota, N. Inoue, K. Akaishi, O. Motojima (NIFS),
K. Iwamoto, I. Fujita, M. Hashiba, T. Hino, T. Yamashina (Hokkaido Univ.),
J. Rice (MIT), K. Okazaki (The Inst. Phys. and Chem. Research),
M. Yamage, H. Toyoda, H. Sugai (Nagoya Univ.)

The importance and the main aims of the boronization study have been already presented in the previous workshop in Santa Fe[1]. The main aims are summarized as follows:

(1) evaluation of the life time of boronized layers being active for oxygen gettering,

(2) how to reactivate the existing boronized film.

A device named SUT (SUrface modification Teststand) [1], a kind of plasma simulator, has been constructed in Toki site and boronization studies have started this year.

The first boronization experiment was carried out in February 1992. Voltage and current of the glow discharge were around 250 volt and 0.2 A. A gas-mixture of 10 % diborane (B_2H_6) in helium was used as the working gas. The total pressure was around 18.5 mTorr. Mass-peaks originated from B_2H_6, namely m/e=10-13, 22-27, all disappeared during the glow discharge. On the other hand, the peaks m/e=1, 2 (H, H_2) increased during the discharge. These correspond to hydrogen molecules due to dissociation of B_2H_6. The thickness of the boron-coated layer was estimated to be several tens nanometer in the first one hour boronization. After improvement in effective pumping speed, coating rate was increased to be 4 nm/s.

After boronization, a glow discharge with 10% oxygen in helium was applied in order to estimate the capacity of oxygen on the boronized surface, which may have a relation to the lifetime of gettering effect of the boron-coated layer. The mass-peak m/e=32 decreased just after the discharge started and m/e=28 (CO) , 44 (CO_2) increases. Origin of CO and CO_2 is not clear at the moment.

In order to get the net amount of absorbed oxygen atoms, number of them released as CO and CO_2 must be subtracted from the number of O_2 absorbed. Net amount of absorbed oxygen was obtained by time integration of the and 1.2 X $10^{17}/cm^2$ in a coating layer of 200 nm in thickness. Not only a few monolayer on the top surface, but more than several hundreds atomic layers contribute the oxygen adsorption.

References

[1] N. Noda et al., Proc. of the last workshop, SAND92-0222 (1992) p.5 -52.

Experimental Study

on Boronization using SUT

N. Noda, A. Sagara, Y. Kubota, N. Inoue, K. Akaishi, O. Motojima (NIFS),

K. Iwamoto, I. Fujita, M. Hashiba, T. Hino, T. Yamashina (Hokkaido Univ.),

J. Rice (MIT),

K. Okazaki (The Inst. Phys. and Chem. Research),

M. Yamage, H. Toyoda, H. Sugai (Nagoya Univ.)

Contents

Aims

(1) Evaluation of effectiveness and the lifetime of oxygen-gettering ability of the boronized surface

(preliminary discussion on the lifetime)

(2) Recovery of the gettering ability for the existing boron film

(a preliminary experimental result)

[This is important with respect to a long period operation beyond the next step reactor]

(3) Hydrogen-recycling control with a boronized wall

(not related in this talk)

Present status of SUT

(1) A good vacuum condition in the main chamber and in the analyzing chamber

close to 1 .0 E-9 torr

(2) Available diagnostics

RGA, optical spectroscopy, in-situ AES, quartz oscillator (real time monitor of thickness)

(3) Liner temperature up to 600 °C

(4) Data acquisition by ADC/MAC system

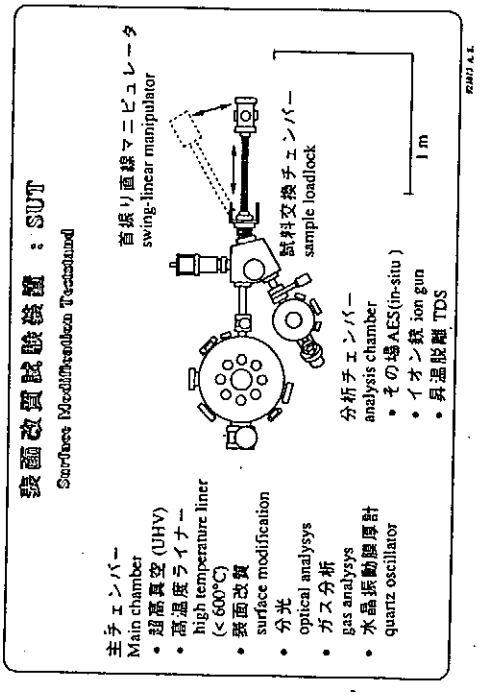

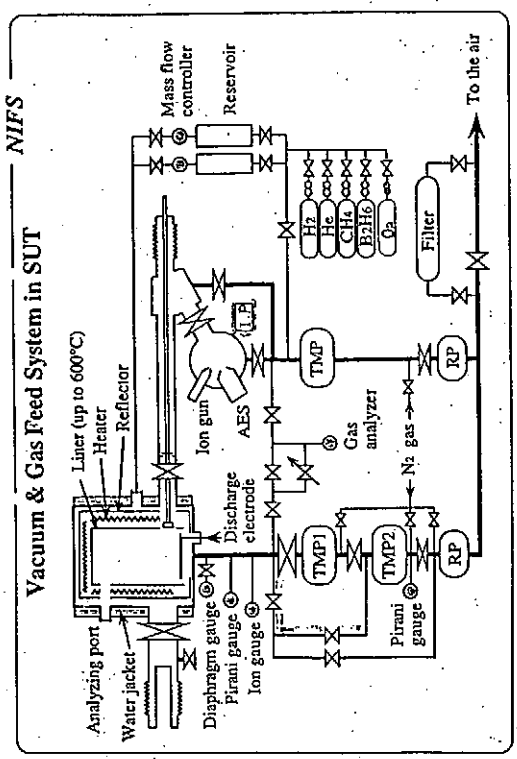

Experimental procedures

(1) Pump-down and baking (~200°C)

(2) Hydrogen-glow discharge

(3) Boronization

Glow discharge in a gas mixture of 10% B_2H_6 in He

Total pressure is around 20 mtorr

Current ~ 0.3 A, Voltage ~ 250 - 350 V

(4') exposed to atmosphere

(4) Oxygen absorption

Glow discharge in a gas mixture of 10% O_2 in He

(5) Recovery (He-glow discharge)

(6) Oxygen absorption (same as the procedure 4)

Experimental Results

(1) Oxygen is strongly absorbed during O_2/He glow discharge by a boronized wall

absorbed amount

1.2E17/cm^2 with a boronized wall

1.5E16/cm^2 with a bare SS wall

(2) CO and CO_2 were released during O_2/He glow discharge after boronization

(observed with RGA and optical spectroscopy)

origin of the carbon is not clear

(3) Boronized film can contain a lot of gaseous components of the air after exposing it to atmosphere

(4) Gettering effect was recovered after He glow discharge applied to the boronized wall

(5) B/O ratio on the top surface is 3/2

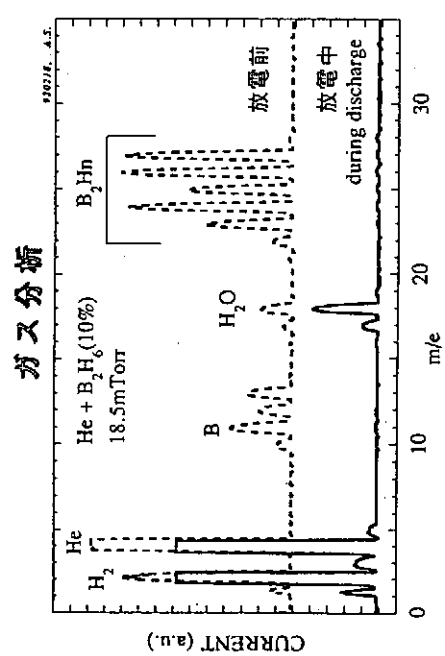

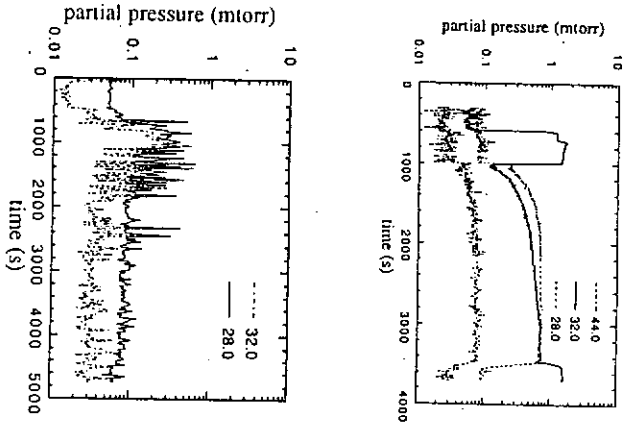
partial pressure (mtorr)
0.01
0.1
1
10
time (s)
1000
2000
3000
4000
5000
32.0
28.0
partial pressure (mtorr)
0.01
0.1
1
10
time (s)
1000
2000
3000
4000
44.0
32.0
28.0

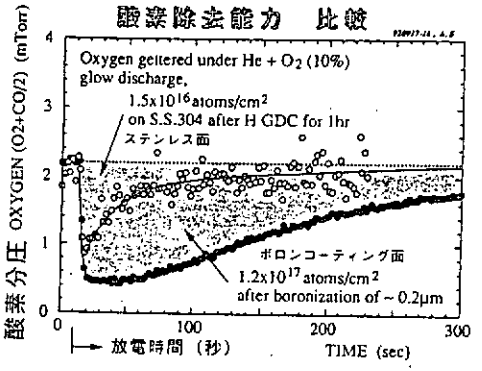
酸素除去能力　比較
Oxygen gettered under He + O2 (10%) glow discharge,
1.5x10^16 atoms/cm^2 on S.S.304 after H GDC for 1hr
ステンレス面
ボロンコーティング面
1.2x10^17 atoms/cm^2 after boronization of ~ 0.2μm
酸素分圧 OXYGEN (O2+CO/2) (mTorr)
0
1
2
3
4
0
100
200
300
放電時間（秒）
TIME (sec)

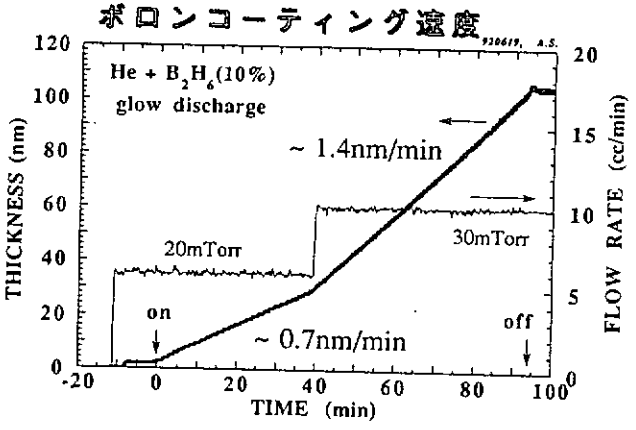
ボロンコーティング速度
He + B2H6(10%)
glow discharge
~ 1.4nm/min
~ 0.7nm/min
20mTorr
30mTorr
on
off
THICKNESS (nm)
FLOW RATE (cc/min)
TIME (min)
0
20
40
60
80
100
120
5
10
15
20
-20
0
20
40
60
80
100

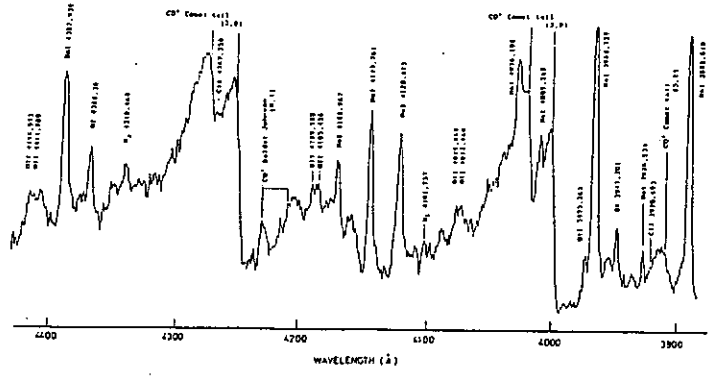
分光測定　（He 90%+O2 10%）
WAVELENGTH (Å)

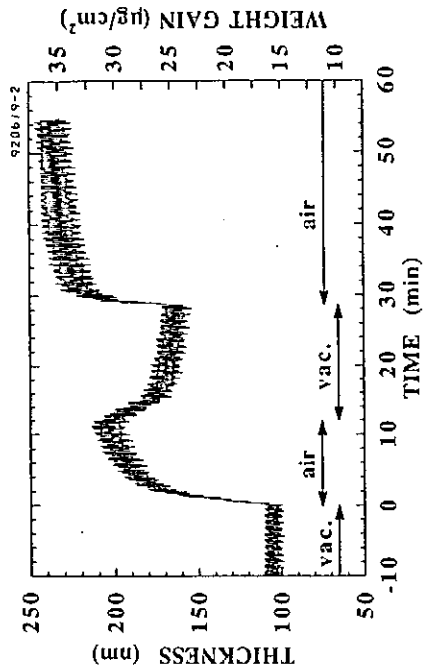

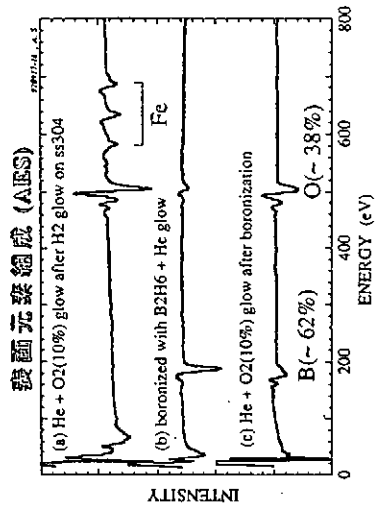

A preliminary discussion

(1) Oxygen atoms are absorbed in hundreds monolayers from the top surface

(2) preliminary estimation of the lifetime

$Q_{limit} \sim A_{LHD}\, C_{smax} = 1.2\ e22$

$C_{smax} = 1.2e17\ cm^{-2}$ (saturation density)

$A_{LHD} = 1.0e5\ cm^2$ (total surface area of divertor legs in LHD)

$N_{ox}/\tau_p = 0.03\, n_e V_{LHD}/\tau_p = 3.0\ e20\ /s$

$V_{LHD} = 2.0\ e7\ cm^3$

$\tau_p = 0.1\ s$ [particle confinement time]

$n_e = 5.0\ e13\ cm^{-3}$

$Q_{[1shot]} = 3.0\ e21$ for 10 second discharge

$Q_{limit} / Q_{[1shot]} \sim 1.2\ e22 / 3.0\ e21 = 4$ shots

Future Plan

(1) Oxygen absorption amount as a function of wall temperature, impact energy of ions, etc.

(2) A detailed comparison with a post-mortem analysis in Hokkaido University

(3) Comparison of the gettering ability of the boronized surface with tat of titanium flashed surface

(4) Detail analysis for evaluation of the lifetime

(5) Experiments on hydrogen recycling control

(6) Boronization for a graphite liner

Summary

(1) Present status of SUT and some results of boronization experiment are presented

amount of absorbed oxygen is 1.2 e7 cm^{-2}

B/O ratio on the top surface is 3/2

(2) This suggests that oxygen is absorbed in more than hundreds monolayers on the surface

(3) Preliminary estimation of the lifetime shows that it could be a problem if the oxygen recycling would occur only in divertor legs

gettering on the wall may reduce this problem but more precise study is necessary on this subject

Basic Experiments on Boronization with Use of Decaborane

H. Sugai, M. Yamage and T. Ejima

Department of Electrical Engineering, Nagoya University
Furo-cho, Chikusa-ku, Nagoya 464-01, Japan

1. Use of Decaborane

Diborane used in conventional boronization is extremely toxic and explosive, while the use of a less hazardous gas, $B(CH_3)_3$, gives carbon-containing boron films (B/C $\sim$ 0.6). In order to deposit carbon-free films, we have proposed the use of a much less hazardous boride, decaborane ($B_{10}H_{14}$), which is sublimated in vacuum at low temperatures such as 40 - 100 °C. This method has successfully been applied to the boronization of JT-60U since August, 1992.

2. Scaling Law for Non-Uniformity of Deposition

The glow discharge decomposition of decaborane in helium gives rise to the deposition of boron films whose thickness exponentially decreases with the distance from a gas inlet. The measured dependence of the e-folding length for the non-uniformity agreed with the prediction in a one-dimensional fluid model for the plasma CVD. In addition, a fairly uniform deposition of boron has been demonstrated using pulsed glow discharges.

3. Boron Coating without Glow Discharges

Boron thin films were deposited by thermal decomposition (pyrolysis) of decaborane in the absence of a glow plasma. High deposition rates on a hot wall (> 350 °C) were obtained with the activation energy of 39 kcal/mol.

4. Oxygen Gettering and Hydrogen Recycling

After boronization, a pulsed glow discharge in a mixture of O_2 and He was turned on to investigate the activity on oxygen impurity. The boronized walls by both the plasma CVD and the thermal CVD in decaborane absorbed a considerable amount of oxygen, which is comparable with the oxygen gettering by the diborane-based boronization. A pulsed glow discharge in deuterium after the decaborane-based boronization showed the hydrogen recycling bahavior similar to that observed after the boronization by a diborane discharge.

Basic Experiments on Boronization with Use of Decaborane

H. Sugai, M. Yamage and T. Ejima
Dept. of Electrical Eng., Nagoya University

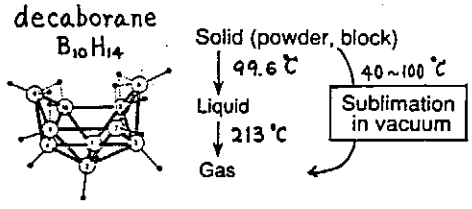

Why Decaborane ?

1) Handling
Less Hazardous, Non-Explosive
Easy to Treat, Inexpensive

2) Carbon-Free, Less H-Content

$B(CH_3)_3 \rightarrow \frac{B}{C} \sim 0.6$ $\quad B_4C$

$B_{10}H_{14} \rightarrow \frac{H}{B} = \frac{14}{10} = 1.4$

$B_2H_6 \rightarrow \frac{H}{B} = \frac{6}{2} = 3$

Laboratory Experiment on

[redacted]

Long Cylindrical Vessel at Room Temp.
2 m long, 0.6 m diam.

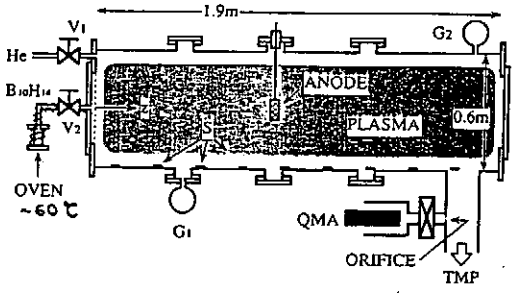

DC Glow Discharge (350 V, 0.5 A)
in 10% $B_{10}H_{14}$/He (1 Pa)

Axial Distribution of Film Thickness

UNIFORMITY OF DEPOSITION

$d \propto \exp(-z/L)$

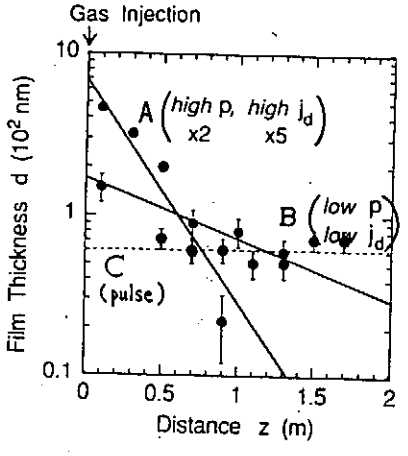

Case	Pressure $B_{10}H_{14}$ (Pa)	Discharge V_d (V)	Deposition Time (hour)	Length L (m)	Scaling Factor $L(p')^{1/2}$
A	0.0067 ~0.0200	310	2.5	0.22	0.13
B	0.0665	370	1.0	0.43	0.15

Boronization without Glow Discharge (Plasma CVD)

Thermal CVD (Pyrolysis)

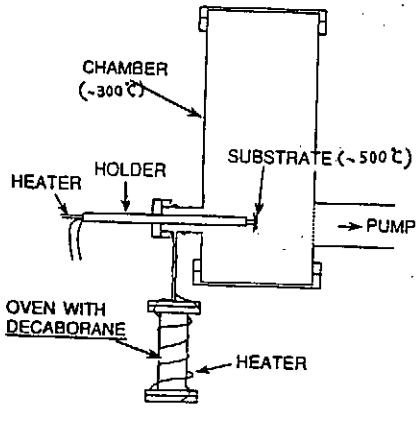

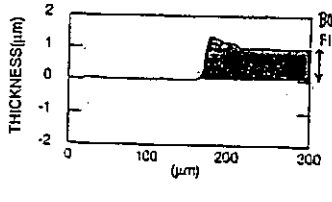

T_s=372℃
P_{db}=0.027~0.029Pa
t_d=60min

Pulsed Glow Discharge
after Boronization (Pyrolysis)
300 °C

(1) Test of Hydrogen Recycling

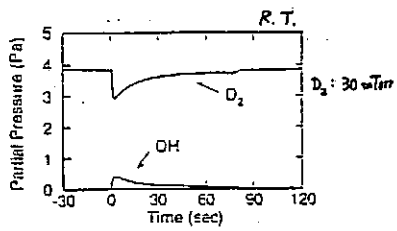

(2) Test of Oxygen Gettering

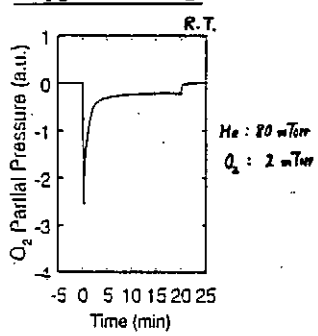

SUMMARY

1. New Boronization Based on Decaborane
   Les Hazardous, Carbon-Free
2. Scaling for Non-Uniform Deposition
   e-Folding Length $\propto (p j_d)^{-1/2}$
3. Boronization by Pyrolysis of Decaborane
4. Oxygen Gettering Effect

Applied to the Boronization of **JT-60U**
since August, 1992.

Erosion Profiles on Graphite under PISCES-B Plasma

A.Sagara
National Institute for Fusion Science, Nagoya 464, Japan
-- the US-Japan collaboration work with Y.Hirooka, R.W.Conn and M.Khandagle of UCLA, and O.Motojima of NIFS in 1991 --

Plasma bombardment of materials in a magnetic field gives rise to deformation of surface topography due to erosion and redeposition with self-sputtering. Particularly, in such as ITER and LHD, deformation due to net erosion of actively cooled divertor plates is expected to limits their lifetime, demanding their repairs many times a year. However, it is also true that there is few experiments performed to evaluate surface deformation by measuring net erosion profile of target materials under well controlled conditions, where it is important to use nonuniform plasma with sufficiently short ionization mean free path of sputtered neutrals in the scale of target size [1].

High-flux, steady-state hydrogen or helium plasma has been conducted perpendicularly along the magnetic field lines to target disks of 50 mm in diameter using the PISCES-B facility at UCLA. The targets used here are isotropic graphite IG430U and they have been prepared very carefully to have highly flat surface within 1 mm over 50 mm. In both cases of hydrogen and helium, the electron density profile measured by a fast scanning probe has the maximum at the target center with the FWHM of about 50mm, but the electron temperature profile is almost flat. The surface temperature is measured with an infrared pyrometer which is focused to the target center.

Net erosion profiles have been measured with surface profilometry. The erosion profile due to helium is easily explained by sputtering with little redeposition, because the sputtering yield estimated from the weight loss is comparable to that from ion beam experiments, and because the calculated ionization mean free path of physically sputtered carbon atoms is as long as about 100mm in this experiment.

In case of hydrogen, the net erosion profile clearly differs from that of helium. The initial surface level can be estimated from the volume change estimated from the weight loss by assuming the weight density of the redeposited layer to be the same as that of the bulk. The result indicates that there is net growth at the center region and net erosion at the outer region. In fact the SEM photos show a thick layer due to redeposition at the center region and a heavily eroded surface at the outer region.

The net growth in the center region is explained by redeposition of carbon under a condition of not only a short ionization mean free path of about 10mm for CH_4 gas at 1,000°C but also an excessive supply from the outer region. Though the H flux Φ is 50% lower at the outer, this excessive supply is likely to take place, because it is conjectured that the surface temperature is lower at the outer than 950°C at the center and the chemical erosion yield Y has the maximum at about 600 ~ 700°C [2], thus giving a larger erosion rate ΦY at the outer than the center region.

[1] A.Sagara et al., 10th PSI conf.(1992), in press in J.Nuclear Materials
[2] A.Sagara et al, 16th SOFT conf.(1990) p.361.

Erosion Profiles on Graphite under PISCES-B Plasma

A. Sagara

NIFS

1. Performed as part of US-J collaboration in May,'92
   - *UCLA : Y.Hirooka, R.W.Conn and M.Khandagle*
   - *NIFS : A.Sagara and O.Motojima*
   - View point of erosion lifetime of divertor plates in LHD and ITER

2. Required experimental conditions
   - Ionization mean-free path of sputtered particles
     $\lambda i \ll D$ of sample plates
   - Nonuniform plasma flux with
     FWHM << D

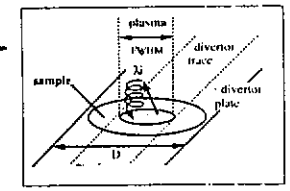

Ne and Te Profiles

- In both cases of hydrogen and helium, the electron density profile was intentionally made narrow as far as possible.
- In both cases of H and He, we could control the density profile to be peaked at the target center with the FWHM of about 50mm measured by a fast scanning probe. But the electron temperature profile was almost flat.
- The surface temperature was measured with an infrared pyrometer which was focused to the target center.

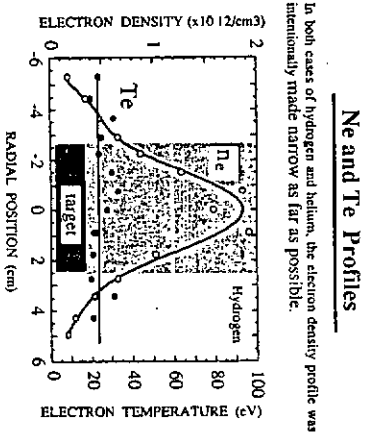

NIFS, 921218, A. Sagara

Flatness of Sample Surfaces

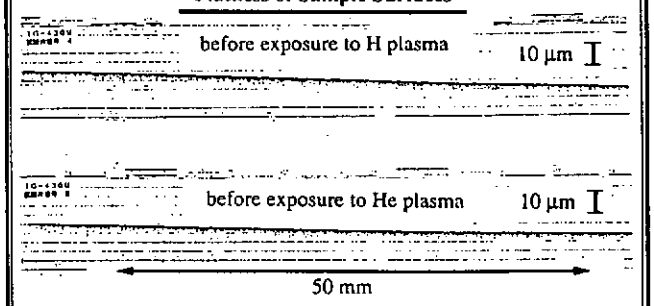

The targets used here are isotropic graphite IG430U and they have been prepared very carefully to have highly flat surface within 1 μm over 50 mm.

NIFS, 921218, A. Sagara

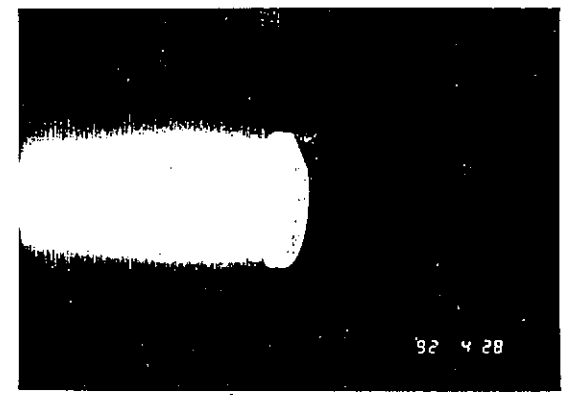

High-flux, steady-state hydrogen or helium plasma has been conducted perpendicularly along the magnetic field lines to target disks of 50 mm in diameter using the PISCES-B facility at UCLA.

Net Erosion Profiles

measured with surface profilometry

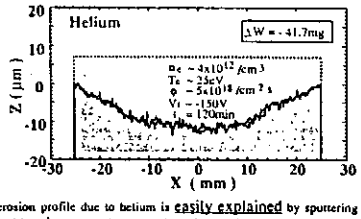

The erosion profile due to helium is easily explained by sputtering with little redeposition, because the sputtering yield estimated from the weight loss is comparable to that from ion beam experiments, and because the calculated ionization mean free path of physically sputtered carbon atoms is as long as about 100mm in this experiment.

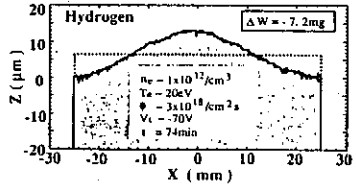

In case of hydrogen, the net erosion profile clearly differs from that of helium.

The initial surface level can be estimated from the volume change estimated from the weight loss by assuming the weight density of the redeposited layer to be the same as that of the bulk.

- The result indicates that there is net growth at the center region and net erosion at the outer region.

NIFS, 921218, A. Sagara

SEM Photos

show a thick layer due to redeposition at the center region and a heavily eroded surface at the outer region.

(a) center region

10 μm

(b) outer region

Bombarded with H plasma.
View 30° from normal

NIFS, 921218, A. Sagara

Discussion

edge center

Φ < Φ ------ Hydrogen Flux

Y > Y ------ Erosion yield

YΦ > YΦ ---- Erosion rate

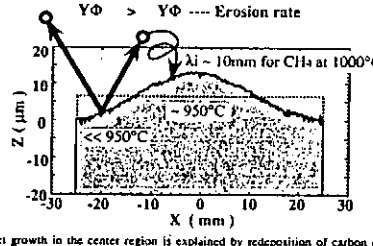

The net growth in the center region is explained by redeposition of carbon under a condition of not only a short ionization mean free path of about 10mm for CH_4 gas at 1,000°C but also an excessive supply from the outer region. Though the H flux is 50% lower at the outer, this supply is likely to take place, because it is conjectured the surface temperature is lower at the outer than 950°C at the center and the chemical erosion yield has the maximum at about 700°C, thus giving a larger erosion rate at the outer than the center region.

A. Sagara et al, 14th SOFT (1990) p.361.

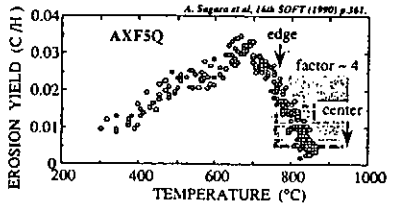

NIFS, 921218, A. Sagara

Summary

- The first experiment have been performed to bombard graphite sample with high-flux, steady-state H or He plasma in PISCES-B under conditions of peaked flux-profile with short ionization mean free path of sputtered neutrals in the scale of sample size.
- In spite of a peaked flux-profile of H plasma, there were observed net growth at the sample center and net erosion at the edge region.
- The net growth was explained by an excessive supply of carbon from the outer region where the erosion rate was conjectured to be larger than the center region due to surface temperature lower than 950°C at the center.
- The surface temperature is very important to control erosion profiles on divertor plates made of a kind of graphite in particular.

NIFS, 921218, A. Sagara

Mass Balance Equations and Their Physical Parameters for Prediction of Hydrogen Recycling and Inventory during D-T Discharge Shots

Kenji MORITA

Department of Crystalline Materials Science, School of Engineering

Nagoya University, Furo-cho, Chikusa-ku, Nagoya 464-01, JAPAN

In magentically confined fusion devices, evaluation and prediction of hydrogen isotopes re-emission from and retention in wall materials, espcially, carbon and carbon-metal composite materials before and after each discharge shot are of essential importance to control plasma parameters and to establish the ignition condition in D-T burning experiments, because the retained number of hydrogen in the wall materials is much larger than the confined number in core plasma. A number of data on retention and re-emission have been accumulated by many authors. The tritium data describing its retention and re-emission have been accepted to be extrapolated using the isotopic effects from the protium and deuterium data on diffusion, trapping, ion-induced and thermal detrapping and molecular recombination. For evaluation of hydrogen recycling, the modelling and the elementary processes, applicable to both the retention and re-emission experiments, should be well established.

So far, our group has proposed the mass balance equations of hydrogen in graphite and has determined the rate constants of the elementary processes by applying them to analysis of the experimental data on retention and ion-induced and isothermal re-emission of protium and deuterium. Moreover, we have reasonably explained the isotope difference in the experimental data on protium and deuterium.

In this report, the mass balance equations for single hydrogen are modified to describe retention and re-emission behaviors during D-T dual irradiation. The rate constants of elementary processes for H and D are present and the isotopic effects are shown for extrapolation of the T data.

Japan-US Workshop P196 on High Heat Flux Components
and Plasma Surface Interaction for Next Devices
Kasuga-shi, Fukuoka, JAPAN Nov. 17-19, 1992

Mass Balance Equations and Their Physical Parameters for Prediction of Hydrogen Recycling and Inventory during D-T Discharge Shots

Kenji MORITA

Department of Crystalline Materials Science
School of Engineering, Nagoya University

We have investigated retention behavior of H and D during single implantation of H or D and re-emission behavior of H and D due to isothermal annealing and ion bombardment after the implantation. The mass balance equations were used for analysis of the experimental data on retention and re-emission and the rate constant of relevant elementary processes : diffusion, thermal and ion-induced detrapping, trapping (or retrapping) and local molecular recombination for H and D were determined. The isotope difference between the rate constants of H and D was derived for prediction of T data

In this report, the mass balance equations are proposed to describe Hydrogen Recycling during D-T discharge shots. The rate constants of the elementary processes for H and D are presented and the isotopic effects are derived for extrapolation of T data

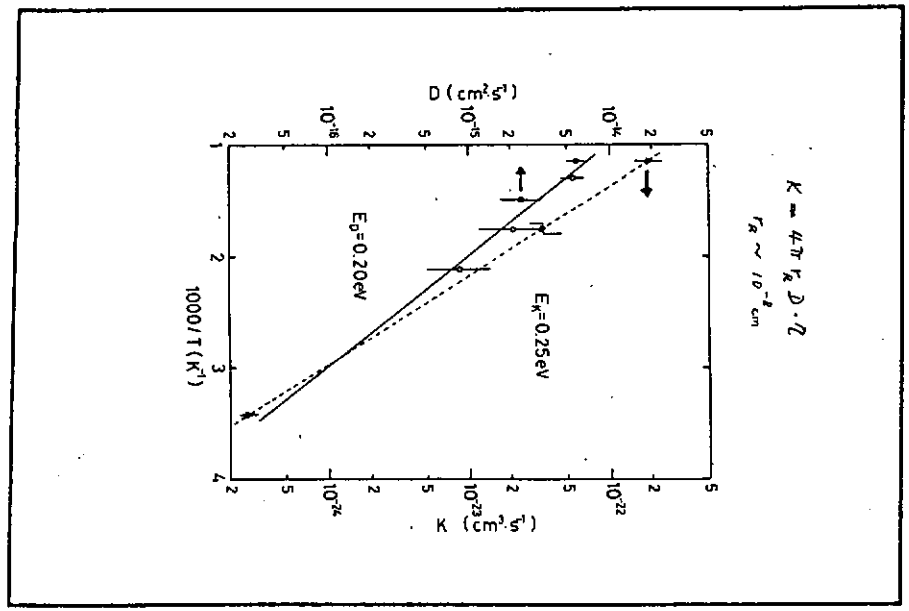

$K = 4\pi r_R D \cdot Q$

$r_R \sim 10^{-8}$ cm

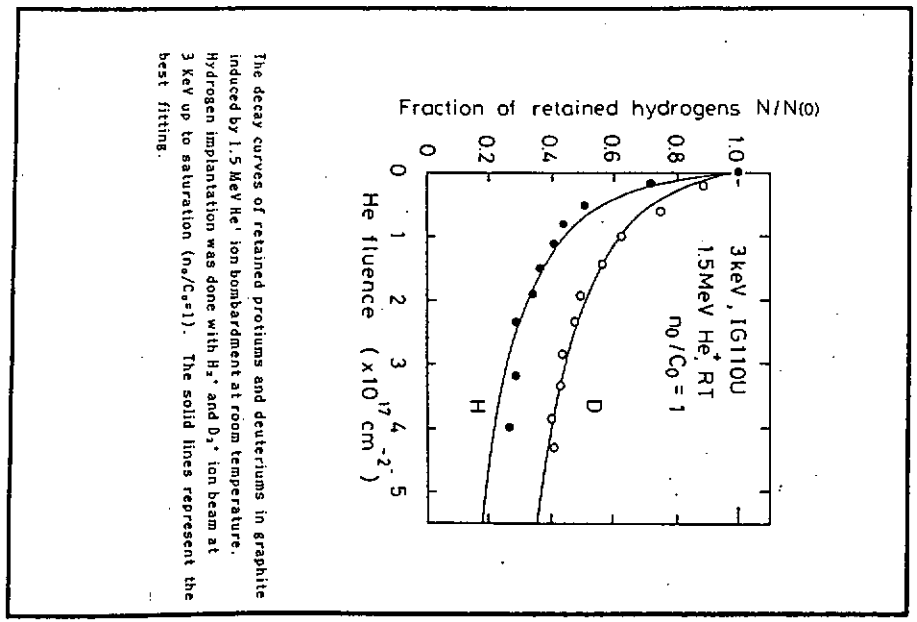

The decay curves of retained protiums and deuteriums in graphite induced by 1.5 MeV He^+ ion bombardment at room temperature. Hydrogen implantation was done with H_2^+ and D_2^+ ion beam at 3 KeV up to saturation ($n_0/C_0=1$). The solid lines represent the best fitting.

Mass Balance Equations for Prediction of Recycling of D and T during D-T Discharge shot

For free T

$$\frac{\partial N^T(z,t)}{\partial t} = D^T \frac{\partial^2 N^T(z,t)}{\partial z^2} + (v^T + v^D)\frac{\partial N^T(z,t)}{\partial z} + f^T(z,t) - \Phi_{out}^T(z,t) - N_c^T(z,t)k_c^T$$

$$- N^T(z,t)\Sigma_t^T(C_0 - N_t^T(z,t) - N_t^D(z,t)) + (\sigma_d^{TT}\phi_{in}^T + \sigma_d^{DT}\phi_{in}^D + \Sigma_d^T)N_t^T(z,t) \qquad (1)$$

$$- N^T(z,t)(K^{TT}N_t^T(z,t) + K^{TD}N_t^D(z,t)) + N^T(z,t)(2K_1^{TT}N^T(z,t) + K_1^{TD}N^D(z,t))$$

For trapped T

$$\frac{\partial N_t^T(z,t)}{\partial t} = (v^T + v^D)\frac{\partial N_t^T(z,t)}{\partial z} + N^T(z,t)\Sigma_t^T(C_0 - N_t^T(z,t) - N_t^D(z,t))$$

$$- (\sigma_d^{TT}\phi_{in}^T + \sigma_d^{DT}\phi_{in}^D + \Sigma_d^T)N_t^T(z,t) - N_t^T(z,t)(K^{TT}N^T(z,t) + K^{TD}N^D(z,t)) \qquad (2)$$

For free D

$$\frac{\partial N^D(z,t)}{\partial t} = D^D \frac{\partial^2 N^D(z,t)}{\partial z^2} + (v^T + v^D)\frac{\partial N^D(z,t)}{\partial z} + f^D(z,t) - \Phi_{out}^D(z,t) - N_c^D(z,t)k_c^D$$

$$- N^D(z,t)\Sigma_t^D(C_0 - N_t^T(z,t) - N_t^D(z,t)) + (\sigma_d^{TD}\phi_{in}^T + \sigma_d^{DD}\phi_{in}^D + \Sigma_d^D)N_t^D(z,t) \qquad (3)$$

$$- N^D(z,t)(K^{DT}N_t^T(z,t) + K^{DD}N_t^D(z,t)) + N^D(z,t)(2K_1^{DD}N^D(z,t) + K_1^{DT}N^T(z,t))$$

For trapped D

$$\frac{\partial N_t^D(z,t)}{\partial t} = (v^T + v^D)\frac{\partial N_t^D(z,t)}{\partial z} + N^D(z,t)\Sigma_t^D(C_0 - N_t^D(z,t) - N_t^T(z,t))$$

$$- (\sigma_d^{TD}\phi_{in}^T + \sigma_d^{DD}\phi_{in}^D + \Sigma_d^D)N_t^D(z,t) - N_t^D(z,t)(K^{DT}N^T(z,t) + K^{DD}N^D(z,t)) \qquad (4)$$

Out-flux

$$\phi_{out}(t) = \sum_{D,T}\int_0^\infty [2K_1^{ii}(N^i(z,t))^2 + 2K_1^{ij}N^i(z,t)N^i(z,t)$$

$$+ 2K^{ii}N_t^i(z,t)N^i(z,t) + 2K^{ij}N_t^i(z,t)N^j(z,t)]dz + \sum_{D,T} N^i(z,t)\,k_c^i \qquad (5)$$

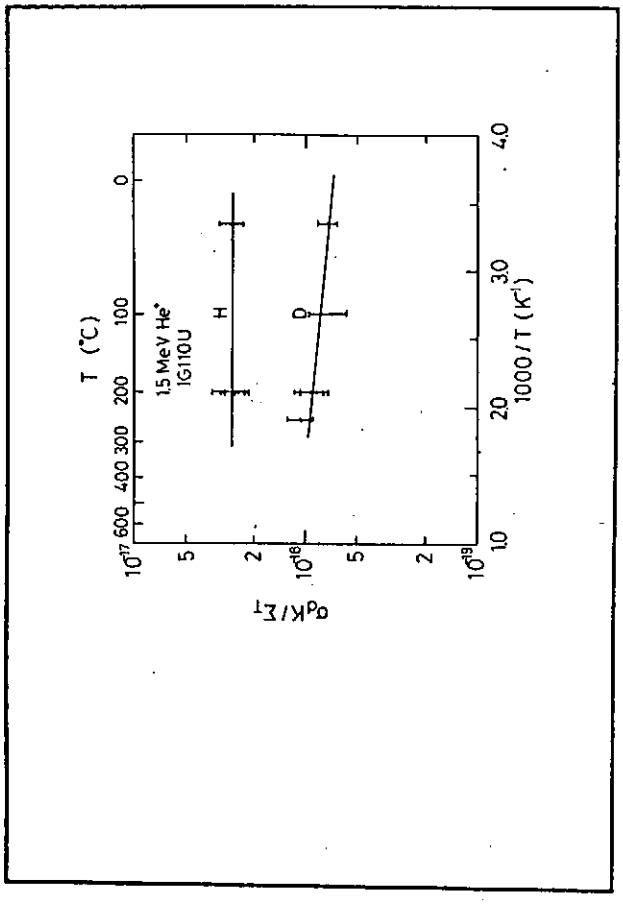

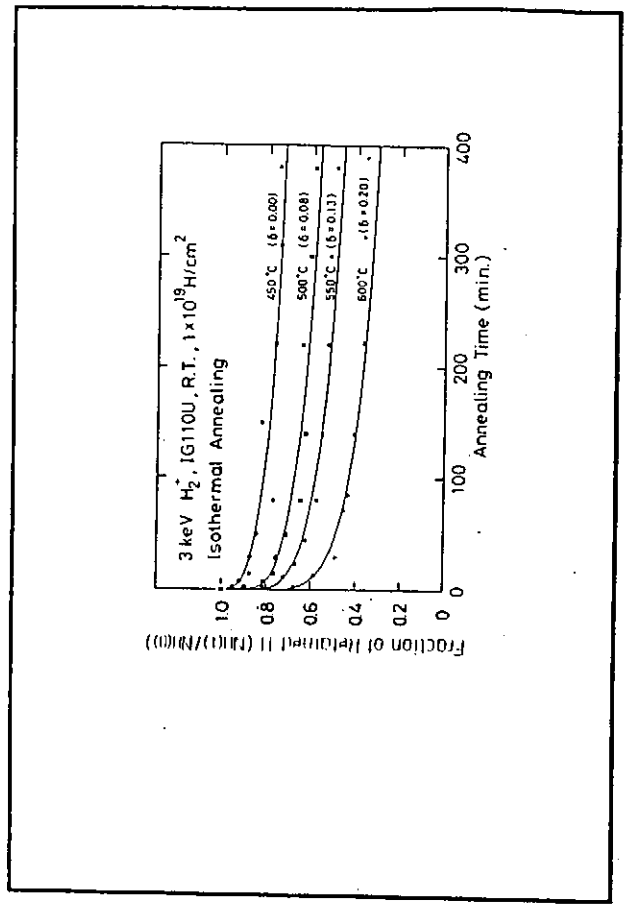

Isotopic Effect in Ion-Induced Re-emission

	$\sigma_d K/\Sigma_T (10^{-18}\,cm^2)$	$\sigma_{d,theor} (10^{-17}\,cm^2)$	K/Σ_T
H	2.9	2.8	0.10
D	0.77	2.5	0.031

Based on the diffusion-limited reaction model

$$\Sigma_T = 4\pi r_T D_a' \xi$$
$$K = 4\pi r_R D_a' \eta$$

D_a' : diffusion constant of hydrogens activated due to ion-induced detrapping $D_a' \gg D$ (thermal)

When $\Sigma_T C_0 \gtrsim 1/sec$, $\Sigma_T C_0$ shows no isotopic effect.

K is responsible for isotopic effect in K/Σ_T.

D_a' is propotional to $1/\sqrt{M}$

η and r_T are propotional to the mean amplitude or the frequency of thermal vibration, namely to $1/\sqrt{M}$

K/Σ_T is propotional to $1/(\sqrt{M})^3$

Table I The theoretical detrapping cross-section $\sigma_{d,\,theor}$ for H, D and T atoms trapped in graphite of 1.5MeV He^+ ion, the effective detrapping cross-sections $\sigma_d K/\Sigma_I$, the estimated ratios of K/Σ_I, the pre-exponential factors of Σ_d and $\left(\frac{\kappa_1}{c_1}\right)\left(\frac{\Sigma_1}{\Sigma}\right)$ and their isotope ratios.

Hydrogen isotope	$\sigma_{d,\,theor}$ (10^{-17}cm^2)	isotope ratio	$\sigma_d K/\Sigma_I$ exp.(10^{-17}cm^2)	isotope ratio	K/Σ_I exp.	isotope ratio	$\Sigma_d^0\left(\frac{\kappa_1}{c_1}\right)\left(\frac{\Sigma_1}{\Sigma}\right)$ exp.	isotope ratio
				exp. theor.				exp. theor.
H	2.8	1	2.9	0.10 1.0	0.10	1 1	5.6	45 1 1
D	2.5	0.89	0.77	0.27 1/2	0.033	0.40 $1/2\sqrt{2}$	4.0	18 0.40 $1/2\sqrt{2}$
T	2.1	0.75	0.41[a]	0.14 1/3	0.019[a]	... $1/3\sqrt{3}$	...	... ... $1/3\sqrt{3}$

a) The values were extrapolated K/Σ_I from =0.1 for H using the isotope ratio of K/Σ_I for T.

Isotopic Effect in Isothermal Re-emission

Σ_d : themal detrapping
the pre-exponential factor is proportional to $1/\sqrt{M}$
Based on the diffusion-limited reaction model
$\Sigma_T = 4\pi r_T D\xi$
$K_1 = 4\pi r_R D\eta$
D : diffusion constant
the pre-exponential factor is proportional to $1/\sqrt{M}$
r_T and r_R: effective radii for trapping and recombination
ξ and η : the probabilities for trapping and molecular fomation
r_T is independent of M
r_R is proportional to diffusion length
ξ is independent of M
η is proportional to the frequency factor of thermal vibration of partner hydrogen: $1/\sqrt{M}$

Finally,
$(K_1/C_0)(\Sigma_d/\Sigma_T)^2$ is proportional to $1/M\sqrt[4]{M}$.
Theoretical D/H ratio is 2.4.

Summary

The mass balance equations developed for single hydrogen isotope have been modified to describe retention and re-emission behavior during D-T dual irradiation. The rate constants of elementary processes for H and D available for them have been shown, which were obtained in the experiments of retention and re-emission. The isotopic effects have been derived for extrapolation of T data.

In order to establish the mass balance equations, the experiments on retention and re-emission during H-D dual irradiation of isotropic graphite are being planned in future.

RELEASE OF HYDROCARBON FROM GRAPHITE
– Modeling and Its Application to Isotropic and Boron-doped Graphites –

Michio YAMAWAKI, Satoru TANAKA, Kenji YAMAGUCHI
and
Tetsuhiro NAKAGUMA

Nuclear Engineering Research Laboratory
University of Tokyo

During the course of hydrogen-graphite interaction, a hydrogen atom (H) is considered to undergo a series of trapping, detrapping, diffusion and recombination. These fundamental kinetic processes combine to determine the overall rate of hydrogen uptake, ion- and/or thermally induced desorption, chemical sputtering, radiation enhanced sublimation, etc. hydrocarbon from graphite, and the model is applied to the experimental data of thermal desorption.

According to the present model, the principal equations describing the hydrocarbon formation can be expressed as follows.

$$\frac{dN_H}{dt} = -\Sigma_T N_{vac} N_H - \Sigma_T^* N_{CH} N_H + \Sigma_d N_{CH} - 2K_R N_H^2 , \quad (1)$$

$$\frac{dN_{vac}}{dt} = -\Sigma_T N_{vac} N_H + \Sigma_d N_{CH} , \quad (2)$$

$$\frac{dN_{CH}}{dt} = \Sigma_T N_{vac} N_H - \Sigma_d N_{CH} - \Sigma_T^* N_{CH} N_H , \quad (3)$$

$$\frac{dN_{CH_x}}{dt} = \Sigma_T^* N_{CH} N_H \equiv J_{C_xH_y}/x_R , \quad (4)$$

where N_H, N_{vac}, N_{CH} and N_{CH_x} are the concentrations of mobile (untrapped) hydrogen (in solution site), vacant trap sites, C-H, C-H_x, which leads to the spontaneous release of hydrocarbon, respectively, $J_{C_xH_y}$ is the release flux of hydrocarbon, Σ_d is the detrapping rate constant, Σ_T and Σ_T^* are the trapping rate coefficients, x_R is the implantation depth and K_R is the (bulk) recombination rate coefficient. It should be noted that Σ_T^* is specially assigned to describe the formation of hydrocarbon, assuming that the nature of trapping should be different when the host carbon atom is already occupied by another hydrogen.

The solution of the above differential equations can be obtained with the help of experimental data of thermal desorption. However, in the present model, Σ_T^*, N_H and K_R are unknown, so that a pair of desorption spectra of hydrogen and hydrocarbon alone is not sufficient to determine these parameters uniquely. Hence, additional information, for instance, a time dependence of trapped hydrogen, N_{CH}, or more than two sets of desorption spectra with different temperature profiles is needed. In applying the present model to B-doped graphite, a detailed knowledge of the effect due to doping is required; B-doping is likely to have simultaneous effects on trapping, detrapping and recombination.

RELEASE OF HYDROCARBON FROM GRAPHITE

Modeling and Its Application to Isotropic and Boron-doped Graphites

M. YAMAWAKI, S. TANAKA, K. YAMAGUCHI
and
T. NAKAGUMA

Nuclear Engineering Research Laboratory
University of Tokyo

presented at
Japan-US Workshop P196
Nov.17-19, 1992
Kyushu University

INTRODUCTION

- Fundamental Transport Processes in Graphite
  1. trapping or re-trapping
  2. detrapping
  3. diffusion
  4. (bulk) recombination
- These processes combine to determine the overall rate of
  1. hydrogen uptake
  2. ion- and/or thermally-induced desorption
  3. chemical sputtering
  4. radiation enhanced sublimation, etc.
- Chief interest is to incorporate these processes into one comprehensive model, and to apply it to the above mentioned graphite phenomena.

DESCRIPTION OF THE MODEL

The principal equations

$$\frac{dN_H}{dt} = -\Sigma_T N_{vac} N_H - \Sigma_T^* N_{CH} N_H + \Sigma_d N_{CH} - 2K_R N_H^2 \quad (1)$$

$$\frac{dN_{vac}}{dt} = -\Sigma_T N_{vac} N_H + \Sigma_d N_{CH} \quad (2)$$

$$\frac{dN_{CH}}{dt} = \Sigma_T N_{vac} N_H - \Sigma_d N_{CH} - \Sigma_T^* N_{CH} N_H \quad (3)$$

$$\frac{dN_{CH_x}}{dt} = \Sigma_T^* N_{CH} N_H \equiv J_{C_xH_y}/x_R \quad (4)$$

Trapping rate coefficients

$$\Sigma_T = 4\pi R_T D = (\Sigma_T)_0 \exp(-\frac{E_T}{RT}) \quad (5)$$

$$\Sigma_T^* = (\Sigma_T)_0 \exp(-\frac{E_T + E^*}{RT}) \quad (6)$$

SOLVING DIFFERENTIAL EQUATIONS

1. Addition of eqs. (2), (3) and (4)

$$\frac{d}{dt}[N_{vac} + N_{CH} + N_{CH_x}] = 0$$

$$N_{vac} + N_{CH} + N_{CH_x} = N_T^0 \quad (7)$$

2. Estimation of N_H from experiment

$$N_H = \frac{J_{C_xH_y}/x_R}{\Sigma_T^* N_{CH}} \quad (8)$$

3. Rewriting eq.(3)

$$\frac{dN_{CH}}{dt} = \Sigma_T(N_T^0 - N_{CH} - N_{CH_x})\frac{J_{C_xH_y}/x_R}{\Sigma_T^* N_{CH}} - (\Sigma_d N_{CH} + \frac{J_{C_xH_y}}{x_R}) \quad (9)$$

where

$$N_{CH_x} = \int_0^t \frac{J_{C_xH_y}}{x_R}\, dt \quad (10)$$

4. Determination of K_R.

$$J_{H_2} = \frac{K_R}{x_R} N_H^2 \quad (11)$$

RELATION WITH HYDROGEN RELEASE MODELS

- If hydrocarbon formation is negligible,

$$\frac{J_{C_xH_y}}{x_R} = \Sigma_T^* N_{CH} N_H \to 0 \qquad (12)$$

then,

$$\frac{dN_H}{dt} = -\Sigma_T(N_T^0 - N_{CH})N_H + \Sigma_d N_{CH} - 2K_R N_H^2 \qquad (13)$$

$$\frac{dN_{CH}}{dt} = \Sigma_T(N_T^0 - N_{CH})N_H - \Sigma_d N_{CH} \qquad (14)$$

- Eqs. (13) and (14) can be compared to the models of Morita et al. [1] and Brice [2].

REFERENCES

[1] K. Morita et al., J. Nucl. Mater. 162-164 (1989) 990.
[2] D. K. Brice, Nucl. Instr. Meth. B44 (1990) 302.

CALCULATIONS

- Assumption for Σ_T^*
  1. $\Sigma_T^* = \Sigma_T$; that is, $E^* = 0\,\mathrm{kJ/mol}$
  2. $E^* = 19.3\,\mathrm{kJ/mol}$

- Data employed in the calculation
  1. $D/\mathrm{m^2\,s^{-1}} = 1.1 \times 10^{-17} \exp(-\frac{19.3}{RT})$
  2. $\Sigma_d/\mathrm{s^{-1}} = 1.2 \times 10^{-1} \exp(-\frac{38.6}{RT})$
  3. $x_R/\mathrm{m} = 5.0 \times 10^{-8}$
  4. $N_T^0/\mathrm{m^{-3}} = 4.0 \times 10^{28}$
  5. $R_T/\mathrm{m} = 1 \times 10^{-10}$

  where activation energies are expressed by kJ/mol.

SUMMARY

- An attempt was made to model hydrocarbon release from hydrogen- implanted graphite.
  1. The present model incorporates such important transport processes as diffusion, trapping, detrapping, recombination, etc.
  2. According to the model, the following desorption mechanisms are assumed.
     (a) hydrogen → recombination of two mobile hydrogen (K_R).
     (b) hydrocarbon → continuous trapping of hydrogen and dissociation of C-C bond (Σ_T^*).
  3. Experimental results allow to estimate the rate constants corresponding to the above processes. However, one set of desorption spectra of hydrogen and hydrocarbon is insufficient to determine these constants uniquely.
- Application to B-doped graphite requires close examination of hydrogen-graphite systems; B-doping should have simultaneous effects on trapping, detrapping and recombination.

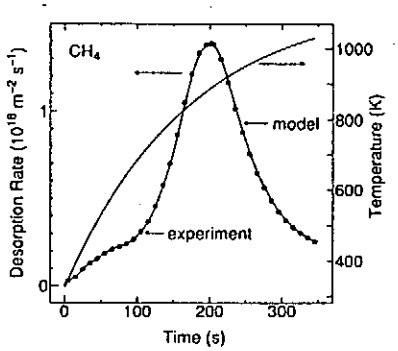

Fig. Confirmation of the calculation. Desorption spectrum of methane (CH_4) is reproduced by the model.

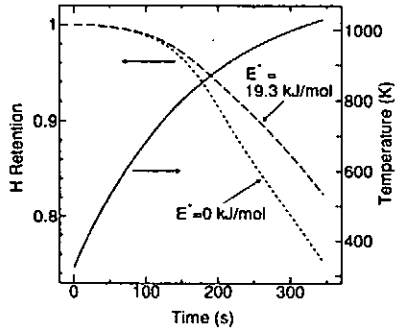

Fig. Effect of activation energy, E^*, on the retained fraction, N_{CH}/N_T^*, of H.

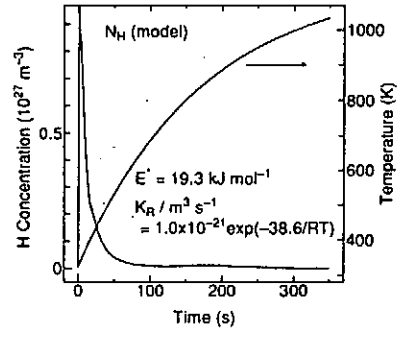

Fig. H concentration (N_H) profile predicted by the model.

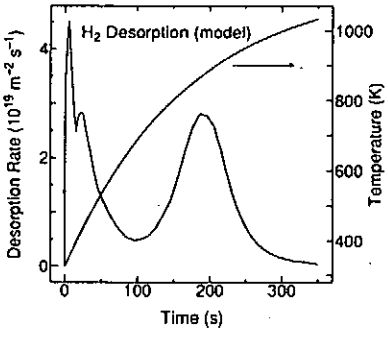

Fig. Hydrogen (H_2) desorption curve predicted by the model. The rate constants are same as those used in the previous figure.

Hydrogen Retention in Graphite
- Correlation with the Structure -

Hisao ASUMI*, Michio ISEKI** and Tatsuo SHIKAMA***

* Department of Nuclear Reactor Engineering, Kinki University, Kowakae 3-4-1, Higashi-Osaka, Osaka 577, Japan
** Department of Nuclear Engineering, Nagoya University, Furo-cho, Chikusa-ku, Nagoya 464-01, Japan
*** The Oarai Branch, Institute for Materials Research, Tohoku University, Naritacho, Oaraimachi, Higashi-ibarakigun, Ibaraki 311-13, Japan

In order to obtain fundamental information on hydrogen recycling process in fusion reactor environment, hydrogen absorption experiments have been performed on various graphite materials (thirteen isotropic graphites and two CFCs).

X-ray powder diffraction study was performed as a characterization of the samples, and the correlation with hydrogen retention in graphite has been discussed. The degrees of graphitization determined for the samples were in the range of 49-77%. CFC materials (PCC-2S and CX-2002U) had higher values.

Hydrogen solubilities are significantly different among samples, whose maximum is approximately 16 times. A strong correlation could be observed between hydrogen solubilities and the degrees of graphitization. The higher degree of graphitization appears to make hydrogen solubilities become lower.

After neutron irradiation up to 5.4×10^{20} n/cm^2, the hydrogen solubilities became 20-50 times larger those for unirradiated samples. The increase of hydrogen solubility was saturated above the damage level of ~ 0.3 dpa. These behavior of hydrogen solubility also correlated to the changes of the degrees of graphitization. These results suggest that the hydrogen atoms are trapped at defects in graphite.

Experimental

Samples (15 brands)

IG-110U, IG-430U, ISO-630U
ISO-880U, CX-2002U*(Toyo Tanso, Japan)
T-4MP, T-6P, ETP-10 (Ibiden, Japan)
PD-330S, PCC-2S*(Hitachi Chem., Japan)
EK-47, EK-98 (Ringsdorf, Germany)
AXF-5Q1 (POCO Graphite, U.S.A.)
ATJ (Union Carbide, U.S.A.)
CL-5890PT (Le Carbone, France)
*CFC

Solubility measurement

Determine the pressure change with Baratron manometer

Temperature: 700-1050℃ (mainly 1000℃)
Pressure : ~10 kPa
Time : 6-40 hours

Degree of graphitization

X-ray powder diffraction study
Measurement of lattice spacing d_{002}
Degree of graphitization=1-p
$d_{002}=3.440-0.086(1-p^2)$

Neutron irradiation

JMTR
Temperature: 200℃
Fluence :
~5.4×10^{20}n/cm^2

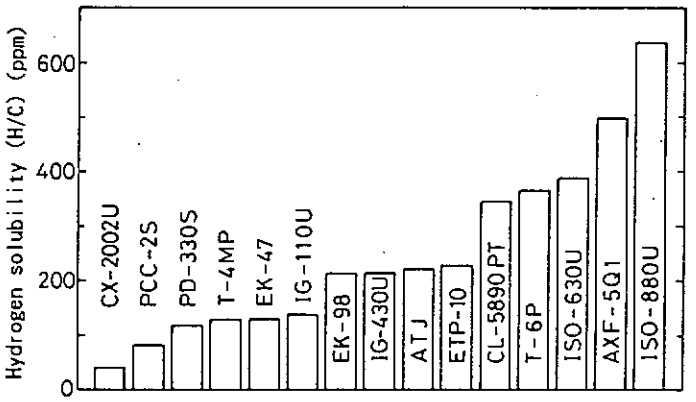

Fig. 1 Hydrogen solubilities in graphite samples.

Hydrogen Retention in Graphite

-Correlation with the Structure-

H. ATSUMI : Department of Nuclear Reactor Engineering, Kinki University
M. ISEKI : Department of Nuclear Engineering, Nagoya University
T. SHIKAMA: Institute of Materials Research, Tohoku University

Hydrogen Recycling on Graphite

1. Mechanisms

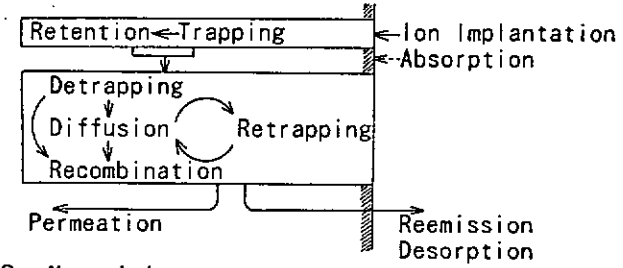

2. Material
   Graphite—Behavior is varied among brands
   Requirement of Characterization
3. Items of Determination
   Hydrogen absorption, Dissolution,
   Diffusion, Irradiation effects

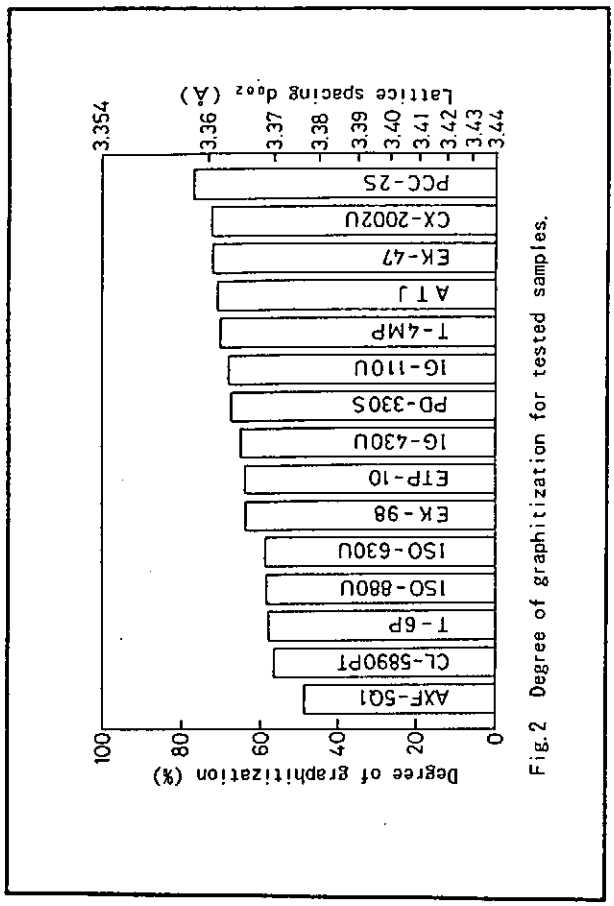

Fig. 2 Degree of graphitization for tested samples.

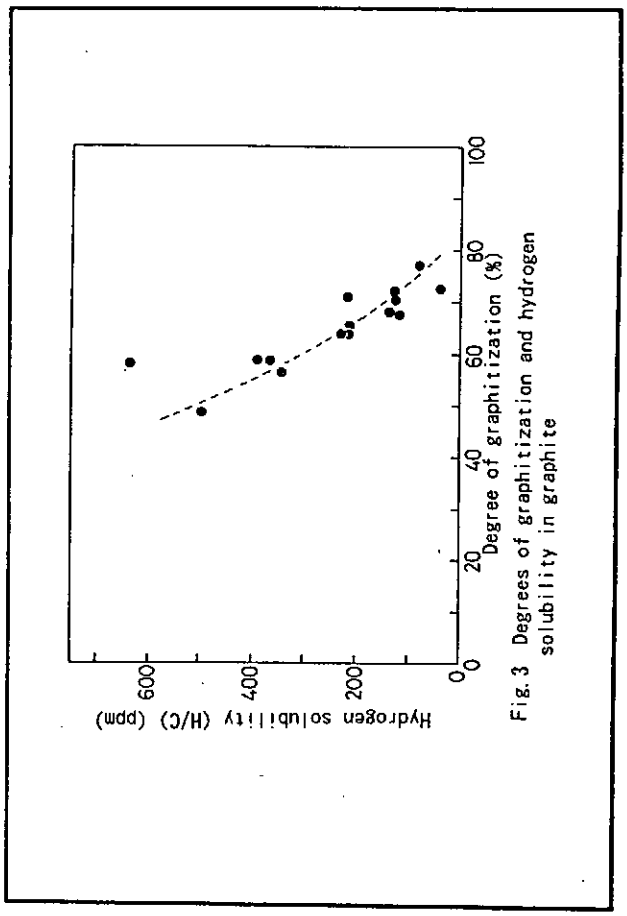

Fig. 3 Degrees of graphitization and hydrogen solubility in graphite

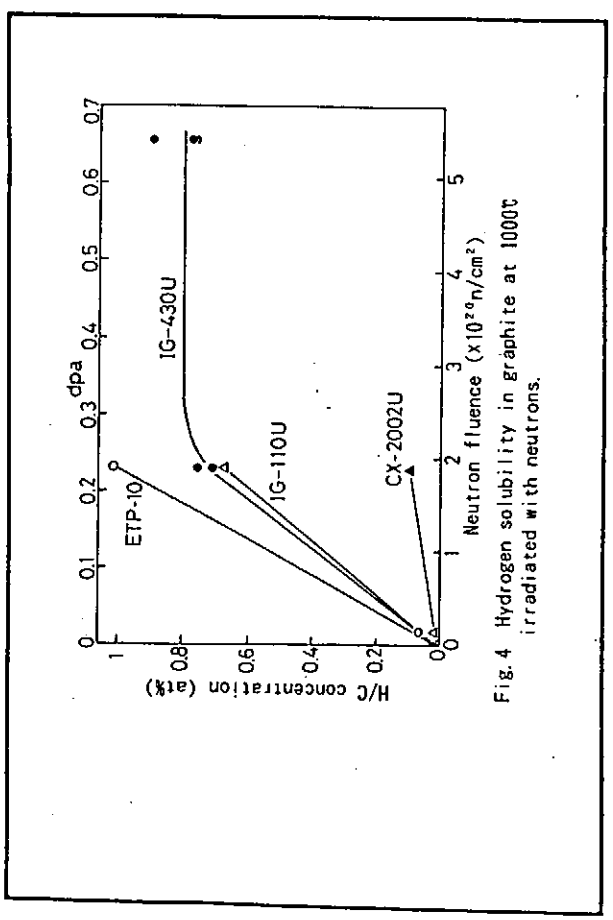

Fig. 4 Hydrogen solubility in graphite at 1000℃ irradiated with neutrons.

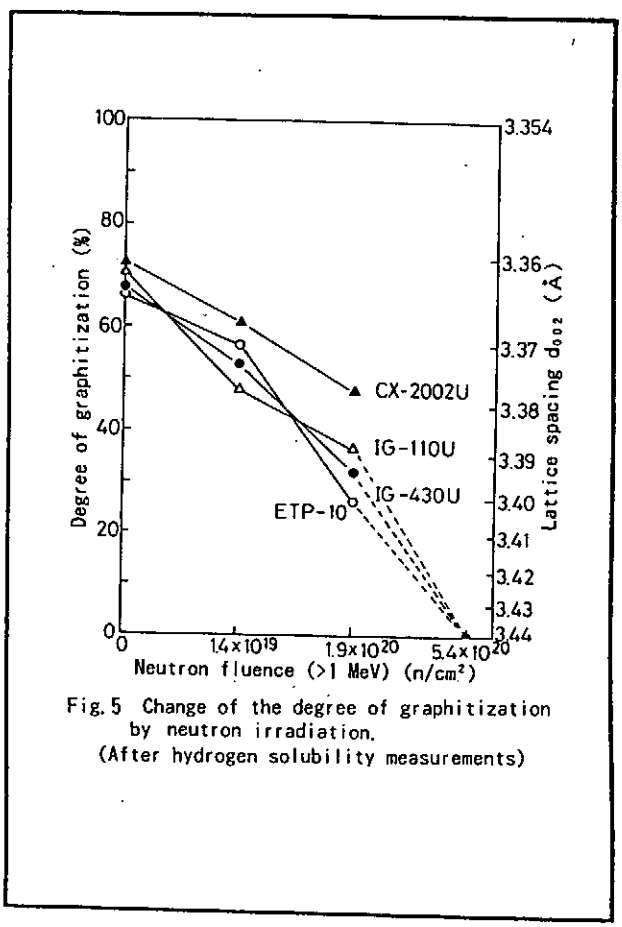

Fig. 5 Change of the degree of graphitization by neutron irradiation.
(After hydrogen solubility measurements)

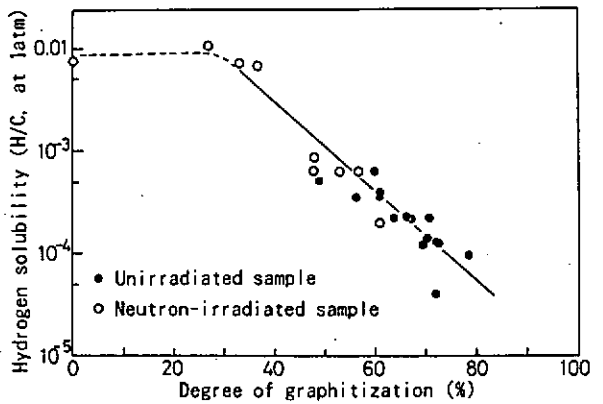

Fig. 6 Correlation between the degrees of graphitization and hydrogen solubility in graphite.

Conclusions

1. Strong correlation between hydrogen solubilties and the degrees of graphitization
   Higher degree of graphitization
   → Lower hydrogen solubility
2. Neutron irradiation effects
   ①Hydrogen solubility : 50 times
   Radiation defects → Lower degree of graphitization → Higher hydrogen solubility
   ②Hydrogen solublity ⇔ Degree of graphitization
   (CFC gave only a little change in the degree of graphitization → 22 times of increase)

D_2/CD_4-TDS of Sputter B/C-Film

Hitachi Research Laboratory, Hitachi Ltd.,
Y. GOTOH, T. YAMAKI

Boron, of the lower-Z number than carbon, is now expected to be an useful element for plasma facing material. It has recently been revealed that addition of small amount of boron into graphite effects drastic suppression of chemical sputtering. Boronization experiments in real tokamaks, on the other hand, showed both considerable reduction of oxygen impurity in the core plasma and improvement of H/D recycling properties of the wall.

In the present thermal desorption spectroscopy(TDS), effects of boron addition on the D_2/CD_4-thermal desorption characteristics of carbon(graphite) are investigated. The TDS are made in a 400-1300K range at an 1 K/s temperature ramp rate, on sputter B/C-films of B-concentration from 0 to 74 at% after irradiation of 1keV D (3keV D_3^+) to 2×10^{17} D/cm^2 at 473K.

Three peaks, a broad peak at around 1050K and the narrower peaks centered at 850K and 650K, are identified in the D_2-TDS of the B/C films. Only an 1050K peak is observed in the 400-1300K range for graphite(B:0%). As the B concentration is increased from 0 to 3%, the 850K peak increases in intensity, while the 1050K peak decreases. With further increasing the B concentration over 23% to 74%, the 650K peak starts increasing, while the 850K peak decreases. On the other hand, a CD_4-TDS peak, located at 800-900K, is observed to decrease with increasing the B concentration.

The B/C films are assumed to be graphite(with substitutional B) + B_4C phase. The observed 1050K peak is attributable mainly to D-detrapping from C-D in graphite, while the 850K peak to detrapping from C-D in B-neighborhood, and the 650K peak to B-D detrapping.

D_2/CD_4-TDS of B/C Sputter Film

Hitachi Research Laboratory,
Hitachi Ltd.,

Y. GOTOH, T. YAMAKI

[Background]

Boron addition to carbon

- Suppressing chemical sputtering
- Improving D-recycling properties (Oxygen gettering)

[Aim]

Elucidation of B effects on D_2/CD_4 thermal desorption

- D_2/CD_4-TDS (400K-1300K)
- Sputter B/C-films(B=0-74at%)

[Test Samples]

B/C Sputter Film/isographite

Thickness : 0.5-2 μm
B :0, 3, 6, 23, 74 at%
(0 :less than 3 at%)
Heat treatment at 1300K

Reference material : CVD-B_4C
B : 59%

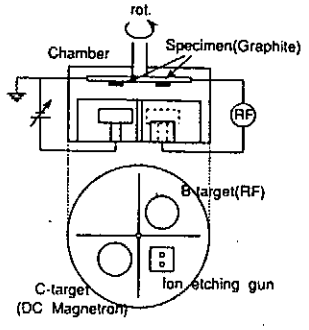

Fig. Sputtering apparatus

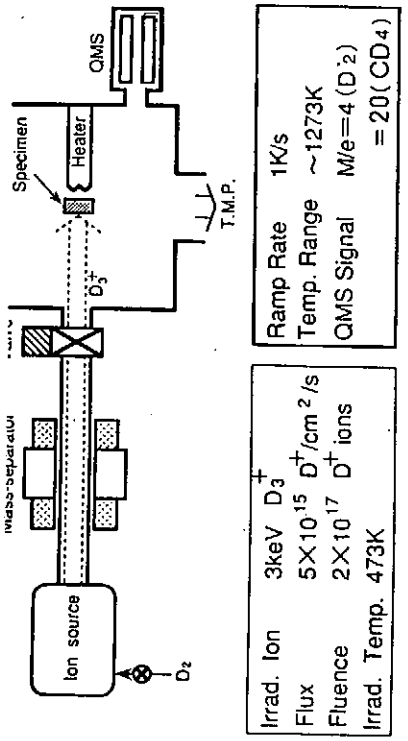

Ramp Rate	1K/s
Temp. Range	~1273K
QMS Signal	M/e=4 (D_2)
	=20(CD_4)

Irrad. Ion	3keV D_3^+
Flux	5×10^{15} $D^+/cm^2/s$
Fluence	2×10^{17} D^+ ions
Irrad. Temp.	473K

Fig. Schematic Diagram of TDS Apparatus and Experimental Conditions

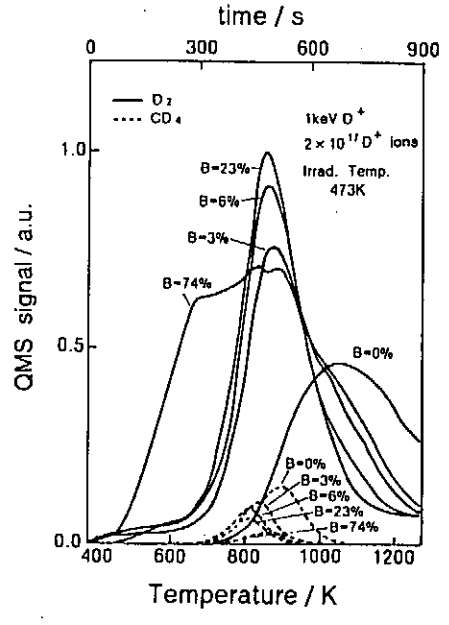

Fig. D_2- and CD_4-TDS of B/C-Sputter Film

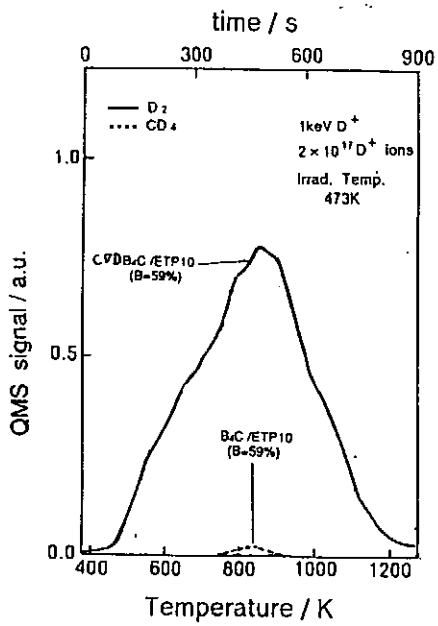

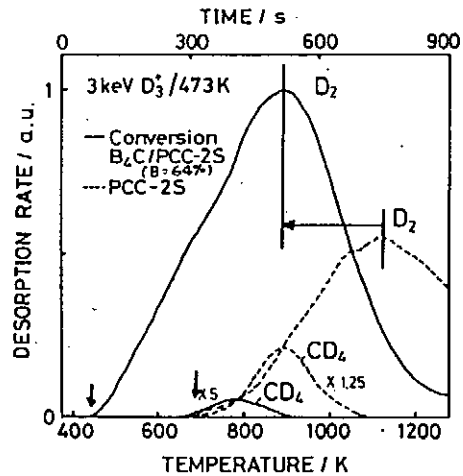

Fig.3 D_2-TDS and CD_4-TDS spectra from conversion-B_4C/PCC-2S and bare PCC-2S with a linear temperature ramp rate at 1K/s, after irradiation of 1keV D^+ to 2×10^{17}D/cm² at 473K.

Conclusion

1. Three D_2-TDS peaks were found for the B/C films, a broad 1050K peak, narrow 850K and 650K peaks.

2. For graphite(B:0%), only 1050K peak was found in 400-1300K range.

3. As the B/C ratio was increased, the lower temperature peak increased in intensity.

4. The 1050K peak is due to D-detrapping from C-D in graphite, the 850K peak to C-D in B neighbor, and the 650K peak to B-D in the B neighbors.

5. CD_4-TDS peak, at 800-900K, was observed to decrease with increasing the B concentration.

JPN-US Workshop P196 11/17-19,1992 Kyushu University

PFC and PSI Studies in Hokkaido University

Tomoaki Hino and T.Yamashina
Department of Nuclear Engineering, Hokkaido University
Kita-13,Nishi-8,Kita-ku,Sapporo,060 Japan

Recent studies on plasma facing components and plasma surface interactions are introduced. In the fiscal year of 1992, we have the following researches;

(1) Erosion yield measurements of boron mixed graphites and vanadium mixed graphites using ECR hydrogen ion source

(2) Boronization experiments using surface modification test stand (SUT) of NIFS, Toki-site

(3) Water desorption from graphite dipped in water

(4) Heat load experiments for boron mixed graphite using active cooling test facility of NIFS, Toki-site

The items (2) and (3) have been carried out by the collaborations with NIFS and Toyo Tanso.

In the followings, major results are described in the vu-graphs.

11/18/92
5-2 12)

PFC and PSI Studies in Hokkaido Univ.

T. Hino and T. Yamashina

Fusion Studies in 1992

1. Erosion Yields of B, V Mixed Graphites
2. Boronization Experiments Using SUT of NIFS
   with NIFS, Toyo Tanso
3. H_2O Desorption from Graphite
4. Heat Load Experiments for B Mixed Graphite Using ACT of NIFS
   with NIFS, Toyo Tanso

Hino-1

1. Erosion Yields of B and V Mixed Graphites due to Hydrogen Ions

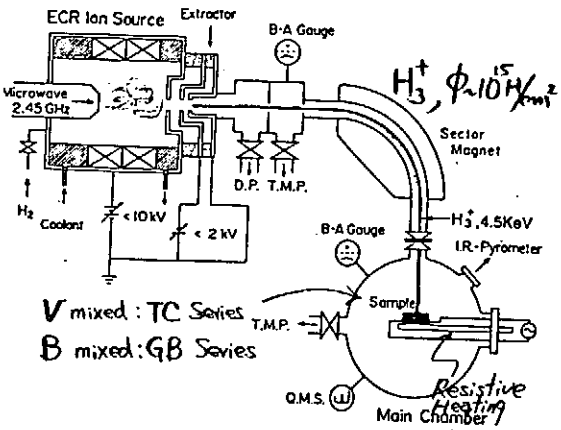

V mixed : TC Series
B mixed : GB Series

Yield → Weight Loss

Hino-2

VANADIUM MIXED GRAPHITE 17th SOFT '92

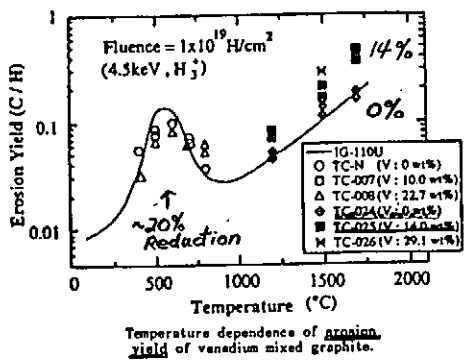

Temperature dependence of erosion yield of vanadium mixed graphite.

Vanadium evaporation rate.

Temp.(°C) \ V Conc.(wt%)	Vanadium Evaporation Rate Per Day (%/Day)	
	14.0	29.1
1200	0.73	—
1500	5.12	5.06
1700	13.82	—

Hino-3

BORON MIXED GRAPHITE 10th PSI '92

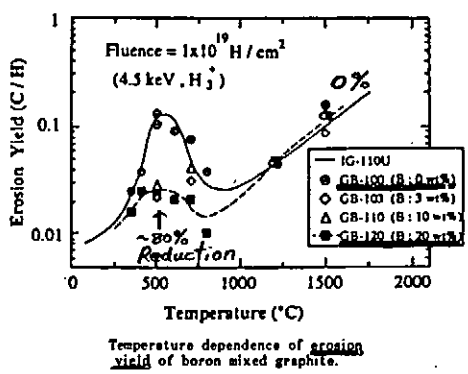

Temperature dependence of erosion yield of boron mixed graphite.

Boron evaporation rate

Temp.(°C) \ B Conc.(wt%)	Boron Evaporation Rate Per Day (%/Day)			
	1	3	10	20
1200	—	1.03	—	0.29
1500	2.14	7.45	2.84	2.13

Hino-4

2. Boronization Experiments Using SUT of NIFS

(H.U.) K. Iwamoto, I. Fujita, T. Hino, T. Yamashina
(NIFS) Y. Kubota, N. Noda, A. Sagara, O. Motojima
(T.T.) T. Matsuda, T. Sogabe, K. Kuroda

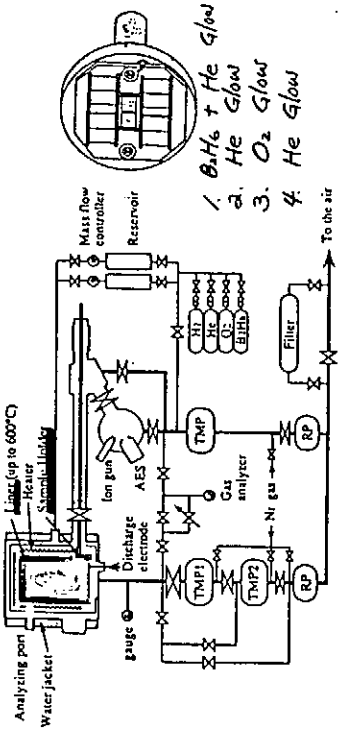

Hino-

XPS

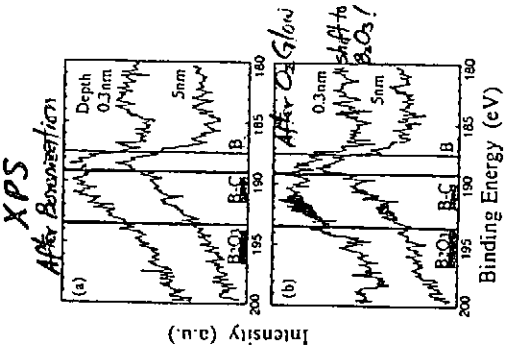

AES

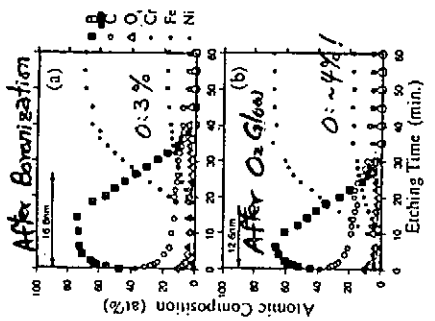

Hino-6

3. H_2O Desorption from Graphite

M. Okita, Y. Hirohata, T. Hino, T. Yamashina

IG 110U : Prebaked at 1000°C, 30 min
(10×10×1 mm) dipped in water, 2-3 days
baking at 120°C, 12 hrs

TDS : RT → 1000 °C

↓

Activation Energy

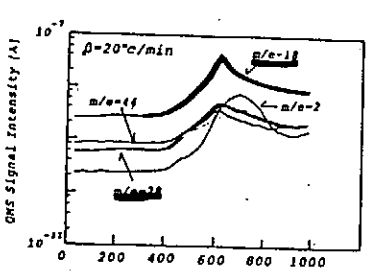

Hino-7

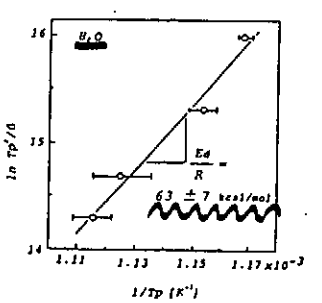

	H_2O	CO	CO_2	H_2
E_d (kcal/mol)	63	49	43	23
文献値		64-83	21-51	

Chemical Adsorption
-H & -OH

Hino-8

4. Heat Load Experiments for B Mixed Graphite Using ACT of NIFS

(JAERI I. Fujita, T. Hino, T. Yamashina
NIFS Y. Kubota, N. Noda, A. Sagara,
O. Motojima
T.T. T. Matsuda, T. Sogabe, K. Kuroda

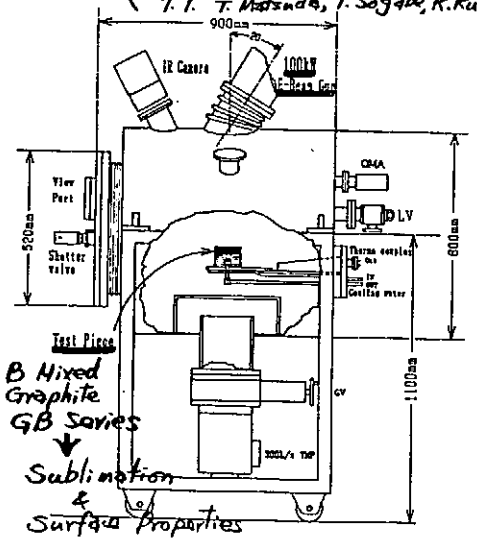

Active Cooling Test Facility

Hino-9

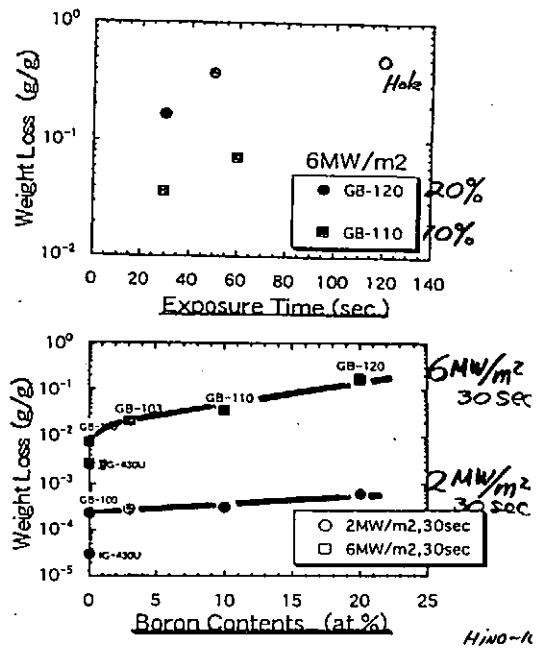

Hino-11

HYDROGEN ISOTOPE RETENTION FOR CFC, ISOTROPIC GRAPHITE AND CARBON CONTAINED COPPER MATERIALS

S. Amemiya, M. Natsir, T. Masuda and Y. Tsurita

Department of Nuclear Engineering, University of Nagoya, Furocho chikusaku, Nagoya, Japan

Abstract

The retention of deuterium in carbon fiber composites(CFC), Isotropic graphite(ISO) and carbon contained copper materials were measured at room temperature as a function of fluences from 2.2×10^{16} up to 2.2×10^{18} D/cm^2 for 200 eV incident energies. The measurement of retained deuterium was carried out by using D(^{3}He,p)^{4}He nuclear reaction analysis technique(NRA). The experimental results have showed that the retention grade of carbon fiber composites is higher if compared with isotropic graphite, which is the retention ratio of CFC/ISO is 1.3 as shown in figure. 1.
This curve is comparable to the curve 300 eV measured for deuterium irradiated in carbon.[1] For fluences less than 2.2×10^{16} all the incident fluences has been retained, at higher fluences the indication of saturation observed. And also shown in fig.2 are depth profiles resulted on both carbon materials.

Fig. 1. Deuterium retention on isotropic graphite & carbon-fiber-composites

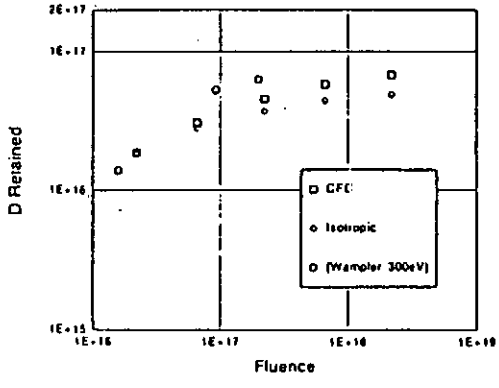

The retention of deuterium on copper containing carbon materials are lower than carbon material. Three kinds of composition of copper containing carbon were used here. Since the carbon atom larger than copper atom on the surface, they induced a deuterium retention on surface higher. The concentration of carbon highly affect the deuterium retention in copper containing carbon materials.

Fig. 2. Depth profile of deuterium (2.2×10^{18} D atoms/cm^2 Irradiated)

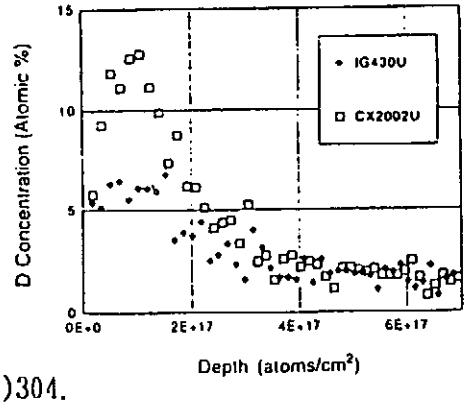

(1)W.R. Wampler, et all, J. Nucl. Mater.102(1981)304.

HYDROGEN ISOTOPE RETENTION FOR CFC, ISOTROPIC GRAPHITE AND CARBON CONTAINED COPPER MATERIAL

S. Amemiya, M. Natsir, T. Masuda and Y. Tsurita

DEPARTMENT OF NUCLEAR ENGINEERING, NAGOYA UNIVERSITY, FUROCHO-CHIKUSAKU NAGOYA JAPAN

PURPOSE :

-TO DETERMINE THE RETENTION OF DEUTERIUM IN CFC, ISOTROPIC GRAPHITE AND COPPER CONTAINED CARBON MATERIAL

-TO COMPARE THE DEUTERIUM RETENTION GRADE OF CFC AND ISO.

➡CARBON FIBER COMPOSITES(CFC) AS WELL AS ISOTROPIC GRAPHITE IS NOW IN A GREAT NUMBER USED FOR PLASMA FACING MATERIAL.

➡RECYCLING PROBLEM, THE HYDROGEN RECYCLING IS ENHANCED BY THE HYDROGEN RETAINED IN PLASMA FACING MATERIAL.

➡DATA ABOUT THE INTERACTION OF DEUTERIUM UPON CFC MATERIAL STILL RARE.

THEREFORE, IN THIS STUDY WERE CARRIED OUT THE MEASUREMENT OF DEUTERIUM RETENTION ON CFC AND ISO GRAPHITE.

ALSO, ON COPPER CONTAINING CARBON AS ALTERNATIVE MATERIAL IN A LARGE DEVICES.

EXPERIMENT

THE SAMPLES WERE PREPARED ARE AS FOLLOW

- CARBON FIBER COMPOSITES;
  - -CX2002U
  - -CC312 SIZES: 2X2 cm, THICKNESS 2 mm
- ISOTROPIC GRAPHITE
  - -IG110U
  - -IG430U SIZES: 2X2 cm THICKNESS 2 mm
  - -ETP10

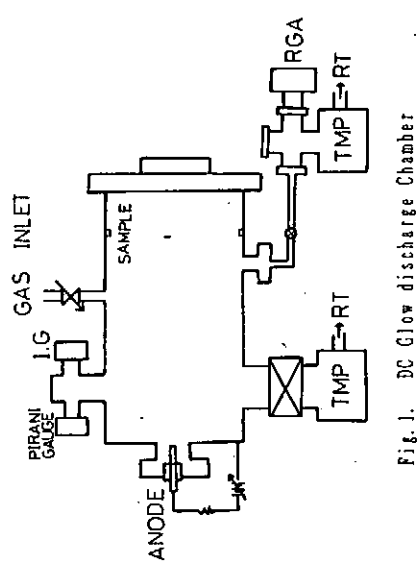

Fig. 1. DC Glow discharge Chamber

Deuterium Retained Monitor

-The amount of deuterium retained in samples was monitored using ;
D(^{3}He, p)^{4}He nuclear reaction.

-Accelerator Van de Graaff
^{3}He Energy 800 keV
Detected (alpha particles)

5

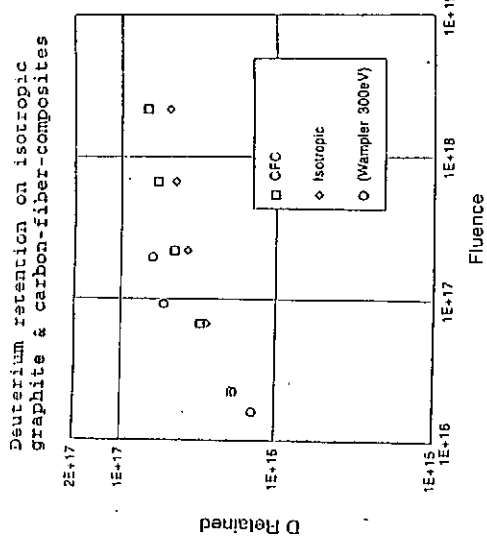

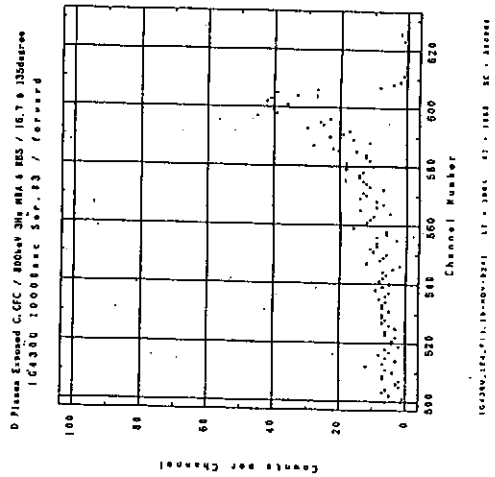

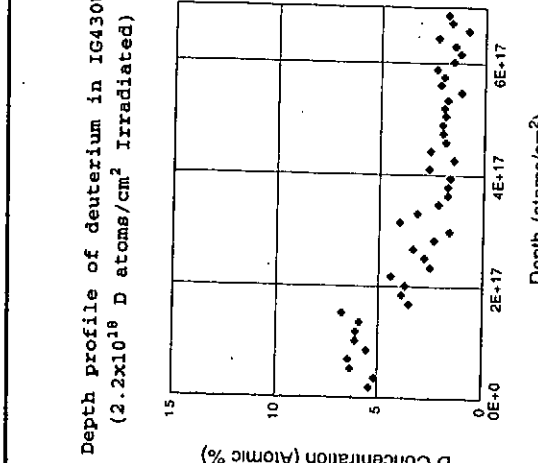

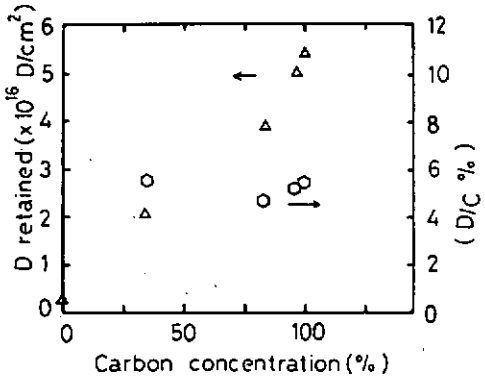

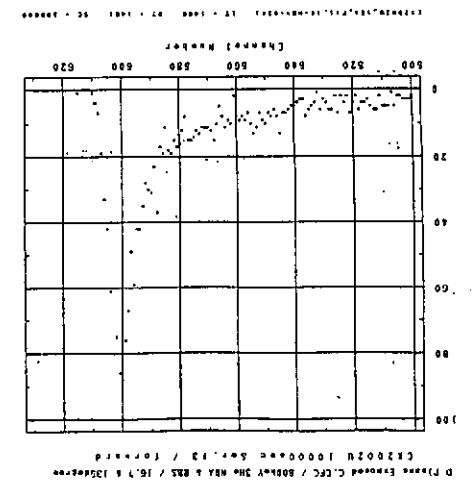

Depth profile of deuterium in CX2002
(2.2×10^{18} D atoms/cm^2 Irradiated)

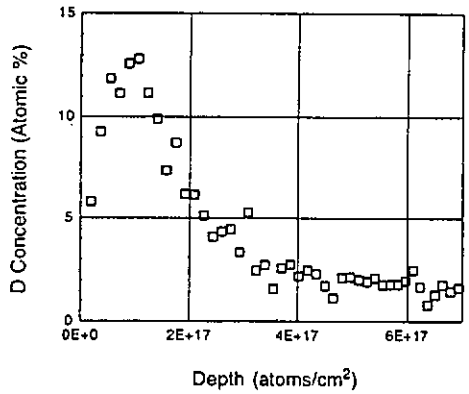

Deuterium retention on Cu-C Mareria1
exposed in DC discharge plasma

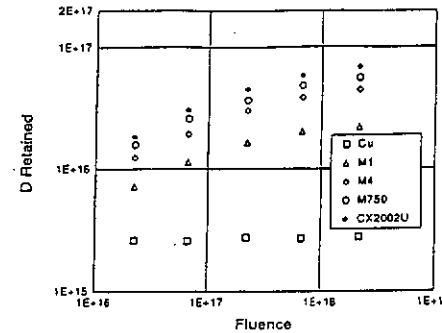

Retention of deuterium irradiated in copper contained carbon material with diffrences concention of carbon at 200 eV.

CONCLUSION

-THE SATURATION BEHAVIOR WAS THE SAME FOR TWO DIFFERENT KINDS OF CARBON ; CFC AND ISO GRAPHITE.

-THE RETENTION GRADE OF CFC IS HIGHER THAN ISOTROPIC GRAPHITE, WHICH IS THE RETENTION RATIO OF CFC/ISO IS 1.32

-THE CONCENTRATION OF CARBON HIGHLY AFFECT THE DEUTERIUM RETENTION IN COPPER CONTAINING CARBON MATERIAL.

Session 5: Tritium Inventory and Handling

TRITIUM INVENTORY IN BERYLLIUM

K. L. WILSON
SANDIA NATIONAL LABORATORIES
LIVERMORE CA 94550 USA

JAPAN - US WORKSHOP P196
KYUSHU UNIVERSITY
NOVEMBER 17-19, 1992

TOPICS

- Introduction
- Diffusivity and Solubility
- Molecular Recombination Constant
- Trapping
  - Ion Beam Experiments
  - JET PFCs
  - Neutron Damage
- Retention Modelling
- Outgassing
- Steam Reactions

Unlike Graphite, Redeposited Beryllium Does Not Co-Deposit with Tritium

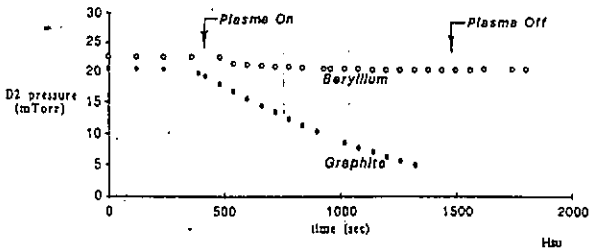

This observation has important implications for both fuel recycling and in-vessel tritium inventory

The database from 1965 to 1985 was simple, and probably totally wrong

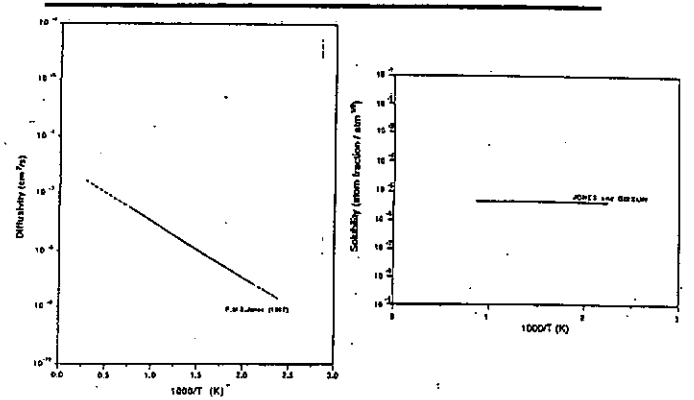

In many ways, beryllium is the ideal plasma facing material

- Very low atomic number
- Excellent thermal properties
- Reasonable mechanical properties
- Acceptable sputtering characteristics
- Low tritium affinity

Plasma driven permeation depends strongly on the surface oxide layer

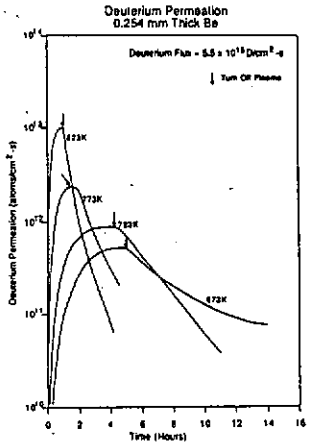

Permeation Results

Post-irradiation examination of the permeation membranes showed them to have an oxide layer 0.4 μm thick on the back, and a layer of beryllium oxide and carbide 0.9 μm thick on the plasma-facing side. Part of these layers may have formed during heating after the plasma was turned off.

The magnitude of the deuterium permeation through the beryllium membranes did not scale with the membrane thickness. In all cases, the permeation was higher for the higher temperatures. The magnitude of the permeation was likely controlled by a combination of factors including recombination at both surfaces, diffusion through the surface layers, and diffusion through the beryllium metal.

The logarithm of the release rate after the plasma was turned off decreased linearly with time for all of the experiments. At each of the different temperatures, the slopes of the logarithm of release rates did not change with sample thickness. This can only be explained by assuming that all of the deuterium released after the plasma was terminated came from the oxide layer on the rear of the sample.

The database for hydrogen diffusion in beryllium is meager

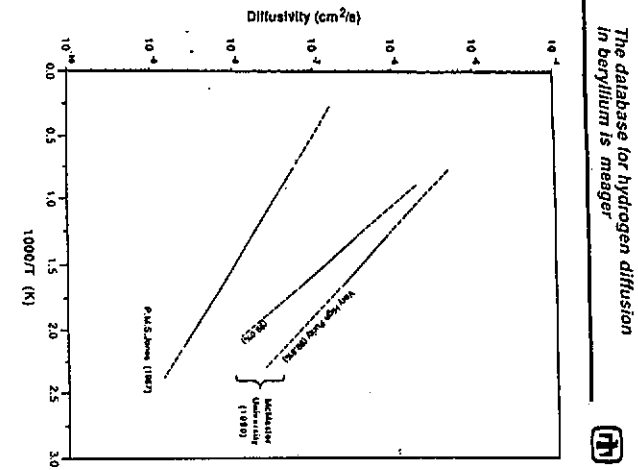

Surface effects also play a strong role in hydrogen release kinetics from beryllium

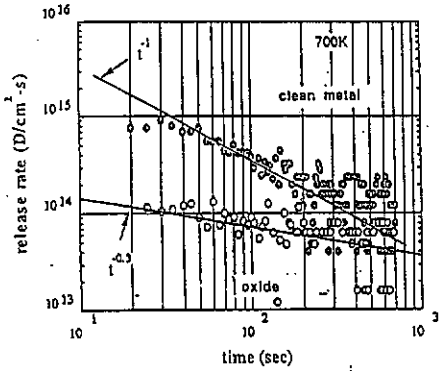

A controversy exists for the hydrogen solubility in beryllium

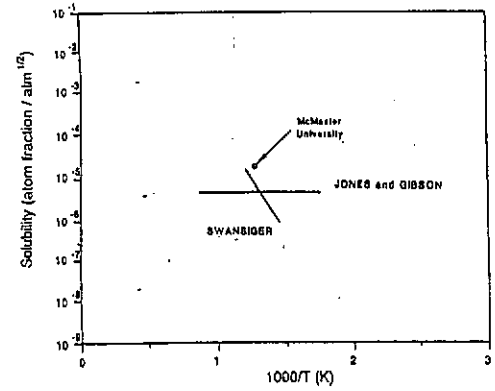

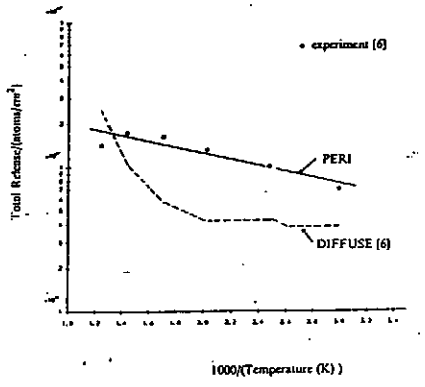

5. The total release of deuterium as measured (·) and calculated (----) by Hsu et al [6]. Solid line is the result of the present interpretation using either of the least squares fits in Fig.4 together with the lower curve in Fig.3.

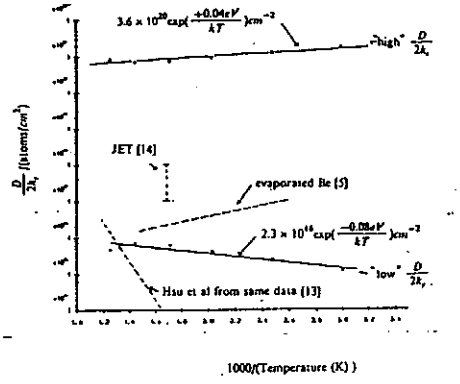

4. Pumping parameter for deuterium/beryllium versus reciprocal temperature. Open circles represent values taken from the lower curve in Fig.3 given the release/fluence measurements of Hsu et al [6]. Solid lines represent least squares fits to the above, while dashed lines show several values taken from the literature.

Beryllium is Often Said to Have Less Tritium Trapping Than Graphite

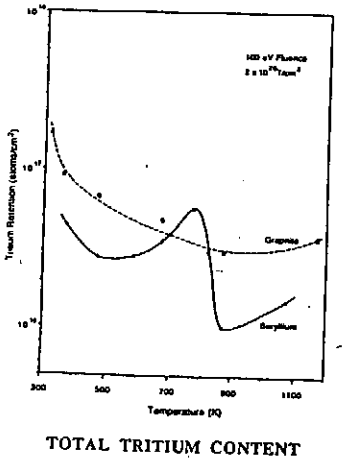

- The saturated layer of beryllium is one-half the tritium concentration of graphite at room temperature
- This near surface retention decreases more rapidly with temperature for beryllium than graphite
- However, the <u>total</u> tritium retention of beryllium can exceed that of graphite under certain conditions

TOTAL TRITIUM CONTENT

Tritium retention in beryllium shows a complex temperature dependence

Tritium retention is measured in TPX and modelled with DIFFUSE

A strong increase in bulk retention occurs above 700K

We postulate that the rapid decrease above 800K is due to the loss of the protective oxide coating, which had been acting as a barrier to tritium recombination

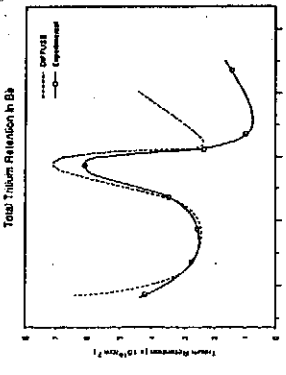

EXPERIMENTAL METHOD

- D and He or H are implanted into Be to different depths. D is trapped at defects created during the implantation.
- Internal redistribution to traps at different depths, and release of D is monitored by nuclear reaction analysis while the sample temperature is increased.
- Activation energy Q for detrapping is determined from a model for H diffusion with trapping.

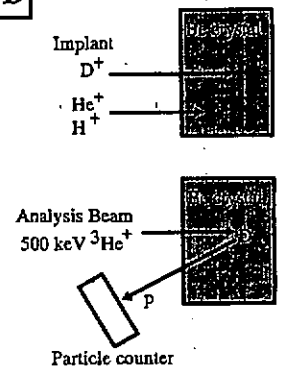

Trapped deuterium exhibits two distinct release stages from beryllium

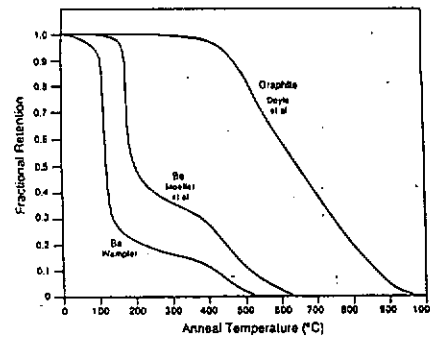

- Two traps are observed
  - a hydride-like phase (0.3 D/Be) with a 1.0 eV detrapping energy
  - Point defect trapping (< 0.05 D/Be) with a 1.8 eV detrapping energy
- Hydrogen is trapped far more strongly in graphite

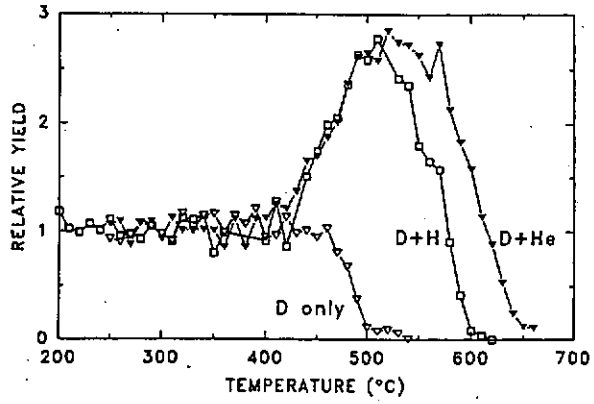

High dose H and He implants form bubbles which collect D when it is detrapped at about 470°C.

PLASMA-BERYLLIUM INTERACTIONS

W. R. Wampler
Sandia National Laboratories
Albuquerque, NM

RELEASE BY PERMEATION FROM GAS IN BUBBLES

Permeability $\Gamma = \Phi R/P^{1/2} = NDS$

PERMEATION OF D FROM BUBBLES

- Bubbles formed by high dose H and He implants accumulate D released from defect traps.
- D gas is released from bubbles by permeation through the Be to the external surface.
- D release rate $\Phi = 10^{12}/cm^2$ s at 600°C.

  Permeability $\Gamma = \Phi R/P^{1/2} = 2x10^{5}$ D/(cm s $atm^{1/2}$)
- Permeability predicted from published solubility S and diffusivity D is much larger.

  Permeability $\Gamma = NDS = 4x10^{12}$ D/(cm s $atm^{1/2}$) at 600°C.

RELEASE OF DEUTERIUM FROM Be

1. Hydrogen is strongly trapped at lattice damage and helium bubbles in Be.
2. Hydrogen is released from bubbles by permeation.
3. Permeation rate from the bubbles is 10^7 times smaller than predicted from published solubility and diffusivity.
4. Effects of damage and He from neutron irradiation on properties of H in Be need better characterization.

Outgassing efficiency as a function of temperature for beryllium samples in air and in argon.

A.T. Peacock[1], J. P. Coad[1], K.J. Dietz[1], A.P. Knight[2]
[1]JET Joint Undertaking, Abingdon, Oxfordshire OX14 3EA, UK
[2]Winfrith Atomic Energy Establishment, Dorchester, Dorset DT2 8DH, U.K.

TRITIUM MONITOR

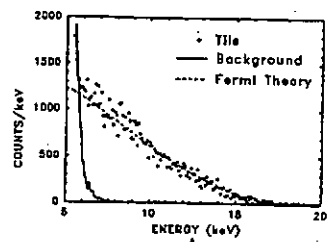

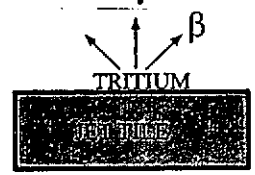

The range of tritium betas in carbon is ~1 micron

We are studying beryllium from JET's DT run

SANDIA NATIONAL LABORATORIES

- Tritium Dissolution Counting — Total tritium
- Beta Detector Scans — Near surface tritium
- SIMS — Tritium depth profiles
- Nuclear Reaction Analysis — Tritium depth profiles
- Scanning Electron Microscopy — Morphology
- Auger Electron Spectroscopy — Composition

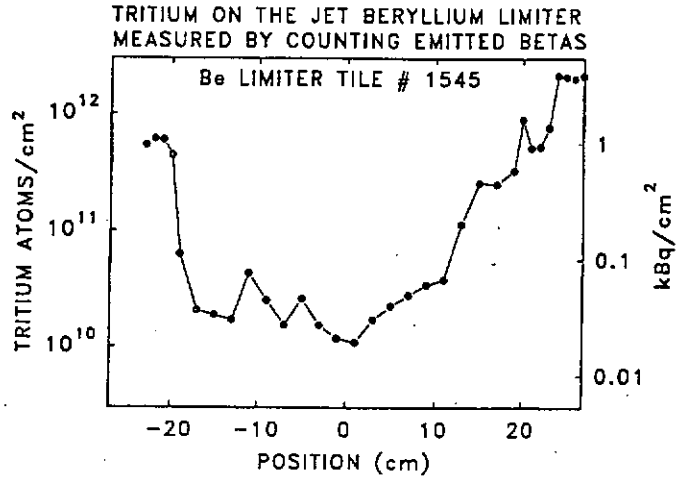

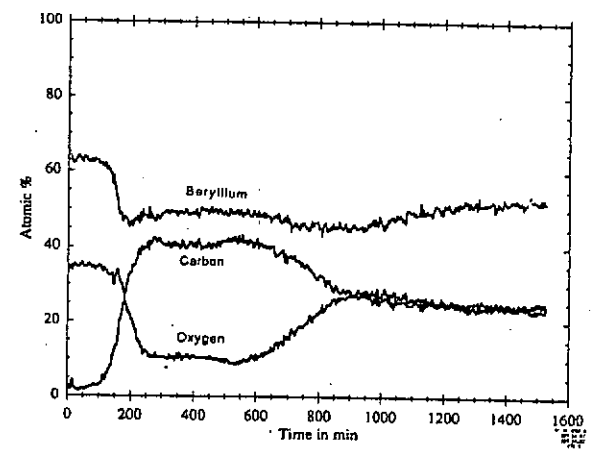

SENT BY:Dewar Level 5115 11-17-92 ; 8:16PM ; Sandia Natl. Labs.-

Tritium in the JET Be Divertor tile #SC42

Activity in units of kBq/cm^2

1 kBq/cm^2 = 5.6 x 10^{11} T/cm^2

	0.12			0.23	0.74
	0.10	0.17		0.08	1.1

Tritium Retention in JET Beryllium

Two beryllium samples from the JET fusion reactor were tested for tritium retention in experiments performed in the Sandia National Laboratories Tritium Research Laboratory (TRL). Sections of the beryllium limiter and divertor were sent to Sandia from the JET fusion reactor. These samples were cut into smaller samples using an electrical band saw in a plastic bag located in a TRL high velocity air hood. One sample each of the limiter and divertor were then dissolved in dilute sulfuric acid. As each sample dissolved, sweep gas consisting of 99% helium and 1% hydrogen was sent over the acid solution in a sealed glass beaker, through a liquid nitrogen cold trap, and then through an ionization chamber. During the dissolution of beryllium, part of the tritium in the beryllium is retained in the acid and part is released as gas. The results are as follows:

Limiter Tile

Retained in Acid - 6.1x10^{11} T/cm^2 Retained in Acid- 3.3x10^{11} T/cm^2

Released as Gas - 3.0x10^{12} T/cm^2 Released as Gas - 9.7x10^{11} T/cm^2

Divertor Tile

For the divertor tile, the sample was removed from a section that did not show significant melting. There was also no evidence of a thick redeposited carbon layer. The limiter sample was taken from the middle of the tile. This was not an area showing significant redeposition of carbon. There were areas near the ends of the tile that did show redeposition.

The results from these experiments can be compared to those performed in July of 1991. A beryllium sample removed from JET at that time was analyzed for tritium content. It contained approximately 2x10^{13} T/cm^2.

X-NRA SYSTEM TO MEASURE TRITIUM IN JET TILES USING THE T(p,n) REACTION

- THE SYSTEM IS CURRENTLY SENSITIVE TO ~ 10^{14} T/cm^2 IN GRAPHITE.
  - * ANALYSIS RANGE IS ~ 10 μm IN GRAPHITE.
  - * NO T DETECTABLE ON GRAPHITE JET TILE 7165.
- SIMULTANEOUS MEASUREMENT OF Be ON GRAPHITE TILES WITH ^{9}Be(p,n) IS POSSIBLE.
  - * 1.6 x 10^{19} Be/cm^2 OR ~ 1.25 μm MEASURED AT CENTER OF GRAPHITE TILE 7165.
  - * βBS MEASUREMENTS ON SIMILAR TILES SHOWED ~ 2μm OF DEPOSITED Be.
- SOLID Be TILES HAVE VERY HIGH BACKGROUND FROM ^{9}Be(p,d)→^{9}Be(d,n) SECONDARY REACTION.
  - * X-T(p,n) IS UNSUITED FOR MEASURING T IN SOLID Be TARGETS.

Jet Be Limiter Sample 2A

Tritium release from 100%-dense hot-pressed Be (1.7 wt. % BeO) with 2500 appm tritium and 26000 appm He.

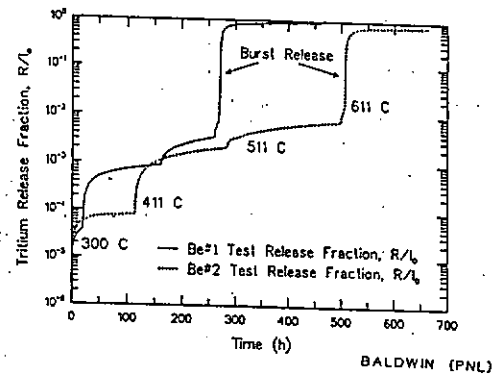

BALDWIN (PNL)

Jet Be Limiter Sample 2A

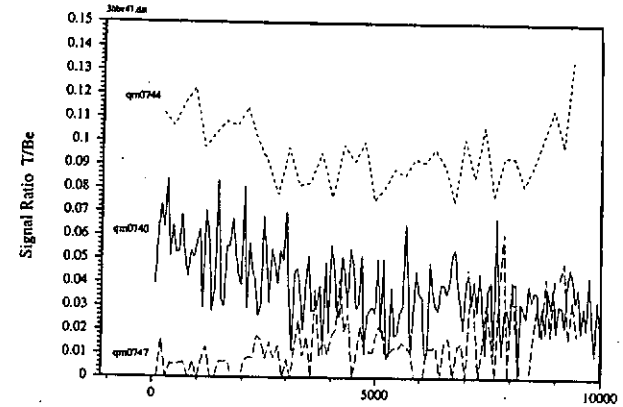

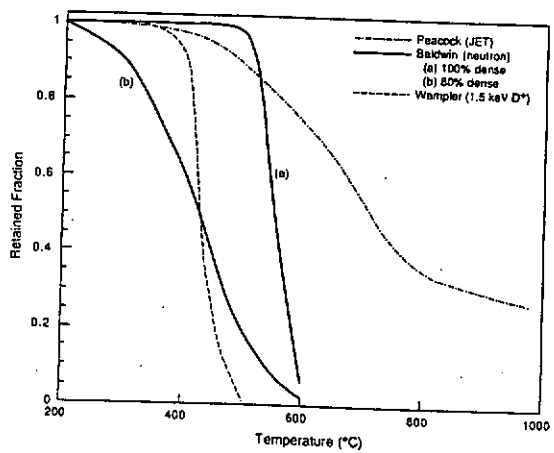

Tritium Is Strongly Trapped in Neutron Irradiated Beryllium

4.75 gram sample of beryllium

0.2 % TRITIUM II

Sample #	Mass Removed (gms)	Concentration (Ci/gm)
1	1.35	7.4
2	1.10	7.3
3	0.85	6.5
4	1.45	6.4

Beryllium was irradiated at INEL to 5×10^{22} n/cm^2

Tritium was created by (n,T) and (n,α) nuclear reactions

Results show 100% tritium retention at 40 C

101289F KW

Steady-State Temperatures

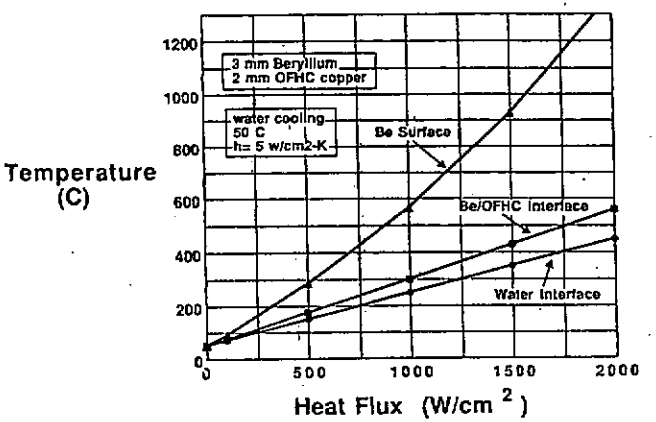

RDW Sandia 3/92

A "standard" re-emission calculation has been done for each material

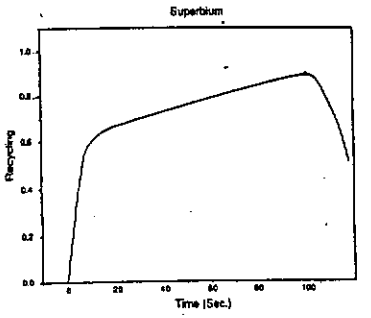

- Steady state re-emission for a 100s discharge at 20% duty cycle
- 5 A/cm^2 at 200 eV (10 MW/m^2)
- Water temperature of 100° C
- Surface temperature (thickness)

Tungsten	1100°C	(10mm)
Beryllium	800°C	(4mm)
Graphite	1200°C	(10mm)

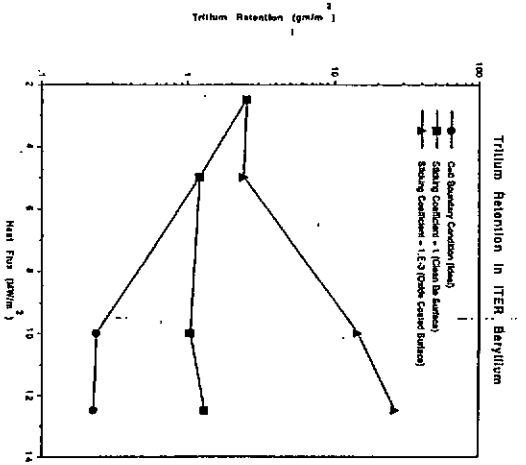

The "standard" re-emission calculation for beryllium

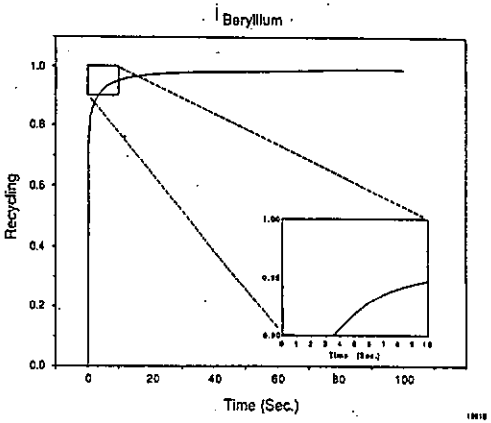

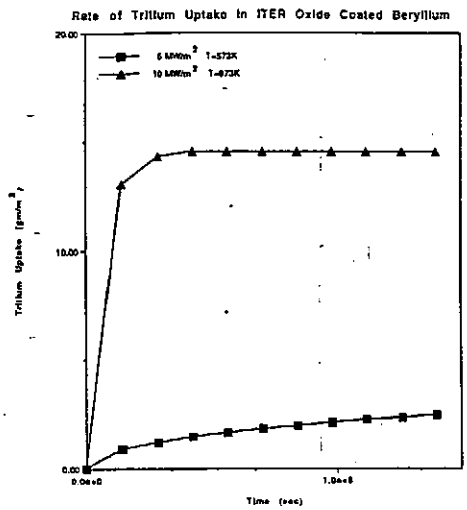

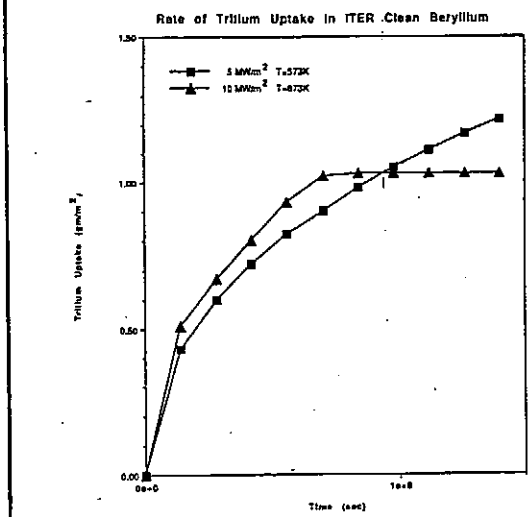

Beryllium's bulk tritium inventory may not be better than graphite's

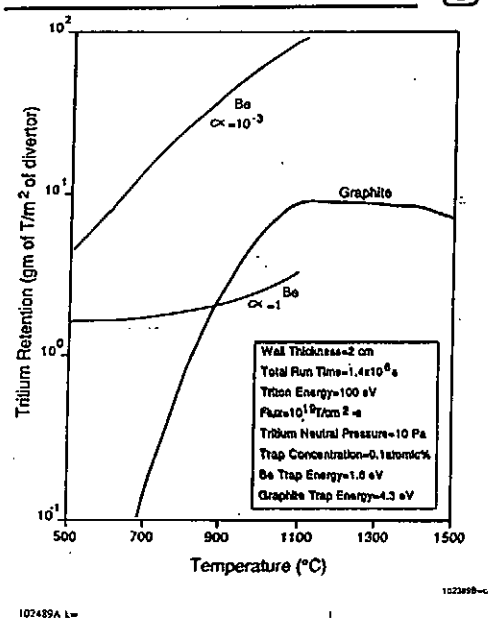

Critical Issues: Beryllium-Tritium Interaction

- Solubility
  Large differences in the database will require further study.
  Thermal diffusion (Soret effect) must be assessed
- Surface Effects
  The role of surface contamination (carbon, oxygen) needs to be studied
- Wall Pumping
  The differences between laboratory and JET observations need to be clarified
- Neutron Effects
  The database for tritium trapping at neutron damage needs significant improvement

Extend the laboratory measurements to ITER relevant fluxes and energies

Beryllium also shows significant outgassing

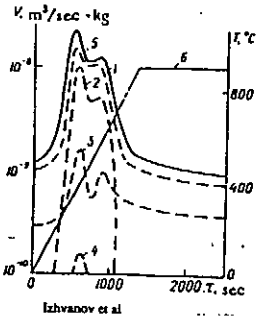

Izhvanov et al

Hot pressed 3h at 1410 K at 5 MPa

Hydrogen and water vapor are the main gases evolved

Chemisorbed gases and surface reactions dominate the release

1: H_2 2: H_2O 3: N_2 4: CO_2 5: Sum

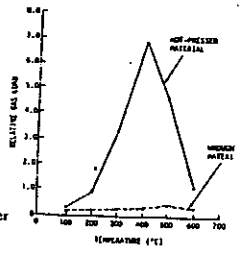

Hot-pressed material outgases much more than wrought material

Moreau and Paaschier

Beryllium outgassing is quantitatively less than that of graphites

1021189A kw

Beryllium Outgasses Air Components To 500°C

- Outgassing of 1 gm, air-exposed Be and POCO samples were compared by ramping to 600°C at ~0.2°C/s.
- Be outgassing is 100X lower at 50-100°C 5 to 10X lower at 400-500°C
- Be outgasses water to 500°C.
- Be exhibits a broad CO or N2 peak from 300 to 500°C.

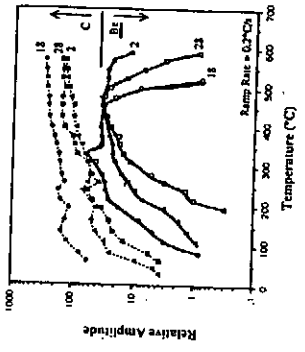

TRITIUM/BERYLLIUM SAFETY RESEARCH AT THE INEL IS IN FIVE MAIN AREAS

- Implantation-driven permeation experiments on PFC materials such as tungsten and beryllium
- Measurement of the mechanical properties of neutron-irradiated beryllium
- Studies to evaluate routine tritium effluents from fusion components and to support design of tritium management systems (magnetic and ICF)
- Safety code development, certification to Quality Level A, and promulgation (e.g., TMAP4)
- Oxidation-driven volatility experiments

INEL

EG&G

INEL Tests Have Explored Oxidation-Driven Volatility and Chemical Reactivity

- Volatility results are used to calculate maximum offsite accident doses
- Results from tests are used in the development of an ITER mid-plane LOCA model
  - Temperature sensitivity to boundary conditions
  - Various PFC materials will be incorporated
  - Hydrogen production will be calculated
- Measured hydrogen production rates as a function of temperature for various PFC materials is given below

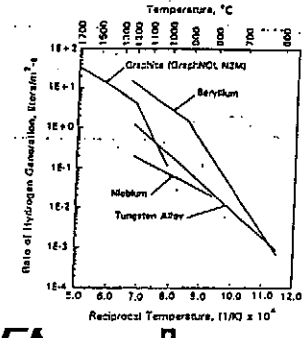

INEL

EG&G Idaho, Inc.

IMPLANTATION DRIVEN PERMEATION OF DEUTERIUM THROUGH MOLYBDENUM

W.H. SHU[1], K. OKUNO[1], AND Y. HAYASHI[2]
1) Japan Atomic Energy Research Institute
2) Department of Material Science and Technology, Kusyu University

From a viewpoint of tritium safety in fusion reactors, Ion-Driven Permeation (IDP) behavior on pure molybdenum has been studied using deuterium ions with relatively low incident energy. Permeation fluxes of deuterium through Mo were measured at steady state as a function of incident ion energy (200 eV-2 keV), incident ion flux (4-13x10^{18} D^+/m^2), and target temperature (450-690 K).

The experimental result for dependence of incident ion flux on permeation flux suggests that the IDP process of deuterium implanted into Mo was found to be controlled by the diffusion of deuterium in both the front and back regions, DD-regime defined by Doyle.

In the case of 1.5 keV incident energy, the permeation flux decreased with increasing temperature in the lower temperature region, and became nearly constant in the higher region. This suggests that the irradiation by 1.5 keV ions would produce trapping sites for the diffusion of deuterium at lower temperature region, which might be annealed at higher temperature. On the other hand, in the case of 500 eV, as temperature increases, the permeation flux increased significantly at temperature below 600 K, and decreased gradually at temperature above 600 K. It is suggested that the irradiation by 500 eV D^+ ions would form a short path (H-SIA) at lower temperature, and that some trapping sites would be formed by the dissolving of the H-SIA at higher temperature.

The permeation flux increased rapidly with increasing incident ion energy at lower temperature and gradually at higher temperature for the incident ion energy ranging from 1.5 to 2 keV. It is suggested that the higher energetic ions would produce more trapping sites or stronger trap binding energy at lower temperature. For the incident ion energy ranging from 200 to 500 eV, on the other hand , the permeation flux increased significantly with increasing incident ion energy at lower temperature, and decreased at higher temperature. The experimental results suggest that for the lower incident ion energy, the H-SIA complexes would be more produced at lower temperature, and that trapping sites would be more effective at higher temperature.

IMPLANTATION DRIVEN PERMEATION OF DEUTERIUM THROUGH PURE MOLYBDENUM

W.M. SHU[1,2], K. OKUNO[1] and Y. HAYASHI[2]

1: *Japan Atomic Energy Research Institute, Tokai-mura, Ibaraki-ken 319-11, Japan*

2: *Department of Materials Science and Engineering, Kyushu University, Fukuoka 812, Japan*

1) For D-T fusion reactors, one of key safety issues is behavior of tritium implanted into plasma facing materials.

2) A number of experimental studies have been carried out using ion beam or discharge methods.
   Typical energy region : > a few keV for ion beam method
   < a few 100 eV for discharge method
   Important energy region : < a few keV

3) An experimental apparatus has been developed to study tritium permeation behavior using a tritium accelerator which can produces tritium ions with incident energy ranging from several 10 eV to 2 keV.

4) In the present work, ion implantation driven permeation (IDP) behavior of D^+ ions implanted into Mo has been studied. Our attention was focused on measurements of a steady- state permeation as a function of incident ion energy, incident ion flux and target temperature. Based on the experimental results, the mechanism of IDP process of D^+ ions in Mo will discussed.

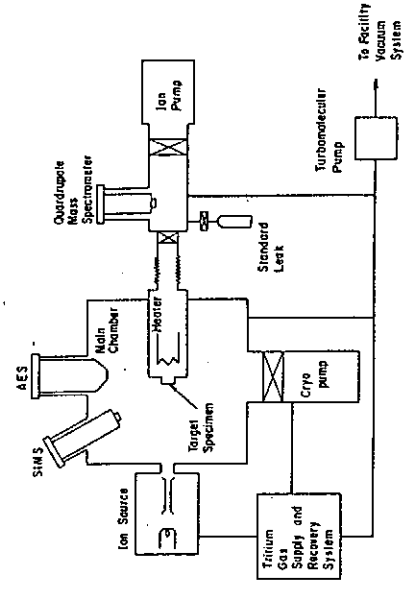

SAMPLE SPECIFICATION

pure molybdenum: 99.95 %wt
thickness: 5×10^{-5} m
implatation size: 2.5×10^{-2} m in diameter

EXPERIMENTAL CONDITION

(1) Incident ion flux: 4~13x 10^{18} D^+/m^2

(2) incident ion energy: 200~2000 eV

(3) membrane temperature: 450~690 K

(4) base pressure:

below 2x 10^{-6} Pa on upstream side

below 1x 10^{-6} Pa on downstream side

(5) upstream pressure:

1.5x 10^{-4} Pa during implantation

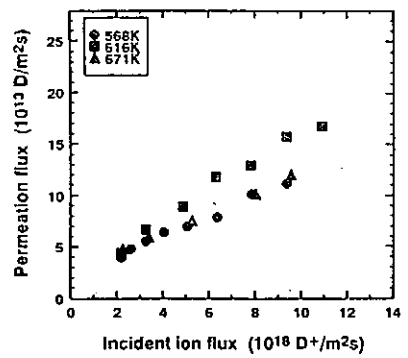

Fig. Incident ion flux dependence of IDP flux for deuterium implanted into pure molybdenum (thickness:5x 10^{-5}m; incident ion energy: 500eV)

5

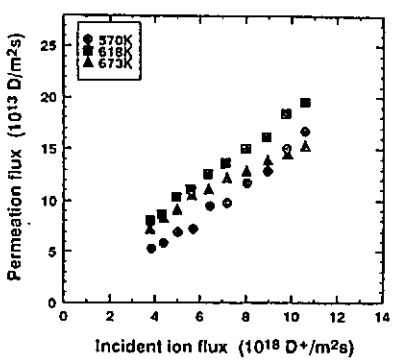

Fig. Incident ion flux dependence of IDP flux for deuterium implanted into pure molybdenum (thickness:5x 10^{-5}m; incident ion energy: 1.0ke

7

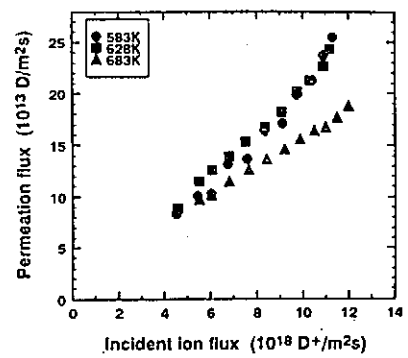

Fig. Incident ion flux dependence of IDP flux for deuterium implanted into pure molybdenum (thickness:5x 10^{-5}m; incident ion energy: 2.0keV)

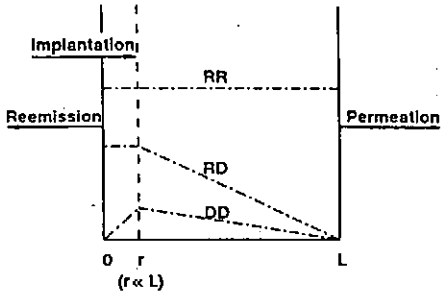

r: projected range ; L: thickness
RR: recombination on both sides
RD: recombination on front side and diffusion on back side
DD: diffusion on both sides

Fig. Simplified model for implatation permeation at steady state

$$\text{RR regime: } \Phi_p = \frac{k_b}{k_f + k_b}\Phi_i$$

$$\text{RD regime: } \Phi_p = \frac{D_b}{L}\sqrt{\frac{\Phi_i}{k_f}}$$

$$\text{DD regime: } \Phi_p = \frac{D_b}{D_f}\frac{r}{L}\Phi_i \quad (r \ll L)$$

Φ_p: permeation rate; Φ_i: incident ion flux
k: recombination coefficient; D: diffusion coefficient
subscripts f and b: front and back sides respectively
r: projected range; L: thickness of membrane

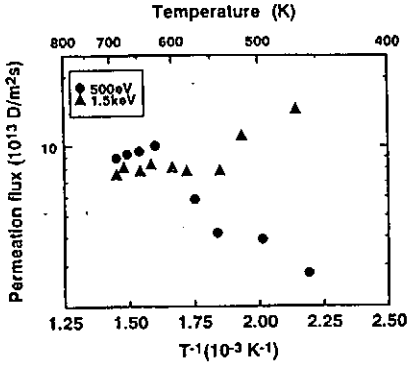

Fig. Permeation flux of deuterium implanted into pure molybdenum (5x 10⁻⁵ m; 6.37x 10¹⁸ D⁺/m²s)

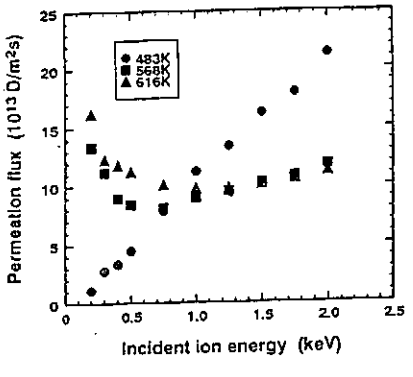

Fig. Incident ion energy dependence of IDP flux for deuterium implanted into pure molybdenum (thickness:5x 10⁻⁵m; incident flux:6.37x 10¹⁸D⁺/m²s)

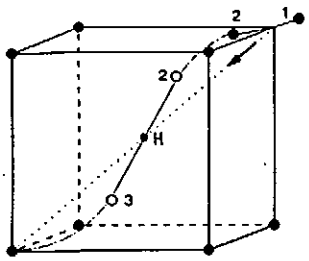

SIA : Self Interstitial Atom

Fig. Scheme of displacement of SIA-H comlex in a bcc lattice

The circles 2 and 3 denote the position of a split interstice with a hydrogen atom in the middle after a diffusion jump. Atom Mo1 occupies a lattice site while Mo2 forms a new dumbbell with Mo3, which was previously at the regular lattice site at the center of the cube. In the jump the hydrogen atom moves along a diagonal of the cube.

A.P. Zakharov, et.al.
Sov. Phys. Dokl. 25 (1980) 309

SUMMARY

(1) The permeation process was controlled by the diffusion of deuterium in both the front and back regions (DD regime).

(2) The irradiation by the higher energy (1.5 ~ 2 keV) ions will produce the defects, which act as trapping sites for the diffusion of deuterium in the front region.

(3) The irradiation by the lower energy (200 ~ 500 eV) ions will form a short diffusion path in the front region due to the production of H-SIA complexes (SIA : Self Interstitial Atoms).

DD regime: $\Phi_p = \frac{Db}{Df}\frac{r}{L}\Phi_i$

	Low Energy Irradiation (produce) ↓ H-SIA complex → Increase Dr →	High Energy Irradiation (produce) ↓ Hydrogen trap → Decrease Dr →
Low T	H-SIA stable Dr: large ϕ_p: small	Hydrogen trap stable Dr: small ϕ_p: Large
High T	H-SIA annealed Dr: middle ϕ_p : middle	Trap annealed Dr: middle ϕ_p : middle.

INTERACTION OF TRITIUM WITH PIPING MATERIALS, CATALYSTS AND ADSORBENTS

Masabumi Nishikawa

Kyushu University,Faculty of Engineering,
Department of Nuclear Engineering
Hakozaki 6-10-1, Higashi ku, Fukuoka 812 , Japan

It is necessary to grasp the tritium mass balance in a fusion reactor through the whole system and at every part of subsystems for assurance of radiation safety to get the social acceptance or for development of effective use of tritium to ease breeding requirements.

In discussions of behaviors of tritium on the surface of various materials contacting with gas stream containing tritium, the mass transfer phenomena as follows should be taken in count.

(1) water adsorption.
(2) hydrogen isotopes adsorption.
(3) isotope exchange reaction between gaseous hydrogen in gas stream and surface water.
(4) isotope exchange reaction between water in gas stream and surface water.
(5) transfer of hydrogen isotopes and water through bulk of piping material.
(6) transfer of hydrogen isotopes and water through surface layer formed on materials or pores.
(7) oxidation of gaseous hydrogen on surface.

It is observed in this study that steps (3) and (6) are mostly effective in case when oxide film layer formed on the material surface as stainless steel.

The amount of tritium sorbed on the stainless steel is correlated and compared with that observed for copper or quartz.

The memory effect observed for an ionization chamber having stainless steel electrodes is also compared with that having copper electrodes.

(1) water adsorption
(2) hydrogen isotopes adsorption
(3) isotope exchange reaction between gaseous hydrogen in gas stream and surface water
(4) isotope exchange reaction between water in gas stream and surface water
(5) transfer of hydrogen isotopes and water through bulk of material
(6) transfer of hydrogen isotopes and water through pores and interface
(7) oxidation of hydrogen on surface

Kyushu University Tritium Laboratory

This facility, installed in the Department of Nuclear Engineering, was built to clarify tritium behavior in a fusion reactor in terms of chemical engineering.

The initial purpose of research in this facility was to establish safety confinement technology through experiments on the following:

1. tritium reaction kinetics in a catalyst bed for oxidation of tritiated gaseous components, a catalyst bed for isotope exchange reactions, an adsorption bed, or an absorption bed
2. decontamination methods to release tritium from piping materials and surfaces of glove boxes
3. treatment of tritiated waste materials
4. tritium monitoring at various levels in different atmospheres.

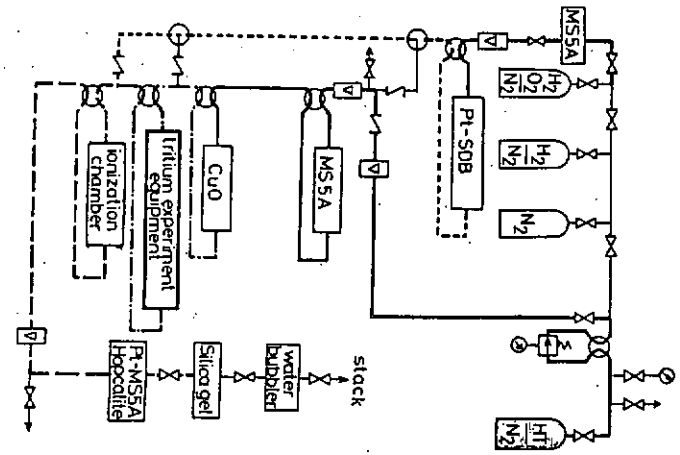

Research programs on safety confinement technology are progressing satisfactorily, and we are attempting to optimize the operating conditions of various types of tritium cleanup systems.

Research into tritium behavior in the fueling system of a fusion reactor is also done in this laboratory. The areas listed below are being studied:

1. behavior of tritium in a packed bed of solid breeder materials and systems to recover tritium
2. physical and chemical behavior of tritium in various candidate structural materials for fusion reactors.

Table Comparision of Sorption Characteristics
(pH_2O = 10Pa, room temperature)

	Copper	SUS 304	Quartz
Tritiated water adsorbed on top-surface	~20 Ci/m^2	1/4~1/6 of copper	1/6~1/10 of copper
Tritiated water in surface layer	~20 Ci/m^2	~50 Ci/m^2	~3 Ci/m^2
Time to get steady state on sudface	relatively slower	relatively faster	relatively faster
Time to get saturation on surface layer	relatively faster	relatively slower	relatively faster
Decontamination using water vapor	effective once purge	effective repetitive purge	effective once purge
Decontamination using protium gas	not effective	not effective	not effective
Decontamination using dry gas	not effective	not effective	partly effective

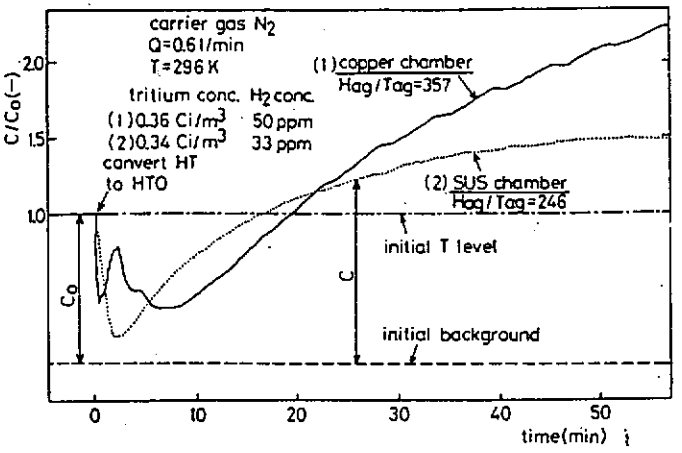

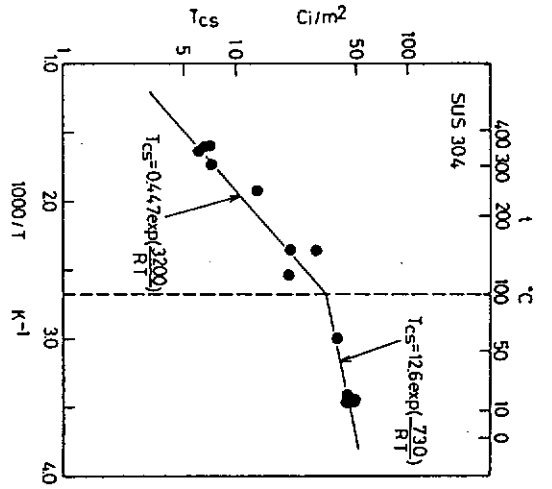

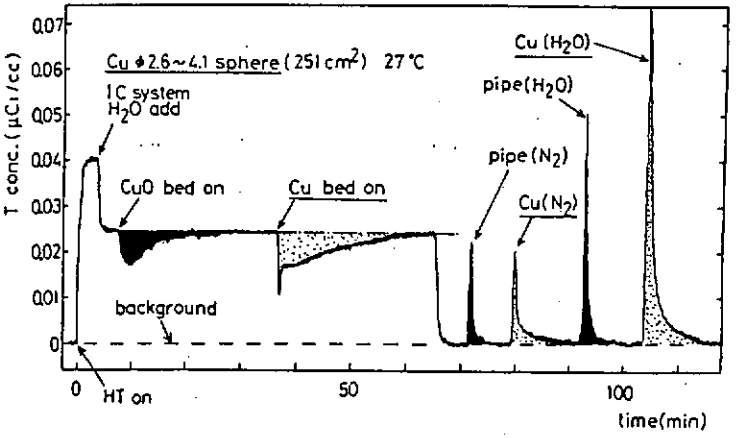

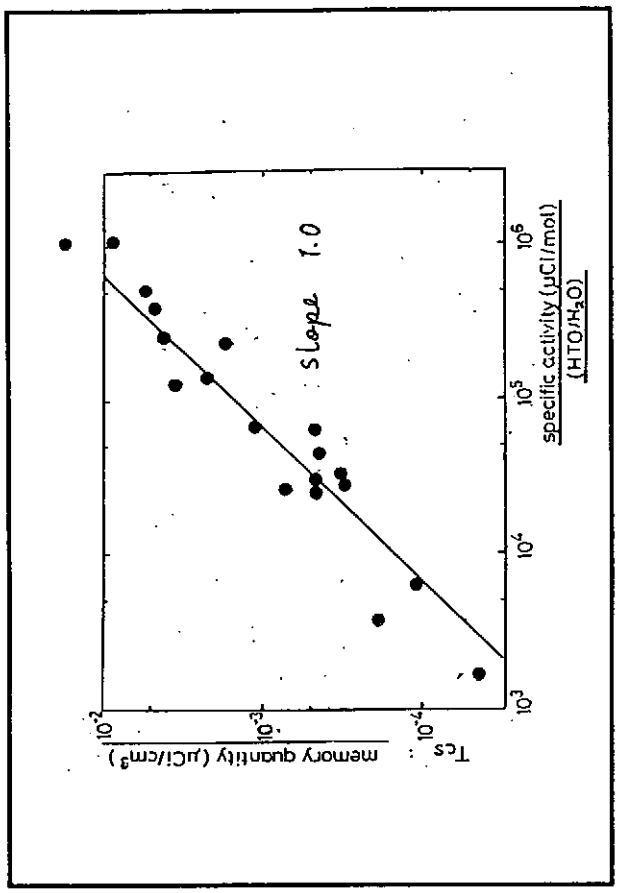
Slope 1.0
specific activity (μCi/mol) / (HTO/H2O)
memory quantity (μCi/cm³)
Tcs :

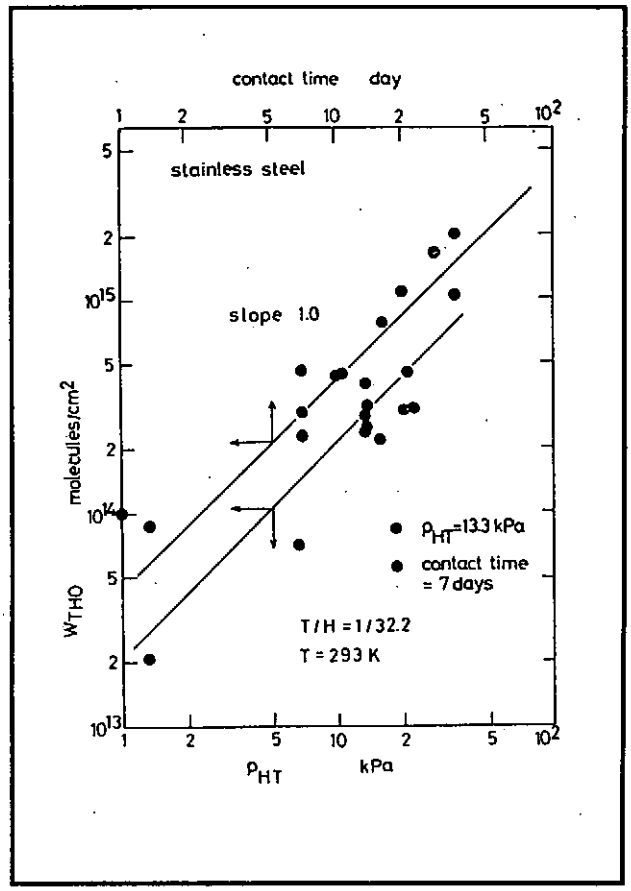
contact time day
stainless steel
slope 1.0
ρHT=13.3 kPa
contact time = 7 days
T/H = 1/32.2
T = 293 K
WTHO molecules/cm²
ρHT kPa

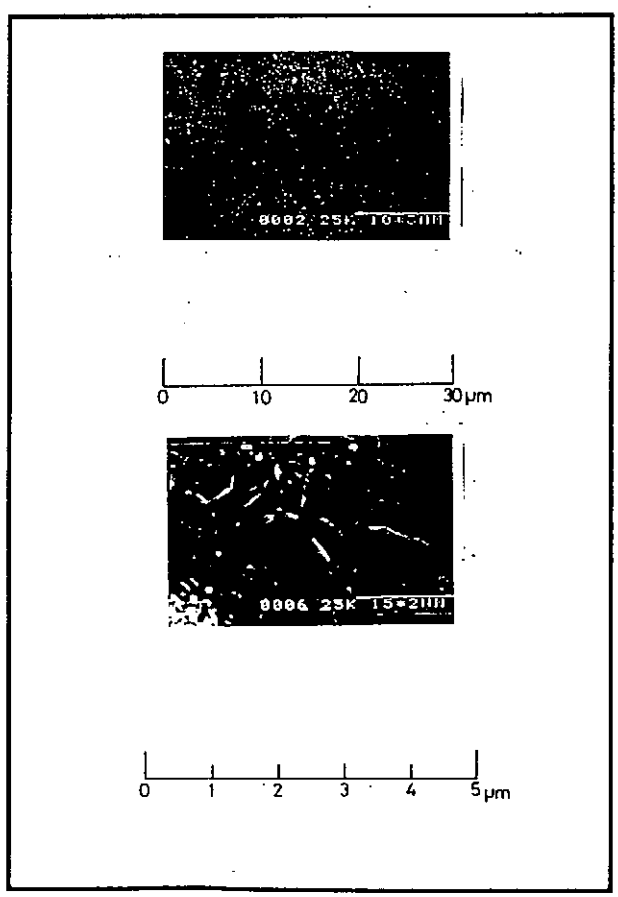
0 10 20 30 μm
0 1 2 3 4 5 μm

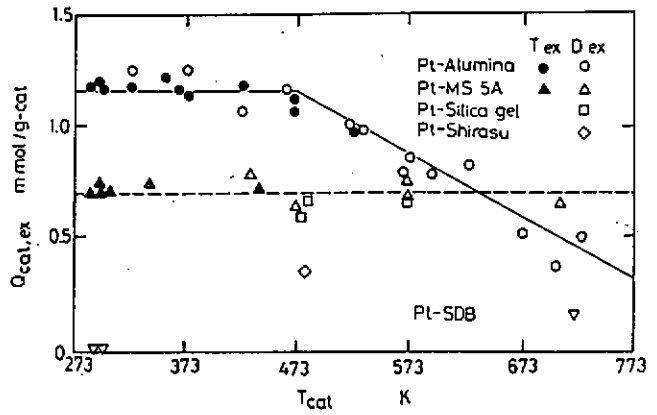

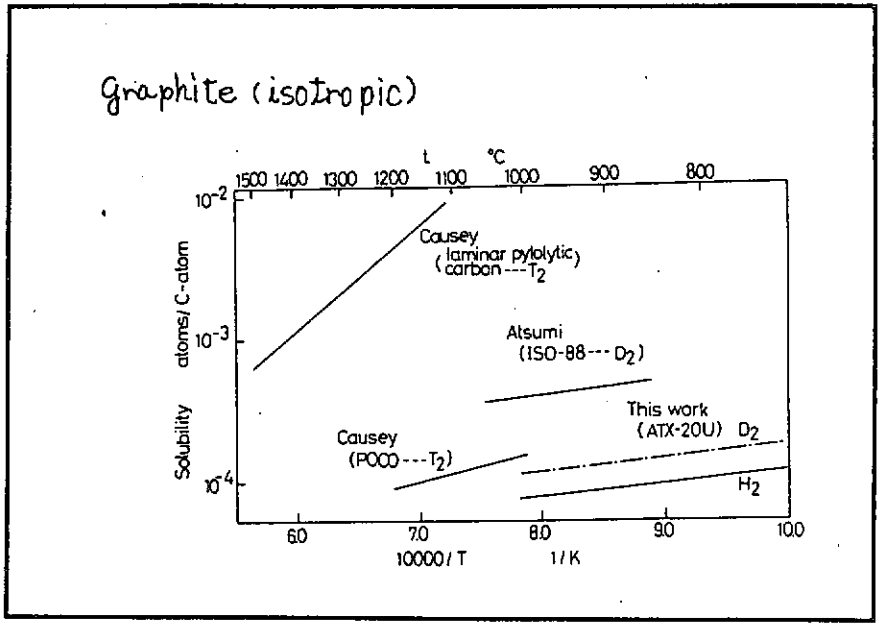

Wherever OH group or crystal water exists, tritium can be easily trapped to the surface in the form which can hardly be released by drying or evacuation, though it can be easily released by isotope exchange reaction.

The isotope exchange reaction for tritium of T_2O form in gas stream is much faster than that for tritium in T_2 form.

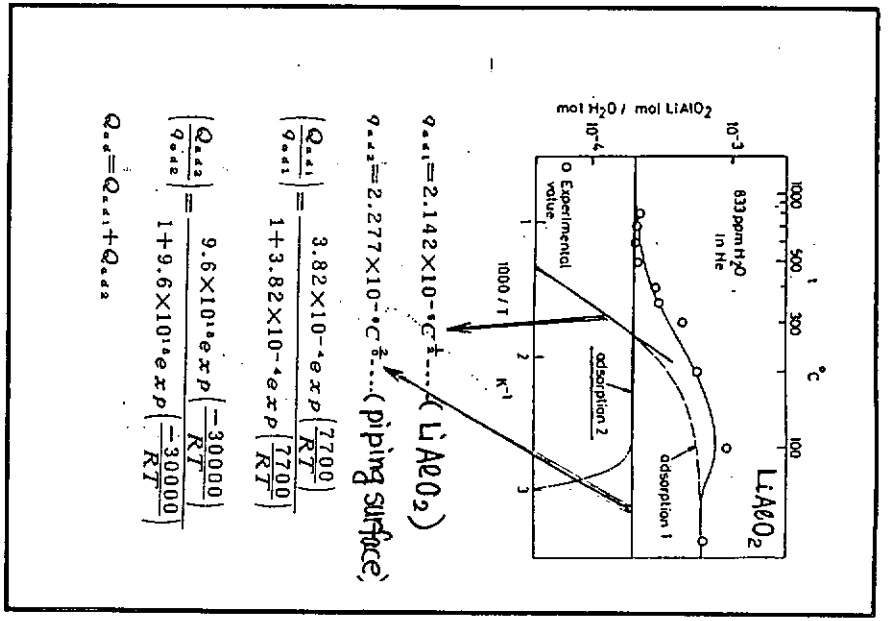

- oxide film on metal surface
  (SUS, copper, iron, aluminium)
  — piping, chemical reactor, glove box,
  ionization chamber, cryopanel

- porous adsorbent
  (molecular sieves, silica gel, kieselguhr,
  activated aluminum)
  — catalyst bed, adsorption bed

- ceramics
  (breeding materials, quartz)
  — blanket, glove box, piping

Session 6: Neutron Damage

Abstract of :

U. S. Plasma Facing Components Irradiation Program

L. L. Snead, T. D. Burchell, W. P. Eatherly, S. J. Zinkle
Metals and Ceramics Division, Oak Ridge National Laboratory

The current irradiation program in the United States for ITER relevent materials is focusing on three areas:

1) Thermal conductivity and dimensional stability of C/C composite material.
2) Characterization of unirradiated and irradiated mechanical properties of Glidcop dispersion strengthened copper.
3) Effects of radiation on tritium retention and embrittlement of beryllium.

This talk will summarize the irradiation studies in these areas and lay out the planned irradiation and post irradiation testing in each area. Emphasis will be given to the thermophysical properties of C/C materials which have been irradiated in the HTFC 1 and 2 capsules in HFIR.

Radiation Effects in C/C Composite Materials

- Radiation response of C/C composites following HFIR irradiation:
  - varied architectures
  - PAN and Pitch based fibers
- General Properties of Interest are:
  - Strength
  - Dimensional Stability
  - Thermal Conductivity
- Results from two irradiation capsules will are summarized:
  - HTFC1 : 1.6 dpa, 600 C HFIR target region
  - HTFC2 : 5 dpa, 600 C in HFIR target region

ORNL

U. S. Plasma Facing Components Irradiation Program

L. L. Snead
T. D. Burchell
W. P. Eatherly
S. J. Zinkle

Presented at the U. S. - Japan Workshop P-196
on High Heat Flux Components and
Plasma Surface Interactions

Kyushu University, Japan
November 17-19, 1992

ORNL

EXPERIMENTAL DETAILS

IRRADIATION CONDITIONS

HIGH FLUX ISOTOPE REACTOR TARGET REGION
FLUX ~ 1.5 x 10^{15} n/cm^2•s [E>0.183 MeV]
CAPSULE PEAK TO MINIMUM FLUENCE RATIO ~ 3.0

- HFIR CYCLE 289, CAPSULE HTFC-I
  - 600°C, 2.44 x 10^{25} n/m^2 [E>50 keV], 1.6 dpa
- HFIR CYCLES 295-297, CAPSULE HTFC-II
  - 600°C, 7.28 x 10^{25} n/m^2 [E>50 keV], 4.7 dpa

ornl

Introduction

- Neutron effects for ITER relevant diverter materials is currently in three general areas
  1) Thermal conductivity and dimensional stability of C/C composite material.
  2) Characterization of unirradiated and irradiated mechanical properties of Glidcop dispersion strengthened copper.
  3) Effects of radiation on tritium retention and embrittlement of beryllium.

ORNL

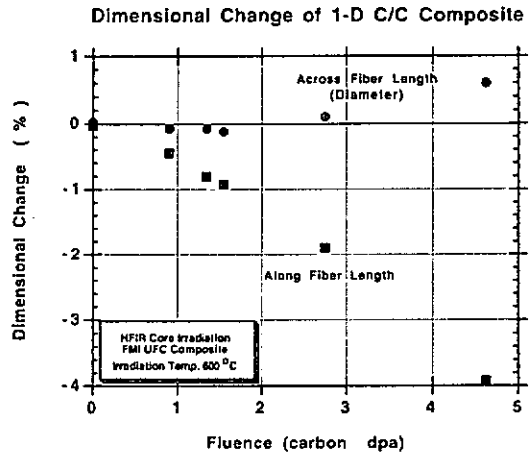

Summary of materials in HFIR capsules HTFC-1 and -2

Designation	Description	Heat Treatment Condition
H-451	Near-isotropic nuclear graphite (reference material).	As received
A05	Carbone Lorraine. 2D C/C composite. PAN Fibers.	As received
UFC	Fiber Materials, Inc. 1D C/C composite. PAN Fibers.	3100°C
RFC	Fiber Materials, Inc. Random fiber composite. PAN Fibers (chopped).	2650 and 3100°C
223	Fiber materials, Inc. 3D C/C composite. PAN Fibers.	2650 and 3100°C
222	Fiber Materials, Inc. 3D C/C composite. Pitch Fibers (P55).	2650 and 3100°C

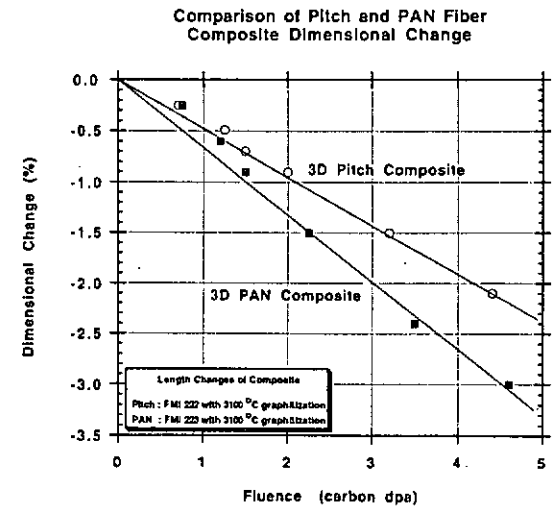

Dimensional Changes

- Dimensional changes dominated by fibers:
- 3-D composites show least anisotropic behavior
- Pitch based fiber composites exhibit least dimensional change

ORNL

RADIATION INDUCED DIMENSIONAL CHANGES
GRAPHITE AND ORTHOGONAL 3D C/C COMPOSITES

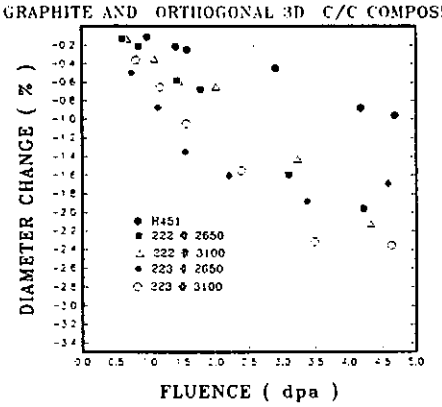

RADIATION INDUCED DIMENSIONAL CHANGES
GRAPHITE AND ORTHOGONAL 3D C/C COMPOSITES

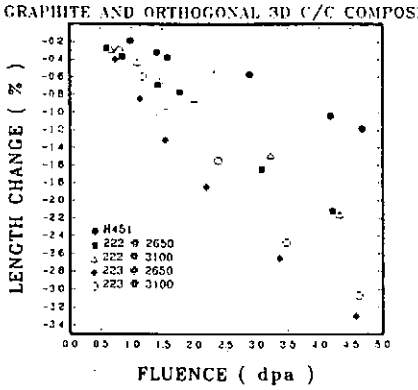

RADIATION INDUCED VOLUME CHANGES
GRAPHITE AND ORTHOGONAL 3D C/C COMPOSITES

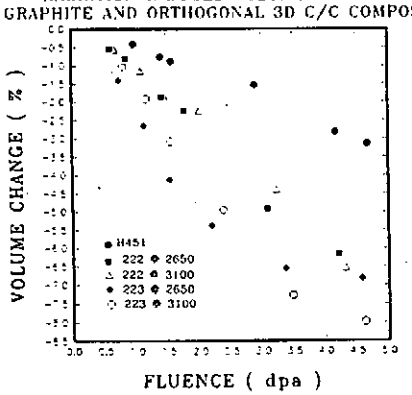

RADIATION INDUCED DIMENSIONAL CHANGE
.PHITE AND 1D,2D AND RANDOM FIBER C/C COMPOSITES

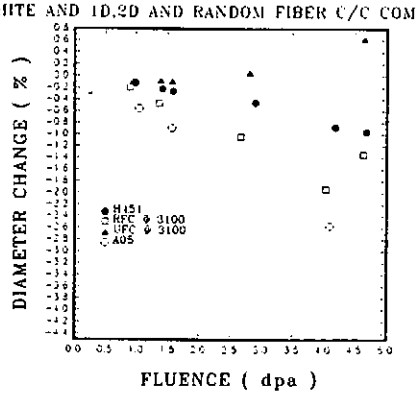

DIATION INDUCED DIMENSIONAL CHANGES IN GRAPHITE
1D,2D AND RANDOM FIBER C/C COMPOSITES

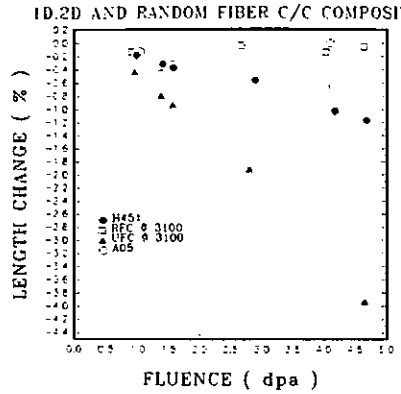

ADIATION INDUCED VOLUME CHANGES IN GRAPHITE
1D, 2D AND RANDOM FIBER C/C COMPOSITES

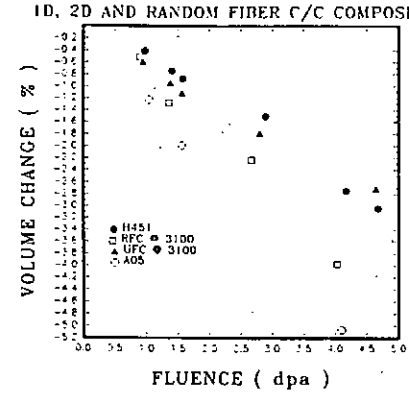

DIMENSIONAL CHANGES OF 2D COMPOSITES
ARE VERY ANISOTROPIC

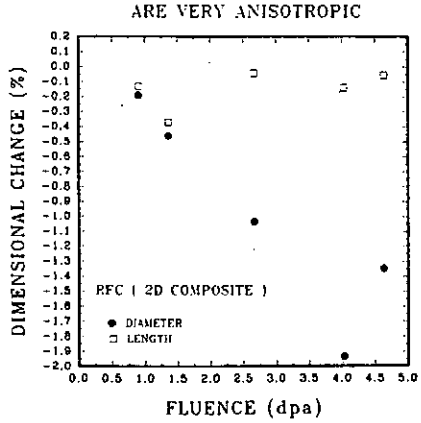

DIMENSIONAL CHANGES OF 3D COMPOSITES
ARE MORE ISOTROPIC THAN 2D MATERIALS

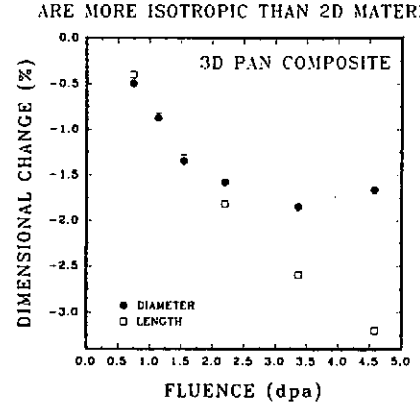

Annealing of Irradiated Pitch Based C/C Composite

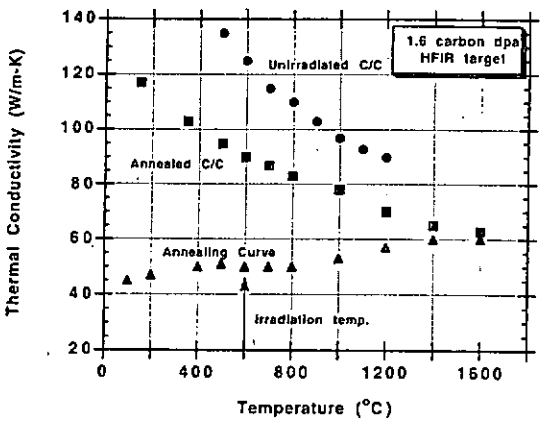

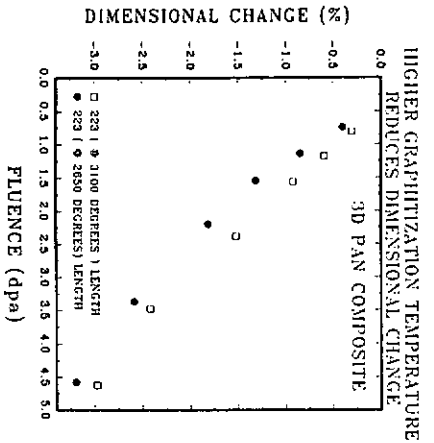

Annealing of Irradiated PAN Based Fiber

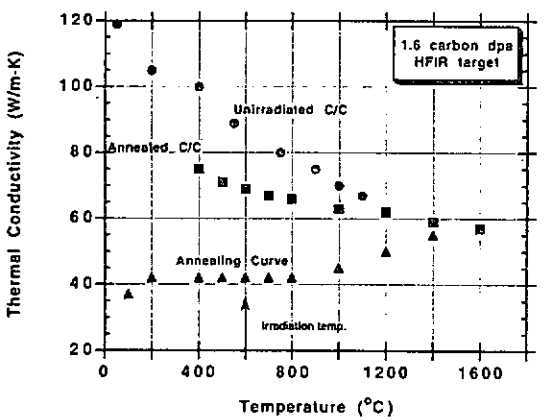

Thermal Conductivity

- 3-D pitch fiber composite reduced by 60 %
- 3-D PAN fiber composite reduced by 50 %
- Post-irradiation annealing above the irradiation temperature allows large recovery in thermal conductivity

ORNL

Loading List - HTFC 3

Sample ID (900°C; 1/2" discs) 1.6 dpa	Composition	Weave	PIE					Supplier	Date Expected
			TC	S	D	M	TS		
H 451	Reference Graphite		X	X	X		X	ORNL	In possession
FMI 222	Pitch Fiber (P55)	3D balanced	X	X	X		X	ORNL	In possession
FMI 223	PAN Fiber	3D balanced	X	X	X			ORNL	In possession
FMI UFC	PAN Fiber	1D continuous	X	X	X			ORNL	In possession
FMI TC	Pitch Fiber (K 1100)	1D continuous	X	X	X	X		ORNL	In possession
NAMCO	Pitch Fiber (K 1100)	Angle interlock	X	X	X	X		Glen Engle	In possession
MKC-1PH	Pitch Fiber	1D continuous	X	X	X		X	Bob Watson	By 11/1
MFC-1	Pitch Fiber	1D continuous	X	X	X			Mitsubishi (JAERI)	In possession
Hercules NGR 04	CVD Impregnated, A70 PAN Fiber	N_2Z	X		X	X		Paul Walsh	In possession
Hercules NGR-04, 52	Pitch Impregnated, A70 PAN Fiber	N_2Z	X		X	X		Paul Walsh	In possession
Hercules HTC	Pitch Fiber (P 120)	3D unbalanced	X	X	X		X	Paul Walsh	In possession
UCLA Redeposited Carbon	Redeposited carbon on graphite	–	X			X	X	Yoshi Hirooka	By 12/1
Plasma Sprayed Re	Free standing	–	X			X	X	Bob Watson	By 12/1
Plasma Sprayed W	Free standing	–	X			X	X	Bob Watson	By 12/1
TRA Cu/C-C TRA Cu/G	FMI 222 brazed to Cu H451 brazed to Cu	Balance weave (Pitch)	X	X		X	X	Joe Weeks	By 11/1
MER Cu/C-C MEP Cu/G	FMI 222 brazed H441 brazed to Cu	Balance weave (Pitch)	X	X		X	X	Sumit Gulia	By 11/1

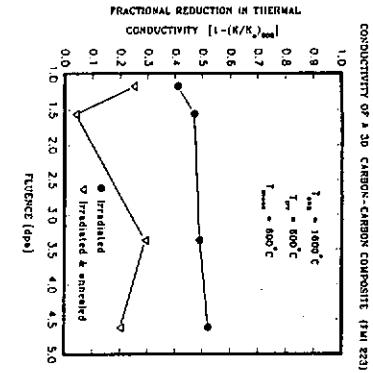

THE EFFECT OF POST IRRADIATION ANNEALING ON THE THERMAL CONDUCTIVITY OF A 3D CARBON-CARBON COMPOSITE (FMI 223)

ISTC1 (In-Situ Thermal Conductivity)

- 0 to 4 dpa in HFIR reflector region
- 200 and 900 °C irradiation temperature
- Thermal conductivity measurement during HFIR irradiation
- In-situ annealing to 1200 C
- Samples will include:
  - High Thermal conductivity C/C
  - H451 and Highly Ordered Pyrolitic Graphite

ORNL

Planned Irradiations (1993)

HTFC3 (HFIR target, begin irradiation Feb. 1993)

- 900 and 1200 °C, 1.6 dpa
  - Complete HTFC 1,2 test matrix
  - Sprayed Tungsten
  - Cu-Graphite and Cu-C/C brazed materials
  - Redeposited Carbon
- TEM discs will be included with fusion relevant He/dpa generation
- Testing of irradiated materials will include:
  - Thermophysical properties (ORNL)
  - Tritium retention (SNL)
  - Thermal Shock (KFK Juelich)
  - Microscopy (ORNL)

ORNL

Radiation Effects in Glidcop

- Glidcop has been irradiated up to ~ 150 dpa (FFTF- 450 °C) with promising results for use of material for ITER
- ORNL/PNL program in MP of unirradiated Glidcop (tensile, fatigue, fatigue crack growth, fracture toughness)

ORNL

Tritium Retention in Beryllium

Trapped Fraction as a Function of Annealing Temperature

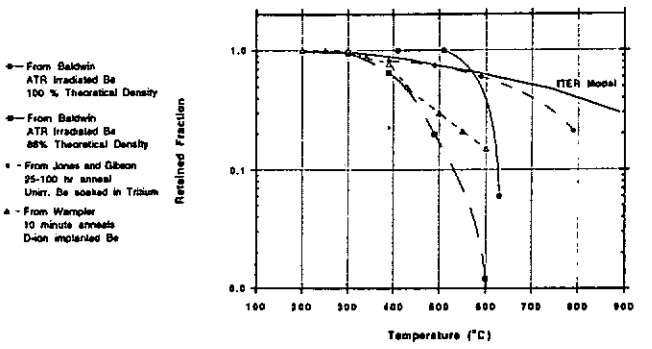

Planned Irradiations (1993)

- Spectral Tailored Capsules (200J, 400J - HFIR shield)
  - ITER relevant He/dpa ratios
  - ITER relevant transmutation products
- Joint US/Russia Glidcop Irradiations (SM3 - Dimitrovgad)
  - identical specimens to 200J and 400J
  - larger specimens for mechanical properties
- Post Irradiation Testing Includes:
  - tensile, fatigue, fatigue crack growth, fracture toughness, swelling, microstructure

ORNL

Radiation Effects in Beryllium

- Currently, irradiation of Be materials is being conducted in blanket community
- Microstructural studies (Gellis) of FFTF irradiated HIP Be concludes:
  - severe ductility loss found following irradiation at 420 °C
  - Irradiation hardening caused by small (c-type) dislocation loops and He bubble formation on grain boundaries
  - cavities found on dislocations and grain boundaries (may indicate swelling for temperatures above 500 °C)
- Tritium retention is being studied for FFTF irradiated Be

PNL

Neutron Irradiation Effect on the Thermal Conductivity of Graphite Materials

Tadashi Maruyama

Power Reactor and Nuclear Fuel Development Corporation

Japan-US Workshop P-196 on "High Heat Flux Components and Plasma Surface Interactions for Next Devices"
Kyushu University
November 17-19 ,1992

Graphite and C/C composites for PFM

- high thermal conductivity
- high thermal shock resistance

Next device ⇨ neutron irradiation effect on the thermal conductivity

⇨ fine-grain isotropic graphites
C/C composites
bulk boronized graphites

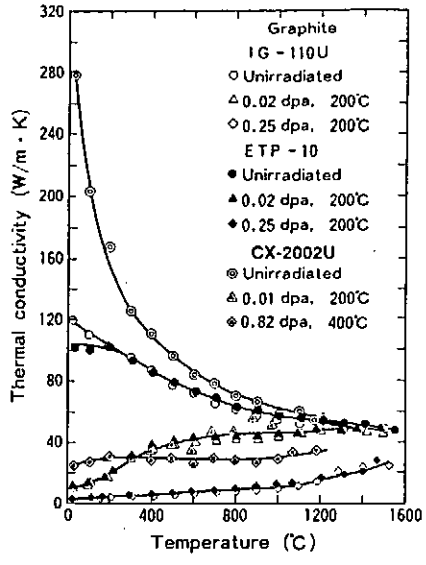

Fig. 1.

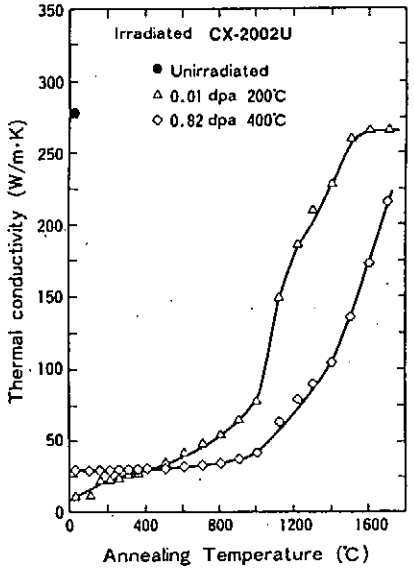

Fig. 3.

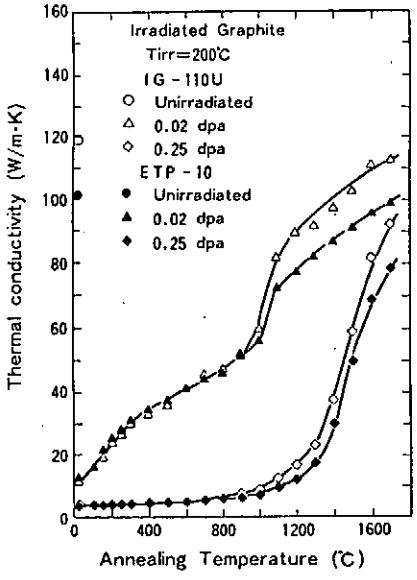

Fig. 2.

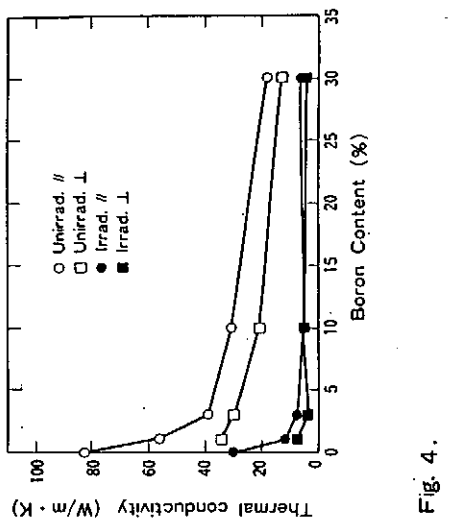

Fig. 4.

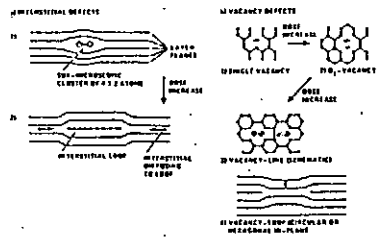

SCHEMATIC OF LATTICE DEFECTS INTRODUCED BY RADIATION IN GRAPHITE (FROM REF. 10)

FIGURE 1

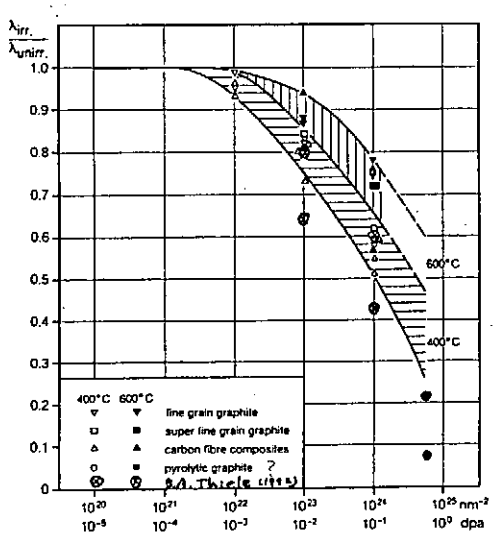

Normalized thermal conductivity of various graphitic materials at 400 and 600°C in dependence of the accumulated neutron fluence.
GRIPS (GRaphite Irradiation in the PoolSide facility of HFR-Petten)

Work performed under NET-task PPM 0-2 by Forschungszentrum Jülich (KFA).

● IG-110U ◍ PyC (400°C)
● CX-2002U ◍ PyC (600°C)

Summary of results

1) The neutron irradiation at low temperature (200 ~ 400°C) and low fluencies (0.01 ~ 0.1 dpa) markedly reduced the thermal conductivity. The room temperature thermal conductivity of CX-2002U became about 2% of the unirradiated value after irradiatrion at 200°C to 0.01 dpa.
2) The recovery in the thermal conductivity becomes very difficult when it is irradiated to over 0.1 dpa. It needs at least 1500°C to reach 50% of unirradiated value by post irradiation annealing.
3) The reduction in thermal conductivty and dimensional change of bulk boronized graphites were lerger than those of isotropic graphites or C/C composites.

Is it possible to develop carbon based materials which shows little degradation in thermal conductivity upon neutron irradiation?

⇨ it is very unlikely to have such material, because irradiation induced defects almost determine thermal conductivity of carbon materials at low temperature

⇨ carbon materials should be used at high temperature to avoid large decrease in thermal conductivity

Use of C/C-Cu graded structure
(Functionally Gradient Materials : FGM)

Advantages of C/C-Cu FGM :

(1) The plasma facing surface is made of carbon 100%.
(2) The thermal conductivity can be > 300 W/(m K) at R.T.
(3) Brazing with cooling structure is easy.
(4) Reduce thermal stresses at brazed region.
(5) Carbon rich portion can be maintained at relatively high temperature, while Cu rich portion is kept at low temperature, which reduces neutron-irradiation-induced degradation of thermal conductivity.

Research and development items:

(1) development of fabrication technology
(2) high temperature stability of C/C-Cu graded structure
(3) neutron irradiation effect on integrity of C/C-Cu FGM

C/C-Cu FGM

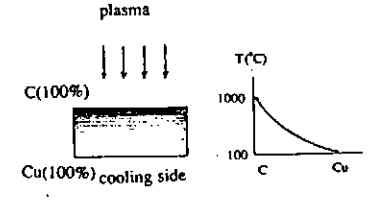

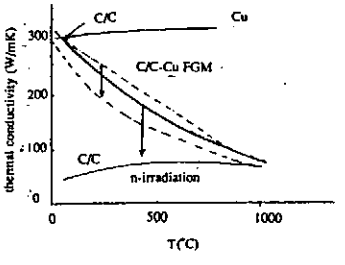

X-ray Diffraction Analysis of Neutron Irradiated Some Graphite Materials

M. ISEKI[1], H. ATSUMI[2] and T. MARUYAMA[3]

1. Nagoya University; Furo-cho, Chikusa-ku, Nagoya 464

2. Kinki University; Kowakae, Higashiosaka

3. PNC; Oarai-cho, Ibaraki, 311-13

Some isotropic graphite and C/C composite are concidered as one of the candidate materials for use in the plasma facing materials because its low atomic number, its low activity after neutron exposure, and its excellent thermal shock resstance. Hoeever, very little data exist on the behavior of these materials neutron irradiation. This experiment was carried out in part of the irradiation reserch group for graphite materials.

Rod like specimens(2 x 2 x 25 mm) of isotropic graphite, C/C composite and glassy carbon were thermal treatt at 1000C Hin vacuum furnace. The irradiation of some graphite and C/C composite were carried out in JMTR(Japan Material Test Reactor), the fast neutron fluence ranged from 1.4 x 10^{19} to 5.4 x 10^{20} n/cm^2 (E>1MeV) and the irradiation temperature under 200C.

Irradiation volume change were mesured with a traveling microscope, lattice parameter changes and graphitization were mesured by X-ray diffraction analysis, and changes in apparent electric resistivity were mesured by D.C. 4-probe method.

Post irradiation annealing treatment consisted of isothermal puls annealing for 1 hr in a vacuum. After annealing properties were mesured at room temperature.

Changes in length and cross section for spesimens irradiated up to 1.9 x 10^{20} n/cm^2 showed clear expansion. Contrary, the glassy carbon and the C/C composite showed lonitudional shurinkage. The demensional changes were very dependent on the fabrication and thermal treatment. X-ray diffraction analysis on the graphite crystalwere shown expands along its C-is and contracts in the two a directions.

Post irradiation annealing test were made on the volume change mesurement, lattice parameter changes and electricalresis mesurement. Expanded lattice parameter and the volume are recovered with increasing annealing temperature. On the contrary, the electrical resistivity increasing with increasing annealing temperature. There is an indication that the electriresistivity is not directly concerned with volume changes.

X-ray Diffraction Analysis of Neutron Irradiated Some Graphite Materials

Michio ISEKI Nagoya University
Hisao ATSUMI Kinki University
Tadashi MARUYAMA Power Reactor and Nuclear Fuel Development Corporation

JAERI-US Workshop p195 HHP components and Plasma Surface Interactions for Next Devices

November 17-19, 1992

Experimental

1. Samples
   - Isotropic Graphite:
     - IG-110U(Toyo Tanso)
     - IG-430U(Toyo Tanso)
     - EPT-10(Ibiden)
   - C/C composite:
     - CX-2002U(Toyo Tanso)
   - Glassy Carbon:
     - GC-3000(Tokai Carbon)

2. Neutron Irradiation
   - JMTR(Japan Material Test Reactor)
   - Fluence: 1.4×10^{25}n/cm², 1.9×10^{25}n/cm², 5.4×10^{25}n/cm²
   - Irradiation Temperature: 200℃

3. Post Irradiation Test
   - X-ray diffraction analysis:
     (powder or rod(1 : 1 : 2mm), S Standard)
     - Lattice Parameter Changes: C, a
     - Graphitization: G-I-P.
       $d_{(002)}=3.440-0.086(1-P^2)$
   - Swelling measurement(Volume Change)
     (1 : 1 : 2, 1 : 1 : 2mm)
   - Electric Resistivity Measurement:
     DC 4 Probe Method, (1 : 1 : 2, 1 : 1 : 2mm)
   - Annealing Behavior:
     Lattice Parameter, Volume Change, Electrical Resistivity etc.
     (Vacuum, 10⁻⁶Torr, Pulse Annealing, Hot Hold, 350-650℃, 100° step)

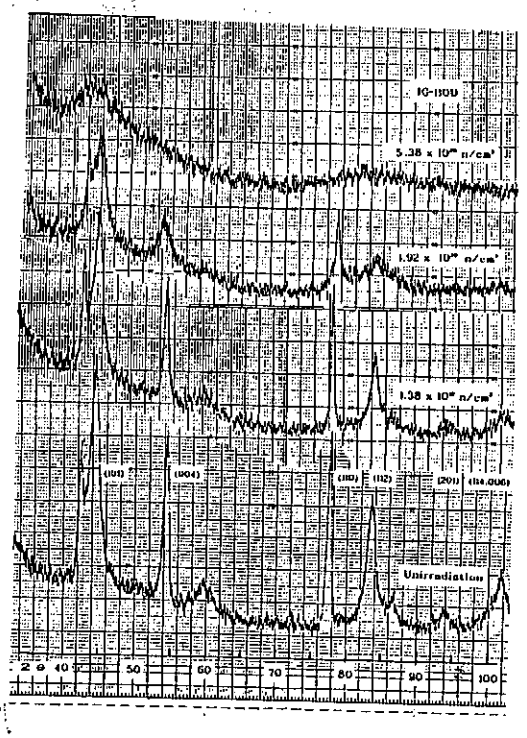

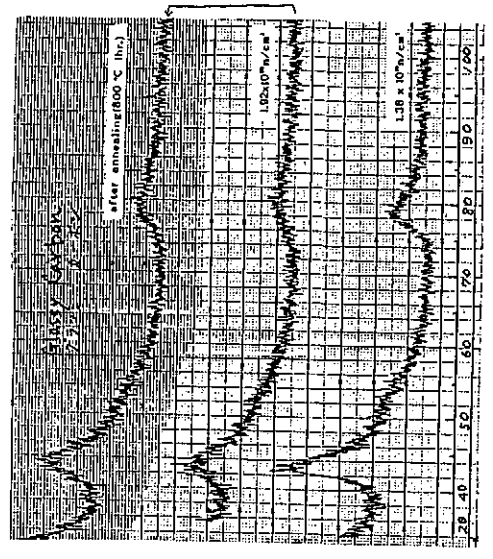

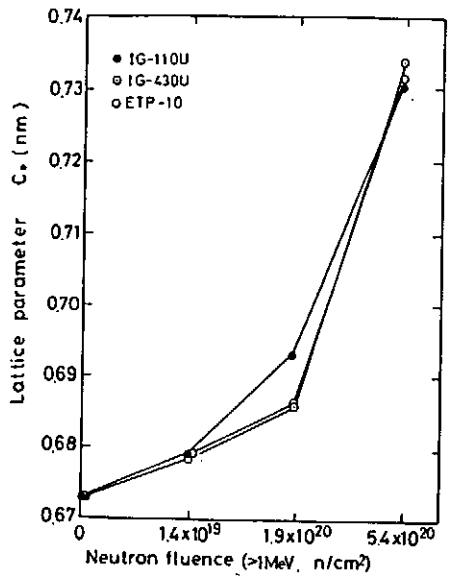

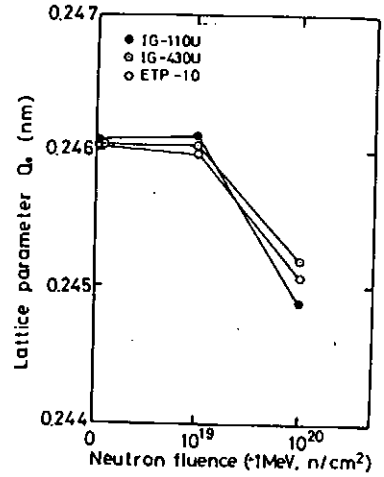

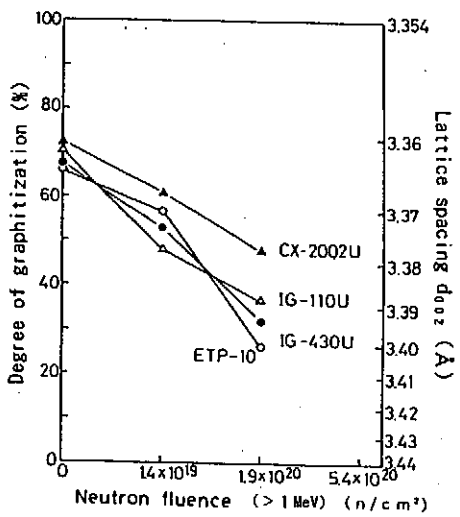

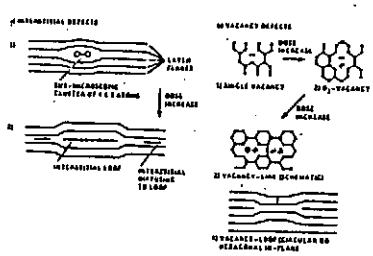

SCHEMATIC OF LATTICE DEFECTS INTRODUCED BY RADIATION IN GRAPHITE (FROM REF. 10)

FIGURE 1

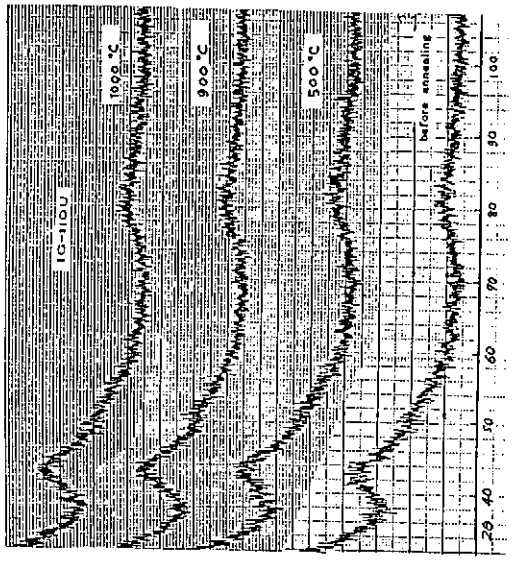
IG-110U
1000 °C
900 °C
500 °C
before annealing

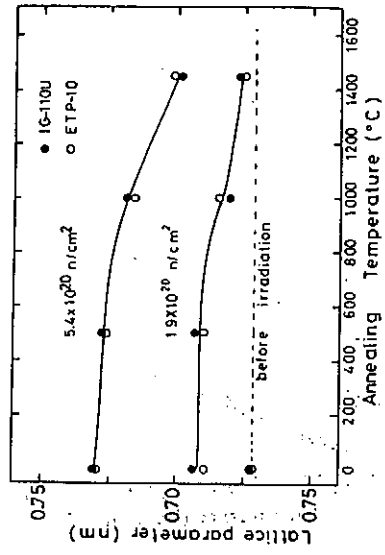
IG-110U
ETP-10
5.4x10²⁰ n/cm²
1.9X10²⁰ n/cm²
before irradiation
Lattice paramater (nm)
Annealing Temperature (°C)

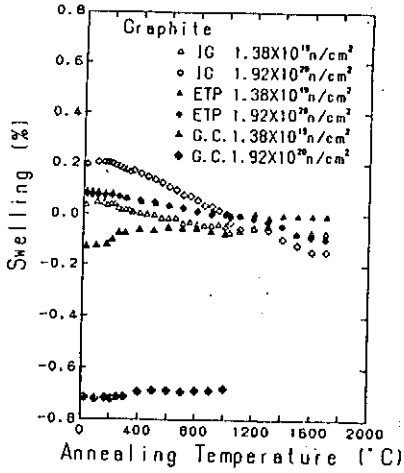
Graphite
IG 1.38X10¹⁹n/cm²
IG 1.92X10²⁰n/cm²
ETP 1.38X10¹⁹n/cm²
ETP 1.92X10²⁰n/cm²
G.C. 1.38X10¹⁹n/cm²
G.C. 1.92X10²⁰n/cm²
Swelling (%)
Annealing Temperature (°C)

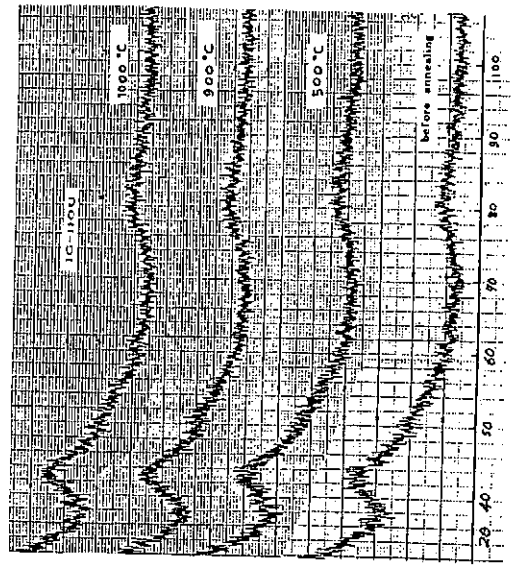
IG-110U
1000 °C
900 °C
500 °C
before annealing

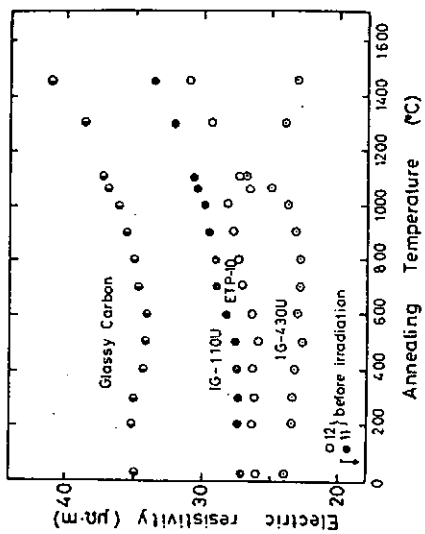

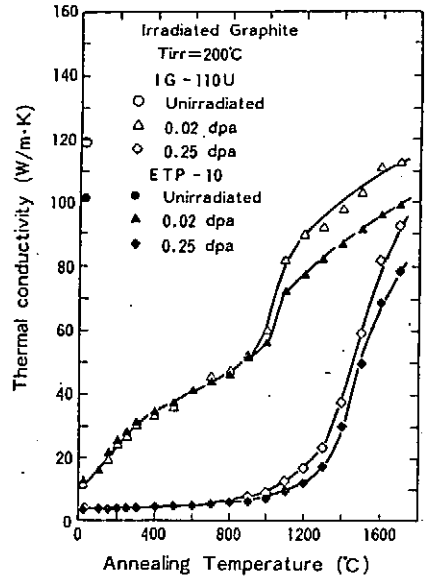

Fig. 2.

Conclusions

Changes in lattice parameter of C-axis and size demension for specimens irradiated up to 1.9 x 10^{20} n/cm²(0.24dpa) showed clear expansion. Contraly, the glassy carbon showed a shurinage.

In post irradiation annealing test, the lattice parameter, volume change and the thermalconductivity are recovered withh increasing temperature. On the contraly, the electrical resistivity increasing with increasingannealing temperature.

MATERIALS DAMAGE STUDIES IN TRIAM

T. Muroga

Research Institute for Applied Mechanics
Kyushu University

ABSTRACT

The flux and energy of the charge exchange neutral hydrogen particles at the SOL of TRIAM-1M have been estimated by comparison of microstructures between specimens exposed to TRIAM-1M plasma and those irradiated with low energy hydrogen ions. The effects of the hydrogen particle bombardment in future devices are discussed.

Specimens of 316SS, Mo, Al, and Cu, prepared for Transmission Electron Microscopy (TEM) observations, were introduced to SOL of TRIAM-1M and exposed to plasma for 1302 sec (2 discharges). Microstructural observatipons by TEM showed interstitial type dislocation loops and hydrogen clusters. This implies that the atomic displacements took place by incident hydrogen particles. Damage microstructure in aluminum were found to be almost insensitive to the distance from the plasma edge. Thus the damage seems to be caused by charge exchange neutral hydrogen particles.

In-situ observation of microstructures by TEM during low energy hydrogen ion irradiations have been carried out in Mo and Al using a interface between a low energy ion source and a TEM. Interstitial type dislocation loops and hydrogen clusters were also observed, whose size and density were strong functions of the ion energy and fluence.

The microstructural comparison between TRIAM-1M probe specimens and ion-irradiated specimens showed that the hydrogen particle energy was typically less than 2 keV and that the fluence during the 1302 sec plasma exposure was 1 to $3 \times 10^{21}/m^2$. The fact that the fluence estimated by microstructures of Mo and Al was close to each other demonstrates reliability of the present study.

It is to be noted that about $10^{21}/m^2$ hydrogen particles were bombarded into the probe specimens only during two plasma shots. Thus $10^{25}/m^2$ hydrogen injection is expected after 20,000 shots. Moreover, because they are neutral, the hydrogen particles would bombard all plasma-facing first wall area (not localized) even when the plasma is magnetically well confined. This should affect the fuel cycling and the materials properties strongly in future high temperature long operation devices.

Contributions of N. Yoshida, K. Tokunaga, T. Fujiwara, R. Sakamoto, S. Itoh and the TRIAM group are acknowledged.

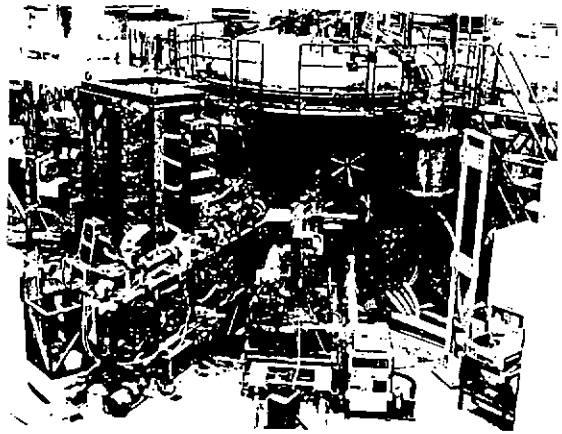

Collector Probe Transportation System
Connected with TRIAM-1M

MATERIALS DAMAGE STUDIES IN TRIAM

T. Muroga

Research Institute for Applied Mechanics,
Kyushu University

Japan-US Workshop P196 on High Heat Flux Components and Plasma Surface Interactions for Next Devices
Nov. 17-19, 1992, Kyushu University

COLLECTOR PROBE TRANSFER SYSTEM

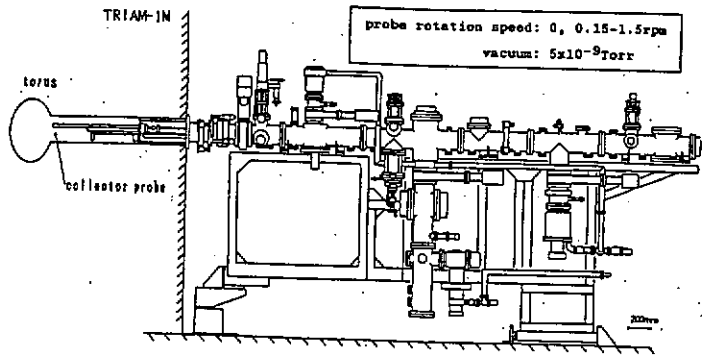

OUTLINE OF PRESENTATION

1. Displacement damage production in TRIAM-1M probe specimens

   TEM observation of defect clusters
   Positional dependence of damage microstructures
   Possible mechanisms of damage production

2. Estimation of particle flux and energy at SOL of TRIAM-1M by comparison with microstructures induced by hydrogen-ion irradiation

   In-situ low energy hydrogen ion irradiation in TEM
   Estimation by microstructural comparison in molybdenum
   Estimation by microstructural comparison in aluminum

3. Implication to PFC materials damage in future devices

CONTRIBUTION : N. YOSHIDA, K. TOKUNAGA, T. FUJIWARA, R. SAKAMOTO
S. ITOH AND THE TRIAM GROUP

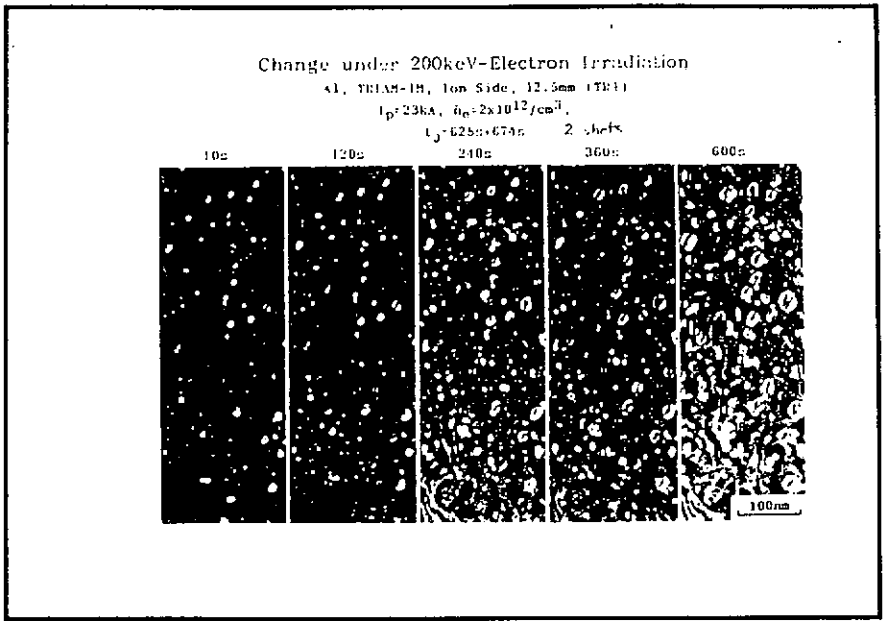

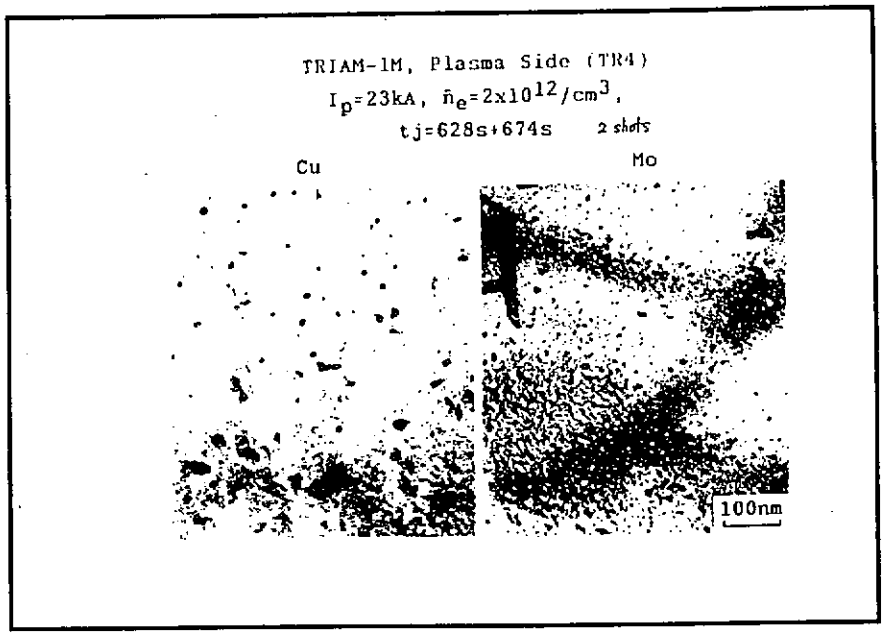

SUMMARY 1. DAMAGE OBSERVED IN TRIAM-1M PROBE SPECIMENS

1. Interstitial loops and hydrogen clusters were observed in 316SS, Mo, Al and Cu. This implies that the atomic displacements took place by incident hydrogen particles.

2. The damage microstructures in Al were not sensitive to the distance from the plasma edge. Thus the damage seems to be caused by charge exchange neutral hydrogen particles.

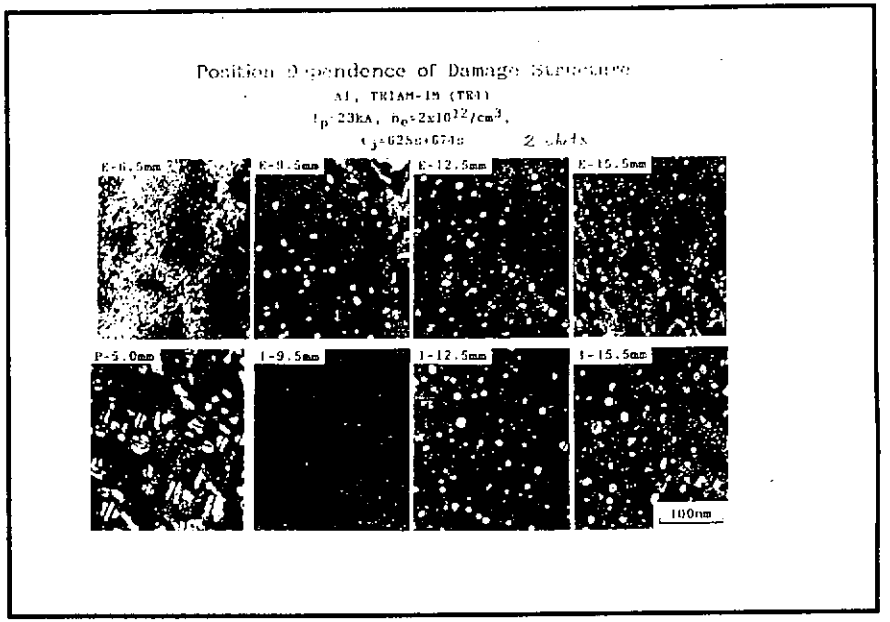

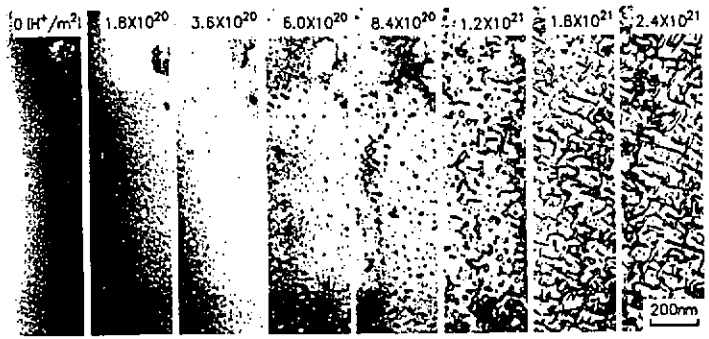

Mo, irradiated with 8.0IkeVI $H^+(2.0X10^{18}IH^+/m^2.sI)$ at R.T.

SUMMARY 2. Estimation of fluence and energy of hydrogen particles subject to TRIAM-1M probe specimens

1. Typical hydrogen energy was less than 2 keV.
2. Hydrogen fluence was 1-3x10^{21}/m^2 for the case of 1302 sec plasma discharge (2 shots).
3. The fact that the fluence estimated by microstructures of Mo and Al was close to each other demonstrates reliability of the present method.

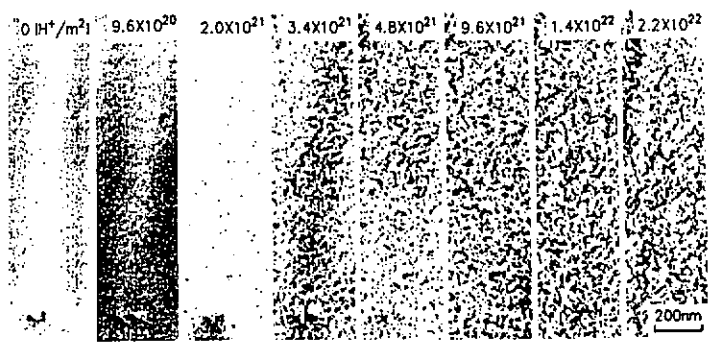

Mo, irradiated with 2.0IkeVI $H^+(8.0X10^{18}IH^+/m^2.sI)$ at R.T.

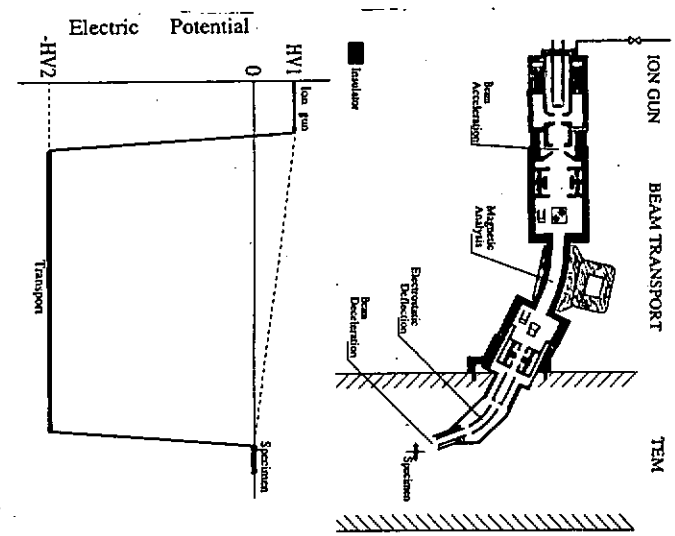

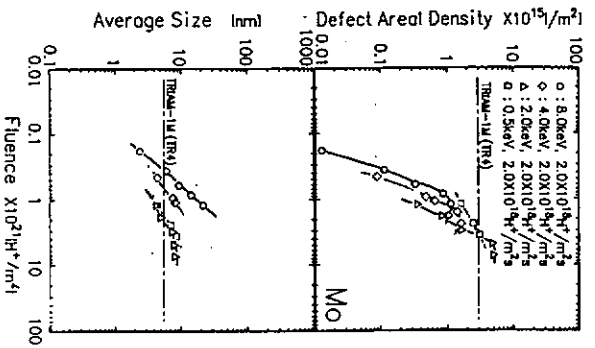

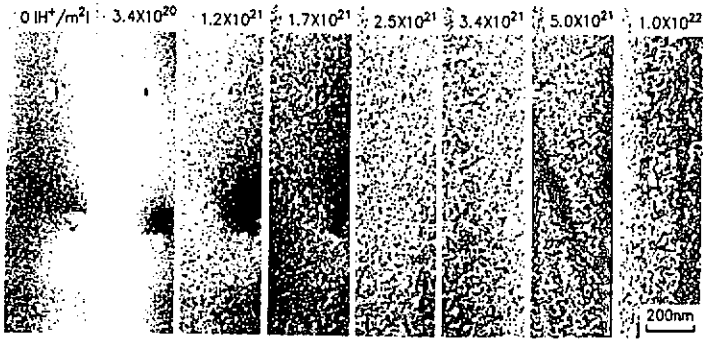

Mo, irradiated with 0.5(keV) $H^+(2.8X10^{18}(H^+/m^2 \cdot s))$ at R.T.

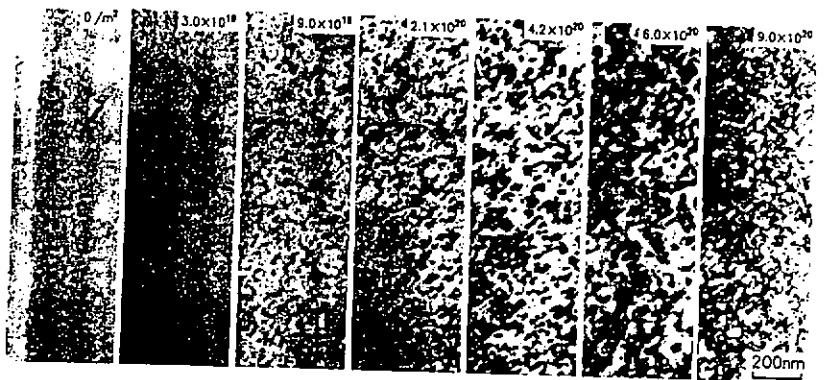

Al, irradiated with 8.0(keV) $H^+(2.0X10^{18}(H^+/m^2 \cdot s))$ at R.T.

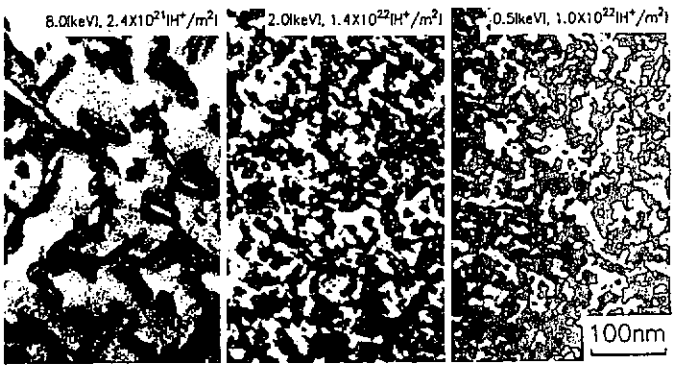

Mo, irradiated with H^+ at R.T.

SUMMARY 2. Estimation of fluence and energy of hydrogen particles subject to TRIAM-1M probe specimens

1. Typical hydrogen energy was less than 2 keV.
2. Hydrogen fluence was 1-3x10^{21}/m^2 for the case of 1302 sec plasma discharge (2 shots).
3. The fact that the fluence estimated by microstructures of Mo and Al was close to each other demonstrates reliability of the present method.

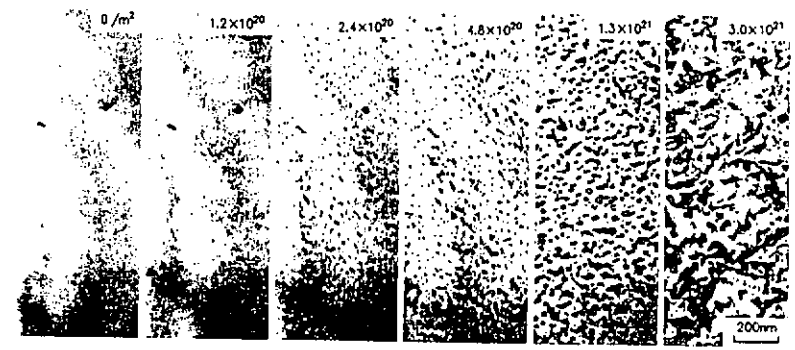

Al, irradiated with 0.5lkeVl H^+(2.0X10^{18}lH^+/m^2·sl) at R.T.

SUMMARY 3. Implication to PFC materials damage in future devices

Order of 10^{21}/m^2 charge exchange neutral hydrogen particles were injected in TRIAM-1M probe specimens. (only after two discharges!)

Number of discharges	Hygrogen fluence expected
200	10^{23}/m^2
20000	10^{25}/m^2

Moreover, because they are neutral, the hydrogen particles would bombard all plasma-facing first wall area (not localized effects) even when the plasma is confined well.

This should affect the fuel cycling and the materials propertis strongly in the future high temperature long operation devices.

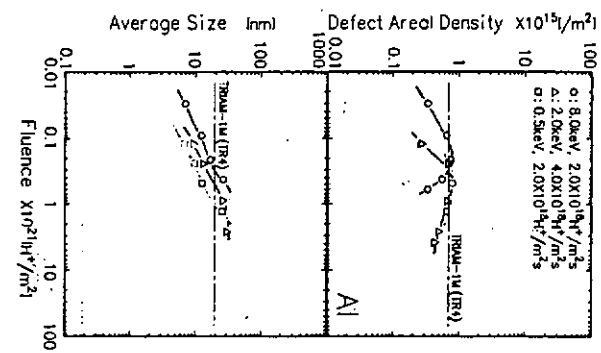

Session 7: Session Summaries

Summary ①

PFC and PSI in Large Devices
M. Ulrickson

D III D

Initial gas target divertor experiments showed ~50% heat flux reduction without changing core plasma

Advanced Divertor Program
Biasing can increase neutral pressure

Pumping being added

Radiative divertor planned

Actively cooled divertor planned

Divertor Material Erosion Experiment ready for operation

TFTR

D retention 44±15% average over 5 years

Retention correlated with average beam power

Distribution

Limiter Surface ~50%

Gaps between tiles ~20%

Walls ~33%

He/O GDC has been tried for removal of codeposited layers

Significant D retained

Boronization required

Low inventory T reprocess. will be installed

Preparations for T in progress

② LHD

In 3rd year of 7 year construction project

Buildings well along

Coils and cryostat under construction

TRIAM-1M

Mo Limiters show evidence of cracking and melting

Low density ops ok

High density ops cause damage

Investigating alloys to lessen damage

③

JT60 U (4)

Boronization performed using $B_{10}H_{14}$ (decaborane)

Reduced recycling
o concentrations
Zeff

Result high performance plasmas.
More inlets planned

B_4C coatings on C tiles

LPPS } melting, exfoliation (edges)
CVD }
CVR (best) melting (edge)

more coverage planned (CVR)

He TDC (5)

GDC

Lower T operation used to lower recycling

TDC not needed after boronization

D_α reduced in H-mode (Cause not sure)

A personal opinion

More attention needs to be paid to development of low activation materials:

examples - SiC
V
Al
Braze materials

Why?

Long development time

New design criteria

Qualification for use in fusion devices.

Summary: Developments of High Heat Flux and Energy Deposition

Prepared by: M. Akiba
and
R. McGrath

I Materials Data Base (continued)

I-2 Disruptions & Run Away Electrons

e-beam simulations (4-1, 13, 15, 16)

Plasma gun simulations (4-1)

Tokamak measurements (3-2, 4-1)

Comments:

- Pulsed e-beam test show ~400μm erosion at 12 MJ/m² while plasma gun simulations show 2μm.
- Modeling of PMI during disruptions is being developed/applied to aid in understanding the data mentioned above. (Not presented at this meeting)
- Measurements on DIII-D using DIMES will assist in evaluating disruption loads and associated materials response.
- Run Away electron generation (not presented) and materials response is being evaluated.

I - Materials Data Base

I-1 Thermal & Mechanical Properties

Be (4-1, 3)*

CFCs (4-1, 4, 15)

W-33Cu (4-7)

C-B-Ti (4-11)

* Number of talk where information was presented

Comments

- Data base for Be is less developed than that for carbon based armors.
- Development of new CFCs with high thermal conductivities is advancing. (e.g. 1D CFCs with 850 w/mk @ 20°C)
- Neutron damage is a major concern. 30-50% loss in thermal conductivity at 0.1 dpa. (See Neutron Damage Session)

III Armor/Heat Sink Bonding, Fabrication and Reliability

- Be + CuCrZr (4-3)
- CFCs + OFHC, small samples (4-1, 4, 5, 6, 8, 9, 10, 12, 15, 16)
- CFC + OFHC, 1 m long samples (4-4, 5, 6)
- CFC + W-33Cu (4-7)
- W + OFHC (4-10)
- CFCs + DS Cu (4-15)
- CFCs + TZM (4-15)
- First Wall optims (4-4, 5)

II Heat Transfer Data Base

Swirl tubes (4-1, 4, 15)

Porous coatings (4-1)

Hypervapotrons (4-1, 3)

Helium coolants (4-1)

Comments

- Heat transfer correlations under one-sided heating conditions, with and without boiling, are required.
- Present structures nearly meet ITER requirements (eg. ~20 MW/m²)
- Helium offers some advantages over water: no phase change instabilities, easier clean-up after coolant leaks, accident/safety concerns, etc.

III Armor/Heat Sink. Bonding, Fabrication and Reliability

Comments (continued)

- The data base on Be armor stress cracking and attachment is being expended at JET (Mark I & II) and SNL
- Support structure performance is an important issue and testing has been initiated in Japan and the EC.
- Performance, Reliability and lifetime testing of full scale PFC proto-types will be required for ITER. At least one new, high power (10s of MWs), large area (~few m^2s) test stand will be required.

III Armor/Heat Sink Bonding, Fabrication and Reliability

Comments:

- Options for armor/heat sink combinations developed to date operate at 20 MW/m^2. These almost meet ITER requirements.
- Reliability & lifetime are serious concerns:
  + Some testing at 5-20 MW/m^2 for ~1000 cycles
  + We need many samples to 10,000 cycles, maybe higher heat fluxes.
- Fabrication quality control is important,
  + thermography and other inspection techniques
  + repair procedures, fab. sequence and in situ

IV PFC R&D Programs Presented At This Workshop Support Many Different Devices

- Applications to Operating Machines Presented
  - + JT-60U
  - + TRIAM-1M
  - + TFTR
  - + DIII-D
  - + Tore Supra
  - + TEXTOR

- Applications To Future Devices
  - + Large Helical Device - LHD
  - + Tokamak Plasma Experiment - TPX
  - + ITER

PFC and PSI Studies in Laboratory

Chairmen: K. Wilson (SNL) and N. Noda (NIFS)

The reports can be divided into three main categories:

- Hydrogen Recycling
- Erosion / Redeposition Studies
- Boronization

Hydrogen Recycling

- Hydrogen is released as atoms rather than molecules from graphite at elevated temperatures. *Haasz*

Models have been developed for hydrogen release under combined ion and thermal release mechanisms. *Morita*

Bulk hydrogen retention in graphite depends on the degree of graphitization. *Atsumi*

Copper-carbon materials have retention behavior between graphite and copper. *Natsir*

Key Requirement: Develop a tritium inventory model for graphite with realistic neutron effects.

Fig. 6 Correlation between the degrees of graphitization and hydrogen solubility in graphite.

Erosion/Redeposition

- Tungsten sputtering is dominated by oxygen sputtering at low energies. *Hirooka*

- The REDEP code has been very successfully benchmarked against laboratory and tokamak data. *Hua*

- Erosion/redeposition of carbon can be very complex in the 900K range. *Sagara*

- A new model for methane release from graphite has been developed. *Yamaguchi*

- Boron has high evaporation rates from boronized carbons at high temperatures. *Hino*

Key Requirement: Develop predictive models of erosion lifetime for various plasma modes.

Net Erosion Profiles

measured with surface profilometry

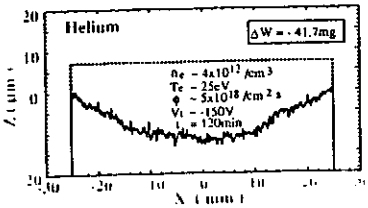

The erosion profile due to helium is easily explained by sputtering with little redeposition, because the sputtering yield estimated from the weight loss is comparable to that from ion beam experiments, and because the calculated ionization mean free path of physically sputtered carbon atoms is as long as about 100mm in this experiment.

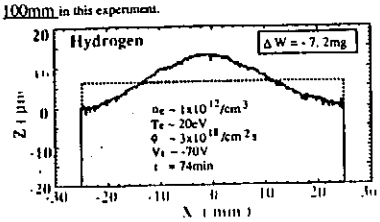

In case of hydrogen, the net erosion profile clearly differs from that of helium.

The initial surface level can be estimated from the volume change estimated from the weight loss by assuming the weight density of the redeposited layer to be the same as that of the bulk.

- The result indicates that there is net growth at the center region and net erosion at the outer region

Boronization

- Solid target boronization has been successfully tested in tokamaks. *Hirooka*

- Gettering properties can be recovered by helium GDC. *Noda*

- Decaborane offers many safety advantages, but the deposition is non-uniform. *Sugai*

- Hydrogen desorbs at lower temperatures for increasing boron to carbon ratio. *Gotoh*

Key Requirement: Optimize boronization technique for steady state operation

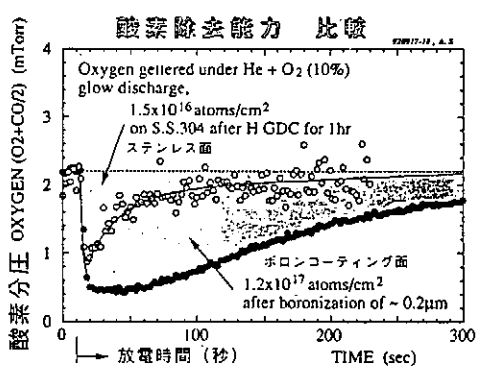

US-JAPAN WSHOP

PSI/HHF

KYUSHU UNIV.

NOV 17-19, 92

SESSION #4

ON

RITIUM INVENTORY AND HANDLING

SUMMARY

M. CROCLIN

PPPL

1

MINI SESSION - 3 TALKS:

1- K. WILSON (SNL)
T INVENTORY IN Be

2- K. OKUNO (JAERI)
IDP OF D THROUGH Mo

3- M. NISHIKAWA (KYUSHU)
T INTERACTION WITH MATERIALS

2

- WILSON - T/Be

- (H,D,T) DATA NOT SATISFACTORY:
  - * SOLUBILITY LOW (DATA SCARCE)
  - * DIFFUSIVITY MODERATE (")
  - * BeO ON SURFACE (??)
  - * SURFACE EFFECTS AND RATE CONSTANTS (?)
  - * EFFECTS OF SURFACE CONTAMINANTS (?)
  - * MODELLING by PERI CODE → JET SHOTS + OLD DIFF. DATA (R. Brown)

WORK UNDER WAY MUST CONTINUE (→ ITER)

3

- JET Be TILES UNDER STUDY FOR TRITIUM
  - ~ 2 Ci LEFT (INPUT ~ 53 Ci)
  - C-Be/O LAYER BURIED UNDER Be/O LAYER

2- OKUNO - IDP D/Mo

T-IDP RIG, 0.2-2 keV

- ss ϕ_p vs ϕ_i IS DD-LIMITED
- TRAPS BY HIGH E EXP (DEFECTS)
- T° SCALING OF ϕ_p vs ϕ_i ?

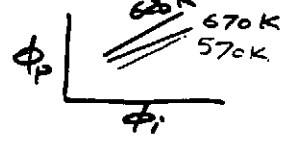

4

3- NISHIKAWA - T-MATLS

- TRITIUM LAB - KYUSHU
  SAFETY ENGRG +
  FUELLING STUDIES

- WARNING - LOTS OF DIFFER.
  PROCESSES (H ISOTOPES/WATER)
  ADS + EXCHANGE etc.

- OH GROUP IMPORTANT -
  HAS IMPACT ON TRITIUM'S
  STICKING ONTO SURFACES

5

Radiation Effects

M. Iseki (Nagoya)
T. Maruyama (PNC)
T. Muroga (Kyushu)
L. Snead (ORNL)

Materials Damage in Triam

- Defect structures observed in:
  SS316, Mo, Al, Cu
  Following keV protium implantation.
- Dislocation loops we observed to be of interstitial type:
  - presence of loops implies H^+ displacements
  - positional independence of damage implies defects are caused by charge exchange neutrals.
- Size of dislocation loops is larger for higher incident proton energies.

Radiation Effects in Glidcop

- Glidcop has been irradiated up to ~ 150 dpa (FFTF- 450 °C) with promising results for use of material for ITER
- ORNL/PNL program in MP of unirradiated Glidcop (tensile, fatigue, fatigue crack growth, fracture toughness)

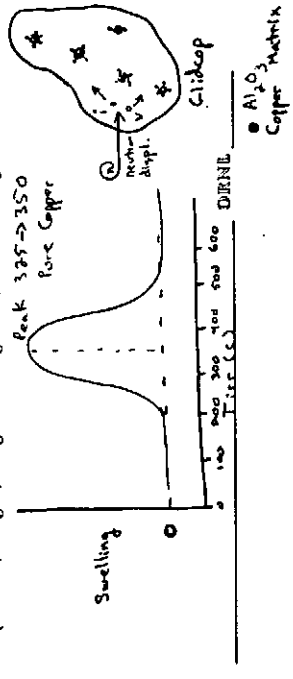

Neutron Irradiation Effects in Graphite

M. Iseki
T. Maruyama
L. Snead

- Dimensional Changes in c/c will be dominated by fibers.
- Thermal Conductivity and Electrical Conductivity were seen to anneal at different temperatures.

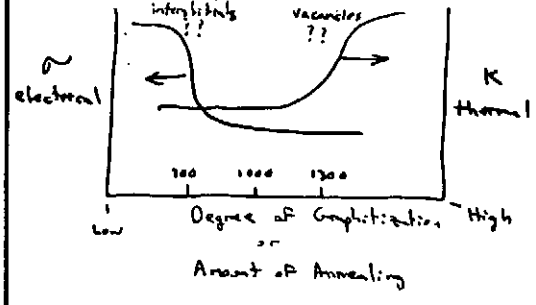

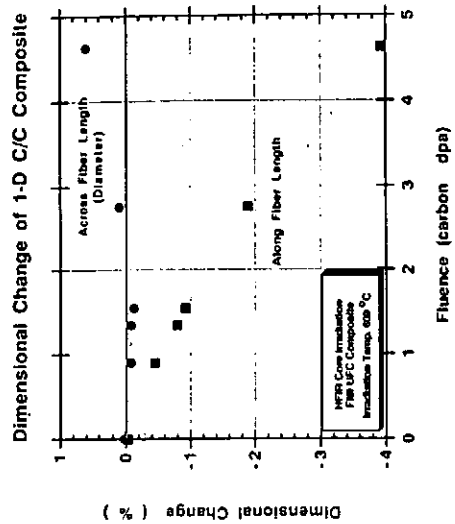

Thermal Conductivity of Graphite

- The amount of radiation induced thermal conductivity degradation is dependent on starting "graphitic perfection."
- Substantial thermal conductivity is regained following annealing (up to or greater than 50%)
  - Simple Defects $T > T_{irr}$
  - Complex Structures, $T > \sim 1000$ °C.
- Boronization of graphite is extremely detrimental to unirradiated and irradiated thermal conductivity.
  - Boron is a substitutional impurity which "pins" dislocations

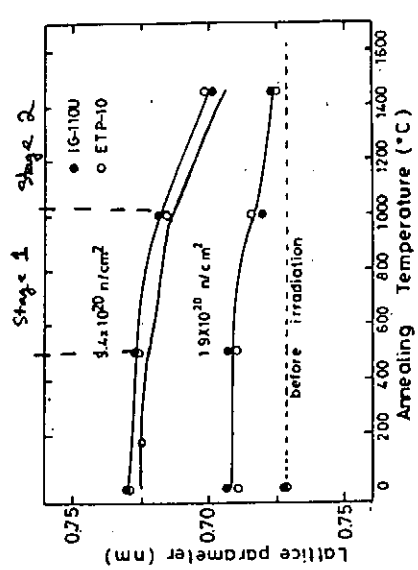

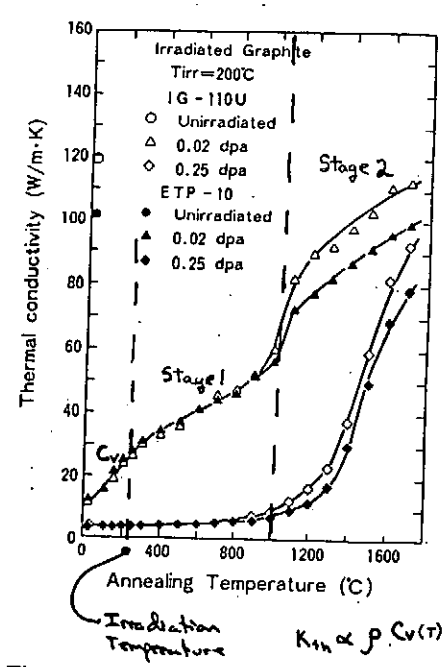

$K_{th} \propto \rho\, C_{v(T)}\, l$

ρ: density
C_v: specific heat
l: mean phonon length

Fig. 2.

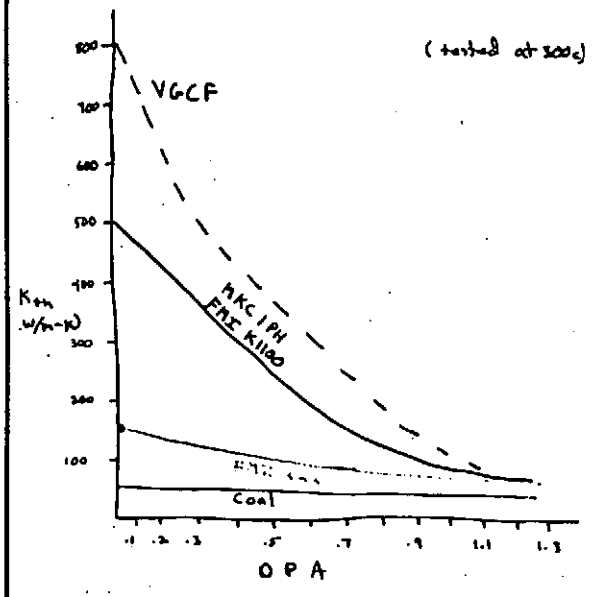

$$K = \frac{\rho}{3} C_v(T)\, \ell$$

$$\frac{1}{\ell} = \underbrace{\frac{1}{\ell_o}}_{\text{initial defect structure}} + \underbrace{\frac{1}{\ell_{irr}}}_{\text{radiation induced defect structure}}$$

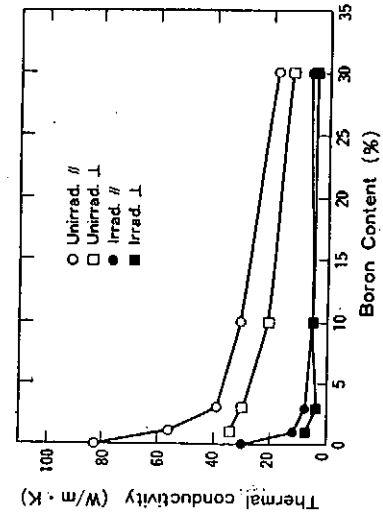

Fig. 4.

Direction for Continued Research in c/c

- Understanding of radiation effects in c/c is fairly good.
- It is important to focus on candidate materials and start bi-lateral studies on these materials.
- Preparation should be made to study irradiation effects of brazed materials.
- Beryllium studies needs to begin !! (more lead time ...)

Functionally Gradient Materials (FGM)

- Proposed FGM (Cu-c/c) for high heat flux material.
  - Reduced thermal stress (only Cu-Cu braze required)
  - Neutron degredation of thermal conductivity reduced.
- Important that only c/c faces plasma

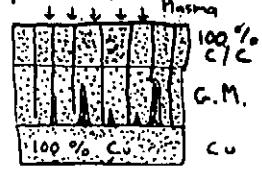

- FGM's are very early in developmental stage.

Cu - C
Cu - Be
C - SiC
:

Appendix A: Agenda

Japan-US Workshop P-196 on "High Heat Flux Components and Plasma Surface Interactions for Next Devices"
November 17-19, 1992
Kyushu University, Chikushi Campus, Kasuga, Fukuoka

Agenda

Tuesday, November 17, 1992

8:40 a.m. **Welcome Talks** — Satoshi Itoh (Kyushu Univ.), T.Yamashina (Hokkaido Univ.), K.Wilson (Sandia National Laboratories)

9:10 a.m. **Session 1: Overviews**
Chairmen: R.McGrath (SNL) and O.Motojima (NIFS)

1-1 "US Activities on Plasma Facing Materials and Components"
K.Wilson (SNL) *20min.*

1-2 "JET as a Testbed for Materials"
K.J.Dietz (JET) *20min.*

1-3 "Japanese Studies on HHFC and PSI"
T.Hino (Hokkaido Univ.) *20min.*

10:10 a.m. - 10:30 a.m. Break

10:30 a.m. **Session 2: PFC and PSI in Large Devices**
Chairmen: M.Ulrickson (PPPL) and N.Yoshida (Kyushu Univ.)

2-1 "The DIII D Divertor Development Program"
L.Sevier (GA) *15 min. + 5 min. discussion*

2-2 "DIMES System Design and 1993 Experimental Plan"
C.Wong (GA) *15 min. + 5 min. discussion*

2-3 "Hydrogen Isotope Retention in TFTR"
M.Caorlin (PPPL) *15 min. + 5 min. discussion*

2-4 "Preparations for DT Operation on TFTR"
M.Ulrickson (PPPL) *15 min. + 5 min. discussion*

2-5 "Present Status of LHD"
O.Motojima (NIFS) *15 min. + 5 min. discussion*

12:10 p.m. - 1:10 p.m. Lunch Break

2-6 "PFC and PSI in TRIAM-1M"
N.Yoshida (Kyushu Univ.) *15 min. + 5 min. discussion*

2-7 "Development and Experiences with JT-60U PFC"
T.Ando (JAERI) *15 min. + 5 min. discussion*

2-8 "Recycling of Hydrogen Isotopes and He Ash in JT-60U"
H.Nakamura and JT-60U Team (JAERI) *10 min. + 5 min. discussion*

2-9 "Initial Boronization of the JT-60U Tokamak by Using Decaborane"
M.Saido (JAERI) *10 min. + 5 min. discussion*

2:20 p.m. **Session 3: Developments of HHFC/Divertor and Energy Deposition**
Chairmen R.McGrath (SNL) and M.Akiba (JAERI)

3-1 "High Heat Flux Testing and Material Development at Sandia"
R.McGrath (SNL) *30min. + 10 min. discussion*

3-2 "SSAT Divertor Design"
M.Ulrickson (PPPL) *15 min. + 5 min. discussion*

3-3 "High Power Tests of Possible First Wall Materials for JET"
H.D.Falter (JET) *15 min. + 5 min. discussion*

3:40 p.m.4:00 p.m. Break

3-4 "Development of Plasma Facing Components for ITER"
M.Akiba (JAERI) *15 min. + 5 min. discussion*

3-5 "Development of Fabrication Technologies for PFC of ITER"
S.Yamazaki (Kawasaki) *10 min. + 5 min. discussion*

3-6 "PFC R&D for ITER in Mitsubishi"
K.Ioki (MAPI) *10 min. + 5 min. discussion*

3-7 "Development of a New MFC-1(1D-CC)/W-33Cu Tubeless Flat Plate Divertor Design"
I.Smid (ANRC/JAERI) *10 min. + 5 min. discussion*

3-8 "High Heat Flux Test of Divertor Materials Using ACT(Active Cooling Teststand in NIFS)"
Y.Kubota (NIFS) *10 min. + 5 min. discussion*

3-9 "Development of Carbon Material Brazed with Metal"
T.Matsuda (Toyo Tanso) *10 min. + 5 min. discussion*

3-10 "Development of PFC in Toshiba Corp."
K.Kitamura (Toshiba) *10 min. + 5 min. discussion*

5:50 p.m. **End of Presentations**

6:00 p.m. - 7:30 p.m. **Banquet in Chikusi Campus**

Wednesday, November 18, 1992

8:40 a.m.

3-11 "Behavior of Carbon-Boron -Titanium Materials under High Heat Load"
H.Shinno, M.Fujitsuka and T.Tanabe (NRIM), T.Shikama (Tohoku Univ.),
A.Ono and T.Baba (NRLM) *10 min. + 5 min. discussion*

3-12 "C/C-OFHC Brazing Structure"
A.Shigenaga (Hitachi) *10 min. + 5 min. discussion*

3-13 "High Heat Flux Experiments on B_4C Overlaid Carbon Brazed Materials for Fusion Application"
K.Nakamura (JAERI) *10 min. + 5 min. discussion*

3-14 "Evaluation of Energy Deposition due to Runaway Electrons"
T.Kunugi (JAERI) *10 min. + 5 min. discussion*

3-15 "Progress in the EC Technology Program on Plasma Facing Components"
A.Cardella (NET) *10 min. + 5 min. discussion*

3-16 "Heating Tests with the New E-Beam Facility in the Hot Cells(JUDITH)"
R.Duwe (KFA) *10 min. + 5 min. discussion*

10:15 a.m. - 10:30 a.m. Break

10:30 a.m. **Session 4: PFC and PSI Studies in Laboratory**
Chairmen K.Wilson (SNL) and N.Noda (NIFS)

4-1 "Hydrogen in Graphite:Transport/Reemission/Retention"
A.A.Haasz (Univ. of Toronto) *15 min. + 5 min. discussion*

4-2 "Recent Results from PISCES"
Y.Hirooka (UCLA) *15 min. + 5 min. discussion*

4-3 "Boronization Studies"
Y.Hirooka (UCLA) *15 min. + 5 min. discussion*

4-4 "Erosion/Redeposition Modeling and Analysis Activities"
Thanh Hua (ANL) *15 min. + 5 min. discussion*

4-5 "Experimental Study on Boronization Using SUT(Surface Modification Teststand in NIFS)"
N.Noda (NIFS) *15 min. + 5 min. discussion*

12:00 p.m. - 1:00 p.m. Lunch Break

1:00 p.m.

4-6 "Basic Experiments on Boronization with Use of Decaborane"
H.Sugai, M.Yamage and T.Ejima (Nagoya Univ.)
15 min. + 5 min. discussion

4-7 "Erosion Profiles on Graphite under PISCES-B Plasma"
A.Sagara (NIFS) *10 min. + 5 min. discussion*

4-8 "Mass Balance Equations and Their Physical Parameters for Predication of Hydrogen Recycling and Inventory During D-T Discharge Shots"
K.Morita (Nagoya Univ.) *10 min. + 5 min. discussion*

4-9 "Release of Hydrocarbon from Graphite - Modeling and its Application to Isotropic and Boron-doped Graphites -"
K.Yamaguchi and M.Yamawaki (Univ. of Tokyo)
10 min. + 5 min. discussion

4-10 "Hydrogen Retention in Graphite - Correlation with the Structure -"
H.Atsumi (Kinki Univ.) *10 min. + 5 min. discussion*

4-11 "Characterization of C/C Armor Materials"
Y.Gotoh (Hitachi) *10 min. + 5 min. discussion*

4-12 "PFC and PSI Studies in Hokkaido Univerity"
T.Hino (Hokkaido Univ.) *10 min. + 5 min. discussion*

4-13 "Hydrogen Isotope Retention for CFC, Isotropic Graphite and Carbon Contained Copper Materials"
S.Amemiya, M.Natsir, T.Masuda and Y.Tsurita (Nagoya Univ.)
10 min. + 5 min. discussion

3:05 p.m. - 3:20 p.m. Break

3:20 p.m. **Session 5: Tritium Inventory and Handling**
Chairmen M.Corlin (PPPL) and K.Okuno(JAERI)

5-1 "Tritium Inventory in Beryllium"
K.Wilson (SNL) *15 min. + 5 min. discussion*

5-2 "Permeation Behavior of Deuterium Implanted into Metals with Low Incident Energy"
K.Okuno (JAERI) *15 min. + 5 min. discussion*

5-3 "Points to be Taken Care at Tritium Experiments - Interaction of Tritium with Piping Materials, Catalysts and Absorbents -"
M.Nishikawa (Kyushu Univ.) *10 min. + 5 min. discussion*

4:15 p.m. **Session 6: Neutron Damage**
Chairman L.Snead (ORNL) and T.Muroga (Kyushu Univ.)

6-1 "Neutron Damage of Graphite and Beryllium"
L.Snead (ORNL) *15 min. + 5 min. discussion*

6-2 "Neutron Irradiation Effect on the Thermal Conductivity of Graphite Materials"
T.Maruyama (PNC) *15 min. + 5 min. discussion*

6-3 "X-ray Diffraction Analysis of Neutron Irradiated Some Graphite Materials"
M.Iseki (Nagoya Univ.), T.Maruyama (PNC), H.Atsumi (Kinki Univ.)
10 min. + 5 min. discussion

6-4 "Material Damge in TRIAM"
T.Muroga (Kyushu Univ.) *10 min. + 5 min. discussion*

5:25 p.m. **End of Presentations**

Evening : Group Discussions and Preparation of Vu-Graphs for Session Summarues

Thursday, November 19, 1992

9:00 a.m. **Session 7: Session Summaries**
Chairmen R.McGrath (SNL) and T.Hino (Hokkaido Univ.)

"PFC and PSI in Large Devices"
M.Ulrickson (PPPL) and T.Ando (JAERI) *10 min.*

"Development of HHFC/Divertor and Energy Deposition"
R.McGrath (SNL) and M.Akiba (JAERI) *10 min.*

"PFC and PSI Studies in Laboratory"
K.Wilson (SNL) and N.Noda (NIFS) *10 min.*

"Tritium Inventory and Handling"
M.Caorlin (PPPL) and M.Nishikawa (kyushu Univ.) *10 min.*

"Neutron Damage"
L.Snead (ORNL) and T.Maruyama (PNC) *10 min.*

9:50 a.m. - 10:10 a.m. Break

10:10 a.m. **Overall Summary**
Chairmen K.Wilson (SNL) and T.Yamashina (Hokkaido Univ.)

"Discussions on Results of P196 and Items for Next Workshop"
K.Wilson (SNL) and T.Yamashina (Hokkaido Univ.)
30 min.

"Plan for Next Workshop"
K.Wilson (SNL) *15 min.*

11:00 a.m. - 12:00 p.m. **TRIAM Tour**

12:00 p.m. - 1:00 p.m. Lunch Break

1:00 p.m. - Tour to Aso Mt. Area for Technicasl Discussion

Appendix B: List of Participants

Japan-US Workshop P-196 on "High Heat Flux Components and Plasma Surface Interactions for Next Devices"
November 17-19, 1992
Kyushu University, Chikushi Campus, Kasuga, Fukuoka

List of Participants

M. Akiba	JAERI	Japan
T. Ando	JAERI	Japan
H. Atsumi	Kinki University	Japan
S. Fukuda	Kyushu University	Japan
Y. Gotoh	Hitachi	Japan
T. Hino	Hokkaido University	Japan
T. Ikeda	Mitsubishi Kasei	Japan
K. Ioki	MAPI	Japan
M. Iseki	Nagoya University	Japan
Sanae I.Itoh	Kyushu University	Japan
Satoshi Itoh	Kyushu University	Japan
Y. Kubota	NIFS	Japan
T. Kunugi	JAERI	Japan
E. Kuramoto	Kyushu University	Japan
T. Matsuda	Toyo Tanso	Japan
T. Maruyama	PNC	Japan
K. Moriyta	Nagaya University	Japan
O. Motojima	NIFS	Japan
T. Muroga	Kyushu University	Japan
H.Nakamura	JAERI	Japan
K. Nakamura	JAERI	Japan
Y. Nakamura	Kyushu University	Japan
N. Noda	NIFS	Japan
B. Oh	Kyushu University	Japan
M. Okada	Toyo Tanso	Japan
K. Okuno	JAERI	Japan
A. Sagara	NIFS	Japan
A. Shigenaka	Hitach	Japan
N. Shikama	Kyushu University	Japan
H. Shinno	NRIM	Japan
H. Sugai	Nagoya University	Japan
T. Suzuki	Kawasaki	Japan
Y. Takao	Kyushu University	Japan
K. Tokunaga	Kyushu University	Japan
M. Toyoda	MAPI	Japan
N. Tsukuda	Kyushu University	Japan
K. Yamaguchi	University of Tokyo	Japan
T. Yamashina	Hokkaido University	Japan
M. Yamawaki	University of Tokyo	Japan
S. Yamazaki	Kawasaki	Japan
N. Yoshida	Kyushu University	Japan
H. Watanabe	Kyushu University	Japan
M. Caorlin	Prinsceton Plasma Physics Lab.	USA
Y. Hiroola	UCLA	USA
Thanh Hua	Argonne National Laboratory	USA
R. McGrath	Sandia National Laboratories	USA
B. E. Mills	Sandia National Laboratories	USA
L. Sevier	General Atomics	USA
L. Snead	Oak Ridge National Laboratory	USA
P. Trester	General Atomics	USA
M. Ulrickson	Princeton Plasma Physics Lab.	USA
K. Wilson	Sandia National Laboratories	USA

C. Wong	General Atomics	USA
A. A. Haasz	University of Toronto	USA
A. Cardella	NET	EC
J. Dietz	JET	EC
R. Duwe	KFA	EC
H. Falter	JET	EC
T. T. C. Jones	JET	EC
I. Smid	ANRC/JAERI	EC/JAERI

Recent Issues of NIFS Series

NIFS-PROC-1 *U.S.-Japan Workshop on Comparison of Theoretical and Experimental Transport in Toroidal Systems Oct. 23-27, 1989* Mar. 1990

NIFS-PROC-2 *Structures in Confined Plasmas –Proceedings of Workshop of US-Japan Joint Institute for Fusion Theory Program–* ; Mar. 1990

NIFS-PROC-3 *Proceedings of the First International Toki Conference on Plasma Physics and Controlled Nuclear Fusion –Next Generation Experiments in Helical Systems– Dec. 4-7, 1989* Mar. 1990

NIFS-PROC-4 *Plasma Spectroscopy and Atomic Processes –Proceedings of the Workshop at Data & Planning Center in NIFS–*; Sep. 1990

NIFS-PROC-5 *Symposium on Development of Intensed Pulsed Particle Beams and Its Applications February 20 1990*; Oct. 1990

NIFS-PROC-6 *Proceedings of the Second International TOKI Conference on Plasma Physics and Controlled Nuclear Fusion , Nonlinear Phenomena in Fusion Plasmas -Theory and Computer Simulation-;* Apr. 1991

NIFS-PROC-7 *Proceedings of Workshop on Emissions from Heavy Current Carrying High Density Plasma and Diagnostics;* May 1991

NIFS-PROC-8 *Symposium on Development and Applications of Intense Pulsed Particle Beams, December 6 - 7, 1990*; Jun. 1991

NIFS-PROC-9 *X-ray Radiation from Hot Dense Plasmas and Atomic Processes*; Oct. 1991

NIFS-PROC-10 *U.S.-Japan Workshop on "RF Heating and Current Drive in Confinement Systems Tokamaks" Nov. 18-21, 1991*, Jan. 1992

NIFS-PROC-11 *Plasma-Based and Novel Accelerators (Proceedings of Workshop on Plasma-Based and Novel Accelerators) Nagoya, Japan, Dec. 1991*; May 1992